UNIVERSITY OF SOUTHAMPTON

FACULTY OF PHYSICAL SCIENCES AND ENGINEERING

OPTOELECTRONICS RESEARCH CENTRE

ULTRAFAST WAVEGUIDE LASERS

by

Amol Choudhary

Thesis for the degree of Doctor of Philosophy

January 2014

UNIVERSITY OF SOUTHAMPTON

ABSTRACT

FACULTY OF PHYSICAL SCIENCES AND ENGINEERING
OPTOELECTRONICS RESEARCH CENTRE
Doctor of Philosophy

ULTRAFAST WAVEGUIDE LASERS

By Amol Choudhary

Mode-locked lasers with repetition-rates in excess of 1 GHz have many applications in areas such as optical sampling, non-linear microscopy, and optical frequency metrology. To date there have been very few demonstrations of such high repetition-rate lasers with sub-picosecond operation and high average power. This thesis deals with the realisation of such compact sources using an integrated-optics platform. Waveguides offer certain key advantages, including a low threshold power, high slope efficiency, compatibility with monolithic devices, and a low mode-locking threshold, making them very promising candidates for such devices. Ultrafast multi-GHz waveguide lasers are described in this thesis, which are compact, mass-producible and low-cost making them very exciting candidates for industrial applications.

Mode-locking was demonstrated in an ion-exchanged Yb:phosphate glass waveguide laser with integrated saturable absorber elements. An average output power as high as 80 mW was achieved at a pulse repetition frequency (PRF) of 4.9 GHz, at a wavelength around 1 µm and with pulse durations as short as 740 fs. Using shorter cavity lengths, waveguide lasers with PRFs of 10.4 GHz, 12 GHz and 15.2 GHz were achieved with pulse durations between 757 fs and 824 fs. A Gires Tournois Interferometer (GTI) effect was used to facilitate soliton mode-locking in the waveguides via accurate control of the gap between the waveguide and the output coupling mirror. This is a convenient technique to control the dispersion without introducing any extra elements in the laser cavity.

Two further Yb-doped ultrafast laser hosts, $RbTiOPO_4$ and $KY(WO_4)_2$, were investigated for their potential as ultrafast waveguide laser sources, having both been previously demonstrated as good bulk ultrafast systems. Laser action was demonstrated for the first time in an (Yb,Nb):$RbTiOPO_4$ planar waveguide laser, fabricated by liquid-phase epitaxy. Ion-beam milling was then used to fabricate the first ever single-mode rib waveguides in (Yb,Nb):$RbTiOPO_4$ fabricated by dry etching techniques but laser action was not possible due to propagation losses of ~3dB/cm. A systematic study of the reactive ion etching of $RbTiOPO_4$ was then carried out to minimise the surface roughness, in an attempt to reduce the propagation losses. The first ever demonstration of single-mode waveguiding in (Yb,Nb):$RbTiOPO_4$ fabricated by reactive ion etching was demonstrated but the propagation losses remained high. Using (Yb,Gd,Lu):$KY(WO_4)_2$ as a gain media, efficient laser action was demonstrated in an “inverted-rib” waveguide laser structure fabricated by ion-beam milling. This laser was found to have a threshold power as low as 13 mW and a maximum slope efficiency of 58% and showed characteristics of a pure 3-level-laser by lasing at 981 nm. However, further loss reduction is again required in order for efficient ultrafast operation to be obtained in the future.

Mode-locked waveguide laser operation was extended to the 1.5µm spectral region based on an ion-exchanged Er,Yb:phosphate glass waveguide laser using a novel SESAM based on a quantum dot in well (DWELL) structure. 2.5 ps pulses at a PRF of 4.8 GHz and an average output power of 9 mW were achieved. With a shorter waveguide sample, a PRF of 6.8 GHz with an average output power of 30 mW and pulse duration of 5.4 ps was achieved. The repetition-rate of the laser was finely tuned by controlling the pump power offering an attractive technique for enabling future frequency-comb stabilisation. This is the highest reported repetition-rate from a mode-locked waveguide laser at 1.5 µm and is also the first ever waveguide laser mode-locked by a quantum dot SESAM.

Finally, as an intitial step towards further extension to the 2µm spectral region, laser action was demonstrated, for the first time, in an ion-exchanged Tm:glass waveguide laser with a threshold power as low as 44 mW and a maximum slope efficiency of 6.8% around 1.9 µm.

Designs for power-scaling of such sources have also been discussed in this thesis.

Table of Contents

List of figures

Declaration of Authorship

I, Amol Choudhary declare that the thesis entitled "Ultrafast waveguide lasers"

and the work presented in it are my own. I confirm that:

- this work was done wholly or mainly while in candidature for a research degree at this University;
- where any part of this thesis has previously been submitted for a degree or any other qualification at this University or any other institution, this has been clearly stated;
- where I have consulted the published work of others, this is always clearly attributed;
- where I have quoted from the work of others, the source is always given. With the exception of such quotations, this thesis is entirely my own work;
- I have acknowledged all main sources of help;
- where the thesis is based on work done by myself jointly with others, I have made clear exactly what was done by others and what I have contributed myself;
- parts of this work have been published as: [please see list of publications on page xix and page xx]

Signed: ....

Date: ....

Acknowledgements

I would like to express my gratitude to my supervisor Prof. Dave Shepherd for taking me on as a PhD student on this very exciting project three years ago. He has been very supportive and patient throughout the course of my PhD. He has been instrumental in the development of my "laser-making" skills by teaching me how to put the mirrors on the waveguides (which is an art!), launching into the waveguides, telling which mirror face is coated, etc. I also appreciate his speed of proof-reading. Thank You!

I would then like to thank my co-supervisor Dr. Jacob Mackenzie for helping me with diodes, Mathcad and for introducing me to the very elegant technique of measuring propagation losses.

I would like to acknowledge Dr. Pradeesh Kannan for his tremendous help in the fabrication and polishing of waveguides, modelling of modes in ion-exchanged waveguides, measurement of refractive indices by the prism coupling technique and the occasional SEM images.

I would also like to thank other collaborators at Southampton:

> Dr. Xian Feng and Dr. Ben Mills for help with our glasses, Alberto Sposito and Prof. Rob Eason for providing Ti:sapphire films, Dr. Harold Chong for advice on the etching of RTP, Prof. James Wilkinson and Dr. Senthil Ganapathy for various useful discussion and Vincent Leonard and Prof. Dan Hewark for help with our quantum dot glass characterisation.

Most of the results obtained in this thesis would not have been possible without our external collaborators:

> Dr. Tom Brown and Prof. Wilson Sibbett at the University of St. Andrews for help with the mode-locking of waveguides. A special thanks to the awesome Dr. Alex Lagatsky! It was a pleasure mode-locking waveguides with him at St. Andrews.
>
> Jaume, Western, Carla, Dr. Rosa Sole, Dr. Joan Carvajal, Dr. Jaume Massons, Prof. Francesc Diaz and Prof. Magdalena Aguilo at URV Tarragona for providing KYW and RTP based devices.

Z.Y.Zhang, K.J.Zhou, Q.Wang and Prof R.A.Hogg at the University of Sheffield and Prof. E. Rafailov at the University of Dundee for providing the quantum dot SESAM.

I would also like to acknowledge Neil Sessions and Dave Sager for their technical advice and support in the ORC clean rooms, Simon Butler and Addie for fabricating things for me in the workshop and Nicole and Agusti at URV Tarragona and Tim at Southampton for helping me with the polishing of waveguides.

I would also acknowledge my MSc Project supervisor, Dr. Friedrich Koenig at the University of St. Andrews for teaching me the necessary lab skills and also for the motivation and useful discussions.

I would also like to thank all the wonderful people at the ORC for various stimulating discussions which has made my stay quite memorable.

I am also grateful to the EPSRC for funding my PhD.

Finally I would like to thank my family, who have supported me with everything. Mom and Dad have always encouraged me to follow what I enjoy and have constantly motivated me throughout this PhD. A big thank you to my wife, Chhavi for the support, the encouragement and everything.

List of abbreviations

Al	aluminium
Ar	argon
Cr	chromium
CW	continuous wave
DWELL	dot in well
Er	erbium
fs	femtosecond
FWHM	full width at half maximum
GDD	group delay dispersion
GTI	Gires-Tournois interferometer
GVD	group velocity dispersion
HR	high reflectivity
KYW	$KY(WO_4)_2$
LPE	liquid-phase epitaxy
mm	millimeter
mW	milli-Watt
MOPA	master oscillator power amplifier
nJ	nano-Joule
nm	nanometre
OC	output coupler
OPO	optical parametric oscillator
OSA	optical spectrum analyser
PRF	pulse repetition frequency
QD	quantum dot
RBW	resolution bandwidth
RF	radio frequency

RIE	reactive ion etching
RTP	$RbTiOPO_4$
SEM	scanning electron microscope
SESAM	semiconductor saturable absorber mirror
SHG	second harmonic generation
SPM	self-phase modulation
Ti	titanium
TIE	thermal ion-exchange
Tm	thulium
TSSG	top-seeded solution growth
VECSEL	vertical external cavity surface emitting laser
YAG	Yttrium aluminium garnet ($Y_3Al_5O_{12}$)
Yb	ytterbium

List of publications

Journal papers

1. J.Cugat, **A.Choudhary**, R.Sole, J.J.Carvajal, J.Massons, D.P.Shepherd, F.Diaz and M.Aguilo, “Ar^+ ion milling rib waveguides on nonlinear optical (Yb,Nb):RTP/RTP epitaxial layers,” Optical Materials Express, 3, 1912-1917, 2013
2. **A.Choudhary**, A.A.Lagatsky, Z.Y.Zhang, K.J.Zhou, Q.Wang, R.A.Hogg, K.Pradeesh, E.U.Rafailov, W.Sibbett, C.T.A.Brown and D.P.Shepherd, “Diode-pumped 1.5 μm waveguide laser mode-locked at 6.8 GHz by a quantum dot SESAM ”, Laser Physics Letters, 10, 105803, 2013
3. A.A.Lagatsky, **A.Choudhary**, K.Pradeesh, D.P.Shepherd, W.Sibbett and C.T.A.Brown “Fundamentally mode-locked, femtosecond waveguide oscillator with a repetition-rate of 15.2 GHz”, Optics Express, 21, 19608–19614, 2013
4. **A.Choudhary**, K. Pradeesh, J. I. Mackenzie, X. Feng and D.P. Shepherd, “Ion-exchanged Tm^{3+}:glass channel waveguide laser” , Optics Letters , 38, 1146-1148, 2013
5. **A.Choudhary**, J.Cugat, K.Pradeesh, R.Solé, F.Díaz, M.Aguiló, H.M.H.Chong and D.P.Shepherd, “Single-mode rib waveguides in (Yb,Nb):$RbTiOPO_4$ by reactive ion etching”, Journal of Physics D: Applied Physics, 46, 145108, 2013
6. K.Pradeesh, **A.Choudhary**, B.Mills, X.Feng, D.P.Shepherd, “Growth of PbSe quantum-dots within high-index lead-phosphate glass for infrared saturable absorbers”, Journal of the American Ceramic Society, 96, 197-200, 2013
7. **A.Choudhary**, A.A.Lagatsky, K.Pradeesh, W.Sibbett, C.T.A.Brown, and D.P.Shepherd, “Diode-pumped femtosecond solid-state waveguide laser with a 4.9 GHz pulse repetition-rate” Optics Letters, 37, 4416-4418, 2012

Conference proceedings

1. K. Pradeesh, **A. Choudhary**, B. Mills, V. M. Leonard, D. W. Hewak, X. Feng and D. P. Shepherd, “PbSe quantum dots grown in a high-index, low-melting-temperature glass for infrared laser applications”, Proc. SPIE 8621, Optical Components and Materials X, 862104, 2013
2. **A.Choudhary**, W.Bolaños, K.Pradeesh, J.J.Carvajal, M.Aguilo, F. Diaz and D.P.Shepherd, “Low-threshold, mirrorless emission at 981 nm in an Yb,Gd,Lu:KYW inverted rib

waveguide laser", Proc. SPIE 8599, Solid State Lasers XXII: Technology and Devices, 859903, 2013

Conference presentations

1. **A.Choudhary**, A.A.Lagatsky, Z.Y.Zhang, K.J.Zhou, Q.Wang, R.A.Hogg, K.Pradeesh, E.U.Rafailov, W.Sibbett, C.T.A.Brown and D.P.Shepherd, "Near-infrared mode-locked waveguide lasers with multi-GHz repetition-rates", Photonics West, San Francisco, USA, 8959-40, 2014 (Accepted)
2. **A.Choudhary**, A.A.Lagatsky, Z.Y.Zhang, K.J.Zhou, Q.Wang, R.A.Hogg, K.Pradeesh, E.U.Rafailov, W.Sibbett, C.T.A.Brown and D.P.Shepherd, "Diode-pumped, 6.8 GHz, solid-state waveguide laser mode-locked at 1.5 µm by a quantum dot SESAM", Advanced Solid State lasers, Paris, France, ATu1A.7, 2013
3. **A.Choudhary**, A.A.Lagatsky, K.Pradeesh, W.Sibbett, C.T.A.Brown, and D.P.Shepherd, "Towards high-power, multi-GHz waveguide lasers" Wilhelm und Else Heraeus-Seminar on "Modern Concepts of Continuous Wave and Pulsed High Power Lasers", Bad Honnef, Germany, 2013
4. **A.Choudhary**, A.A.Lagatsky, K.Pradeesh, W.Sibbett, C.T.A.Brown, and D.P.Shepherd, "Fundamentally mode-locked Yb^{3+} doped glass waveguide laser with a repetition-rate of up to 15.2 GHz", CLEO Europe, Munich, Germany, CF/IE 8.3, 2013
5. **A.Choudhary**, J.Cugat, K.Pradeesh, R.Solé, F.Díaz, M.Aguiló, H.M.H.Chong and D.P.Shepherd, "On the reactive ion etching of RbTiOPO4", CLEO Europe, Munich, Germany, CE 7.1, 2013
6. K.Pradeesh, **A.Choudhary**, J.I.Mackenzie, X.Feng and D.P.Shepherd, "An ion-exchanged Thulium-doped germanate glass channel waveguide laser operating near 1.9µm", CLEO Europe, Munich, Germany, CJ 12.2, 2013
7. **A.Choudhary**, A.A.Lagatsky, K.Pradeesh, W.Sibbett, C.T.A.Brown, and D.P.Shepherd, "Passively mode-locked diode-pumped monolithic channel waveguide laser with a repetition-rate of 4.9 GHz", EPS-QEOD Europhoton Conference, Stockholm, Sweden, POSD5, 2012 (Postdeadline)
8. **A.Choudhary**, H.M.H.Chong, K.Pradeesh, G.S.Murugan, J.S.Wilkinson, J.Cugat, M.Aguilo, F.Diaz, R.Sole and D.P.Shepherd, "Waveguide lasers in (Yb,Nb):RbTiOPO4", European Conference on Integrated Optics (ECIO), Sitges, Spain, 23, 2012

Chapter 1 Introduction

1.1 Motivation

The first ever laser consisted of a flash-lamp-pumped ruby rod and was built by T.H. Maiman in 1960 [1] and since then lasers have captured the imagination of many physicists and the general public alike. Lasers have evolved significantly and now find various applications in areas such as spectroscopy [2], interferometry [3], remote sensing [4], holography [5], material processing [6], medicine [7], in day to day devices like DVD players and laser pointers as well as in more exotic applications such as the simulation of event horizons of black holes in optical fibres [8, 9].

Lasers can operate in the continuous wave (CW) regime, where the intensity remains constant as a function of time or in the pulsed regime where periodic pulses of light are emitted with durations in the order of femtoseconds (mode-locking) to nano-seconds (Q-switching). Over the last decade, there has been a tremendous advancement in mode-locked laser systems, with pulses as short as 4 fs [10] being achieved in the near infrared (NIR) spectral regime. Such laser system are known as “ultrafast” lasers and now find applications in many areas such as telecommunications [11], measurement of the dynamics of chemical reactions [12, 13], micromachining of materials [14] and medicine [15, 16].

Ultrafast lasers can be categorised based on the pulse repetition-rates. Lasers with low repetition-rates (kHz- MHz) can have very high energies making them very attractive for applications such as particle acceleration [17], XUV generation [18] and plasma physics [18]. Repetition-rates in the order of 100 MHz with femtosecond pulse durations are typically achieved from Ti:sapphire lasers [19, 20] and various Yb-doped bulk laser systems [21-23], which are the work-horses for a large number of technological applications like optical frequency metrology [24], optical coherence tomography [15] and non-linear microscopy [25]. Extending ultrafast laser systems to even higher repetition-rates (>1 GHz) brings its own range of applications. In nonlinear microscopy [26], it was demonstrated that a balance could be reached between the high second harmonic signal and unwanted photo-damage by increasing the repetition-rate of an NIR laser. In the field of optical metrology [27] there is a need for stabilised high-repetition-rate lasers for precise measurement of optical frequencies due to the high power per longitudinal mode. Other applications include the calibration of astronomical spectrographs (astro-combs) [28], optical arbitrary waveform generation [29] and optical sampling [30].

In order to realise mode-locked high-repetition-rate sources, the cavity length has to be decreased because of the following relation:

$$f_{rep} = \frac{c}{2nl} \tag{1.1}$$

where, f_{rep} is the repetition-rate of the laser, c is the speed of light, n is the refractive index of the gain medium and l is the length of the cavity. A simplified cavity where the length of the gain medium is equal to the cavity length is shown in Figure 1-1. The train of pulses are separated in time by the inverse of the pulse repetition-rate.

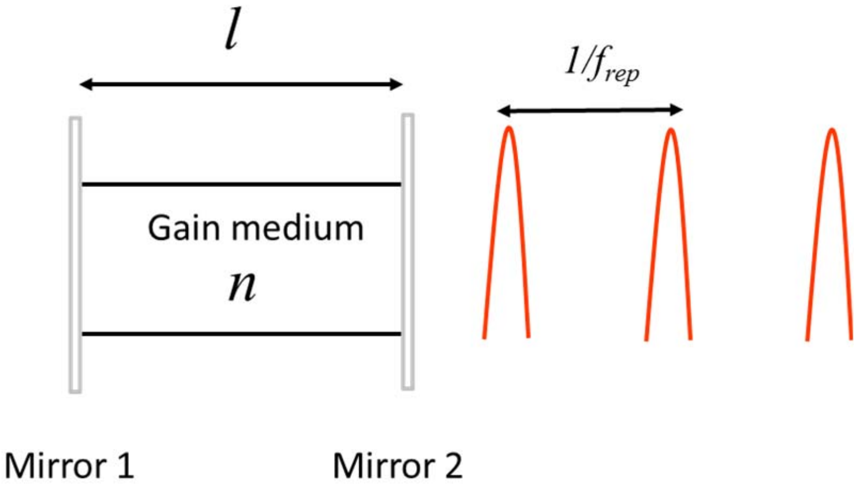

Figure 1-1. An idealised mode-locked cavity showing a train of pulses.

High-repetition-rate (> 1GHz) solid-state lasers operating near 1 μm [31-36] have been demonstrated using a micro-chip laser cavity based on Nd:YVO$_4$. Pulses of ~2 picoseconds were realised around 1064 nm using this system with a repetition-rate as high as 160 GHz [36]. Using carefully engineering micro-cavities, mode-locked operation around 1.5 μm [37-39] was obtained using Er,Yb:glass as the gain medium. A repetition-rate of up to 100 GHz was demonstrated with pulse duration in the picosecond regime. Efficient and compact ultrafast lasers operating in the GHz regime with sub-picosecond pulse duration have also been developed based on diode-pumped ytterbium

(Yb^{3+}) gain media [40-41] and solid-state-laser-pumped titanium (Ti^{3+}) doped sapphire [42, 43]. However, bulk laser approaches to high-repetition-rate sources typically require carefully engineered components (because of the short cavity lengths required) making them expensive and difficult to construct

In general, there is a need for compact ultrafast sources with multi-GHz repetition-rates which have a low-timing-jitter, can be power-scalable, are cheap and are compatible with standard micro-fabrication techniques. In the last decades, there have been various sources developed towards this goal. Vertical external cavity surface emitting semiconductor lasers (VECSELS) [44] and semiconductor lasers [45] can be mass-produced and have high repetition-rates. However, due to the fast gain dynamics during mode-locking, such sources have a high timing jitter of up to one picosecond [46]. The timing jitter can be reduced by using active elements [47] to achieve mode-locking, but such systems suffer from the drawback of having external control components thus making the system more complicated and also leads to the generation of longer pulses.

Harmonic mode-locking is a technique in which multiple pulses oscillate in the cavity synchronously, thus increasing the repetition-rate in integral multiples of the fundamental repetition-rate given by the following expression:

$$f_{rep} = N\frac{c}{2nl} \tag{1.2}$$

where, N is the number of pulses in the cavity. Harmonic mode-locking has also been used in fibre lasers [48] and VECSELS [49] to reach multi- GHz repetition-rates. Also, a repetition-rate of up to 10 GHz has been achieved from a Ti,Er:$LiNbO_3$ waveguide [50] laser using this technique. However, due to the existence of multiple pulses in the cavity, harmonic mode-locking is less stable when compared to fundamental mode-locking.

Diode-pumped waveguide lasers either in a cylindrical geometry (fibres) or in a rectangular geometry (planar/ channel waveguides) with low propagation losses benefit from compactness, low laser threshold powers and high slope efficiencies. When integrated with saturable absorber elements they can have a low mode-locking threshold due to the strong saturation of the gain medium and the saturable absorber due to small mode sizes. Short pieces of Erbium-(Er^{3+}) doped fibres have been used to realise sources with repetition-rates greater than 1 GHz [51-53] but are usually limited in power to about

1 mW. Recently, a sub-centimetre Ytterbium (Yb^{3+})-doped fibre was used to generate 3 GHz pulses with up to 27 mW of average power [54].

In a rectangular geometry, mode-locked waveguide laser sources can be fundamentally mode-locked to develop power-scalable sources at different wavelengths which can be mass-producible, compatible with micro-photonic fabrication techniques, are compact and cheap. A motivation for multi-GHz waveguide lasers could be for optical sampling [30] which at the moment requires two high-repetition-rate mode-locked Ti:sapphire laser sources with slightly different repetition-rates. Many mode-locked lasers can be realised on a single waveguide chip, thus making the setup much more compact and cheap. Another advantage is that by using standard clean-room fabrication techniques, dispersion compensating elements, Bragg-mirror structures and possibly saturable absorbers could be integrated on a single chip. To this end, the first integrated sub-picosecond waveguide laser with a repetition-rate of 400 MHz and wavelength around 1.5 μm was realised by Byun et al. using an Erbium-doped alumina-silicate glass [55]. A p-doped silicate glass was integrated on the chip and was used for dispersion compensation and a saturable Bragg reflector was end-butted on the waveguide to facilitate self-starting mode-locking. Pulses as short as 440 fs at a wavelength of ~1560 nm were achieved; however the output power was limited to only ~1.2 mW. Waveguides have been used as a gain medium in various ultrafast cavities with the saturable absorber in an external cavity configuration, thus resulting in repetition-rates below 1 GHz [56-60]. Recently, picosecond pulses at a repetition rate of 1.5 GHz [61] have been generated from a Q-switched mode-locked laser using femtosecond written waveguides and graphene saturable absorber elements.

The realisation of ultrafast waveguide lasers with repetition-rates in excess of 1 GHz with a footprint of ~1 cm^2 serves as a motivation for this project. Such sources with integrated saturable absorber elements could pave the path to have on-chip mode-locked sources. Such sources can have tremendous potential for the realisation of a compact and robust frequency comb for applications in optical frequency metrology, astronomical spectroscopy and many others.

The goal of the research described in this thesis was the realisation of novel sub-picosecond, multi-GHz waveguide lasers operating around 1 μm, 1.5 μm and 2 μm with power in excess of 10 mW. To achieve this, various gain media like Yb^{3+}-doped IOG-glasses, Yb^{3+}-doped $RbTiOPO_4$, Yb^{3+}-doped $KY(WO_4)_2$, Er^{3+},Yb^{3+}-doped IOG glasses and Thulium (Tm^{3+})-doped germanate glasses were studied during the course of this project to evaluate their potential for mode-locking applications in a waveguide geometry. The key achievements of this research project and the outline of this thesis are described in the following sections.

1.2 Key Achievements

Some of the highlights of the work described in this thesis are:

1. Promising results were achieved using ion-exchanged Yb^{3+}-doped IOG-1 glasses with the realisation of the first femtosecond oscillator based on an Yb^{3+}-doped glass waveguide laser with a repetition-rate of 4.9 GHz. Pulses as short as 740 fs and output power as high as 80 mW was achieved.
2. The highest reported repetition-rate of 15.2 GHz from a waveguide-based femtosecond oscillator using Yb^{3+}-doped IOG-1 glasses.
3. The first waveguide laser mode-locked using a quantum dot SESAM. This was achieved with an ion-exchanged Er,Yb-doped IOG-1 glass waveguide laser. Pico-second operation with a maximum power of 30 mW was demonstrated. A repetition-rate of 6.8 GHz was achieved, which is the highest repetition-rate reported from a fundamentally mode-locked waveguide laser operating near 1.5 µm.
4. The first ion-exchanged Tm^{3+}-doped glass waveguide laser operating near 1.9 µm was demonstrated. This can open up the field for the development of mode-locked sources with multi-GHz repetition-rates near the 2 µm spectral regime. Such sources can be used as pumps for mid-IR frequency comb generation.
5. Mirrorless emission from an inverted Yb^{3+}-doped KYW laser at 981 nm was observed. Emission was also observed at 999.8 nm. KYW has a broad emission near 999.8 nm and near 1030 nm. Traditionally, lasing has been observed near 1030 nm from this laser crystal. However, if the entire emission spectrum from 981 nm to 1030 nm is exploited for mode-locking, sub-50 fs pulses can be potentially achieved.
6. Demonstration of the first channel waveguide in Yb,Nb:$RbTiOPO_4$ waveguide fabricated by reactive ion etching (RIE). RIE was optimised for $RbTiOPO_4$ to produce low-loss waveguides. $RbTiOPO_4$ is a non-linear crystal with a broad emission bandwidth and RIE can be used for fabrication of waveguide-based non-linear devices and mode-locked sources.

7. Demonstration of the first ion-beam milled Yb,Nb: $RbTiOPO_4$ waveguide.

1.3 Thesis synopsis

After this brief introduction and the key achievements of this project, the rest of the thesis has been presented as follows:

Chapter 2 discusses the technological background relevant for this thesis. This includes:

1. All the theoretical concepts relevant to this research: waveguide theory, laser theory, ion-exchange theory and mode-locking theory.
2. A literature survey of the gain media explored in this research.

Chapter 3 discusses all the experimental techniques employed in this project:

1. The fabrication of planar and channel waveguides.
2. The basic experimental setups for CW lasing and mode-locking experiments.
3. 3 methods of estimating the propagation loss in waveguides.

Chapter 4 describes experiments carried out with Yb^{3+}-doped waveguides:

1. CW and mode-locking results obtained with Yb:IOG-1 glass.
2. CW and waveguiding experiments withYb^{3+}-doped $KY(WO_4)_2$ and RTP.

Chapter 5 contains experimental details about mode-locking experiments carried out with ion-exchanged Er^{3+},Yb^{3+}-doped IOG glass waveguides.

Chapter 6 presents the fabrication details and CW experiments carried out with ion-exchanged Tm^{3+}:germanate glass waveguides.

In chapter 7, the conclusions and the future work have been presented.

1.4 References

1. Maiman, T.H., *Stimulated Optical Radiation in Ruby.* Nature, 1960. **187** (4736): p. 493-494.
2. Demtröder, W., *Laser Spectroscopy*. 2003, Berlin: Springer-Verlag.
3. Peterson, D.G. and A. Yariv, *Interferometry and laser control with solid Fabry-Perot etalons.* Applied optics, 1966. **5** (6): p. 985-991.
4. Measures, R.M., *Laser remote sensing: fundamentals and applications* 1984: Wiley.
5. Hariharan, P., *Basics of Holography* 2002: Cambridge University Press.
6. Steen, W.M., *Laser Material Processing* 2003: Springer London, Limited.
7. Duarte, F., *Tunable Laser Applications,* 2010: Taylor & Francis.
8. Choudhary, A. and König, F., *Efficient frequency shifting of dispersive waves at solitons.* Opt. Express, 2012. **20** (5): p. 5538-5546.
9. Philbin, T.G., Kuklewicz, C., Robertson, S., Hill, S., König, F. and Leonhardt, U., *Fiber-Optical Analog of the Event Horizon.* Science, 2008. **319** (5868): p. 1367-1370.
10. Schenkel, B., Biegert, J., Keller, U., Vozzi, C., Nisoli, M., Sansone, G., Stagira, S., De Silvestri, S. and Svelto, O., *Generation of 3.8-fs pulses from adaptive compression of a cascaded hollow fiber supercontinuum.* Opt. Lett., 2003. **28** (20): p. 1987-1989.
11. Mollenauer, L. F., Mamyshev, P. V., Gripp, J., Neubelt, M. J., Mamysheva, N., Gruner-Nielsen, L. and Veng, T., *Demonstration of massive wavelength-division multiplexing over transoceanic distances by use of dispersion-managed solitons.* Optics Letters, 2000. **25** (10): p. 704-706.
12. Zewail, A.H., *Femtochemistry: Recent Progress in Studies of Dynamics and Control of Reactions and Their Transition States.* The Journal of Physical Chemistry, 1996. **100** (31): p. 12701-12724.
13. Zewail, A.H., *Femtochemistry: Atomic-Scale Dynamics of the Chemical Bond.* The Journal of Physical Chemistry A, 2000. **104** (24): p. 5660-5694.
14. Liu, X., Du, D. and Mourou, G., *Laser ablation and micromachining with ultrashort laser pulses.* Quantum Electronics, IEEE Journal of, 1997. **33** (10): p. 1706-1716.
15. Huang, D., Swanson, E. A., Lin, C. P., Schuman, J. S., Stinson, W. G., Chang, W., Hee, M. R., Flotte, T., Gregory, K., Puliafito, C. A. and Fujimoto, J. G., *Optical coherence tomography.* Science, 1991. **254** (5035): p. 1178-1181.
16. Loesel, F. H., Fischer, J. P., Götz, M. H., Horvath, C., Juhasz, T., Noack, F., Suhm, N. and Bille, J. F., *Non-thermal ablation of neural tissue with femtosecond laser pulses.* Applied Physics B, 1998. **66** (1): p. 121-128.
17. Mourou, G., Brocklesby, W.S., Tajima, T. and Limpert, J., *The future is fibre accelerators.* Nat Photon, 2013. **7** (5): p. 258-261.
18. http://www.eli-beams.eu/science/lasers/.
19. Spence, D.E., Kean, P.N. , and Sibbett, W., *60-fsec pulse generation from a self-mode-locked Ti:sapphire laser.* Opt. Lett., 1991. **16** (1): p. 42-44.
20. Ell, R., Morgner, U., Kartner, F. X., Fujimoto, J. G., Ippen, E. P., Scheuer, V., Angelow, G., Tschudi, T., Lederer, M. J., Boiko, A. and Luther-Davies, B., *Generation of 5-fs pulses and octave-spanning spectra directly from a Ti:sapphire laser.* Opt. Lett., 2001. **26** (6): p. 373-375.
21. Carvajal, J. J., Ciatto, G., Mateos, X., Schmidt, A., Griebner, U., Petrov, V., Boulon, G., Brenier, A., Peña, A., Pujol, M. C., Aguiló, M. and Díaz, F., *Broad emission band of* Yb^{3+}

in the nonlinear Nb:RbTiOPO$_4$ crystal: origin and applications. Opt. Express, 2010. **18** (7): p. 7228-7242.

22. Liu, H., Nees, J. and Mourou, G., *Diode-pumped Kerr-lens mode-locked Yb:KY(WO$_4$)$_2$ laser.* Opt. Lett., 2001. **26** (21): p. 1723-1725.
23. Hönninger, C., Morier-Genoud, F., Moser, M., Keller, U., Brovelli, L. R. and Harder, C., *Efficient and tunable diode-pumped femtosecond Yb:glass lasers.* Opt. Lett., 1998. **23** (2): p. 126-128.
24. Udem, T., Holzwarth R., and Hansch T. W, *Optical frequency metrology.* Nature, 2002. **416**: p. 233-237.
25. Mertz, J., *Nonlinear microscopy: new techniques and applications.* Current Opinion in Neurobiology, 2004. **14** (5): p. 610-616.
26. Chu, S.-W., Liu, T.-M., Sun, C.-K., Lin, C.-Y. and Tsai, H.-J., *Real-time second-harmonic-generation microscopy based on a 2-GHz repetition rate Ti:sapphire laser.* Opt. Express, 2003. **11** (8): p. 933-938.
27. Bartels, A., Gebs, R., Kirchner, M. S. and Diddams, S. A., *Spectrally resolved optical frequency comb from a self-referenced 5 GHz femtosecond laser.* Opt. Lett., 2007. **32** (17): p. 2553-2555.
28. Chih-Hao, Li, Benedick, A. J., Fendel, P., Glenday, A. G., Kartner, F. X., Phillips, D. F., Sasselov, D., Szentgyorgyi, A. and Walsworth, R. L., *A laser frequency comb that enables radial velocity measurements with a precision of 1 cm s^{-1}.* Nature, 2008. **452** (7187): p. 610-612612.
29. Jones, D. J., Diddams, S. A., Ranka, J. K., Stentz, A., Windeler, R. S., Hall, J. L. and Cundiff, S. T., *Carrier-envelope phase control of femtosecond mode-locked lasers and direct optical frequency synthesis.* Science, 2000. **288** (5466): p. 635-639.
30. Bartels, A., Cerna, R., Kistner, C., Thoma, A., Hudert, F., Janke, C. and Dekorsy, T., *Ultrafast time-domain spectroscopy based on high-speed asynchronous optical sampling.* Review of Scientific Instruments, 2007. **78** (3): p. 035107.
31. Krainer, L., Paschotta, R., der Au, J. A., Honninger, C., Keller, U., Moser, M., Kopf, D. and Weingarten, K. J., *Passively mode-locked Nd:YVO$_4$ laser with up to 13 GHz repetition rate.* Applied Physics B-Lasers and Optics, 1999. **69** (3): p. 245-247.
32. Krainer, L., Paschotta, R., Spuhler, G., Moser, M. and Keller, U., *29 GHz modelocked miniature Nd:YVO$_4$ laser.* Electronics Letters, 1999. **35** (14): p. 1160-1161.
33. Lecomte, S., Kalisch, M., Krainer, L., Spuhler, G. J., Paschotta, R., Golling, M., Ebling, D., Ohgoh, T., Hayakawa, T., Pawlik, S., Schmidt, B. and Keller, U., *Diode-pumped passively mode-locked Nd:YVO$_4$ lasers with 40-GHz repetition rate.* IEEE Journal of Quantum Electronics, 2005. **41** (1): p. 45-52.
34. Krainer, L., Paschotta, R., Moser, M. and Keller, U., *Passively mode-locked picosecond lasers with up to 59 GHz repetition rate.* Applied Physics Letters, 2000. **77** (14): p. 2104-2105.
35. Krainer, L., Paschotta, R., Moser, M. and Keller, U., *77 GHz soliton modelocked Nd:YVO$_4$ laser.* Electronics Letters, 2000. **36** (22): p. 1846-1848.
36. Krainer, L., Paschotta, R., Lecomte, S., Moser, M., Weingarten, K. J. and Keller, U., *Compact Nd:YVO$_4$ lasers with pulse repetition rates up to 160 GHz.* Quantum Electronics, IEEE Journal of, 2002. **38** (10): p. 1331-1338.
37. Zeller, S. C., Krainer, L., Spuhler, G. J., Paschotta, R., Golling, M., Ebling, D., Weingarten, K. J. and Keller, U., *Passively modelocked 50 GHz Er:Yb:glass laser.* Electronics Letters, 2004. **40** (14): p. 875-877.

38. Zeller, S. C., Sudmeyer, T., Weingarten, K. J. and Keller, U., *Passively modelocked 77 GHz Er:Yb:glass laser.* Electronics Letters, 2007. **43** (1): p. 32-33.

39. Oehler, A. E., Südmeyer, T., Weingarten, K. J., and Keller, U., *100 GHz passively mode-locked Er:Yb:glass laser at 1.5 μm with 1.6-ps pulses.* Opt. Express, 2008. **16** (26): p. 21930-21935.

40. Pekarek, S., Klenner, A., Südmeyer, T., Fiebig, C., Paschke, K., Erbert, G. and Keller, U., *Femtosecond diode-pumped solid-state laser with a repetition rate of 4.8 GHz.* Opt. Express, 2012. **20** (4): p. 4248-4253.

41. Endo, M., Ozawa, A. and Kobayashi, Y., *Kerr-lens mode-locked Yb:KYW laser at 4.6-GHz repetition rate.* Opt. Express, 2012. **20** (11): p. 12191-12197.

42. Nogueira, G. T., Xu, B., Coello, Y., Dantus, M. and Cruz, F. C., *Broadband 2.12 GHz Ti:sapphire laser compressed to 5.9 femtoseconds using MIIPS.* Opt. Express, 2008. **16** (14): p. 10033-10038.

43. Bartels, A., Heinecke D., and Diddams S.A., *Passively mode-locked 10 GHz femtosecond Ti:sapphire laser.* Opt. Lett., 2008. **33** (16): p. 1905-1907.

44. Wilcox, K. G., Quarterman, A. H., Beere, H., Ritchie, D. A. and Tropper, A. C., *High Peak Power Femtosecond Pulse Passively Mode-Locked Vertical-External-Cavity Surface-Emitting Laser.* IEEE Photonics Technology Letters, 2010. **22** (14): p. 1021-1023.

45. Brown, C. T. A., Cataluna, M. A., Lagatsky, A. A., Rafailov, E. U., Agate, M. B., Leburn, C. G. and Sibbett, W., *Compact laser-diode-based femtosecond sources.* New Journal of Physics, 2004. **6** (1)**:** p. 175.

46. Tourrenc, J. P., Akrout, A., Merghem, K., Martinez, A., Lelarge, F., Shen, A., Duan, G. H. and Ramdanc, A., *Experimental investigation of the timing jitter in self-pulsating quantum-dash lasers operating at 1.55 μm.* Optics Express, 2008. **16** (22): p. 17706-17713.

47. Gee, S., Ozharar, S., Quinlan, F., Plant, J. J., Juodawlkis, P. W. and Delfyett, P. J., *Self-stabilization of an actively mode-locked semiconductor-based fiber-ring laser for ultralow jitter.* IEEE Photonics Technology Letters, 2007. **19** (7): p. 498-500.

48. Grudinin, A.B. and Gray, S., *Passive harmonic mode locking in soliton fiber lasers.* Journal of the Optical Society of America B-Optical Physics, 1997. **14** (1): p. 144-154.

49. Quarterman, A. H., Perevedentsev, A., Wilcox, K. G., Apostolopoulos, V., Beere, H. E., Farrer, I., Ritchie, D. A. and Tropper, A. C., *Passively harmonically mode-locked vertical-external-cavity surface-emitting laser emitting 1.1 ps pulses at 147 GHz repetition rate.* Applied Physics Letters, 2010. **97** (25): p. 251101.

50. Wessel, R., Ricken, R., Rochhausen, K., Suche, H. and Sohler, W., *Supermode stabilized coupled-cavity 5- and 10-GHz mode-locked Ti:Er:LiNbO$_3$ waveguide lasers.* Quantum Electronics, IEEE Journal of, 2000. **36** (3): p. 394-399.

51. Byun, H., Sander, M. Y., Motamedi, A., Shen, H. F., Petrich, G. S., Kolodziejski, L. A., Ippen, E. P. and Kartner, F. X., *Compact, stable 1 GHz femtosecond Er-doped fiber lasers.* Applied optics, 2010. **49** (29): p. 5577-5582.

52. Yamashita, S., Inoue, Y., Hsu, K., Kotake, T., Yaguchi, H., Tanaka, D., Jablonski, M. and Set, S. Y., *5-GHz pulsed fiber Fabry-Perot laser mode-locked using carbon nanotubes.* IEEE Photonics Technology Letters, 2005. **17** (4): p. 750-752.

53. Martinez, A. and Yamashita, S., *Multi-gigahertz repetition rate passively modelocked fiber lasers using carbon nanotubes.* Optics Express, 2011. **19** (7): p. 6155-6163.

54. Chen, H. W., Chang, G. Q., Xu, S. H., Yang, Z. M. and Kartner, F. X., *3 GHz, fundamentally mode-locked, femtosecond Yb-fiber laser.* Optics Letters, 2012. **37** (17): p. 3522-3524.

55. Byun, H., Hanjani, A., Frolov, S., Ippen, E. P., Pudo, D., Shmulovich, J. and Kartner, F. X., *Integrated Low-Jitter 400-MHz Femtosecond Waveguide Laser.* Photonics Technology Letters, IEEE, 2009. **21** (12): p. 763-765.
56. Valle, G.D, Osellame, R., Galzerano, G., Chiodo, N., Cerullo, G., Laporta, P., Svelto, O., Morgner, U., Rozhin, A. G., Scardaci, V. and Ferrari, A. C., *Passive mode locking by carbon nanotubes in a femtosecond laser written waveguide laser.* Applied Physics Letters, 2006. **89** (23): p. 231115.
57. Beecher, S. J., Thomson, R. R., Psaila, N. D., Sun, Z., Hasan, T., Rozhin. A. G., Ferrari, A. C. and Kar, A. K., *320 fs pulse generation from an ultrafast laser inscribed waveguide laser mode-locked by a nanotube saturable absorber.* Applied Physics Letters, 2010. **97** (11): p. 111114.
58. Schlager, J. B., Callicoatt, B. E., Silverman, K. L., Mirin, R. P., Sanford, N. A. and Veasey, D. L., *Mode-locked erbium/ytterbium co-doped waveguide laser*. in *Lasers and Electro-Optics, 2001. CLEO '01.*
59. Schlager, J. B., Callicoatt, B. E., Mirin, R. P. and Sanford, N. A., *Passively mode-locked waveguide laser with low residual jitter.* IEEE Photonics Technology Letters, 2002. **14** (9): p. 1351-1353.
60. Schlager, J. B., Callicoatt, B. E., Mirin, R. P., Sanford, N. A., Jones, D. J. and Ye, J., *Passively mode-locked glass waveguide laser with 14-fs timing jitter.* Opt. Lett., 2003. **28** (23): p. 2411-2413.
61. Mary, R., Brown, G., Beecher, S. J., Torrisi, F., Milana, S., Popa, D., Hasan, T., Sun, Z., Lidorikis, E., Ohara, S., Ferrari, A. C. and Kar, A.K., *1.5 GHz picosecond pulse generation from a monolithic waveguide laser with a graphene-film saturable output coupler.* Opt. Express, 2013. **21** (7): p. 7943-7950.

Chapter 2 Technological background

After the motivation for the project presented in the first chapter, this chapter discusses various theoretical concepts relevant to the project. Section 2.1 briefly discusses the basic theory of waveguide propagation modes. Since all the mode-locking results were achieved with ion-exchanged waveguides, ion-exchange theory is presented in more detail in section 2.2, and section 2.3 presents the basic quasi-3-level laser theory relevant to the laser systems utilised in this work. Mode-locking theory and mode-locking schemes are then discussed in section 2.4. The advantages of using waveguides for mode-locking are given in section 2.5 and finally, all the gain media discussed in the following chapters are described in section 2.6.

2.1 Waveguide geometry

The ultrafast high-repetition-rate lasers discussed within this project were based on a planar channel waveguide geometry. In this section, a brief overview of the waveguide theory is presented.

2.1.1 Waveguide theory

An optical waveguide is a device that guides electromagnetic waves for certain wavelengths without divergence in the guided direction [1]. It is possible to have waveguides in a rectangular geometry or cylindrical geometry, optical fibres being an example of the latter.

The propagation modes in the waveguide can be calculated from the wave equation [2]:

$$\nabla^2\bar{E} + \omega^2\mu\varepsilon\bar{E} = 0 \tag{2.1}$$

where, ∇ is the spatial vector operator, ω is the angular frequency, μ is the permeability of the medium, ε is the permittivity of the medium and $\bar{E}$ is a complex phasor describing the spatial variation of the electric field ($\tilde{E}$) with displacement vector $\tilde{r}$ and time t :

$$\tilde{E}(\tilde{r},t) = \bar{E}(\tilde{r})e^{i\omega t} \tag{2.2}$$

The refractive index is related to the permittivity via the expression, $n = \sqrt{\varepsilon/\varepsilon_0}$, where ε_0 is the permittivity of free-space. Consider a simple planar structure shown in Figure 2-1 with a substrate of refractive index n_3 (μ_3,ε_3), a superstrate/cladding layer with index n_1 (μ_1,ε_1) and the guiding layer/core with refractive index n_2 (μ_2,ε_2). A pre-requisite for light to be guided by total internal reflection in layer 2 (with thickness d) at a wavelength λ is that n_2>n_1 and n_2>n_3.

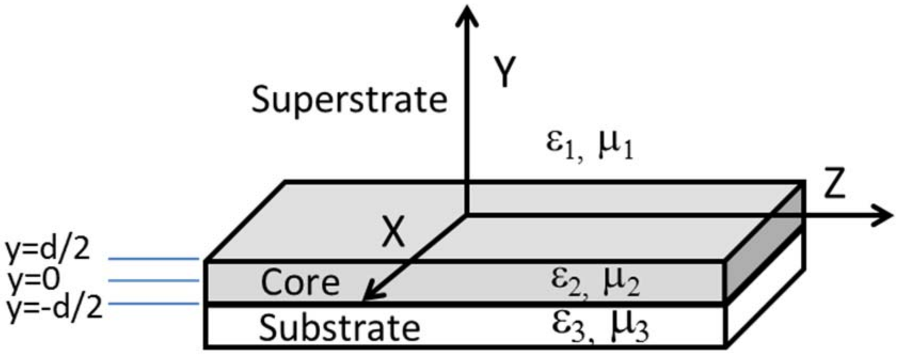

Figure 2-1. A 1-dimensional planar waveguide structure.

The wave propagates along the z-direction and is confined in the y-direction. There are two allowed polarisation states within the waveguide:

1. The transverse electric (TE) mode, where the electric field is polarised along the x-direction (E_y=0, E_z=0 and $H_z\neq 0$)
2. The transverse magnetic (TM) mode, where the magnetic field is polarised along the x-direction (H_y=0, H_z=0 and $E_z\neq 0$)

An important quantity in waveguide optics is the numerical aperture (NA) which describes the maximum angle (θ) at which a launched ray of light will be guided in the waveguide and is given by the following expression:

$$NA = sin\theta = \sqrt{n_2^2 - n_3^2} \tag{2.3}$$

2.1.1.1 TE mode

The field is assumed to have an exponential decay in the substrate and in the cladding and the total internal reflection leads to a standing wave in the core. The field has a common wavevector in the z-direction (k_z) and hence can be expressed as:

$$\tilde{E}(\tilde{r},t) = \bar{E}(\tilde{r})e^{i\omega t}e^{-ik_z z} \tag{2.4}$$

$\tilde{E}(\tilde{r})$ can be written as $E_x(y,z)$ since a planar waveguide is being solved, with no variation in the x direction and the electric field components E$_y$ and E$_z$ are both zero because of the TE condition. Solving the wave equation and using the continuity of the electric and magnetic fields at the interfaces, $E_x(y,z)$ is calculated to be [2]:

$$E_x(y,z) = \begin{array}{l} A_2 \cos\left(\frac{k_y d}{2} + \Psi\right) e^{-\alpha_1\left(y-\frac{d}{2}\right)} e^{-ik_z z},\ y > d/2 \\ A_2 \cos\left(k_y y + \Psi\right) e^{-ik_z z},\ d/2 \geq y \geq -d/2 \\ A_2 \cos\left(\frac{k_y d}{2} - \Psi\right) e^{\alpha_3\left(y+\frac{d}{2}\right)} e^{-ik_z z},\ y < -d/2 \end{array} \tag{2.5}$$

Where, A_2 is the amplitude coefficient, α_1 and α_3 are the decay coefficients in the cladding and in the substrate, k_y is the wave-vector along the y-direction in the core and Ψ is the offset of the field amplitude with respect to the centre of the waveguide, and k_z is the wave-vector of the mode with an effective refractive index (n_{eff}) in the z-direction. Mathematically these quantities are equal to:

$$k_z = \frac{2\pi}{\lambda} n_{eff} \tag{2.6}$$

$$\alpha_1 = \sqrt{k_z^2 - \omega^2 \mu_1 \varepsilon_1} \tag{2.7}$$

$$\alpha_3 = \sqrt{k_z^2 - \omega^2 \mu_3 \varepsilon_3} \tag{2.8}$$

$$k_y = \sqrt{\omega^2 \mu_2 \varepsilon_2 - k_z^2} \tag{2.9}$$

The continuity of E_x and H$_z$ at y= d/2 also gives the following expression:

$$tan\left(\frac{k_y d}{2} + \Psi\right) = \frac{\alpha_1}{k_y} \tag{2.10}$$

Similarly, the continuity of E_x and H$_z$ at y= -d/2 gives:

$$tan\left(\frac{k_y d}{2} - \Psi\right) = \frac{\alpha_3}{k_y} \tag{2.11}$$

From trigonometry it is known that:

$$\tan(A) = \tan(A \pm p\pi) \tag{2.12}$$

Eliminating Ψ using (2.10), (2.11) and (2.12), the following guidance condition is reached:

$$2k_y d - \varphi_1^{TE} - \varphi_3^{TE} = 2p\pi \tag{2.13}$$

Where, p is the mode number and φ_1^{TE} and φ_3^{TE} are giving by the following expressions:

$$\varphi_1^{TE} = 2tan^{-1}\left(\frac{\alpha_1}{k_y}\right) \tag{2.14}$$

$$\varphi_3^{TE} = 2tan^{-1}\left(\frac{\alpha_3}{k_y}\right) \tag{2.15}$$

The first term in expression (2.13) is the phase change due to propagation through one round-trip in the waveguide core and the second and third term are the phase changes due to reflection at the core-cladding interface and the core-substrate interface respectively. This implies that the total phase change of the guided mode over one-round trip should be an integral multiple of 2π. Equation (2.13) can also be written in terms of normalised parameters as:

$$V(1-b)^{1/2} = p\pi + tan^{-1}\left(\frac{b}{1-b}\right)^{1/2} + tan^{-1}\left(\frac{b+a}{1-b}\right)^{1/2} \tag{2.16}$$

Where V is the normalised frequency given by:

$$V = \frac{2\pi}{\lambda} d(n_2^2 - n_3^2)^{1/2} \tag{2.17}$$

b is the normalized guide index given by:

$$b = \frac{\left(n_{eff}^2 - n_3^2\right)}{\left(n_2^2 - n_3^2\right)} \tag{2.18}$$

and a is the asymmetry parameter given by:

$$a^{TE} = \frac{\left(n_3^2 - n_1^2\right)}{\left(n_2^2 - n_3^2\right)} \tag{2.19}$$

From these equations it is possible to calculate the normalised frequency and asymmetry parameter for a given planar waveguide structure and propagation wavelength, and then calculate the normalised guide index that satisfies eqn. (2.16) for a given propagating mode p. This allows the effective index to be found and hence all the spatial properties of that mode.

Light can also be confined in both the dimensions, to give a 2-dimensional waveguide. A geometry widely used in this thesis is the etched rib waveguide as shown in Figure 2-2.

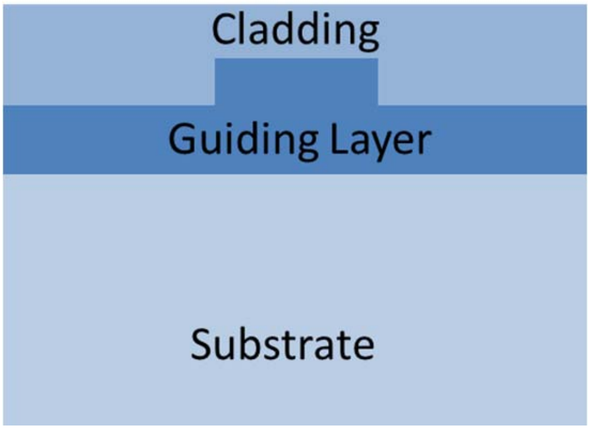

Figure 2-2. Rib waveguide geometry.

The effective-index method [2] can be used to calculate the propagating modes of such 2-dimensional waveguides. This method is summarised in Figure 2-3 for the rib waveguide shown in Figure 2-2.

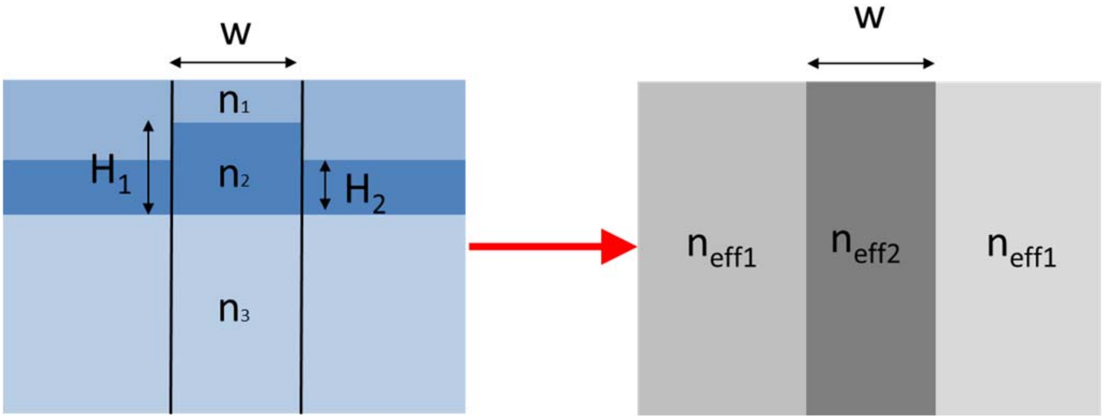

Figure 2-3. The effective-index method.

The waveguide is cut into 3 slices, corresponding to 3 different planar waveguides, and the effective index n_{eff} of a given mode is calculated in each region, using the method described above. Next, the 2-d waveguide is replaced by a simple symmetric planar waveguide structure with a guiding layer of height W and a refractive index n_{eff2} and a substrate and a cladding layer, both with a refractive indices n_{eff1}. Repeating the 1-d waveguide analysis in this transformed waveguide, the effective index for the particular propagation mode of the waveguide can be calculated. Once the effective index of the propagating mode has been found, the spatial properties of the mode can be calculated in both dimensions.

The effective index method was used as a simple starting point for the waveguide designs in the thesis. However, in practice, commercial waveguide numerical modelling packages were used to calculate the spatial properties of the modes presented in the thesis as the real waveguide geometries fabricated by etching a planar film are often more complex (e.g. etched side walls are normally sloped).

Another widely used technique for directly fabricating waveguides is ultrafast laser inscription (ULI) [3]. In this technique an ultrafast pulse is tightly focussed into a dielectric material which modifies the sample. Tracks can be inscribed which cause stress induced change in the refractive index which promotes waveguiding. Using this technique, waveguide lasers have been demonstrated with propagation losses of typically >1 dB/cm [4, 5].

2.2 Ion-exchange

Thermal ion-exchange was also extensively used in this project for realising waveguide lasers and is discussed in this sub-section.

2.2.1 Introduction

Ion-exchange is an elegant technique for fabricating low-loss waveguides in glasses. It involves the exchange of ions within the glass (glass ions) with different ions in the diffusant source (diffusant ions). When heat is used as a diffusing mechanism, it is known as thermal ion exchange (TIE), and when an electric field is used along with heat it is referred to as field-assisted ion-exchange. The first planar waveguide fabricated using field-assisted ion-exchange was demonstrated in 1972 [6] and thermal ion-exchange was demonstrated in 1973 [7].

The glass sample to be ion-exchanged is placed in a crucible, containing a molten mixture, rich in the diffusant ions and heated in a temperature controlled furnace. Due to the concentration-gradient formed between the diffusant-ion-deficient glass and the diffusant-ion-rich melt, there is a flow of the diffusant ions from the melt to the glass. Similarly, the glass-ions diffuse from the glass to the melt.

TIE is usually carried out at a temperature lower than the glass transition temperature (T_g) and therefore nitrate salts, which have low melting points, are preferred as the diffusant source. The glasses used in this project were rich in sodium (Na^+) ions, and the Na^+ ions within the glass were exchanged with other alkali metal ions: silver (Ag^+) and potassium (K^+). Ag^+ ions allow a high-index-contrast but can also lead to high losses; K^+ ions cause a lower index contrast but generally lead to lower propagation losses. Using a combination of Na^+-K^+ ion exchange and Na^+-Ag^+ ion-exchange, propagation losses of <0.3 dB/cm and an index contrast of up to 0.05 were achieved as discussed in the later chapters.

2.2.2 Theory

The diffusion model for the ion-exchange process is described in this section. The concentration of the diffusant ions is directly proportional to the refractive index [8], hence the concentration as a function of the depth has been derived.

Figure 2-4 shows the schematic of the ion-exchanged waveguide in a glass along with the coordinate system used for the derivation of the diffusion equation [9]:

$$\frac{\partial c}{\partial t} + \frac{1}{1-(1-M)c} \mu_A \widetilde{E} \cdot \nabla c = \frac{D_A}{1-(1-M)c} \nabla^2 c \qquad (2.20)$$

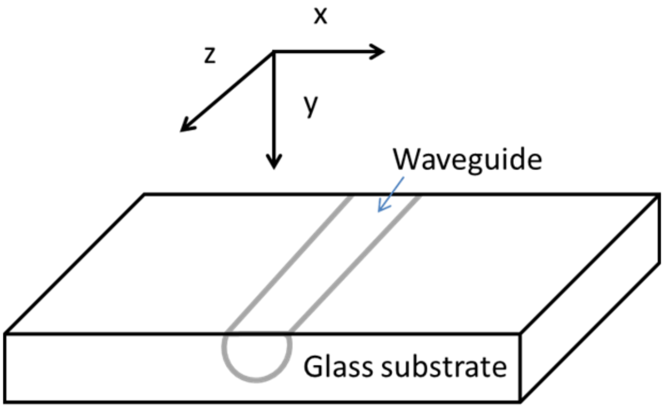

Figure 2-4. Diagram showing the coordinate system for the ion-exchanged waveguides.

Where, $c = c(x, y, z, t) = c_A/c_B^0$ is the normalized diffusant ion concentration, c_A is the concentration of the diffusant ions and c_B^0 is the concentration of the glass ions prior to ion-exchange. M is the ratio of the mobilities of the diffusant and glass ions, μ_A is the mobility of the diffusant ions, $\widetilde{E}$ is the electric field and D_A is the diffusion coefficient of the diffusant ions.

Assuming that diffusion only occurs in one dimension and that the mobilities of the diffusant and glass ions are similar (M≈1), (2.20) reduces to:

$$\frac{\partial c}{\partial t} + \mu_A \widetilde{E}\, \frac{\partial c}{\partial y} = D_A \frac{\partial^2 c}{\partial^2 y} \tag{2.21}$$

The boundary conditions are shown below, where c_s is the concentration of the diffusant ions on the surface of the glass:

$$\begin{gathered} c(y,0) = 0 \\ c(0,t) = c_s \\ c(\infty,t) = 0 \end{gathered} \tag{2.22}$$

The solution for (2.21) is given by [10]:

$$\frac{c}{c_s} = \frac{1}{2}\left[erfc\left(\frac{y-\mu_A E t}{2\sqrt{D_A t}}\right) + \exp\left(\frac{\mu_A E y}{D_A}\right) \cdot erfc\left(\frac{y+\mu_A E t}{2\sqrt{D_A t}}\right)\right] \tag{2.23}$$

and simplifies to the following expression in the absence of an electric field:

$$\frac{c}{c_s} = erfc\left(\frac{y}{W_0}\right) \tag{2.24}$$

where, $erfc$ is the complementary error function and $W_0 = \sqrt{2D_A t}$ is the value at which the argument of the erfc function equals 1, i.e the $erfc(1)$ depth. Since the refractive index is proportional to the concentration of the diffusant ions, the refractive index is given by the following expression with n_s being the refractive index of the substrate and Δn being the maximum change in the refractive index:

$$n(x,y) = n_s + \Delta n \cdot erfc\left(\frac{y}{W_0}\right) \tag{2.25}$$

For a 2-dimensional diffusion profile, the index profile has experimentally been found to be [11]:

$$n(x,y) = n_s + \Delta n \cdot exp\left(\frac{-x^2}{d_x^2}\right) \cdot erfc\left(\frac{y}{d_y}\right) \tag{2.26}$$

where d_x is the 1/e half width and d_y is the $erfc(1)$ depth of the waveguide.

2.2.3 Ion-exchanged waveguide theory

The theory of guided propagation in step-index waveguides was described in section 2.1. However, since ion-exchange results in a graded refractive index profile n(y), the planar waveguide theory must be modified to account for this. Let the maximum refractive index be n_{sur} at the surface of the waveguide and the substrate refractive index be n_s. Since there is not a clear boundary between the core and the substrate, it is difficult to solve the Maxwell's equations. The WKB method [2] is used to evaluate the modes and the effective refractive indices in the ion-exchanged waveguides. The representation of the refractive index structure of the ion-exchanged waveguide is shown in Figure 2-5 with the core assumed to be contained between Y_a and Y_b. The mode should then have a similar behaviour as in the slab waveguide. At any given point (y, z), a ray sees a refractive index n(y) and satisfies the following expression:

$$k^2(y) = k_y^2(y) + k_z^2 = \omega^2 \mu \epsilon(y) \tag{2.27}$$

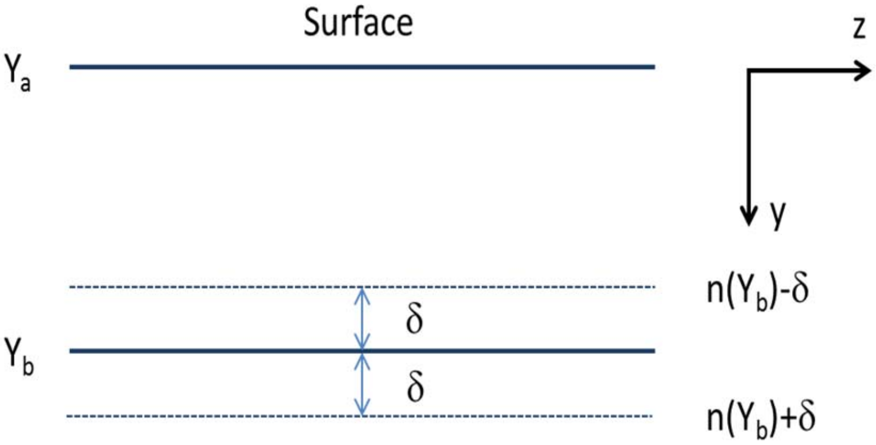

Figure 2-5. Refractive index of the waveguide.

This can be further written as:

$$k_y(y) = k_0 \sqrt{n^2(y) - n_{eff}^2} \tag{2.28}$$

where, $k_0 = \omega\sqrt{\mu_0 \epsilon_0}$. Points Y_a and Y_b represent a turning point defining the effective size of the core region within which a propagating ray can be confined. At these points the $k(y)$ vector is parallel to the z-axis and k_y is 0 implying:

$$k_y(Y_a) = k_y(Y_b) = 0 \tag{2.29}$$

Or:

$$n(Y_a) = n(Y_b) = n_{eff} \tag{2.30}$$

Then (2.13) is rewritten as [2]:

$$2\int_{Y_a}^{Y_b} k_y(y)dy - \varphi_1^{TE} - \varphi_3^{TE} = 2p\pi \tag{2.31}$$

To solve (2.31), the turning point Y_b must be evaluated since Y_a can be set to 0. At the core-air interface using (2.7), (2.9) and (2.14), the phase change of the mode can be written as:

$$\varphi_1^{TE} = 2tan^{-1}\left(\sqrt{\frac{n_{eff}^2 - n_1^2}{n_2^2(y) - n_{eff}^2}}\right) \tag{2.32}$$

The refractive index $n_2(y)$ can be written as n_{sur}, resulting in the following expression:

$$\varphi_1^{TE} = 2tan^{-1}\left(\sqrt{\frac{n_{eff}^2 - n_1^2}{n_{sur}^2 - n_{eff}^2}}\right) \tag{2.33}$$

The index contrast produced due to the ion-exchange is in the order of 10^{-3} hence the value of n_{sur} is very close to that of n_{eff} resulting in a phase change of $\varphi_1^{TE} = \pi$. The value of φ_3^{TE} is calculated at Y_b with the core divided into thin slices. The refractive index at $n(Y_b)$= n_{eff}. The refractive indices δ above and below Y_b is given by:

$$\mathrm{n}(Y_b - \delta) = n(Y_b) - \delta\frac{\partial n(Y_b)}{\partial y} = n_{eff} - \delta\frac{\partial n(Y_b)}{\partial y} \tag{2.34}$$

$$\mathrm{n}(Y_b + \delta) = n(Y_b) + \delta\frac{\partial n(Y_b)}{\partial y} = n_{eff} + \delta\frac{\partial n(Y_b)}{\partial y} \tag{2.35}$$

The expression for φ_3^{TE} is then:

$$\varphi_3^{TE} = 2tan^{-1}\left(\sqrt{\frac{n_{eff}^2 - n^2(Y_b+\delta)}{n^2(Y_b-\delta) - n_{eff}^2}}\right) \tag{2.36}$$

Which reduces to $\varphi_3^{TE} = 2tan^{-1}(1) = \pi/2$ in the limit of $\delta \rightarrow 0$. (2.31) is then approximated as:

$$2\int_0^{Y_b} k_0\sqrt{n^2(y) - n^2(Y_b)}dy - \left(2p + \frac{3}{2}\right)\pi = 0 \tag{2.37}$$

Using iterative modelling, this equation can be solved for each value of p to find Y_b, $n(Y_b)$, and hence n_{eff}. A commercially available software package (RSoft Cad) was used to calculate the mode-profiles of the ion-exchanged waveguides presented in this thesis.

2.3 Quasi-3-level-laser theory

4-level lasers, such as Nd^{3+}-doped yttrium aluminum garnet (YAG) [12], have been traditionally used to develop low-threshold lasers. However, these lasers are pumped at around 800 nm and lase at around 1 μm resulting in a quantum efficiency of about 80%. Yb^{3+}-doped lasers typically have quantum efficiencies exceeding 90%, leading to a lower thermal load and enabling high-power operation. Also, Yb^{3+}-doped lasers have a much broader emission bandwidth compared to Nd^{3+}-doped lasers, making the former very promising for femtosecond laser operation. However, Yb^{3+}-doped gain media fall in the class of lasers known as quasi-three-level lasers. In such laser systems the lower laser level is thermally populated, which increases the threshold power because of re-absorption of the lasing wavelength. A generalised energy-level diagram for a quasi-3-level laser is shown in Figure 2-6.

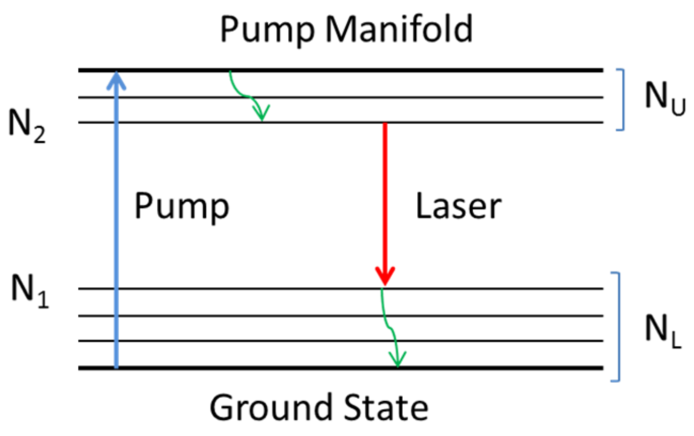

Figure 2-6. Energy level diagram for a quasi-3-level laser.

A pump photon excites an electron from the ground state to the pump manifold, which decays non-radiatively to the metastable upper laser level N_2. Stimulated emission from N_2 to the lower laser level N_1 emits a laser photon. N_1 and N_2 are Stark levels within the lower (N_L) and upper manifolds (N_U) with population densities given by:

$$N_1 = f_1 N_L$$

$$N_2 = f_2 N_U \tag{2.38}$$

where, f_1 and f_2 are the fractions of the total population within the lower laser level of the lower manifold and upper laser level of the upper manifold, respectively. It is assumed that the upper laser level is unpopulated when un-pumped i.e $N_2^0 = 0$ and that the lower laser level population density is $N_1^0 = f_1 N_L^0$ where the superscript "0" denotes equilibrium. Also, spatial hole burning and depopulation of the ground state are neglected in the following analysis [13].

The rate equations for N_2 and N_1 are given by:

$$\frac{dN_2(x,y,z)}{dt} = f_2 R_p r(x,y,z) - \frac{N_2(x,y,z)-N_2^0}{\tau} - \frac{f_2 c\sigma\left(N_2(x,y,z)-N_1(x,y,z)\right)}{n}\Phi\phi(x,y,z) = 0 \tag{2.39}$$

$$\frac{dN_1(x,y,z)}{dt} = -f_1 R_p r(x,y,z) - \frac{N_1(x,y,z)-N_1^0}{\tau} + \frac{f_1 c\sigma\left(N_2(x,y,z)-N_1(x,y,z)\right)}{n}\Phi\phi(x,y,z) = 0 \tag{2.40}$$

where, τ is the upper laser level lifetime, c is the speed of light, σ is the emission cross-section and n is the refractive index of the medium. The pump rate R_p is defined as:

$$R_p = \frac{P_p(1-e^{-\alpha_p l})}{h\upsilon_p} \tag{2.41}$$

where, P_p is the pump power, h is the Planck's constant, υ_p is the frequency of the pump, α_p is the absorption coefficient of gain media at the pump frequency and l is the length of the gain media. The total number of photons in the laser cavity Φ is given by:

$$\Phi = \frac{2nlP_L}{ch\upsilon_L} \tag{2.42}$$

where, υ_L is the laser frequency and P_L is the laser power travelling in one direction. $r(x,y,z)$ is the spatial distribution of the pump energy and is normalised as:

$$\iiint_{cavity} r(x,y,z)\,dxdydz = 1 \tag{2.43}$$

The quantity $\phi(x,y,z)$ is the spatial distribution of the laser energy and is normalised as:

$$\iiint_{cavity} \phi(x,y,z)dxdydz = 1 \tag{2.44}$$

The total population inversion ΔN is given by:

$$\Delta N = N_2 - N_1 \tag{2.45}$$

Therefore, (2.39) and (2.40) can be combined to give:

$$\frac{d\Delta N(x,y,z)}{dt} = (f_1 + f_2)R_p r(x,y,z) - \frac{\Delta N(x,y,z) - \Delta N^0}{\tau} - \frac{(f_1+f_2)c\sigma\Delta N(x,y,z)}{n}\Phi\phi(x,y,z) \tag{2.46}$$

where, $\Delta N^0 = N_2^0 - N_1^0$ is the un-pumped population inversion.

The temporal evolution of the total number of photons in the cavity is governed by the following equation:

$$\frac{d\Phi}{dt} = \frac{c\sigma}{n}\iiint_{cavity} \Delta N(x,y,z)\Phi\phi(x,y,z)dxdydz - \frac{\Phi}{\tau_c} = 0 \tag{2.47}$$

Where, $\tau_c = 2nl/c\delta$ is the photon cavity lifetime and δ is the round-trip loss. Rearranging (2.47) and utilising the fact that for stable laser operation, round-trip loss (δ) must be equal to round trip gain (G):

$$G = 2\sigma l \iiint_{cavity} \Delta N(x,y,z)\phi(x,y,z)dxdydz = \delta \tag{2.48}$$

The round-trip loss δ consists of the passive cavity losses L_{RT} and the output coupling losses $-lnR$ where R is the reflectivity of the output coupler and the reflectivity of the other mirror is assumed to be 100%. The population inversion at thermal equilibrium can be found by replacing $f_1 + f_2$ by f and ΔN^0 by $-N_1^0$ as $N_1^0 \gg N_2^0$ and using (2.46):

$$\Delta N(x,y,z) = \frac{f\tau R_p r(x,y,z) - N_1^0}{1 + \frac{f\tau c\sigma}{n}\Phi\phi(x,y,z)} \tag{2.49}$$

The useful output power P_{out} is given by TP_L, where T is the transmission of the output coupler. Using this and replacing the value of $\Delta N(x,y,z)$ from (2.49) in (2.48) gives:

$$2\sigma l \int_0^l \int_{-\infty}^{\infty} \int_{-\infty}^{\infty} \frac{\frac{f\tau}{h\nu_p} P_P \eta_{abs} r(x,y,z) - N_1^0}{1 + 2l\frac{P_{out}}{TI_{sat}}\phi(x,y,z)} \phi(x,y,z)dxdydz = L_{RT} - lnR \tag{2.50}$$

Where, $\eta_{abs} = 1 - e^{-\alpha_p l}$ and $I_{sat} = \frac{h\upsilon_L}{f\sigma\tau}$. The threshold power ($P_{th}$) is defined as the minimum pump power required to achieve laser action and can be evaluated by setting the P_{out} to 0 and P_P to P_{th}:

$$P_{th} = \frac{\frac{h\upsilon_p}{2\sigma l f\tau\eta_{abs}}(L_{RT} - lnR + 2\sigma N_1^0 l)}{\int_0^l \int_{-\infty}^{\infty}\int_{-\infty}^{\infty} r(x,y,z)\phi(x,y,z)dxdydz} \tag{2.51}$$

The pump and laser spatial distributions are expressed as [13]:

$$r(x,y,z) = \frac{2\alpha_p}{\pi\eta_{abs}\omega_{Px}\,\omega_{Py}} e^{\left(-\frac{2x^2}{\omega_{Px}^2}\right)} e^{\left(-\frac{2xy^2}{\omega_{Py}^2}\right)} e^{-\alpha_P z} \tag{2.52}$$

$$\phi(x,y,z) = \frac{2}{\pi\omega_{Lx}\,\omega_{Ly} l} e^{\left(-\frac{2x^2}{\omega_{Lx}^2}\right)} e^{\left(-\frac{2xy^2}{\omega_{Ly}^2}\right)} \tag{2.53}$$

The final expression for the threshold power can thus be written as:

$$P_{th} = \frac{\pi h\upsilon_p}{4\sigma f\tau\eta_{abs}}(L_{RT} - lnR + 2\sigma N_1^0 l)\sqrt{\omega_{Lx}^2 + \omega_{Px}^2}\sqrt{\omega_{Ly}^2 + \omega_{Py}^2} \tag{2.54}$$

where, ω is the 1/e^2 beam size for the laser (L) and pump (P) in the vertical (x) and horizontal (y) direction.

In order to achieve a low threshold power, the lifetime and emission cross section should be high, which is fixed for a particular gain media. However, the mode sizes, the losses and re-absorption losses should be as low as possible. The mode sizes can be reduced in waveguide geometry as both the pump and laser modes are confined in the waveguide throughout propagation. The round trip propagation loss can be minimised by optimised fabrication techniques and as long as they are much less than the combined re-absorption and output coupling losses then they should not act to significantly increase the threshold power.

The slope efficiency (η_s) gives information of the performance of the laser, i.e. how efficiently the pump power is converted to laser power after reaching threshold. This is given by the following expression [13]:

$$\eta_s = \frac{\nu_L}{\nu_p}\frac{dS}{dF}\eta_q\left(\frac{T}{L+T}\right) \tag{2.55}$$

where, ν_L is the laser frequency, T is the percentage transmission of the output coupler, L is the total percentage loss in the cavity, $\frac{dS}{dF}$ is a measure of the mode-overlap between the population inversion and the laser beam and η_q is the internal quantum efficiency. In a waveguide, the overlap between the population inversion and the laser beam is normally very high. However, the propagation losses are now required to be low in comparison to the output coupling in order for high slope efficiencies to be obtained.

2.4 Mode-locking

In a laser with a sufficiently large emission bandwidth, many longitudinal modes can be phase locked together to generate ultra-short pulses [14, 15], which is called mode-locking. If there are 'n' longitudinal modes and the n^{th} mode has an electric field amplitude E_n, then the total electric field E(t) is given by:

$$E(t) = \sum_n E_n \exp i[(\omega_o + n\Delta\omega)t + n\Delta\varphi] \quad (2.56)$$

where, ω_o is the central frequency, $\Delta\omega$ is the mode separation and $\Delta\varphi$ is the phase difference between successive modes. Mode-locking implies that the phase difference is a constant denoted by φ_o. Therefore the electric field is simplified to the following expression, which is an equation for an electric field modulated by a trigonometric envelope function:

$$E(t) = E_o \exp i[\omega_o t + \varphi_o] \frac{sin\left[\frac{n\Delta\omega t}{2}\right]}{sin\left[\frac{\Delta\omega t}{2}\right]} \quad (2.57)$$

Mode-locking can be achieved actively, for example by using modulators based on the acousto-optic or the electro-optic effects, or passively for example using saturable absorbers or Kerr-lens mode-locking. The first actively mode-locked laser [16] was a He-Ne laser and the first ever passively continuous wave (CW) mode-locked laser was a dye laser [17]. Since active mode-locking requires an external signal and also because it generally leads to the generation of longer pulses [18], passive mode-locking is the preferred choice for this project. If the value of the number of modes n is increased in (2.57), the resulting pulse duration becomes shorter. Thus, it can be concluded that in order to achieve short pulses, the laser medium must have a large spectral bandwidth. Therefore, materials with a broad emission spectrum were chosen as potential candidates for mode-locking in this project.

2.4.1 Saturable absorption

A saturable absorber exhibits a high loss at low intensities and low-loss at high intensities, thus favouring pulsed operation. The most intuitive way to understand saturable absorption is by considering a simple 2-level electronic system. Initially, when all the electrons are in the ground state, then any incident pump photon is absorbed, thus exciting the electron from the ground state to the upper level. As the intensity of incident photons increases, the photon can either be absorbed or can induce emission. Therefore, the absorption decreases with intensity until at high intensities, the upper and lower level reach equilibrium and there is no further absorption. This is the state of low-loss for the pump.

In any laser system, the net gain should be greater than the total loss in the cavity in order for laser oscillations to circulate in the cavity. This means that in a laser with a saturable absorber it is possible to introduce sufficient loss for the low intensity light, to suppress its circulation in the cavity. For the high intensity pulse, the loss is saturated for a short time interval. The dynamics of the gain medium and the loss modulation introduced by the saturable absorber are shown in Figure 2-7.

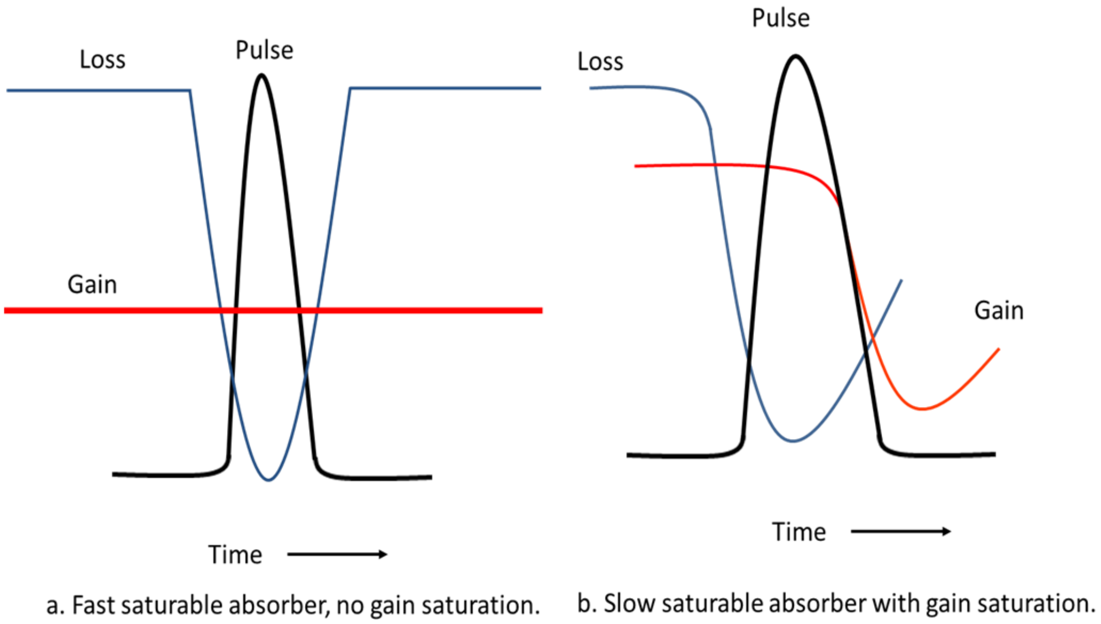

a. Fast saturable absorber, no gain saturation.

b. Slow saturable absorber with gain saturation.

Figure 2-7. Gain-loss dynamics resulting in a short pulse.

Figure 2-7 (a) shows the dynamics of a mode-locked laser with no gain saturation and a fast saturable absorber. The saturable absorber is modulated in the fs scale, and when the loss falls below the saturated gain of the laser gain medium, a pulse is generated. This is the mode-locking mechanism in Kerr-lens mode-locking of Ti:sapphire [19]. The mode-locking mechanism in dye lasers [17, 20] is shown in Figure 2-7 (b). Here, the gain and the saturable absorber are both modulated, with the response of the saturable absorber being slow in comparison to the previous case. There is a short window in which the gain exceeds the loss resulting in the generation of a short pulse.

There are various saturable absorbers that can be used to generate sub-ps pulses. However, semiconductor saturable absorber mirrors (SESAMs) [21] and quantum-dot (QD)-doped glasses [22] have been discussed in the following sub-sections as these were investigated to generate short pulses in this project. Graphene [23] and carbon nanotubes [24] have also shown considerable promise as saturable absorbers for mode-locking and are briefly discussed in section 2.4.1.3.

2.4.1.1 SESAM

Since its invention in 1992 [21], semiconductor saturable absorber mirrors or SESAMs are one of the most popularly used saturable absorbers to generate sub-picosecond pulses. These consist of either a bulk semiconductor or a quantum well or a QD absorbing region that acts as the saturable absorber embedded within a Bragg mirror. The major advantage of using SESAMs is that almost all parameters can be custom designed using semiconductor fabrication techniques. Band-gap engineering and defect engineering can be used to control the operating wavelength and recovery times of the saturable absorber layer, whereas careful design of the dielectric mirrors can give almost any desired reflectivity.

A photon when absorbed by the semiconductor layer excites an electron from the valence band to the conduction band as shown by the blue arrow in Figure 2-8. Initially, there is a fast intra-band relaxation (red arrow in Figure 2-8) in the time scale of 10-100 fs followed by the carrier recombination, which is usually an order of magnitude slower (green arrow in Figure 2-8) .The slower response leads to a reduced saturation intensity, which helps in self-starting while the faster response helps in pulse shaping [25].

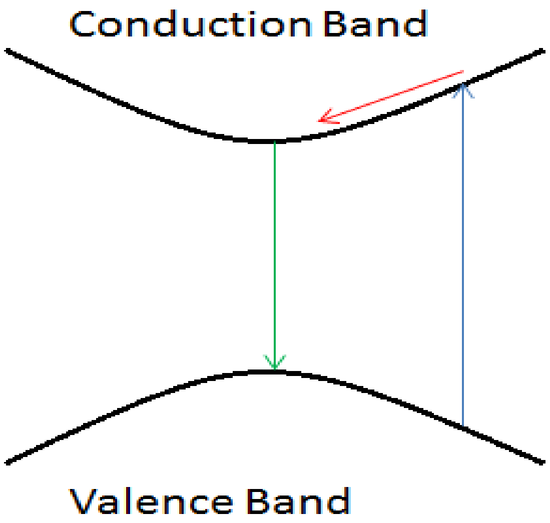

Figure 2-8. Absorption and relaxation processes in a semiconductor.

Usually semiconductors have a carrier recombination time in the range of nanoseconds, which is too slow for CW mode-locking [25]. In order to decrease the slow time constant, low-temperature-grown III-V semiconductors are used [26]. The excess group V atoms formed during the low-temperature growth lead to point defects, which result in fast carrier trapping [27, 28].

The key parameters of a SESAM are: the modulation depth (ΔR) defined as the change of reflectivity due to saturable absorption, saturation fluence (F_{sat}) defined as the required pulse energy fluence to change the reflectivity by 1/e of the modulation depth, linear reflectivity (R_{lin}) defined as the unsaturated reflectivity and the unwanted losses known as the non–saturable losses (ΔR_{ns}). These parameters are clearly marked in a reflectivity vs. pulse energy fluence diagram shown in Figure 2-9.

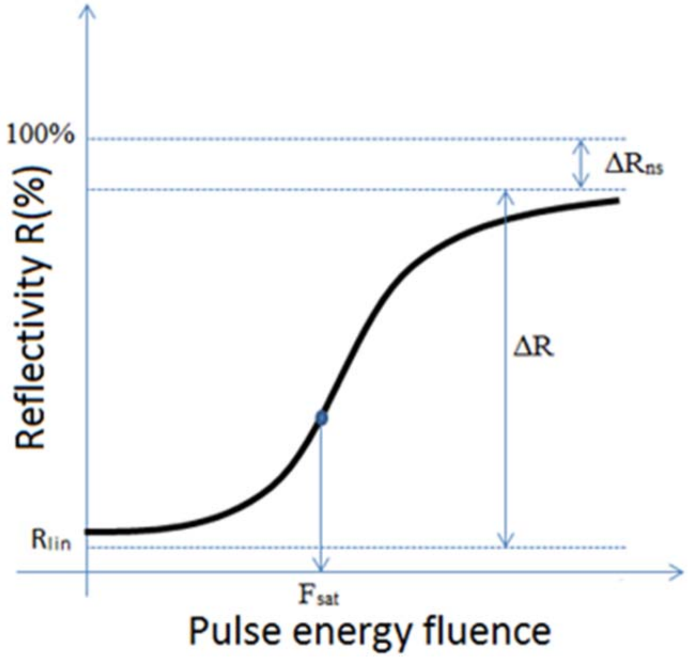

Figure 2-9. Reflectivity vs. pulse energy fluence highlighting the different parameters of a SESAM.

A laser cavity with a saturable absorber may also generate Q-switched mode-locked pulses [29-31]. The condition to prevent Q-switched instabilities in the non-soliton mode-locking case is that [18]:

$$E_p^2 > F_{sat,L}F_{sat,A}A_A A_L \Delta R \qquad (2.58)$$

where, E_p is the pulse energy, $F_{sat,L}$ is the saturation fluence of the laser , $F_{sat,A}$ is the saturation fluence of the saturable absorber, A_A is the area of the laser mode incident on the saturable absorber, A_L is the area of the laser mode in the gain medium and ΔR is the modulation depth of the saturable absorber. The critical pulse energy $E_{p,crit}$ is the minimum pulse energy required to prevent Q-switching instabilities and is found when

$$E_{p,crit}^2 = F_{sat,L}F_{sat,A}A_A A_L \Delta R \qquad (2.59)$$

For the mode-locked Yb:IOG-1 waveguide laser discussed in chapter 4, the value of $F_{sat,L}$ is 72.2 J/cm^2, $F_{sat,A}$ is 90 µJ/cm^2, $A_A = A_L = 6.92 \times 10^{-7}$ cm^2 and ΔR is 0.4% giving a critical pulse energy of 3.5 nJ.

From (2.59) another advantage of using waveguides for ultrafast pulse generation can be deduced: as the effective area of the mode is much smaller than when compared to bulk lasers, it is easier to saturate the absorber and thus avoid Q-switching instabilities.

A brief overview of typical results obtained by mode-locking with SESAMS at different wavelengths is given in Table 2-1.

Table 2-1. Review of typical pulse durations obtained by mode-locking with SESAMs

Gain Medium	**Central Wavelength (nm)**	**Pulse duration (fs)**	**Reference**
Ti:sapphire	840	19	[32]
Cr:LiSAF	875-900	14	[33]
Cr:forsterite	1290	40	[34]
Yb:YAG	1030	1700	[35]
Yb:KYW	1029	66	[36]
Yb:RTP	1053	155	[37]
Yb:glass	1050	58	[38]
Nd:glass	1059	173	[39]
Nd:YLF	1047	3300	[21]
Er,Yb:glass	1533	2500	[40]

Recently, QDs have been used as the saturable absorber layers in SESAMs [41-44]. The densities of states for a quantum dot are a sequence of delta peaks, where each peak corresponds to a QD of a different size. Therefore, the density of charge carriers at a particular energy level is much higher when compared to bulk or a quantum well. QDs also have the following advantages over bulk semiconductor and quantum well structures: broadband absorption due to the inhomogeneous broadening (related to non-uniform dot size distribution), fast recovery times and low saturation fluence.

2.4.1.2 Quantum-dot-doped glass

Even though QD-SESAMs are very widely used, they are expensive and complicated to fabricate because molecular beam epitaxy (MBE) is used. QD-doped glasses offer a cheaper alternative to SESAMs because they are fabricated using much easier and cheaper batch melting techniques [22]. Also, by the variation of the quantum dot diameter, it is possible to tune the absorption over a large bandwidth. II-VI semiconductor crystals like CdS, CdSe and CdTe have been doped in silicate glasses; however they are only suitable for operation in the 500-700 nm regime. The more widely used semiconductor group is IV-VI, which comprises of PbS, PbSe and PbTe, because they can be used for mode-locking from the visible wavelength to 3 μm.

High melting-point quantum dot doped glasses were fabricated by Dr. Pradeesh Kannan and characterised for operation near 1.2 μm [44] during this project. However, the glasses exhibited large losses and it was difficult to control the glass fabrication parameters. Therefore, SESAMs were preferred over these glasses for mode-locking experiments in this project, as they are commercially available with a variety of parameters.

2.4.1.3 Single-wall carbon nanotubes and grapheme

Single-walled carbon nanotubes (SWNT) are allotropes of carbon and have a cylindrical structure. They have been used as saturable absorbers for femtosecond operation [24] owing to their high damage threshold, and low non-saturable losses. The wavelength of operation is dependent on the diameter of SWNT. However, the wavelength tunability is only achieved due to a variation in the diameter which introduces insertion loss at wavelengths where the SWNTs are not in resonance.

Graphene is an allotrope of carbon and has a two-dimensional structure, in which all the carbon atoms form a honeycomb lattice. In contrast to SWNTs, there is an electron-hole pair in resonance for any excitation wavelength due to the negligible band-gap in graphene. In addition, the fast carrier dynamics makes graphene a very promising candidate for fast saturable absorbers [23]. Indeed, graphene will be explored in the future as an alternative to SESAMs for the development of ultrafast waveguide lasers.

2.4.2 Soliton mode-locking

In section 2.4.1, the gain-loss dynamics of a fast saturable absorber and a slow saturable absorber with gain saturation were discussed. It is possible to generate short pulses with a slow saturable absorber and no gain saturation using soliton mode-locking [45], and the dynamics are shown in Figure 2-10. Soliton mode-locking was used for mode-locking the waveguides presented in chapters 4 and 5.

In soliton modelocking the total intra-cavity group delay dispersion (GDD) is made negative by introducing extra elements in the cavity with negative GDD, such as a prism pair, chirped mirrors or GTI mirrors. This negative GDD balances self-phase modulation introduced due to the Kerr non-linearity of gain medium. A SESAM is used to ensure self-starting and it is indeed possible to generate pulses as short as 300 fs with SESAMs with a 10-ps response time [46].

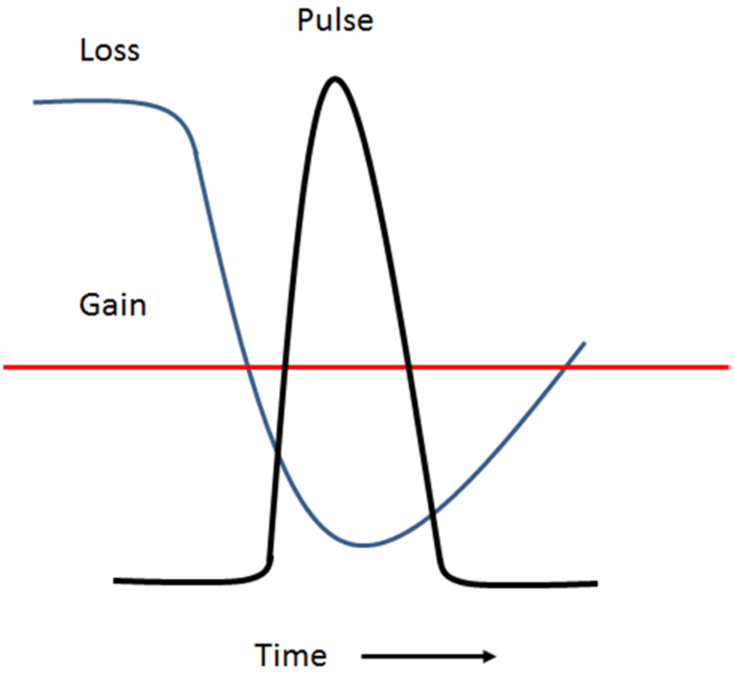

Figure 2-10. Gain-loss dynamics of soliton mode-locking.

In the soliton mode-locking case, the expression for the pulse energy (E_P) in (2.58) is modified to [47]:

$$F_{sat,L}A_L g K^2 {E_P}^3 + {E_P}^2 > F_{sat,L}F_{sat,A}A_A A_L \Delta R \qquad (2.60)$$

where, g is the time-dependant round-trip power gain coefficient and K is a coefficient which depends on the non-linearity of the gain medium and the total round-trip GDD. It is found that the critical pulse energy in this case is usually an order of magnitude lower than when compared to the case of non-soliton mode-locking [48] and is calculated to be 0.095 nJ for the Yb:IOG-1 waveguides discussed in chapter 4.

2.5 Advantages of waveguides

As explained in the previous sub-sections, waveguides can confine light for the entire length of propagation without divergence, thus maintaining high intensities of light. The effective area is therefore smaller when compared to the case of confocal focusing [49, 50]. The threshold power for a laser is directly proportional to the effective area [13] as discussed in the section 2.3, hence a reduction in effective area reduces the threshold power of the laser. The waveguide configuration also automatically allows a good overlap between the pump and the laser beams, thereby resulting in high slope efficiencies if propagation losses can be kept low. Waveguides also have an advantage when it comes to thermal management because of a large aspect ratio [51]. A major attraction for waveguide lasers is their small size and suitability for fully integrated devices with multiple functions on one chip. Finally, as seen from equation (2.59), the critical pulse energy required to overcome Q-switching instabilities in the case of non-soliton mode-locking is directly proportional to the laser and pump mode areas. Since the mode areas in the laser medium and on the saturable are small (and equal), this reduces the mode-locking threshold in waveguides. All these advantages make waveguide lasers very promising candidates for the realisation of ultrafast lasers.

2.6 Ultrafast laser gain media

In this section, all the gain media with which lasing and mode-locking experiments were carried out have been discussed to give an overview of their optical properties, and a brief literature review for each material has also been provided.

2.6.1 Ytterbium-doped gain media

Ytterbium (Yb^{3+}) doped materials [52] are very good active media for making power-scalable solid-state lasers operating around 1 μm as they have a broad absorption band suitable for diode pumping, a small quantum defect (thus a lower thermal load), a long lifetime and almost no losses due to up-conversion and excited state absorption. The trivalent Ytterbium ion has a very simple electronic structure with only 2 sub-levels ($^2F_{7/2}$

and $^2F_{5/2}$) and the sub-levels are further split into several Stark levels. One pump photon excites the ground-state electron in the $^2F_{7/2}$ level to the $^2F_{5/2}$ level, after which it non-radiatively decays to the lowest Stark level of $^2F_{5/2}$. The electron then radiatively decays to the lower laser-level in the ground manifold emitting a photon at the laser wavelength. The lower laser level is thermally populated hence this system acts as a quasi-3-level laser. The electron then decays from the lower laser level to the ground level non-radiatively. The energy diagram for the Yb^{3+} ion is shown in Figure 2-11. Yb^{3+}-doped IOG-1 glass, Yb^{3+}-doped KYW, Yb^{3+}-doped RTP and Yb^{3+} -doped YAG are discussed in the following sections.

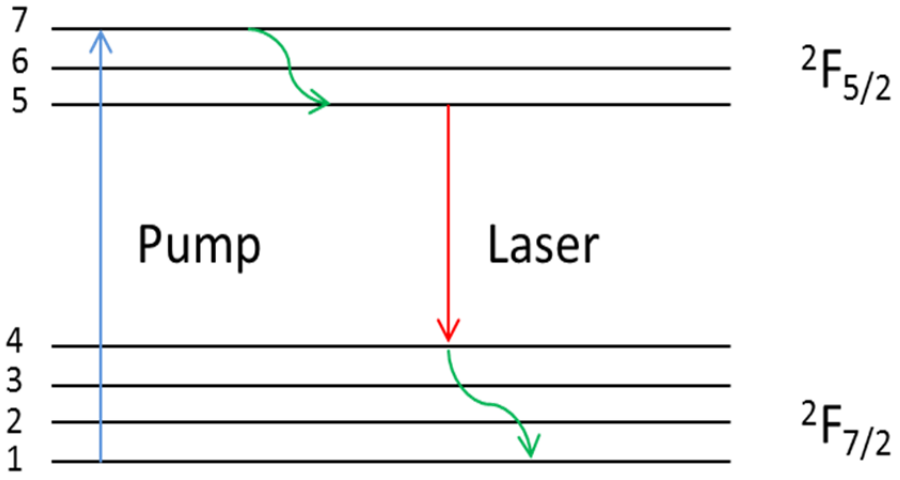

Figure 2-11. Energy diagram of Yb^{3+}-doped gain media.

2.6.1.1 *Yb:IOG-1 glass*

Slope efficiencies of up to 67% have been reported for an Yb^{3+}-doped phosphate glass waveguide laser fabricated by ion-exchange [53]. The absorption and fluorescence spectra for a commercially available phosphate glass (IOG-1 from Schott) doped with 12 wt% Yb^{3+} were measured and are shown in Figure 2-12. It can be seen that this glass has a broad emission spectrum which makes it a very promising candidate for the development of mode-locked sources.

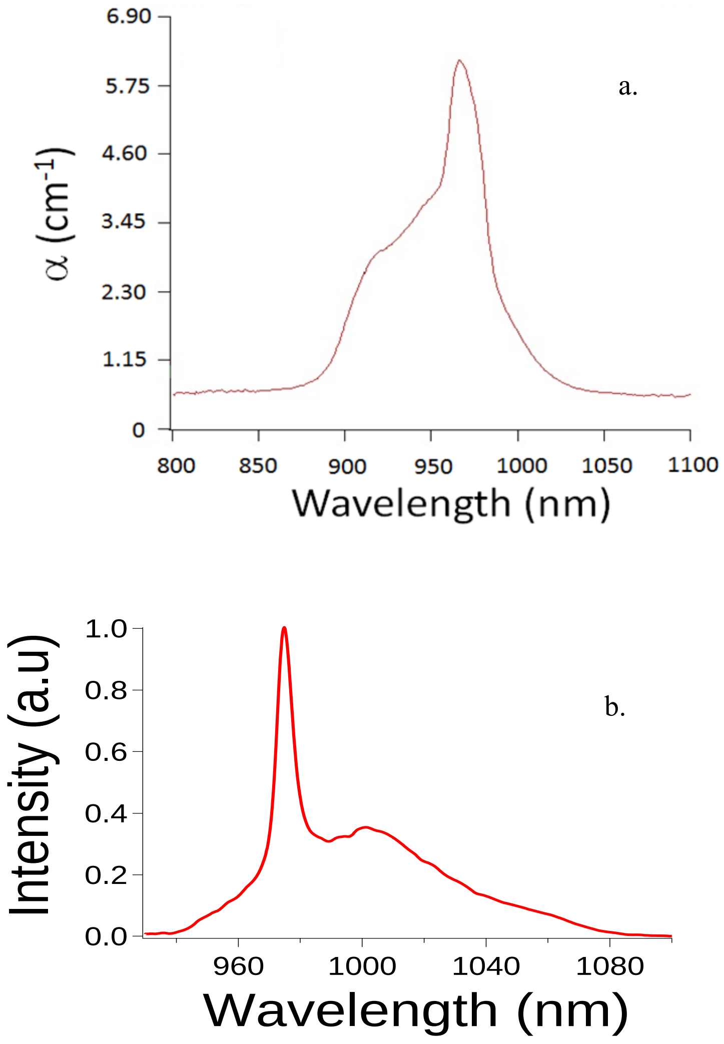

Figure 2-12. a. Measured absorption, and b. emission spectrum for Yb:IOG.

2.6.1.2 Yb:KY(WO$_4$)$_2$

Potassium double tungstates are probably the most common crystal hosts for bulk Yb^{3+}-doped mode-locked lasers. These are biaxial crystals with a chemical formula of KY(WO$_4$)$_2$. The optical axes **N$_m$, N$_p$** and **N$_g$** have refractive indices n_m, n_p and n_g, respectively. They can be pumped by commercially available diode lasers operating at 981 nm. Yb:KY(WO$_4$)$_2$ or Yb:KYW has the highest available gain for the E//N$_m$ polarisation and has a very broad emission spectrum as seen in Figure 2-13 (b) which is conducive for the generation of sub-picosecond pulses. The absorption spectrum is also shown in Figure 2-13 (a) [54]. Femtosecond operation has been demonstrated in bulk Yb:KYW crystals with pulse duration as short as 62 fs [36]. 160 fs pulses with a repetition-rate of 2.8 GHz have been generated by utilizing soliton mode-locking [48] and

114 fs pulses were demonstrated using a QD-based SESAM [41]. 107 fs pulses at a repetition-rate of 294 MHz [55] and a 4.6 GHz oscillator with pulse width of 105 fs [56] have been demonstrated using Kerr-lens mode-locking.

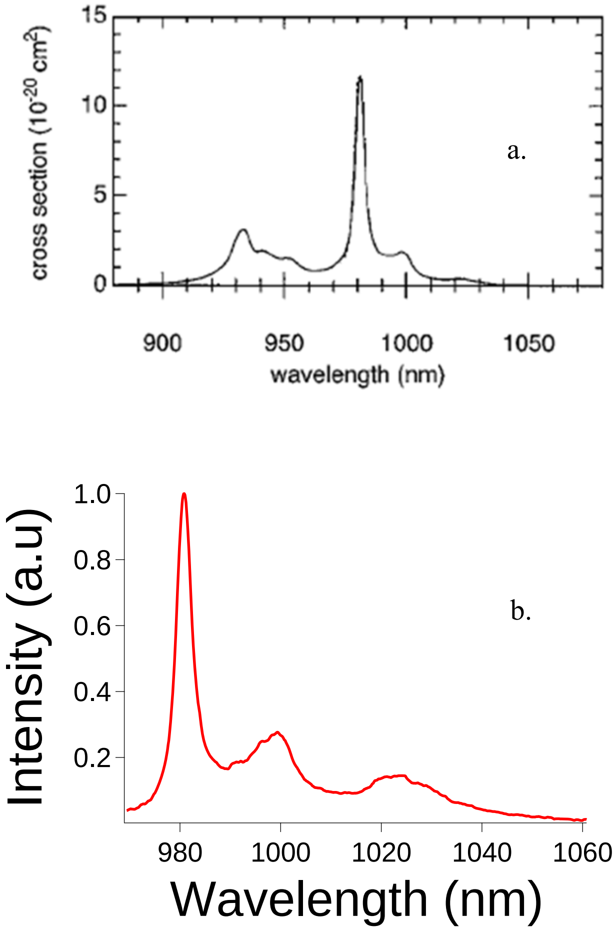

Figure 2-13. a. Absorption spectrum [54], and b. measured emission spectrum of Yb:KYW.

Liquid-phase epitaxy (LPE) is a technique used to fabricate low-loss, single-crystalline waveguides and is discussed in detail in the next chapter. The first Yb:KYW planar waveguide laser was fabricated using LPE [57] and exhibited a slope efficiency of 80%. Q-switched operation has also been demonstrated for LPE-grown Yb:KYW/KYW waveguide lasers [58] which generated pulses of 170 ns duration and 722 kHz repetition-rate. Gd^{3+} and Lu^{3+} co-doped Yb:KYW films have been grown by LPE to increase the refractive index contrast between the substrate and the film. This enabled laser operation at very low threshold power of 18 mW [59] due to the increased confinement of the laser and pump modes.

The first Yb:KYW channel waveguide laser was fabricated by strip-loading a short piece of optical fibre on an LPE-grown Yb:KYW layer [60]. In this case the threshold power and the slope efficiency were measured to be 82 mW and 30% respectively. Ultrafast laser inscription has also been used to fabricate channel waveguides in a doped Yb:KYW crystal, which demonstrated laser action at a threshold power of 18.6 mW [61] with a measured propagation loss of 1.9 dB/cm. More recently, channel waveguides were fabricated by Ar-ion milling of LPE grown Yb^{3+}, Gd^{3+}, Lu^{3+}: KYW layers [62] with a propagation loss of 0.3 dB/cm. A threshold power as low as 4.5 mW and a slope efficiency as high as 62% was reported for this laser.

2.6.1.3 Yb:$RbTiOPO_4$

$RbTiOPO_4$ (RTP) is a nonlinear optical crystal that belongs to the $KTiOPO_4$ (KTP) family. RTP has similar nonlinear optical coefficients to KTP [63] but unlike KTP, it can be doped with Yb^{3+} ions to a high enough concentration to allow efficient laser action [64, 65]. Therefore, by combining the emission of Yb^{3+} with the nonlinear optical properties of the crystal, it is possible to obtain a self-frequency doubling material. RTP has other interesting properties, such as a high laser damage threshold, about 2 times larger than that of KTP [66], large electro-optical coefficients, low dielectric constants [67], high chemical stability and low photorefractive damage susceptibility [68].

Yb^{3+}-doped RTP is also a promising candidate for making ultrafast lasers owing to its large bandwidth as seen from Figure 2-14 (b). The absorption spectra for all polarisations are also shown in Figure 2-14 (a) [69]. Mode-locked operation with pulses as short as 155 fs have also been demonstrated [37]. Planar waveguides in RTP have also been fabricated by LPE with relatively low loss (~0.7dB/cm) [70-72].

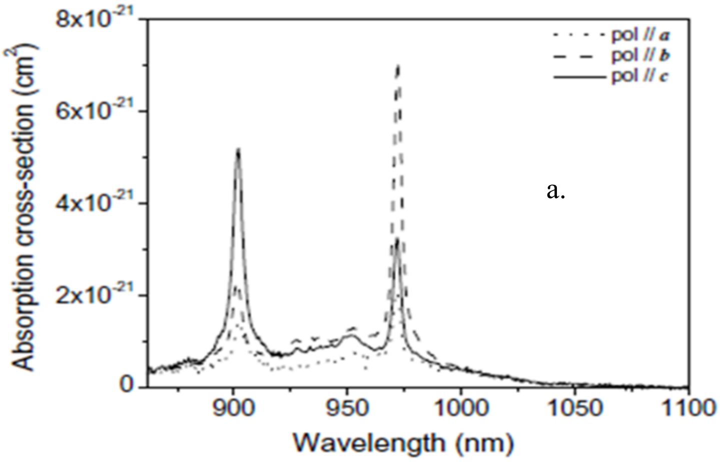

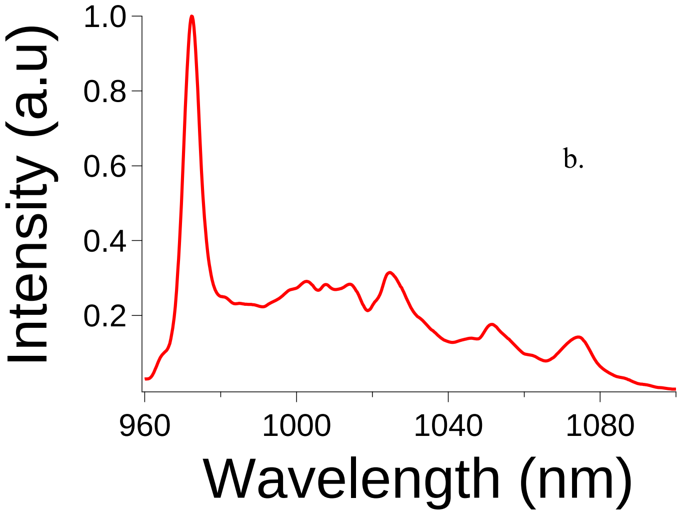

Figure 2-14. a. Absorption spectrum [69], and b. measured emission spectrum of Yb:RTP.

2.6.1.4 Yb:YAG

Yttrium aluminium garnet (YAG) doped with Yb^{3+} (Yb:YAG) [73] has been traditionally used to develop high power lasers [74], owing to the excellent thermal properties of the YAG crystal. Mode-locked operation of Yb:YAG has been demonstrated using a SESAM [35], with pulses as short as 1.7 ps being achieved. An epitaxially grown Yb:YAG waveguide laser with a slope efficiency greater than 77% has also been demonstrated [75]. The absorption spectrum [76] and the measured emission spectrum of Yb:YAG is shown in Figure 2-15, and it can be noted that it is difficult to generate sub-picosecond pulses because of the relatively narrow emission bandwidth. Attempts to mode-lock a low-loss Yb:YAG planar waveguide fabricated by LPE [75] during the course of this project were unsuccessful. The maximum intra-cavity power achieved was <1W, whereas the calculated threshold power for mode-locking was >10 W. The reason behind such a high mode-locking threshold power was that this was a planar waveguide, which increases the effective mode area (equation (2.59)). As this waveguide was clad, it could not be etched to fabricate rib waveguides. Therefore, experiments with this crystal were not pursued further and are not discussed further in this thesis.

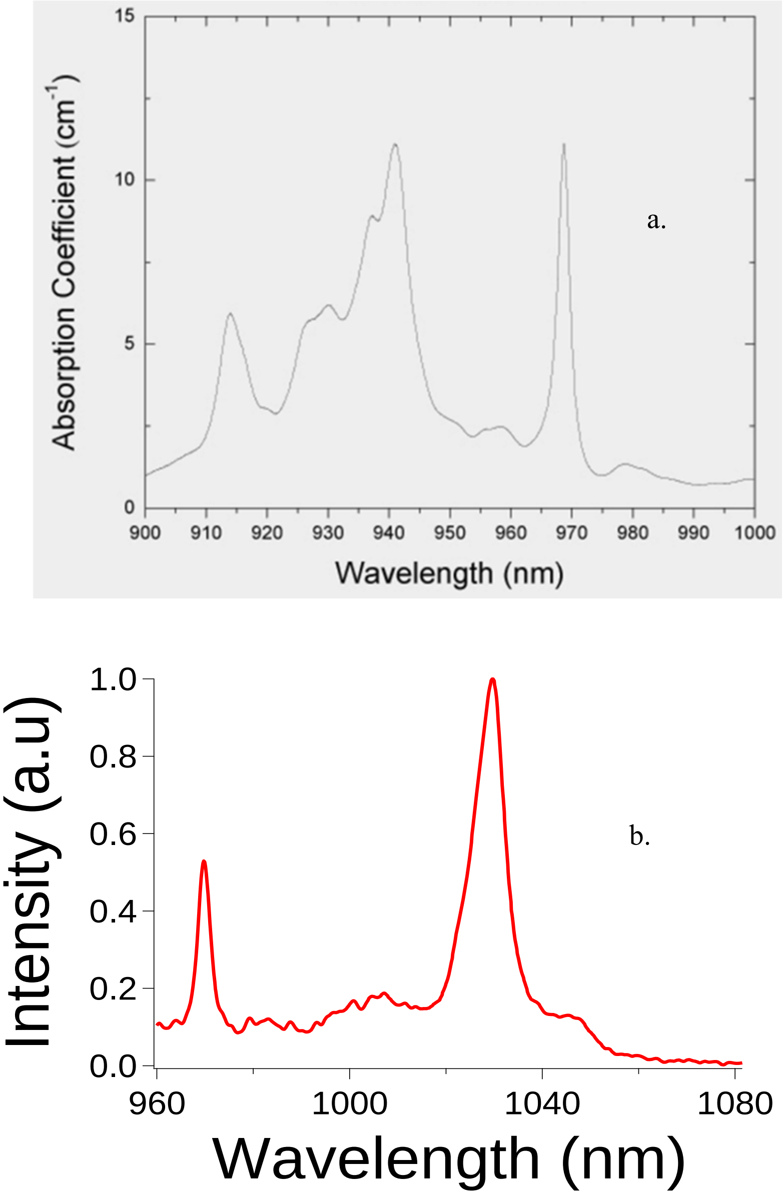

Figure 2-15. a. Absorption spectrum [76], and b. measured emission spectrum of Yb:YAG.

Table 2-2 summarises the optical properties for all the Yb^{3+}-doped gain media that have been discussed in this thesis.

Table 2-2. Optical properties of Yb^{3+}-doped gain media

Property	**IOG-1 Glass [77]**	**Yb:KYW [78]**	**Yb:RTP [69]**	**Yb:YAG [79]**
Emission maxima (nm)	1002	1025	1053	1029
Emission cross-section (m^2)	5.4×10^{-25}	2.9×10^{-24}	3×10^{-25}	2.2×10^{-24}
Absorption maxima (nm)	974.6	981.2	900 (E//c)	941
Absorption cross-section (m^2)	14.5×10^{-25}	1.2×10^{-23}	3.2×10^{-25}	0.8×10^{-24}
Fluorescence lifetime (ms)	1.4	0.3	2.2	0.8
Refractive index	1.52 @ 1 μm	1.98@1μm	1.85 @ 972 nm	1.82 @1μm

2.6.2 (Er,Yb):IOG-1 glass

Development of compact multi-GHz sources operating near 1.5 μm could have potential applications in telecommunications as this wavelength falls in the widely-used third telecoms window, where the losses of the silica sibre are lowest and erbium-doped fibre amplifiers offer very high performance. Er^{3+}-doped waveguides [80] have been used to make laser sources near 1.5 μm. However, the absorption cross-section for pumping from the $^4I_{15/2}$ level to the $^4I_{11/2}$ level is quite low making it difficult to populate the $^4I_{11/2}$ level. Therefore, Yb^{3+} sensitizer ions are often co-doped with the Er^{3+} ions to increase the absorption [81] of the pump. The pump (around 980 nm) excites the ground state electron in the Yb^{3+} ion to the $^2F_{5/2}$ level which transfers energy to the $^4I_{11/2}$ level of a nearby Er^{3+} ion. Following non-radiative decay to the $^4I_{13/2}$ metastable level, a photon at the laser wavelength of around 1.5 μm is emitted from the $^4I_{13/2} \rightarrow {}^4I_{15/2}$ transition. The Er^{3+}, Yb^{3+} energy diagram is shown in Figure 2-16.

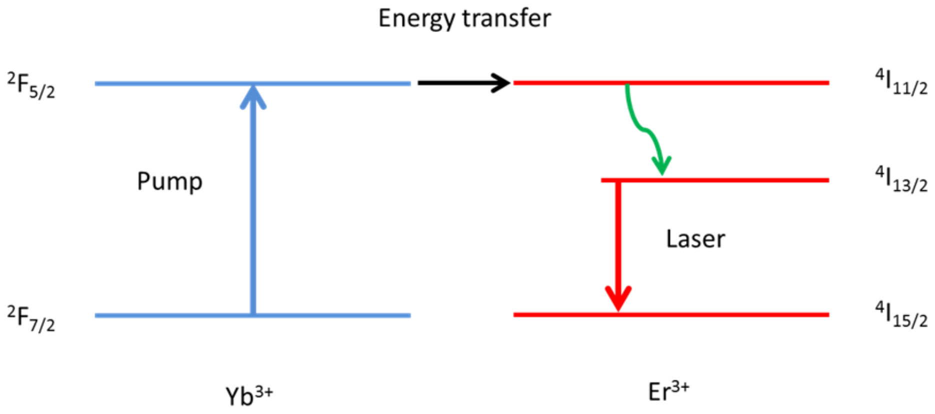

Figure 2-16. Er3+, Yb3+ energy diagram.

CW operation in an ion-exchanged Er^{3+},Yb^{3+}-doped phosphate glass waveguide laser operating near 1.5 µm has previously been demonstrated [53] with a laser threshold of 23 mW and a slope efficiency of 28%. Mode-locking has also been achieved in Er^{3+}, Yb^{3+}-doped phosphate glass waveguide lasers [82-84], however these have typically involved external cavities and have resulted in repetition-rates less than 1 GHz and pulses longer than 1 ps. The measured absorption and emission spectrum of an Er^{3+}, Yb^{3+}: IOG-1 glass (from Schott) is shown in Figure 2-17. Broad-band emission near 1.5 µm is observed, which makes these glasses promising candidates for mode-locked operation in that wavelength range.

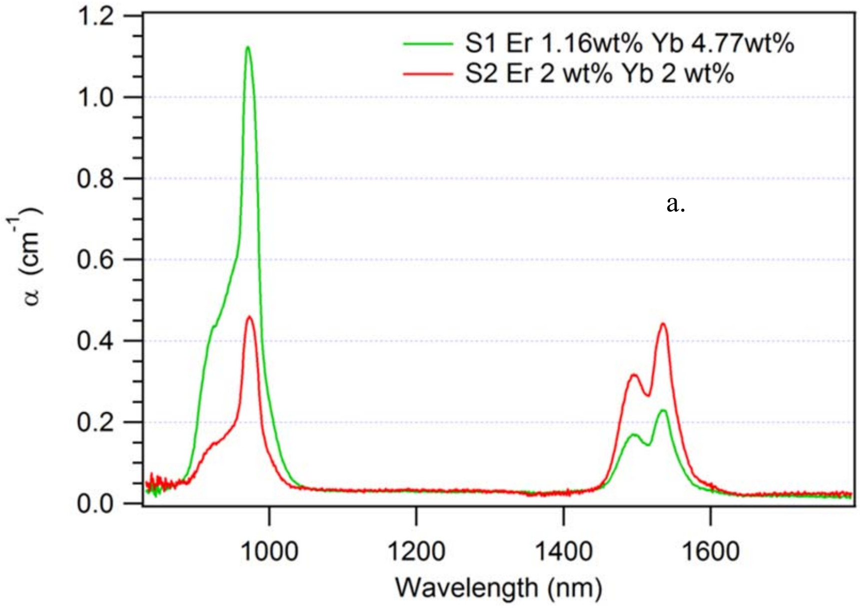

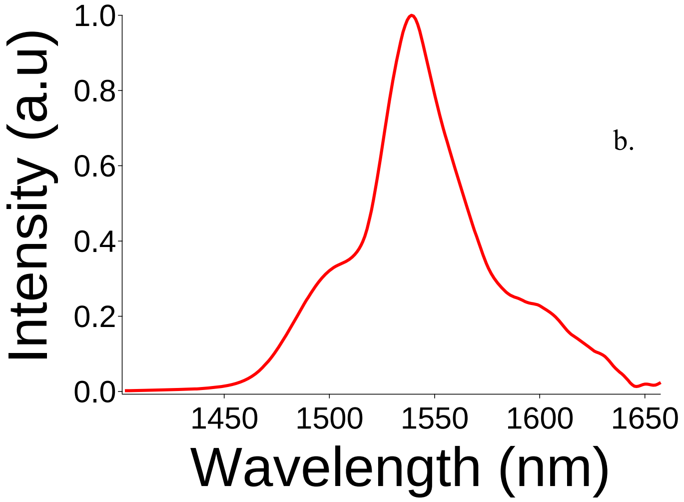

Figure 2-17. a. Measure absorption spectrum for 2 different glass samples, and b. measured emission spectrum for Er^{3+}(1.16 wt%), Yb^{3+}(4.77 wt%): IOG-1.

2.6.3 Tm:germanate glass

Recent development of solid-state lasers operating in the eye-safe region near 2 µm has been motivated by potential applications in spectroscopy [85], medicine [86] and LIDAR [87]. Tm^{3+}-doped lasers have been widely used to develop lasers operating near the 2 µm spectral regime. The energy diagram for a Tm^{3+} ion is shown in Figure 2-18. A pump photon near 800 nm is absorbed to excite the ground-state electron from $^3H_6$ to the $^3H_4$ level, which then decays to the $^3F_4$ level. The lasing action near 2 µm corresponds to the $^3F_4 \rightarrow {}^3H_6$ transition. The $^3H_4 \rightarrow {}^3F_4$ -transition can also promote another nearby Tm^{3+} ion to the $^3F_4$ level from the ground state by a cross-relaxation process. This process can potentially result in an internal quantum efficiency of up to 200%, allowing slope efficiencies approaching 80%. Another advantage of Tm^{3+}-doped gain media is the broad absorption band near 800 nm that can be pumped by commercially available laser diodes.

High-power operation has been demonstrated in a Tm^{3+}-doped fibre laser [88]. Figure 2-19 shows the measured absorption and emission spectra of a Tm:germanate glass developed by Dr. Xian Feng for the work described in the thesis. It can be seen that the emission bandwidth exceeds more than 100 nm, which means that sub 100- fs sources could potentially be developed. An ion-implanted Tm:lead germanate planar waveguide laser has previously been demonstrated at a laser threshold of 89 mW [89] and a femtosecond-written Tm:fluorogermanate glass channel waveguide laser [90] has been demonstrated with a threshold of 80 mW and a slope efficiency of up to 6%.

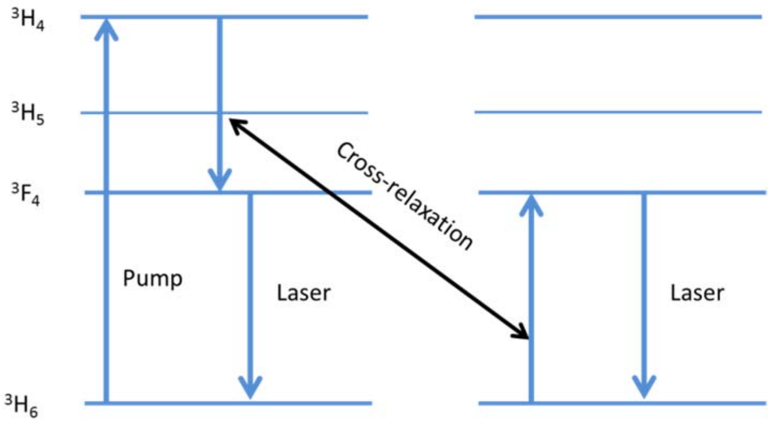

Figure 2-18. Tm^{3+} energy diagram.

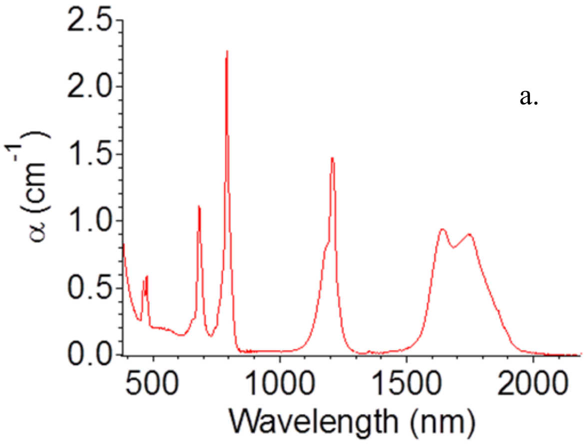

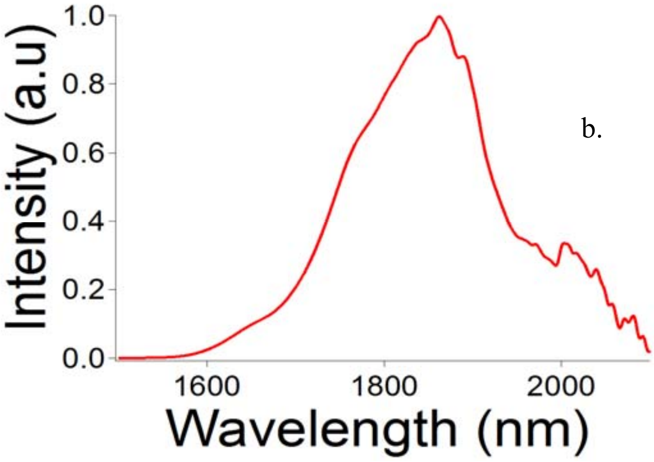

Figure 2-19. a. Measured absorption, and b. emission spectra for the Tm:germanate glass.

2.6.4 Ti:sapphire

Ti:sapphire [91] is a widely used crystal for tuneable and mode-locked lasers with pulses as short as 4 fs being achieved. The absorption spectrum for a bulk Ti:sapphire crystal is shown in Figure 2-20 (a) [92]. The fluorescence spectrum of a thin film grown by pulsed laser deposition (PLD) by Alberto Sposito for this project is shown in Figure 2-20, and it can be seen that emission extends from 650 nm to 1000 nm. The spike near 700 nm is due to the Chromium impurities present in the crystal [93].

PLD has been used to fabricate Ti:sapphire on sapphire waveguide lasers [94] but with relatively high propagation losses. The Ti:sapphire on sapphire waveguides grown by the PLD group at the ORC during the course of this project were also high loss, and therefore this work was not pursued any further and has not been discussed in this thesis.

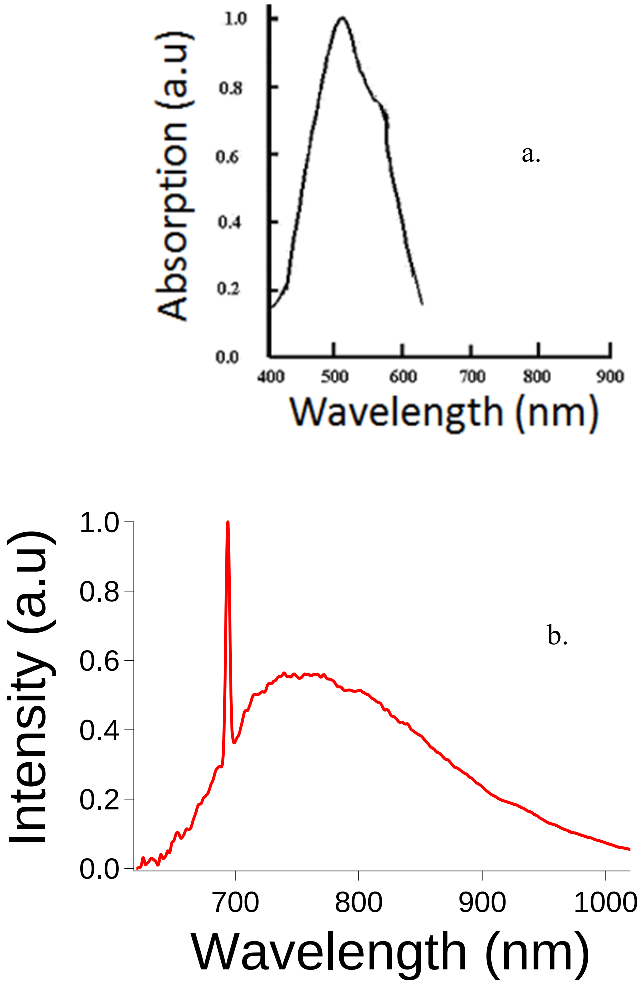

Figure 2-20. a. Absorption spectrum [92], and b. measured emission spectrum of Ti:sapphire.

Table 2-3 summarises the optical properties of the Er^{3+},Yb^{3+}:IOG-1 glass, Tm:germanate glass and Ti:sapphire gain media.

Table 2-3 Optical properties of Er^{3+},Yb^{3+}: IOG-1 glass, Tm:germanate glass and Ti:sapphire

Property	Er^{3+},Yb^{3+}: IOG-1 [77]	Tm:Germanate [95]	Ti:sapphire [96]
Emission maxima (nm)	1534	1865	790
Emission cross-section (m^2)	6.6×10^{-25}	2.3×10^{-25}	41×10^{-24}
Absorption maxima (nm)	974.6	790	492
Absorption cross-section (m^2)	2×10^{-25}	5.6×10^{-25}	6.4×10^{-24}
Fluorescence lifetime (ms)	10	0.8	3.2×10^{-3}
Refractive index	1.5 @ 1.5 µm	1.56 @ 2 µm	1.76 @ 633 nm

2.7 Conclusions

In this chapter, the basic concepts relevant to this project have been discussed. The propagation of modes in a one-dimensional waveguide was first described, followed by the effective-index method for calculating the modes in a two-dimensional waveguide, which is of more interest from the point of view of this project. Since, all the mode-locking results in this project were achieved using waveguides fabricated by ion-exchange, a basic introduction to the diffusion theory was given and an expression for the refractive index profile was derived. Finally, the WKB method for calculating the propagation modes in an ion-exchanged waveguides was discussed.

The laser gain media used for this project fall in the class of quasi-3-level lasers and the theory for such systems was discussed. Starting from the rate equations, the expression for the laser threshold and the slope efficiency was derived. Next, mode-locking theory for generating ultra-short pulses was described with a description of saturable absorption, SESAMs, quantum-dot-doped glasses and soliton mode-locking.

Following which, the rationale behind using waveguide lasers for this project has been explained.

Finally, the properties of the gain media namely: Yb:RTP, Yb,KYW, Yb:IOG-1 glass, Yb:YAG, Er,Yb:IOG-1 glass, Tm:germanate glass and Ti:sapphire were discussed and the emission spectra for each gain medium was presented.

2.8 References

1. Okamoto, K., *Fundamentals of Optical Waveguides* 2006: Academic Press.
2. Lee, D.L., *Electromagnetic principles of integrated optics* 1986: Wiley.
3. Davis, K.M, Miura, K., Sugimoto, N., and Hirao, K., *Writing waveguides in glass with a femtosecond laser*. Opt. Lett., 1996. **21** (21): p. 1729-1731.
4. Bain, F. M., Lagatsky, A. A., Thomson, R. R., Psaila, N. D., Kuleshov, N. V., Kar, A. K., Sibbett, W. and Brown, C. T. A. *Ultrafast laser inscribed Yb:KGd(WO_4)$_2$ and Yb:KY(WO_4)$_2$ channel waveguide lasers.* Opt. Express, 2009. **17** (25): 22417-22422.
5. Siebenmorgen, J., Calmano, T., Petermann, K.,Huber, G. *Highly efficient Yb:YAG channel waveguide laser written with a femtosecond-laser.* Opt. Express, 2010 **18** (15): p.16035-16041.
6. Izawa, T. and Nakagome, H., *Optical waveguide formed by electrically induced migration of ions in glass plates.* Applied Physics Letters, 1972. **21** (12): p. 584-586.
7. Giallorenzi, T. G., West, E. J., Kirk, R., Ginther, R. and Andrews, R. A., *Optical Waveguides Formed by Thermal Migration of Ions in Glass.* Appl. Opt., 1973. **12** (6): p. 1240-1245.
8. Ramaswamy, R.V. and Srivastava, R., *Ion-exchanged glass waveguides: a review.* Lightwave Technology, Journal of, 1988. **6** (6): p. 984-1000.
9. Lilienhof, H. J., Voges, Edgar, Ritter, D. and Pantschew, B., *Field-induced index profiles of multimode ion-exchanged strip waveguides.* Quantum Electronics, IEEE Journal of, 1982. **18** (11): p. 1877-1883.
10. Wilie, C.R., *Advanced Engineering Mathematics* 1995, New York: McGraw Hill.
11. Weiss, M.N. and Srivastava, R., *Determination of ion-exchanged channel waveguide profile parameters by mode-index measurements.* Appl. Opt., 1995. **34** (3): p. 455-458.
12. Geusic, J.E., Marcos, H.M. and Van Uitert L.G., *Laser oscillations in Nd-doped yttrium aluminum, yttrium gallium and gadolinium garnets.* Applied Physics Letters, 1964. **4** (10): p. 182-184.
13. Risk, W.P., *Modeling of longitudinally pumped solid-state lasers exhibiting reabsorption losses.* J. Opt. Soc. Am. B, 1988. **5** (7): p. 1412-1423.
14. Lamb, W.E., Jr., *Theory of an Optical Maser.* Physical Review, 1964. **134** (6A): p. A1429-A1450.
15. Krausz, F., Fermann, M. E., Brabec, T., Curley, P. F., Hofer, M., Ober, M. H., Spielmann, C., Wintner, E. and Schmidt, A. J., *Femtosecond solid-state lasers.* IEEE Journal of Quantum Electronics, 1992. **28** (10): p. 2097-2122.
16. Hargrove, L.E., Fork, R.L., and Pollack, M.A., *Locking of He-Ne laser modes induced by synchronous intracavity modulation.* Applied Physics Letters, 1964. **5** (1): p. 4-5.
17. Ippen, E.P., Shank, C.V. and Dienes, A., *Passive mode locking of the cw dye laser.* Applied Physics Letters, 1972. **21** (8): p. 348-350.
18. Keller, U., *Recent developments in compact ultrafast lasers.* Nature, 2003. **424** (6950): p. 831-838.
19. Keller, U., tHooft, G. W., Knox, W. H. and Cunningham, J. E., *Femtosecond pulses from a continuously self-starting passively mode-locked Ti:sapphire laser.* Opt. Lett., 1991. **16** (13): p. 1022-1024.
20. New, G.H.C., *Mode-locking of quasi-continuous lasers.* Optics Communications, 1972. **6** (2): p. 188-192.

21. Keller, U., Miller, D. A. B., Boyd, G. D., Chiu, T. H., Ferguson, J. F. and Asom, M. T., *Solid-state low-loss intracavity saturable absorber for Nd:YLF lasers: an antiresonant semiconductor Fabry Perot saturable absorber.* Opt. Lett., 1992. **17** (7): p. 505-507.
22. Lagatsky, A. A., Leburn, C. G., Brown, C. T. A., Sibbett, W., Zolotovskaya, S. A. and Rafailov, E. U., *Ultrashort-pulse lasers passively mode locked by quantum-dot-based saturable absorbers.* Progress in Quantum Electronics. **34** (1): p. 1-45.
23. Sun, Z., Hasan, T.,Torrisi, F., Popa, D., Privitera, G., Wang, F., Bonaccorso, F., Basko, D.M. and Ferrari, A.C., *Graphene Mode-Locked Ultrafast Laser.* ACS Nano, 2010. **4** (2): p. 803-810.
24. Rozhin, A. G., Sakakibara, Y., Namiki, Shu, Tokumoto, M.,Kataura, H. and Achiba, Y., *Sub-200-fs pulsed erbium-doped fiber laser using a carbon nanotube-polyvinyl alcohol mode locker.* Appl. Phys.Lett., 2006. **88** (5): p. 051118.
25. Keller, U., Weingarten, K. J., Kartner, F. X., Kopf, D., Braun, B., Jung, I. D., Fluck, R., Honninger, C., Matuschek, N. and Aus der Au, J., *Semiconductor saturable absorber mirrors (SESAM's) for femtosecond to nanosecond pulse generation in solid-state lasers.* Selected Topics in Quantum Electronics, IEEE Journal of, 1996. **2** (3): p. 435-453.
26. Keller, U., Chiu, T.H., and Ferguson, J.F., *Self-starting and self-Q-switching dynamics of passively mode-locked Nd:YLF and Nd:YAG lasers.* Opt. Lett., 1993. **18** (3): p. 217-219.
27. Kaminska, M., Liliental-Weber, Z., Weber, E. R., George, T., Kortright, J. B., Smith, F. W., Tsaur, B. Y. and Calawa, A. R., *Structural properties of As-rich GaAs grown by molecular beam epitaxy at low temperatures.* Applied Physics Letters, 1989. **54** (19): p. 1881-1883.
28. Gupta, S., Whitaker, J.F. and Mourou, G.A., *Ultrafast carrier dynamics in III-V semiconductors grown by molecular-beam epitaxy at very low substrate temperatures.* Quantum Electronics, IEEE Journal of, 1992. **28** (10): p. 2464-2472.
29. Haiml, M., Grange, R. and Keller, U., *Optical characterization of semiconductor saturable absorbers.* Applied Physics B: Lasers and Optics, 2004. **79** (3): p. 331-339.
30. Brovelli, L.R., Keller, U. and Chin, T.H., *Design and operation of antiresonant Fabry-Perot saturable semiconductor absorbers for mode-locked solid-state lasers.* Journal of the Optical Society of America B-Optical Physics, 1995. **12** (2): p. 311-322.
31. Kaertner, F. X., Brovelli, L. R., Kopf, D., Kamp, M., Calasso, I. G. and Keller, U., *Control of solid state laser dynamics by semiconductor devices.* Optical Engineering, 1995. **34** (7): p. 2024-2036.
32. Jung, I. D., Brovelli, L. R., Kamp, M., Keller, U. and Moser, M., *Scaling of the antiresonant Fabry Perot saturable absorber design toward a thin saturable absorber.* Opt. Lett., 1995. **20** (14): p. 1559-1561.
33. Sorokina, I. T., Sorokin, E., Wintner, E., Cassanho, A., Jenssen, H. P. and Szipöcs, R., *14-fs pulse generation in Kerr-lens mode-locked prismless Cr:LiSGaF and Cr:LiSAF lasers: observation of pulse self-frequency shift.* Opt. Lett., 1997. **22** (22): p. 1716-1718.
34. Zhang, Z., Torizuka, K., Itatani, T., Kobayashi, K., Sugaya, T. and Nakagawa, T., *Self-starting mode-locked femtosecond forsterite laser with a semiconductor saturable-absorber mirror.* Opt. Lett., 1997. **22** (13): p. 1006-1008.
35. Hönninger, C., Zhang, G., Keller, U. and Giesen, A., *Femtosecond Yb:YAG laser using semiconductor saturable absorbers.* Opt. Lett., 1995. **20** (23): p. 2402-2404.
36. Rivier, S., Petrov, V., Gross, A., Vernay, S., Wesemann, V., Rytz, D. and Griebner, U., *Diffusion Bonding of Monoclinic Yb:KY(WO_4)$_2$/KY(WO_4)$_2$ and its Continuous-Wave and Mode-Locked Laser Performance.* Applied Physics Express, 2008. **1** (11): p. 112601-3.

37. Carvajal, J. J., Ciatto, G., Mateos, X., Schmidt, A., Griebner, U., Petrov, V., Boulon, G., Brenier, A., Peña, A., Pujol, M. C., Aguiló, M. and Díaz, F., *Broad emission band of* Yb^{3+} *in the nonlinear* $Nb{:}RbTiOPO_4$ *crystal: origin and applications.* Opt. Express, 2010. **18** (7): p. 7228-7242.

38. Hönninger, C., Morier-Genoud, F., Moser, M., Keller, U., Brovelli, L. R. and Harder, C., *Efficient and tunable diode-pumped femtosecond Yb:glass lasers.* Opt. Lett., 1998. **23** (2): p. 126-128.

39. Au, J. Aus der, Kopf, D., Morier-Genoud, F., Moser, M., and Keller, U., *60-fs pulses from a diode-pumped Nd:glass laser.* Opt. Lett., 1997. **22** (5): p. 307-309.

40. Spuhler, G. J., Gallmann, L., Fluck, R., Zhang, G., Brovelli, L. R., Harder, C., Laporta, P. and Keller, U., *Passively modelocked diode-pumped erbium-ytterbium glass laser using a semiconductor saturable absorber mirror.* Electronics Letters, 1999. **35** (7): p. 567-569.

41. Lagatsky, A. A., Bain, F. M., Brown, C. T. A., Sibbett, W., Livshits, D. A., Erbert, G. and Rafailov, E. U., *Low-loss quantum-dot-based saturable absorber for efficient femtosecond pulse generation.* Applied Physics Letters, 2007. **91** (23): p. 231111.

42. Rafailov, E. U., White, S. J., Lagatsky, A. A., Miller, A., Sibbett, W., Livshits, D. A., Zhukov, A. E. and Ustinov, V. M., *Fast quantum-dot saturable absorber for passive mode-locking of solid-State lasers.* Photonics Technology Letters, IEEE, 2004. **16** (11): p. 2439-2441.

43. McWilliam, A., Lagatsky, A. A., Brown, C. T. A., Sibbett, W., Zhukov, A. E., Ustinov, V. M., Vasil'ev, A. P., and Rafailov, E. U., *Quantum-dot-based saturable absorber for femtosecond mode-locked operation of a solid-state laser.* Opt. Lett., 2006. **31** (10): p. 1444-1446.

44. Kannan, P., Choudhary, A., Mills, B., Feng, X. and Shepherd, D.P., *Growth of PbSe Quantum Dots Within High-Index Lead-Phosphate Glass for Infrared Saturable Absorbers.* Journal of the American Ceramic Society, 2013. **96** (1): p. 197-200.

45. Kartner, F.X., Jung, I.D. and Keller, U., *Soliton mode-locking with saturable absorbers.* Selected Topics in Quantum Electronics, IEEE Journal of, 1996. **2** (3): p. 540-556.

46. Jung, I. D., Kärtner, F. X., Brovelli, L. R., Kamp, M. and Keller, U., *Experimental verification of soliton mode locking using only a slow saturable absorber.* Opt. Lett., 1995. **20** (18): p. 1892-1894.

47. Hönninger, C., Paschotta, R., Morier-Genoud, F., Moser, M. and Keller, U., *Q-switching stability limits of continuous-wave passive mode locking.* J. Opt. Soc. Am. B, 1999. **16** (1): p. 46-56.

48. Yamazoe, S., Katou, M., Adachi, T. and Kasamatsu, T., *Palm-top-size, 1.5 kW peak-power, and femtosecond (160 fs) diode-pumped mode-locked* $Yb^{3+}{:}KY(WO_4)_2$ *solid-state laser with a semiconductor saturable absorber mirror.* Opt. Lett., 2010. **35** (5): p. 748-750.

49. Pollnau, M. and Romanyuk, Y.E., *Optical waveguides in laser crystals.* Comptes Rendus Physique, 2007. **8** (2): p. 123-137.

50. Mackenzie, J.I., *Dielectric solid-state planar waveguide lasers: A review.* IEEE Journal of Selected Topics in Quantum Electronics, 2007. **13** (3): p. 626-637.

51. Eggleston, J., Kane, T., Kuhn, K., Unternahrer, J. and Byer, R., *The slab geometry laser--Part I: Theory.* Quantum Electronics, IEEE Journal of, 1984. **20** (3): p. 289-301.

52. Krupke, W.F., *Ytterbium solid-state lasers. The first decade.* Selected Topics in Quantum Electronics, IEEE Journal of, 2000. **6** (6): p. 1287-1296.

53. Veasey, D. L., Funk, D. S., Peters, P. M., Sanford, N. A., Obarski, G. E., Fontaine, N., Young, M., Peskin, A. P., Liu, W. C., Houde-Walter, S. N. and Hayden, J. S., *Yb/Er-*

codoped and Yb-doped waveguide lasers in phosphate glass. Journal of Non-Crystalline Solids, 2000. **263-264**: p. 369-381.

54. Liu, H., Nees, J. and Mourou, G., *Diode-pumped Kerr-lens mode-locked Yb:KY(WO_4)$_2$ laser.* Opt. Lett., 2001. **26** (21): p. 1723-1725.
55. Lagatsky, A., Brown, C. T. A., and Sibbett, W., *Highly efficient and low threshold diode-pumped Kerr-lens mode-locked Yb:KYW laser.* Opt. Express, 2004. **12** (17): p. 3928-3933.
56. Endo, M., Ozawa, A. and Kobayashi, Y., *Kerr-lens mode-locked Yb:KYW laser at 4.6-GHz repetition rate.* Opt. Express, 2012. **20** (11): p. 12191-12197.
57. Romanyuk, Y. E., Borca, C.N., Pollnau, M., Rivier, S., Petrov, V. and Griebner, U., *Yb-doped KY(WO_4)$_2$ planar waveguide laser.* Opt. Lett., 2006. **31** (1): p. 53-55.
58. Bain, F. M., Lagatsky, A. A., Kurilchick, S. V., Kisel, V. E., Guretsky, S. A., Luginets, A. M., Kalanda, N. A., Kolesova, I. M., Kuleshov, N. V., Sibbett, W. and Brown, C. T. A., *Continuous-wave and Q-switched operation of a compact, diode-pumped Yb^{3+}:KY(WO_4)$_2$ planar waveguide laser.* Opt. Express, 2009. **17** (3): p. 1666-1670.
59. Geskus, D., Aravazhi, S., Bernhardi, E., Grivas, C., Harkema, S., Hametner, K., Günther, D., Wörhoff, K. and Pollnau, M., *Low-threshold, highly efficient Gd^{3+}, Lu^{3+} co-doped KY(WO_4)$_2$:Yb^{3+} planar waveguide lasers.* Laser Physics Letters, 2009. **6** (11): p. 800-805.
60. Geskus, D., Bradley, J.D, Aravazhi, S., Wörhoff, K. and Pollnau, M., *Poor Man's Channel Waveguide Laser: KY(WO_4)$_2$:Yb.* in *Conference on Lasers and Electro-Optics/Quantum Electronics and Laser Science Conference and Photonic Applications Systems Technologies*. 2008.
61. Bain, F. M., Lagatsky, A. A., Thomson, R. R., Psaila, N. D., Kuleshov, N. V., Kar, A. K., Sibbett, W. and Brown, C. T. A., *Ultrafast laser inscribed Yb:KGd(WO_4)$_2$ and Yb:KY(WO_4)$_2$ channel waveguide lasers.* Opt. Express, 2009. **17** (25): p. 22417-22422.
62. Geskus, D., Aravazhi, S., Grivas, C., Wörhoff, K. and Pollnau, M., *Microstructured KY(WO_4)$_2$:Gd^{3+}, Lu^{3+}, Yb^{3+} channel waveguide laser.* Opt. Express. **18** (9): p. 8853-8858.
63. Zumsteg, F.C., Bierlein J.D., and Gier T.E., *$K_xRb_{1-x}TiOPO_4$: A new nonlinear optical material.* Journal of Applied Physics, 1976. **47** (11): p. 4980-4985.
64. Carvajal, J. J., Solé, R., Gavaldà, Jna, Massons, J., Aguiló, M. and Díaz, F., *Crystal Growth of $RbTiOPO_4$:Nb: A New Nonlinear Optical Host for Rare Earth Doping.* Crystal Growth & Design, 2001. **1** (6): p. 479-484.
65. Mateos, X., Petrov, V., Peña, A., Carvajal, J. J., Aguiló, M., Díaz, F., Segonds, P. and Boulanger, B., *Laser operation of Yb^{3+} in the acentric $RbTiOPO_4$ codoped with Nb^{5+}* Opt. Lett., 2007. **32** (13): p. 1929-1931.
66. Guillien, Y., Ménaert, B., Fève, J. P., Segonds, P., Douady, J., Boulanger, B. and Pacaud, O., *Crystal growth and refined Sellmeier equations over the complete transparency range of $RbTiOPO_4$.* Optical Materials, 2003. **22** (2): p. 155-162.
67. Satyanarayan, M.N., Deepthy, A. and Bhat, H.L., *Potassium Titanyl Phosphate and Its Isomorphs: Growth, Properties, and Applications.* Critical Reviews in Solid State and Materials Sciences, 1999. **24** (2): p. 103-191.
68. Suhara, T. and Fujimura, M., *Waveguide Nonlinear-Optic Devices* 2003: Springer.
69. Carvajal, J. J., Solé, R., Gavaldà, Jna, Massons, J., Segonds, P., Boulanger, B., Brenier, A., Boulon, G., Zaccaro, J., Aguiló, M. and Díaz, F., *Spectroscopic and second harmonic generation properties of a new crystal: Yb-doped $RbTiOPO_4$.* Optical Materials, 2004. **26** (3): p. 313-317.

70. Cugat, J., Solé, R. M., Carvajal, J. J., Pujol, M. C., Mateos, X., Aguiló, M. and Díaz, F., *Green light waveguide demonstration on Yb:Nb:RbTiOPO$_4$/RbTiOPO$_4$ epitaxial layers.* Physics Procedia, 2010. **8**: p. 136-141.
71. Cugat, J., Solé, R., Pujol, M. C., Carvajal, J. J., Mateos, X., Díaz, F. and Aguiló, M., *Waveguiding demonstration on Yb:Nb:RbTiOPO$_4$/RbTiOPO$_4$(0 0 1) epitaxies grown by LPE.* Optical Materials, 2010. **32** (12): p. 1648-1651.
72. Cugat, J., Solé, R., Carvajal, J. J., Mateos, X., Pujol, M. C., Massons, J., Díaz, F. and Aguiló, M., *Efficient Type II phase-matching second-harmonic generation in Ba:Yb:Nb:RbTiOPO$_4$/RbTiOPO$_4$ waveguides.* Opt. Lett., 2011. **36** (10): p. 1881-1883.
73. Lacovara, P., Choi, H. K., Wang, C. A., Aggarwal, R. L. and Fan, T. Y., *Room-temperature diode-pumped Yb:YAG laser.* Opt. Lett., 1991. **16** (14): p. 1089-1091.
74. Honea, E. C., Beach, R. J., Mitchell, S. C., Skidmore, J. A., Emanuel, M. A., Sutton, S. B., Payne, S. A., Avizonis, P. V., Monroe, R. S. and Harris, D. G., *High-power dual-rod Yb:YAG laser*. in *Lasers and Electro-Optics, 2000. (CLEO 2000). Conference on*. 2000.
75. Pelenc, D., Chambaz, B., Chartier, I., Ferrand, B., Wyon, C., Shepherd, D. P., Hanna, D. C., Large, A. C. and Tropper, A. C., *High slope efficiency and low threshold in a diode-pumped epitaxially grown Yb:YAG waveguide laser.* Optics Communications, 1995. **115** (5-6): p. 491-497.
76. http://www.scientificmaterials.com/products/yb-yag.php
77. http://www.schott.com/
78. Bain, F.M., *Yb:tungstate waveguide lasers*, PhD thesis 2010, University of St.Andrews, St. Andrews.
79. http://www.rp-photonics.com/yag_lasers.html.
80. Bradley, J.D.B. and Pollnau, M., *Erbium-doped integrated waveguide amplifiers and lasers.* Laser & Photonics Reviews, 2011. **5** (3): p. 368-403.
81. Obaton, A. F., Bernard, J., Parent, C., Flem, G. Le, Fernandez-Navarro, J. M., Adam, J. L., Myers, M. J. and Boulon, G., *New laser material for eye-safe sources: Yb^{3+}Er^{3}-codoped phosphate glasses*. 1999. in Advanced Solid State Lasers, Vol. 26 of OSA Trends in Optics and Photonics (Optical Society of America, 1999), paper WB12.
82. Schlager, J. B., Callicoatt, B. E., Silverman, K. L., Mirin, R. P., Sanford, N. A. and Veasey, D. L., *Mode-locked erbium/ytterbium co-doped waveguide laser*. in *Lasers and Electro-Optics, 2001. CLEO '01.*
83. Schlager, J. B., Callicoatt, B. E., Mirin, R. P. and Sanford, N. A., *Passively mode-locked waveguide laser with low residual jitter.* IEEE Photonics Technology Letters, 2002. **14** (9): p. 1351-1353.
84. Schlager, J. B., Callicoatt, B. E., Mirin, R. P., Sanford, N. A., Jones, D. J. and Ye, J., *Passively mode-locked glass waveguide laser with 14-fs timing jitter.* Opt. Lett., 2003. **28** (23): p. 2411-2413.
85. Walsh, B.M., *Review of Tm and Ho materials; spectroscopy and lasers.* Laser Physics, 2009. **19** (4): p. 855-866.
86. Theisen, D., Ott, V., Bernd, H.-W., Danicke, V., Keller, R. and Brinkmann, R., *Cw high-power IR laser at 2 μm for minimally invasive surgery.* Proc. SPIE 5142, Therapeutic Laser Applications and Laser-Tissue Interactions, 2003: p. 96-100.
87. Henderson, S. W., Suni, P. J. M., Hale, C. P., Hannon, S. M., Magee, J. R., Bruns, D. L. and Yuen, E. H., *Coherent laser radar at 2 μm using solid-state lasers.* Geoscience and Remote Sensing, IEEE Transactions on, 1993. **31** (1): p. 4-15.

88. Wu, J., Yao, Z., Zong, J. and Jiang, S., *Highly efficient high-power thulium-doped germanate glass fiber laser.* Opt. Lett., 2007. **32** (6): p. 638-640.
89. Shepherd, D. P., Brinck, D. J. B., Wang, J., Tropper, A. C., Hanna, D. C., Kakarantzas, G. and Townsend, P. D., *1.9-µm operation of a Tm:lead germanate glass waveguide laser.* Opt. Lett., 1994. **19** (13): p. 954-956.
90. Fusari, F., Thomson, R. R., Jose, G., Bain, F. M., Lagatsky, A. A., Psaila, N. D., Kar, A. K., Jha, A., Sibbett, W. and Brown, C. T. A., *Lasing action at around 1.9 µm from an ultrafast laser inscribed Tm-doped glass waveguide.* Opt. Lett., 2011. **36** (9): p. 1566-1568.
91. Moulton, P.F., *Spectroscopic and laser characteristics of* $Ti:Al_2O_3$. J. Opt. Soc. Am. B, 1986. **3** (1): p. 125-133.
92. http://www.worldoflasers.com/lasertypes-solid.htm.
93. Buchert, J., Katz, A. and Alfano, R., *Laser action in emerald.* Quantum Electronics, IEEE Journal of, 1983. **19** (10): p. 1477-1478.
94. Anderson, A. A., Eason, R. W., Hickey, L. M. B., Jelinek, M., Grivas, C., Gill, D. S. and Vainos, N. A., *Ti:sapphire planar waveguide laser grown by pulsed laser deposition.* Opt. Lett., 1997. **22** (20): p. 1556-1558.
95. Choudhary, A., Kannan, P., Mackenzie, J. I., Feng, X. and Shepherd, D.P., *Ion-exchanged* Tm^{3+}*:glass channel waveguide laser.* Opt. Lett., 2013. **38** (7): p. 1146-1148.
96. http://www.rp-photonics.com/titanium_sapphire_lasers.html

Chapter 3 Experimental techniques

3.1 Introduction

In this chapter all the experimental techniques used during the course of the project have been described. First, a description of the waveguide fabrication techniques applied in this work is presented. Liquid-phase epitaxy (LPE) is described as a method of growing rare-earth-doped single-crystal thin films as active planar waveguides. These films can then be etched by ion-beam milling or reactive ion etching (RIE) to create channel waveguides. Direct channel waveguide fabrication via ion-exchange in rare-earth-doped glass is also discussed. This is followed by the description of the continuous-wave laser experimental setup and three methods of estimating the losses in a waveguide. Finally, the experimental setup for mode-locking experiments is discussed.

3.2 Fabrication of waveguides

In this section, the various methods of fabricating waveguides are discussed.

3.2.1 Liquid-phase epitaxy

LPE [1, 2] is an elegant way of growing a single-crystal layer from a molten solution onto a seed crystal. For waveguide laser applications, the layer is normally the same crystal as the substrate (ensuring good epitaxial growth) but with additional rare-earth doping to enable lasing and to give the small increase in refractive index required for optical confinement. A platinum crucible filled with a molten solution with the required constituents is kept at a controlled temperature by a resistance-heated furnace. On cooling, the solution becomes super-saturated and a seed crystal is immersed into the solution. The crystal is rotated and pulled out of the solution slowly (~1 μm/min) to avoid thermal stress. This results in the deposition of a good quality epitaxial layer on the crystal.

This method has the advantage of being a thermodynamic equilibrium process and thus good quality layers with thickness ranging from 1-100 μm can be grown at a fast rate. Low-loss waveguide laser operation has previously been demonstrated in several laser systems, including Yb:KYW [3] and Yb:YAG [4]. Waveguiding has also been demonstrated in Yb:RTP systems with low propagation losses [5]. Therefore, LPE is a method of choice for the fabrication of Yb^{3+}-based waveguide laser systems with the potential for ultra-short pulse operation. LPE-grown Yb^{3+}-doped waveguides were obtained from the Scientific and Practical Materials Research Centre in Minsk, Belarus and from the FICMA (Physics and Crystallography of Materials) group at the Universitat Rovira i Virgili (URV), Tarragona, Spain.

3.2.2 Fabrication of channels

After the growth of single-crystalline films by LPE by our collaborators, I structured the films by either ion-beam milling or RIE in the Integrated Photonics Cleanroom (IPC) at the University of Southampton to form channel waveguides. Alternatively, the substrate may be etched before the LPE-growth and then polished after growth to leave “inverted-rib” waveguides. This fabrication technique is discussed in detail in chapter 4. Ion-exchange can be carried out in glasses through photolithographically patterned masks to directly give channel waveguides. These channel fabrication techniques are discussed in the following sub-sections.

3.2.2.1 Ion-beam milling

Ion milling is a physical etching technique. It involves energetic argon (Ar^{+}) ions bombarding the substrate at high velocities in a vacuum chamber. A mask can be deposited on the substrate that protects the underlying region from the ions. As a result, exposed areas are etched, forming waveguides. Rib waveguides have been formed in Ti: sapphire using a combination of pulsed-laser deposition (PLD) and Ar-ion milling [6-8] and in Yb:KYW [9] using a combination of LPE and Ar-ion milling. A typical ion-beam milling process, as used in this thesis, involves the following steps (summarised in Figure 3-1):

1. A photoresist layer is spun on the active layer.
2. The resist is then exposed to ultra-violet (UV) light through a chromium mask which has the desired waveguide features. Subsequent development of the resist results in the mask pattern being transferred onto the photoresist layer.
3. The sample is then etched using Ar^{+} ion-beam milling with a current of 100 mA and a voltage of 500 V.
4. After this, the resist is removed by solvents and plasma-ashing for 20 minutes with RIE power of 200 W, pressure of 50 mTorr and O_2 flow rate of 10 sccm, which removes any organic impurities present on the substrate.

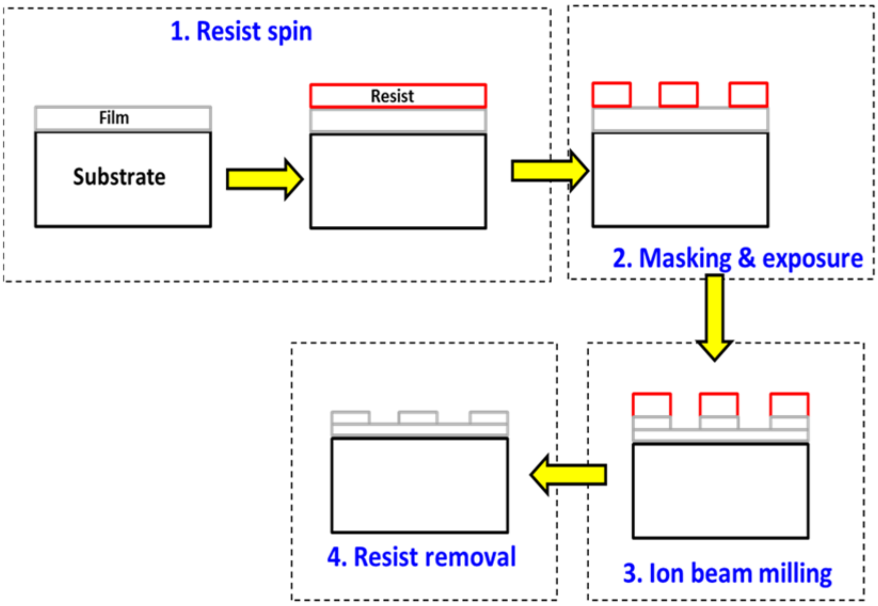

Figure 3-1. Ion-beam milling process to fabricate channel waveguides.

3.2.2.2 Reactive ion etching

RIE is a commonly used method for etching materials in the semiconductor industry and it is a combination of chemical and physical etching. The masked substrate that needs to be etched is placed on an electrode, which is inside a vacuum chamber filled with the chemical reactants. An RF field is applied between the electrode and the chamber (which acts as the ground), resulting in the formation of a plasma. This creates an electric field in the chamber and the substrate becomes negatively charged. The positive ions in the plasma are attracted towards the substrate and they collide with it, dissociate the chemical bonds and thus etch the material.

This technique has previously been used to fabricate waveguides in both Ti:sapphire [10] and Yb:KYW [11]. The advantages of RIE over physical processes like ion-beam milling are that this process is more selective (between the etching of the substrate and the mask) and gives nearly perpendicular side walls. A typical RIE process for etching substrates is described below (and summarised in Figure 3-2):

1. A thin layer of metal mask (Chromium) is deposited on a substrate by e-beam evaporation.
2. After which a layer of photoresist is spun on the sample.
3. The resist is then photolithography patterned to give rib features.

4. The Cr layer is then wet etched to transfer the resist pattern onto the Cr layer.
5. The resist is removed by solvent cleaning.
6. The hard-masked substrates are then etched in an RIE chamber where the pattern of the Cr mask is transferred on the substrate.
7. Following this, the Cr mask is chemically removed.

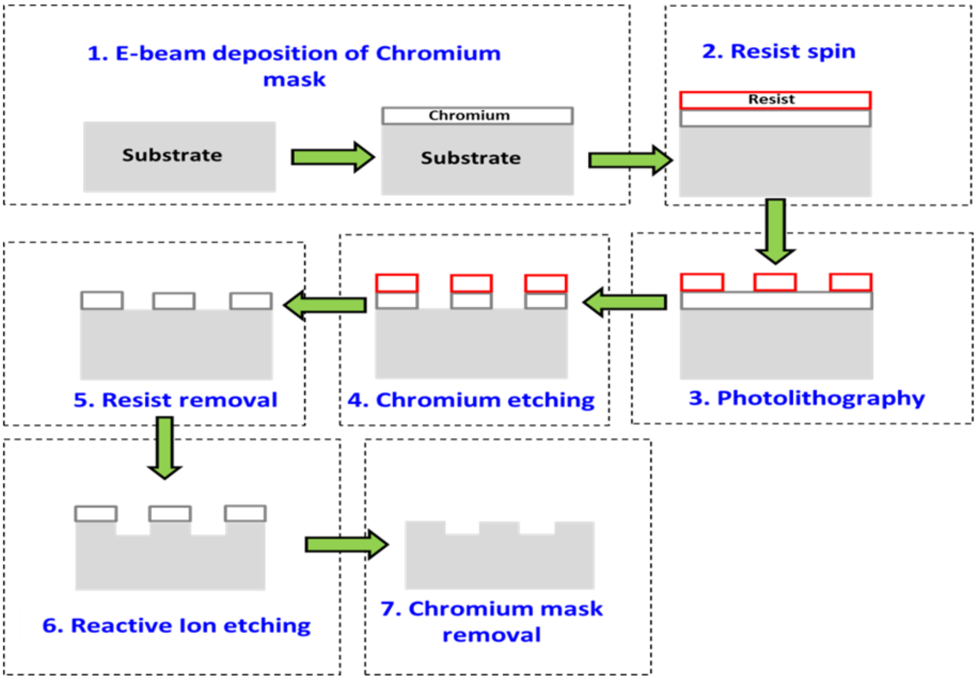

Figure 3-2. A typical RIE process to etch rib features in a substrate.

After the etching conditions were optimised on a bare substrate, the optimised conditions were then used for etching the active layers to fabricate waveguides.

3.2.2.3 Ion-exchange

Ion-exchange is a well-established technique of directly fabricating low-loss channel waveguides in glasses [12] as discussed in the previous chapter. The polished glass samples, which are rich in sodium (Na^+) ions, are coated with an aluminium (Al) film by e-beam evaporation, following which standard photolithography techniques are applied to define channel openings widths in a photoresist layer deposited on top of the Al-film. The Al film is then chemically etched and the resist mask is then removed. These metal patterned samples are then immersed in a molten solution of salt containing both K^+ ions and Ag^+ ions as discussed in the previous chapter. The Na^+ ions are exchanged with the K^+ and Ag^+, which increases the refractive index. The duration and time of the ion-exchange determines the index contrast and the diffusion depth. The ion-exchange process is outlined in Figure 3-3.

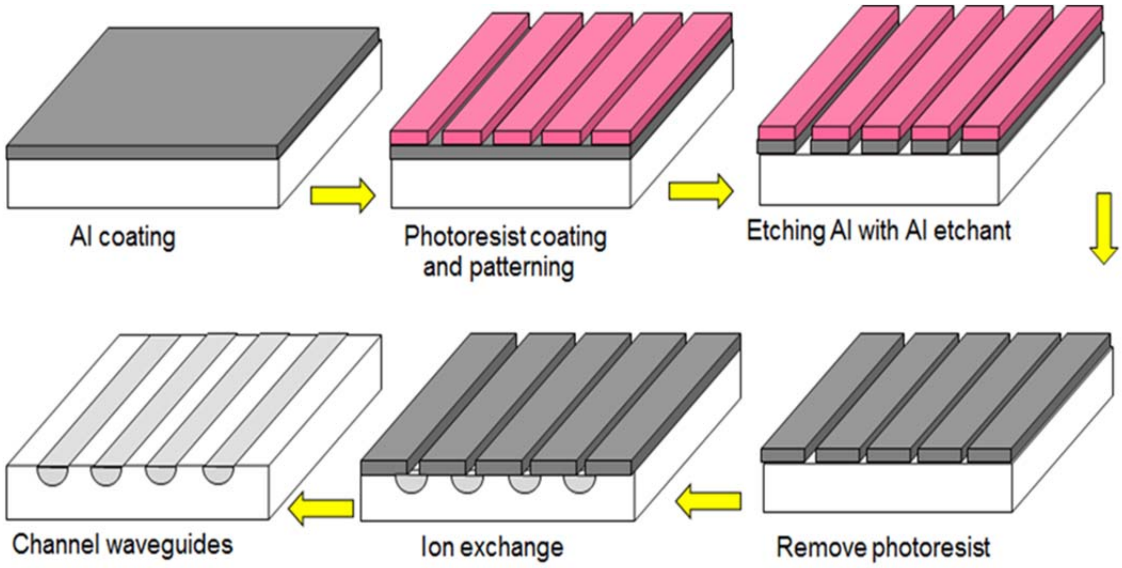

Figure 3-3. An ion-exchange technique.

3.2.3 Polishing and characterisation of waveguides

After the waveguides were fabricated, they were end-polished to minimise scattering losses off the end-facets and to define the monolithic laser cavity. The waveguide samples were sequentially lapped by powdered Al_2O_3 with particle sizes 9 µm, 3 µm and 1 µm until no scratches were visible on the surface. Following the lapping procedure, the waveguides were polished by a chemical (SF1) to optical quality i.e. such that the waveguide features were clearly distinguishable under an optical microscope.

A non-contact profiler (Zescope from Zemetrics) was used for surface topography and a scanning electron microscope (SEM) was used for qualitative analysis of the waveguides. M-line measurements [13] were used for the measurement of the effective indices of the propagation modes.

3.3 Laser Experiments

In this sub-section, various experimental details are presented. First, the experimental setup used for continuous wave laser experiments is presented. Following which, three different methods for loss estimation in waveguides: Caird plots, relaxation oscillation frequency measurements and transmission measurements are discussed. Finally, the experimental setup for mode-locking experiments is presented.

3.3.1 Experimental setup for continuous-wave laser operation

The polished waveguide samples were mounted on copper blocks using silver paint to enable a good thermal contact. The mounts were held on a 4-axis stage to optimise the launch of the pump into the waveguide. The pump laser, which was either a Ti:sapphire laser or a single-mode, fibre-coupled laser diode, was tuned to a wavelength that coincided with the peak of the absorption of the rare-earth dopant. A mechanical chopper was installed in the beam path to help observe when the laser action occurred by the transition from the slow time-response of the fluorescence to the fast response of the laser-action. A neutral density filter was used to vary the incident power on the waveguide and a half-wave plate controlled the polarisation. An aspheric lens or a microscope objective of the appropriate focal length was used to efficiently launch the pump into the waveguide. Thin dielectric mirrors (thickness < 200 μm) or bulk mirrors were end-butted on the waveguide facets using fluorinated liquid (Sigma Aldrich, FC-70) to form the laser cavity. A collimating lens or an objective was used to collimate the output from the waveguide and a dichroic filter was used to separate the pump and the laser wavelengths. The laser beam was then incident on various diagnostic tools to characterise the performance of the waveguide.

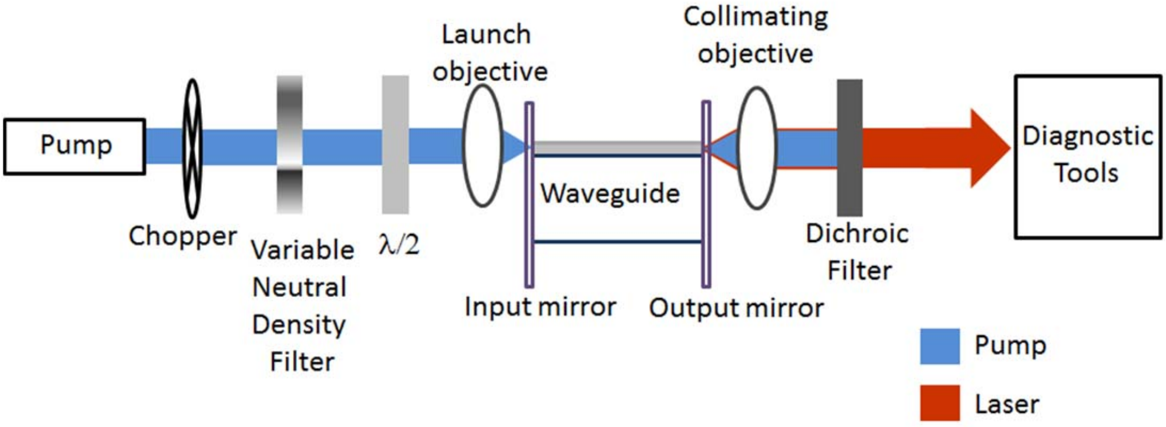

Figure 3-4. Setup for CW lasing experiments.

The diagnostic tools included:

1. Power meter, to study the input-output power characteristics.

2. Fibre–coupled optical spectrum analyser (OSA) to measure the laser spectral characteristics. Alternatively, a fibre was placed on top of the waveguide and connected to an OSA to measure the fluorescence spectra unaffected by re-absorption for quasi-three-level laser systems such as Yb^{3+}.
3. CMOS camera to capture and measure the mode profiles.
4. A mode profiler to measure the beam quality (M^2).
5. Photodiode to measure the fluorescence lifetime.

When the laser diode was used as the pump source, a combination of a half wave plate and optical isolator were additionally installed in the pump path to minimise feedback into the laser diode from the waveguide.

3.3.2 Estimation of losses

For waveguide lasers, the estimation of propagation losses (L) is quite important; as they are much higher than in bulk and can adversely affect the performance of the laser. In this sub-section, three methods of estimating losses in waveguides have been discussed.

3.3.2.1 Caird plots

Waveguide losses for 4-level lasers are often determined via the Findlay-Clay method [14]. In this method equation (2.54) can be rewritten as:

$$\mathrm{P_{th}} = K(L_{tot} - \mathrm{lnR}) \tag{3.1}$$

where, all the physical constants and spatial properties have been written as K, L_{tot} is the round-trip loss including the re-absorption loss (for quasi-3-level systems) and the propagation loss (L_{RT}) and R is the reflectivity of the output coupler. The threshold powers can be plotted against –lnR and the x-intercept gives the value of the total round-trip propagation loss (excluding the output coupler loss).

However, for quasi-3-level lasers the total round-trip losses may be dominated by the re-absorption loss making the determination of the propagation loss less accurate. A more accurate method to calculate the propagation losses in a quasi-3-level laser is the Caird plot method [15]. Equation (2.55) can be rearranged as:

$$\frac{1}{\eta_s} = \frac{1}{\eta_\mathrm{o}} + \frac{L}{\eta_\mathrm{o}}\frac{1}{T} \tag{3.2}$$

where, η_o is the intrinsic slope efficiency (the theoretical maximum efficiency) and L is the percentage round-trip propagation loss. Plotting $1/\eta_s$ vs. $1/T$ allows the estimation of the propagation losses. This method has been used to calculate the propagation losses in the following chapters. Using Findlay-Clay and Caird plots together, the re-absorption losses can also be estimated.

3.3.2.2 Relaxation oscillations

An alternative method of calculating the total cavity loss can be derived from the relaxation oscillations of the laser [16]. For a quasi-3-level waveguide laser with fluorescence lifetime τ, doping concentration N, effective absorption cross section at the laser wavelength σ, refractive index n and speed of light c, the angular frequency of relaxation oscillations ω is given by:

$$\omega^2 = \frac{\gamma_c}{\tau}(r-1)(1+\frac{N\sigma c}{n\gamma_c}) \tag{3.3}$$

where, r is the ratio of pump power to the threshold power (P/P_{th}) and cavity decay rate (γ_c) of the laser cavity is the inverse of the photon cavity lifetime (τ_c) and is given by:

$$\gamma_c = \frac{\beta c}{2nl} \tag{3.4}$$

β is the total loss including the mirror loss and l is the length of the waveguide.

By plotting ω^2 versus $r-1$, the cavity decay constant can be determined from the slope (m) of the linear fit to the data. Rearranging equation (3.3) gives:

$$\gamma_c = m\tau - \frac{N\sigma c}{n} \tag{3.5}$$

The total propagation loss can be determined using equation (3.5) and (3.4) and then subtracting the mirror loss.

3.3.2.3 Transmission measurements

For waveguides that did not lase, transmission measurements were used to give a rough estimate of the propagation losses as well as the degree of absorption. The measurement of absorbed powers in waveguides is difficult in comparison to bulk lasers due to the uncertainty in launch efficiencies and the higher propagation losses in waveguides. In this section a simple method to calculate the absorption, loss and launch efficiency from transmission measurements is described. Two cases have been discussed: low-loss waveguides and high-loss waveguides.

a. *Measurement of absorption in low-loss waveguides*

In the case of a low loss waveguide, the loss is assumed to be negligible. The pump is tuned at the absorption wavelength of the waveguide under test and launched into the waveguide using a suitable objective (at low pump power) and the output power is collected directly by a power meter (no output objective, see Figure 3-5). The transmission (T_{guide}) is given by equation 3.6 [4], assuming that only the core is doped and that un-launched light passes through the substrate:

$$T_{guide} = T_{obj} T_F^2 (1 - \eta_L A) \tag{3.6}$$

where T_{obj} is the transmission of the objective, T_F is (1-Fresnel loss), η_L is the launch efficiency and A is the absorption.

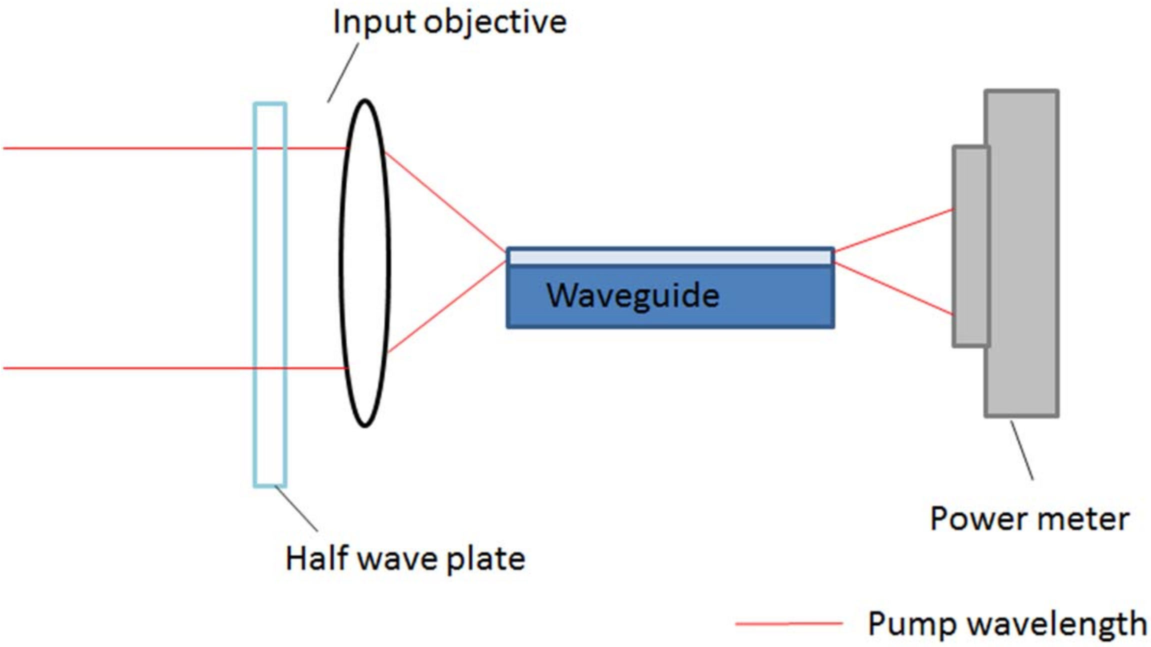

Figure 3-5. Experimental setup to measure $\eta_L A$ for the low-loss case.

The pump is then allowed to pass through the substrate and the transmission (T_S) is given by:

$$T_S = T_{obj} T_F^2 \tag{3.7}$$

It is possible to calculate the product $\eta_L A$ from this method, and by assuming 100% launch efficiency the lower limit on the absorption (A) can be calculated.

b. Measurement of loss, absorption and launch efficiency in high-loss waveguides

The previous approach assumes 100% launch efficiency and is only applicable for low-loss waveguides and does not allow the estimation of propagation losses. When the losses are unknown for a waveguide or a tuneable laser is available, it is preferable to modify the above method as described below.

A similar experiment as described in the low-loss case is carried out and when the pump is launched into the waveguide, T_{guide} is modified as (assuming that the light which is not launched into the waveguide propagates in the substrate only):

$$T_{guide} = T_{obj}T_F^2(\eta_L(1-A)(1-L_s) + (1-\eta_L)) \tag{3.8}$$

Where, L_s is the percentage single-pass propagation loss. An output objective is installed next and the non-guided light is spatially filtered and the transmitted power (T_{go}) is measured and is given by the following expression:

$$T_{go} = T_{obj}^2\eta_L T_F^2(1-A)(1-L_s) \tag{3.9}$$

Then the pump is tuned away from absorption and the spatially filtered output is measured. The transmission (T_{ga}) is given by:

$$T_{ga} = T_{obj}^2\eta_L T_F^2(1-L_s) \tag{3.10}$$

Using equation 3.7 to 3.10 it is possible to evaluate A, L_s and η_L. This is the least accurate method of the three that have been described because of the high errors in the estimation of each value. However, it is a useful experiment to carry out before lasing experiments to get a rough estimate of the propagation losses.

3.3.3 Mode-locking experiments

For the mode-locking experiments, the setup described in section 3.3.1 was modified as shown in Figure 3-6. A fibre-coupled laser diode (3S photonics) operating at either 974 nm or 981 nm was used as the pump source as all the mode-locked lasers reported in this thesis are based on Yb^{3+} or Er^{3+},Yb^{3+} doping. The pump was collimated by an aspheric lens, after which a combination of a half-wave plate and an optical isolator was installed to protect the laser diode from power reflected from the waveguide. An aspheric lens was used to couple the pump into the waveguide through an output-coupler mirror which had >99% transmission at the pump wavelength. The waveguide cavity was terminated by a SESAM, which was either directly end-butted to the waveguide using fluorinert or aligned to the waveguide using a 5-axis stage. A dichroic mirror placed just before the input lens reflects the waveguide laser output towards the diagnostic tools as shown in Figure 3-6. There were two additional diagnostic tools that were used when compared to CW experiments:

1. Autocorrelator, to measure the pulse duration.
2. Radio frequency spectrum analyser to measure the repetition-rates.

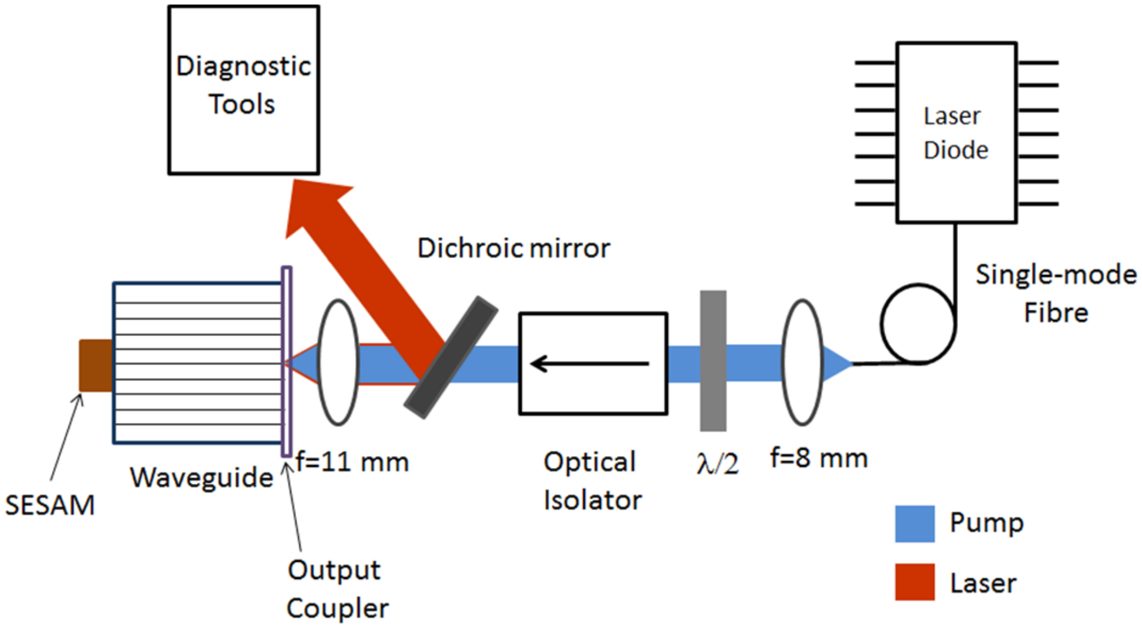

Figure 3-6. Setup for mode-locking experiments.

3.4 Conclusions

In this chapter, all the experimental techniques relevant to this thesis have been discussed. The growth of active layers by LPE was explained first, following which the procedure for the patterning of the active film via RIE or ion-beam milling was summarised. Then the ion-exchange technique for making channel waveguides directly in active glasses was presented.

The experimental setup for continuous-wave (CW) characterisation of waveguides was presented next. In this section, three techniques for estimating propagation losses in the waveguides: Caird plots, relaxation oscillations technique and transmission method were discussed. Finally, the setup used for the mode-locking experiments carried out with the Yb^{3+}-doped IOG-1 Glass and Er^{3+},Yb^{3+}-doped IOG-1 was presented.

3.5 References

1. Pollnau, M. and Romanyuk, Y. E., *Optical waveguides in laser crystals.* Comptes Rendus Physique, 2007. **8** (2): p. 123-137.
2. Ferrand, B., Chambaz, B. and Couchaud, M., *Liquid phase epitaxy: A versatile technique for the development of miniature optical components in single crystal dielectric media.* Optical Materials, 1999. **11** (2-3): p. 101-114.
3. Romanyuk, Y. E., Borca, C.N., Pollnau, M., Rivier, S., Petrov, V. and Griebner, U., Yb-doped KY(WO4)2 planar waveguide laser. Opt. Lett., 2006. 31 (1): p. 53-55.
4. Pelenc, D., Chambaz, B., Chartier, I., Ferrand, B., Wyon, C., Shepherd, D. P., Hanna, D. C., Large, A. C. and Tropper, A. C., *High slope efficiency and low threshold in a diode-pumped epitaxially grown Yb:YAG waveguide laser.* Optics Communications, 1995. **115** (5-6): p. 491-497.
5. Cugat, J., Solé, R., Pujol, M. C., Carvajal, J. J., Mateos, X., Díaz, F. and Aguiló, M., *Waveguiding demonstration on Yb:Nb:RbTiOPO*$_4$*/RbTiOPO*$_4$*(0 0 1) epitaxies grown by LPE.* Optical Materials, 2010. **32** (12): p. 1648-1651.
6. Pollnau, M., Grivas, C., Laversenne, L., Wilkinson, J., Eason, R. and Shepherd, D., *Ti:Sapphire waveguide lasers.* Laser Physics Letters, 2007. **4** (8): p. 560-571.
7. Grivas, C., Shepherd, D. P., May-Smith, T. C., Eason, R. W., Pollnau, M., Crunteanu, A. and Jelinek, M., *Performance of* Ar^+ *milled Ti:sapphire rib waveguides as single transverse-mode broadband fluorescence sources.* Quantum Electronics, IEEE Journal of, 2003. **39** (3): p. 501-507.
8. Grivas, C., Shepherd, D., May-Smith, T., Eason, R. and Pollnau, M., *Single-transverse-mode Ti:sapphire rib waveguide laser.* Opt. Express, 2005. **13** (1): p. 210-215.
9. Geskus, D., Aravazhi, S., Grivas, C., Wörhoff, K. and Pollnau, M., *Microstructured* $KY(WO_4)_2:Gd^{3+}, Lu^{3+}, Yb^{3+}$ *channel waveguide laser.* Opt. Express. **18** (9): p. 8853-8858.
10. Lancok, J., Jelinek, M., Bulir, J. and Machac, P., *Study of the fabrication of the channel waveguide in Ti:sapphire layers.* Laser Physics, 1998. **8** (1): p. 303-306.
11. Borca, C. N., Romanyuk, Y. E., Gardillou, F., Pollnau, M., Bernal, M. P. and Moretti, P., *Optical channel waveguides in* $KY(WO_4)_2:Yb^{3+}$ .in *2006 Conference on Lasers & Electro-Optics/Quantum Electronics and Laser Science Conference (CLEO/QELS)*. 2006. Long Beach, CA, USA.
12. Ramaswamy, R.V. and Srivastava, R., *Ion-exchanged glass waveguides: a review.* Lightwave Technology, Journal of, 1988. **6** (6): p. 984-1000.
13. Ulrich, R. and Torge, R., *Measurement of Thin Film Parameters with a Prism Coupler.* Appl. Opt., 1973. **12** (12): p. 2901-2908.
14. Findlay, D. and Clay, R. A., *The measurement of internal losses in 4-level lasers*. *Phys. Lett*, 1966 **20**: p.277
15. Caird, J. A., Payne, S. A., Staber, P. R., Ramponi, A. J., Chase, L. L. and Krupke, W. F., *Quantum electronic properties of the* $Na_3Ga_2Li_3F_{12}:Cr^{3+}$ *laser.* Quantum Electronics, IEEE Journal of, 1988. **24** (6): p. 1077-1099.
16. Salcedo, J.R., Sousa, J.M. and Kuzmin, V.V., *Theoretical treatment of relaxation oscillations in quasi-three-level systems.* Applied Physics B, 1996. **62** (1): p. 83-85.

Chapter 4 Yb-doped waveguides

4.1 Introduction

In the previous chapters, the necessary background relevant for this project has been presented. In this chapter, the results obtained with different Ytterbium (Yb^{3+})-doped waveguides are discussed. Mode-locking results obtained with Yb^{3+}-doped phosphate glass (IOG-1 Schott [1]) are discussed first, followed by the continuous wave (CW) lasing and waveguiding results obtained with Yb:RTP, and finally by the lasing results achieved with an inverted Yb:KYW rib waveguide laser.

4.2 Yb^{3+}:IOG-1 glass

As discussed in 2.6.1.1, Yb:IOG-1 glass is a very promising candidate for the development of mode-locked waveguide lasers owing to a broad emission bandwidth and ease of fabrication of waveguides via ion-exchange.

4.2.1 Fabrication

The waveguides were fabricated by Dr. Pradeesh Kannan using a standard ion-exchange technique discussed in 3.2.2.3. A 200-nm-thick layer of aluminium (Al) was deposited on the polished Yb^{3+}:IOG-1 glass samples, following which a 1.3-μm-thick photoresist layer (S1813) was spin-coated onto them. Using photolithography, channel openings of widths 1 μm to 10 μm in steps of 0.2 μm were opened and the resist-masked samples were chemically etched to transfer the photoresist mask into the metal layer. After removal of the photoresist by solvents, the samples were immersed in a molten salt mixture comprising of 45 mol% KNO_3 − 50 mol% $NaNO_3$ − 5 mol% $AgNO_3$ and kept at a temperature of 325°C for 10 minutes in an ion-exchange furnace. The Na^+ ions in the glass mixture were exchanged with the K^+ and the Ag^+ ions in the ion-exchange melt, leading to a local increase in the refractive index. Next, the metal mask was chemically removed and the glass samples were polished to lengths of 20 mm, 9.4 mm, 8 mm and 6.5 mm. The refractive index contrast at 632.8 nm was measured in a planar waveguide fabricated with the same ion-exchange parameters using the prism-coupling technique [2]. An index contrast of 0.066 with respect to the bare glass and a diffusion depth of 6.9 μm was calculated by fitting the expected ion-exchange refractive-index profile to the measured mode indices [3].

4.2.2 Experimental setup

The experimental setup was as shown schematically in Figure 3-6. The waveguides were pumped by a single-mode, fibre-coupled laser diode from 3S photonics delivering a power of up to 850 mW in the 980 nm absorption band of Yb:IOG-1. The output was collimated by an aspheric lens of focal length 8 mm and was coupled into the waveguide through an output coupling mirror (R=98% or R=96% at the lasing wavelength and R<0.1% at the pump wavelength) by an aspheric lens with focal length 11 mm such that beam spot radius of 4.4 μm was made at the waveguide facet. After the 8-mm lens, a combination of a half-wave plate and an optical isolator protected the laser diode from back reflections from the waveguide. The waveguide cavity was completed by end-butting a high reflectivity (HR) mirror on a thin substrate to the other end-facet of the waveguide for continuous wave characterisation. A dichroic mirror at an angle of 30º to the incident pump beam, transmitted >99% of the pump and reflected >97% of the laser beam. The reflected laser beam off the dichroic mirror was then isolated by a combination of a half-wave plate and an isolator and then coupled into a single-mode fibre, the output of which was split by a 3 dB coupler and fed into a spectrometer and a radio frequency (RF) spectrum analyser. A flip mirror was placed before the coupling stage, which could be used to steer the beam to an autocorrelator. The output power was measured before the isolator.

The CW characterisation was carried out with an HR mirror terminating the cavity and the mode-locking experiments were carried out by replacing the HR mirror with a SESAM (Batop GmbH, 0.4% modulation depth, 0.3% non-saturable losses, 0.5 ps relaxation time, 90 $\mu J/cm^2$ saturation fluence). The SESAM was initially directly end-butted onto the waveguide for the 5 GHz experiments [4] and then put on a copper block for the 10 GHz, 12 GHz and 15 GHz experiments [5]. The copper block was mounted on a 3-axis stage, to enable accurate control of the gap between the SESAM and the waveguide facet. The gap was monitored by placing a ×100 objective and a CCD camera above the setup. Figure 4-1 shows a photograph of the waveguide laser cavity, the input objective and the monitoring ×100 objective.

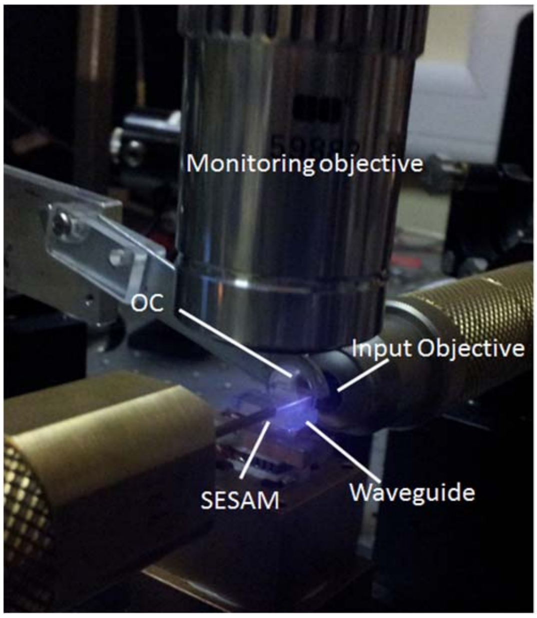

Figure 4-1. Photograph of the mode-locked waveguide laser.

4.2.3 Experimental results

In this section, the experimental results obtained with the 20-mm, 9.4-mm, 8-mm and 6.5-mm-long samples have been presented. The first set of experiments was carried out with the 20-mm-long sample and the CW characterisation and beam characteristics have been discussed in the first sub-section. The mode-locking results with the 9.4-mm-long, 8-mm-long and 6.5-mm-long waveguides have been discussed in the subsequent sub-sections.

4.2.3.1 20-mm-long waveguide

The CW characterisation of the 20-mm-long sample was carried out using a cavity formed by an HR mirror on one end and no output coupler (OC) on the other end. This is effectively a 96% OC due to the 4% Fresnel reflection from the glass. The pump had a central wavelength of 980.6 nm and a maximum output power of 750 mW. All the waveguides were characterised to identify the waveguides with the highest output power. Approximately 90 of the 100 fabricated guides were found to lase with the maximum pump power. The ~10 waveguides that did not lase could have had some fabrication imperfections. It was found that the waveguides fabricated using mask opening widths between 2 μm and 6 μm all had very similar performance. At an incident power of 608 mW, a maximum output power of 164 mW was measured giving a slope efficiency of 66.2%.

A 2% OC was then put on a flexure mount and aligned with respect to the waveguide to optimise the laser performance. A maximum output power of 108 mW and a slope efficiency of 27.3% were observed. Finally, with a 4% OC, a maximum output power of 156 mW and a slope efficiency of 31.5% were observed. The input-output characteristics for all 3 cavities are shown in Figure 4-2. From the Caird analysis described in section 3.3.2.1, the propagation losses were calculated to be <0.1 dB/cm.

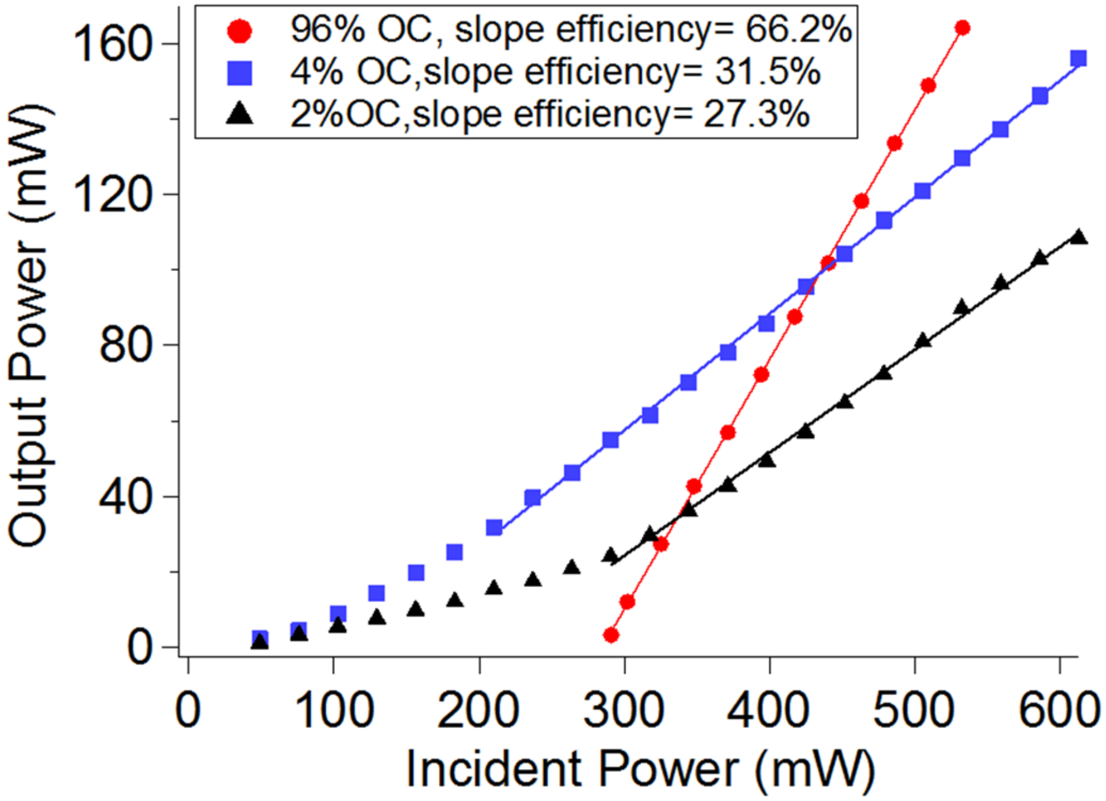

Figure 4-2. CW input-output characteristics of the 20-mm-long waveguide laser.

The collimated laser output was focussed by a 100-mm-focal-length lens on to a beam profiler kept on a translation stage. The beam profiler was translated along the propagation direction of the laser and the beam radii were measured at different positions and were plotted against the position (Z). From these measurements the M^2 was calculated [6] to be 1.05 in the horizontal (parallel to the plane of the waveguides) direction (x) and 1.08 in the vertical directions (y) implying a nearly diffraction limited beam. The M^2 measurements for both the directions are shown in Figure 4-3.

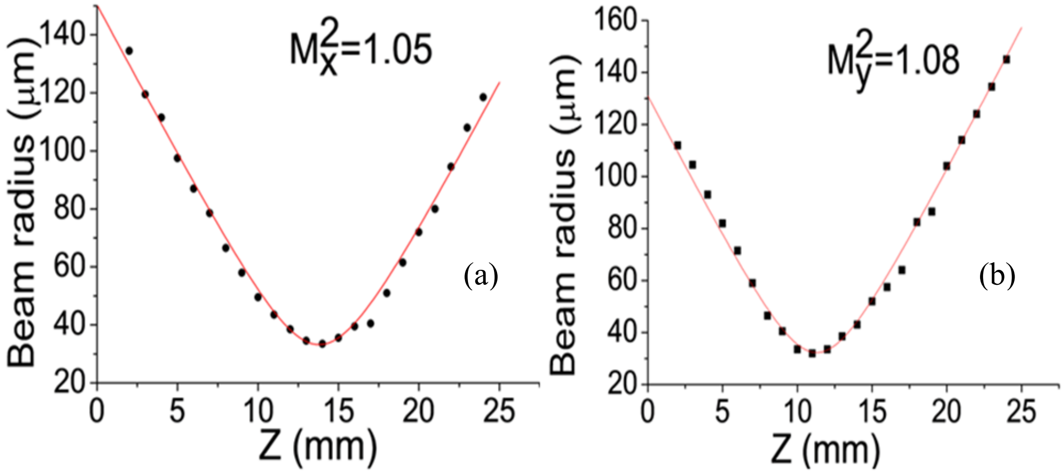

Figure 4-3. M^2 measurements for (a) x-direction, and (b) y-direction directions with fit (red lines) to the experimental data.

The lasing mode was then imaged onto a CCD camera using a ×10 objective with the result shown in Figure 4-4. The output was observed to be single mode with beam diameters of 11.6 μm in the x-direction and 7.6 μm in the y-direction, which is in good agreement with the theoretical values of 12.1 μm and 7.1 μm in the x and y-direction respectively (simulated using OlympIOs). This result corresponds to a mask opening width of 5 μm and only one mode is supported at the laser wavelength.

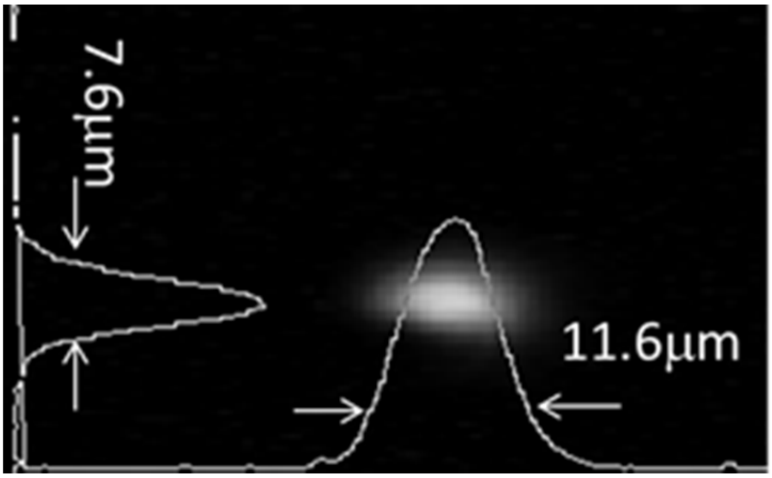

Figure 4-4. Image of the near-field laser mode on a CCD camera.

The HR mirror was then replaced by the SESAM for mode-locking experiments. The SESAM was end-butted against the waveguide using fluorinated liquid (Fluorinert, FC-70, Sigma Aldrich) to hold it in place and a 2% OC was used at the other end of the cavity. It was found that mode-locked operation could only be achieved by introducing micrometre-scale gaps between the waveguide and the OC. No mode-locking was observed when the OC was in direct contact with the waveguide. On increasing the gap, it was found that for a small range of the separation, stable mode-locking was achieved. On increasing the gap even further, the power decreased and mode-locking was lost. This is attributed to the Gires-Tournois Interferometer (GTI) effect, which is discussed later. The GTI effect introduces controllable group velocity dispersion (GVD) into the cavity and the laser operates in the soliton mode-locking [7] regime.

The output power as a function of the incident power is shown in Figure 4-5. With the 2% OC, CW operation was observed up to a pump power of 183 mW (and an output power of 7.7 mW). On increasing the pump power further, Q-switched mode-locking was observed through characteristic multiple peaks on the RF spectrum up to a pump power of 344 mW. Beyond this pump power, stable and self-starting mode-locking was achieved. Pure mode-locking was confirmed via the observation of a sharp peak in the RF spectrum (Figure 4-6), measured with a resolution bandwidth (RBW) of 1 kHz and a span of 1 MHz. The repetition-rate was measured to be 4.9 GHz.

The mode-locking threshold in terms of the output power was 19.7 mW, which corresponds to a critical pulse energy ($E_{p,\mathrm{crit}}$ in equation 2.59) of 0.2 nJ (within the cavity). A maximum output power of 31.6 mW was obtained at a pump power of 505 mW. Beyond this pump power, it was found that the RF spectrum became unstable, with multiple peaks being observed possibly due to the onset of multi-pulsing. Stable mode-locking was observed for output powers between 19.7 mW and 31.6 mW, with a corresponding slope efficiency of 7.4% with respect to the incident power.

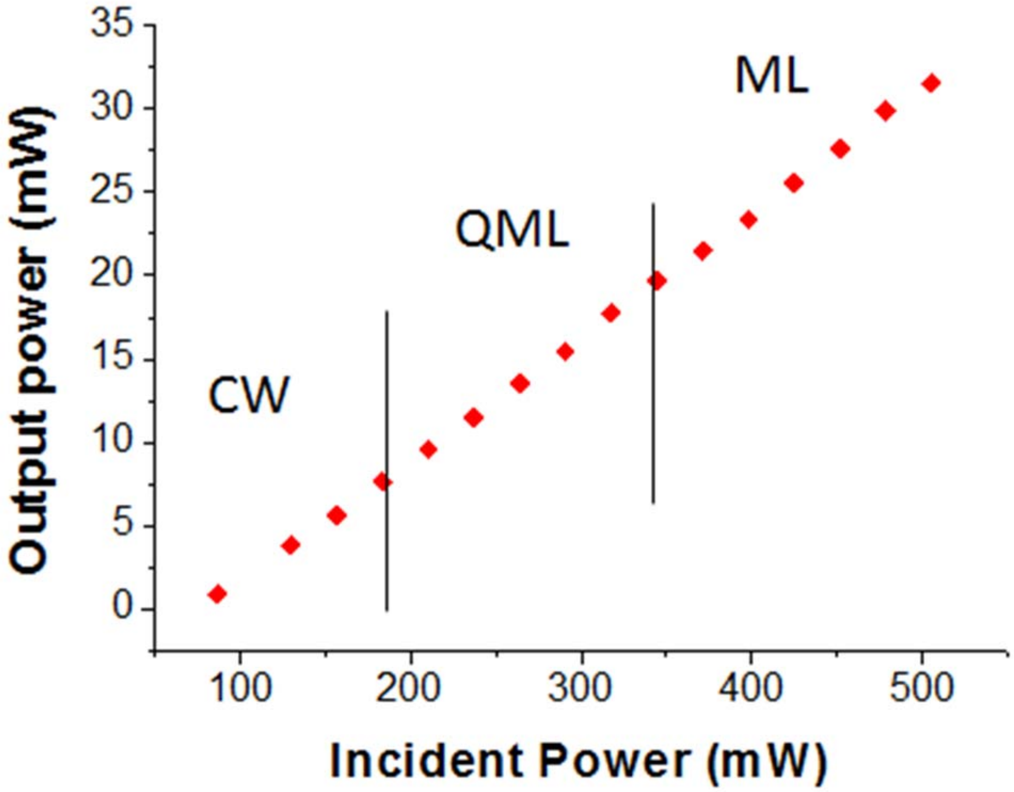

Figure 4-5. Input-output characteristics for the mode-locked waveguide laser with a 2% OC.

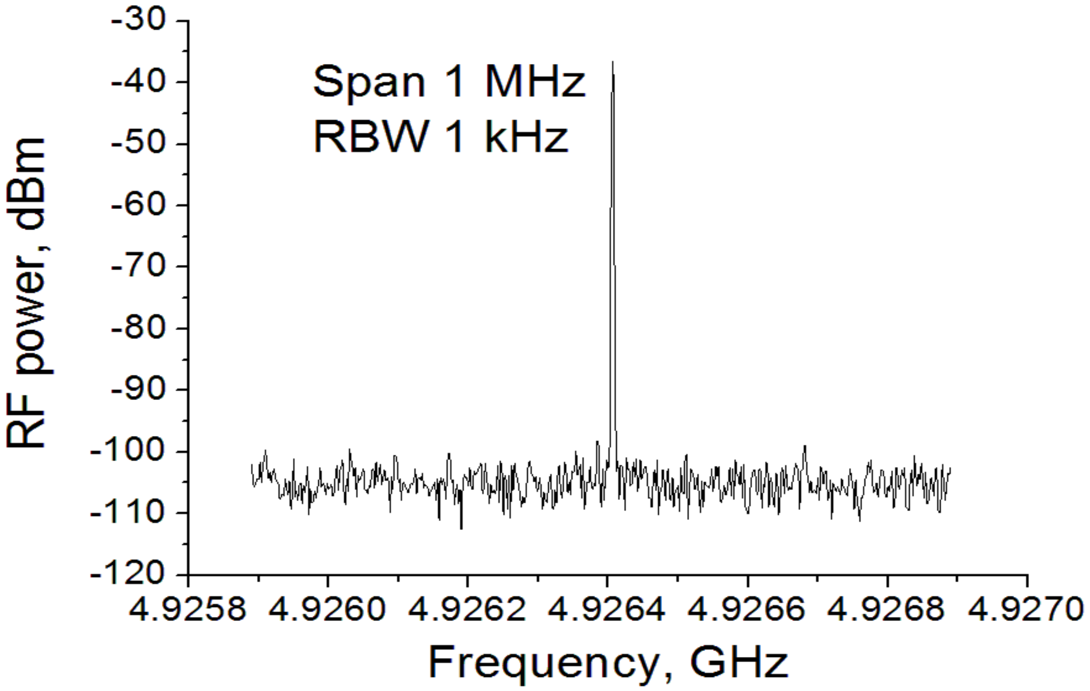

Figure 4-6. The RF spectrum for the mode-locked waveguide laser (span = 1 MHz and RBW = 1 KHz).

The RF spectrum, measured at a span of 30 GHz and a RBW of 1 MHz, is shown in Figure 4-7 showing the fundamental frequency at 4.9 GHz and 5 harmonics.

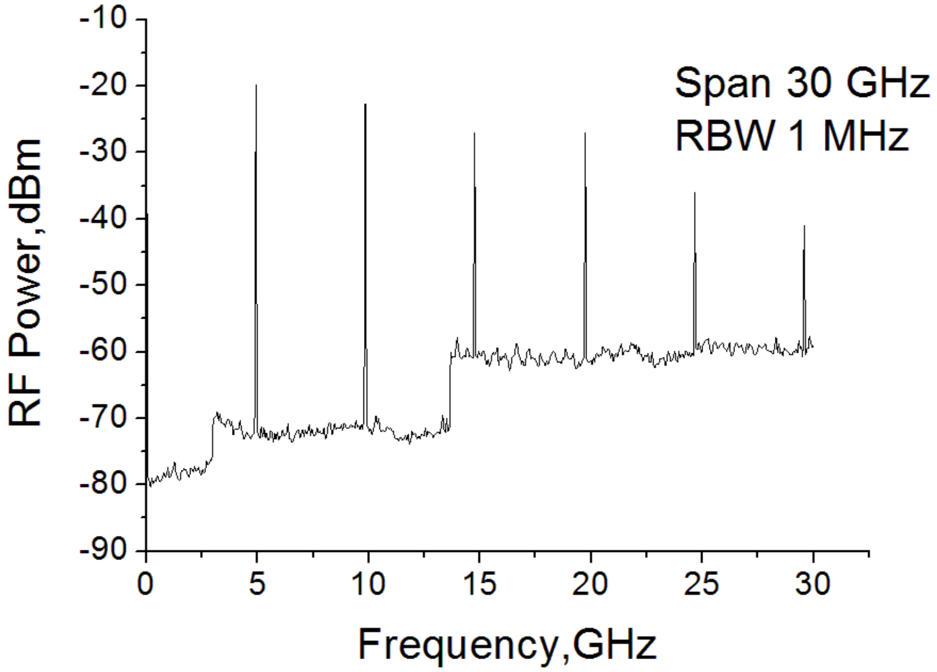

Figure 4-7. The RF spectrum for the mode-locked waveguide laser (span = 30 GHz and RBW = 1 MHz).

The autocorrelation trace was measured at an output power of 30 mW and is shown in Figure 4-8 (a). A good sech^2 fit to the experimental data was observed with a full-width-at-half-maximum (FWHM) pulse width of 740 fs. The optical spectrum is shown in Figure 4-8 (b) and it can be seen that the optical spectrum was centred on 1058.3 nm and had a FWHM bandwidth of 2.3 nm. The time-bandwidth product was calculated to be 0.46, which is larger than the ideal value of 0.315 for a bandwidth-limited sech^2 pulse. The bandwidth-limited value of pulse was 530 fs, suggesting that using external pulse compression could lead to even shorter pulses.

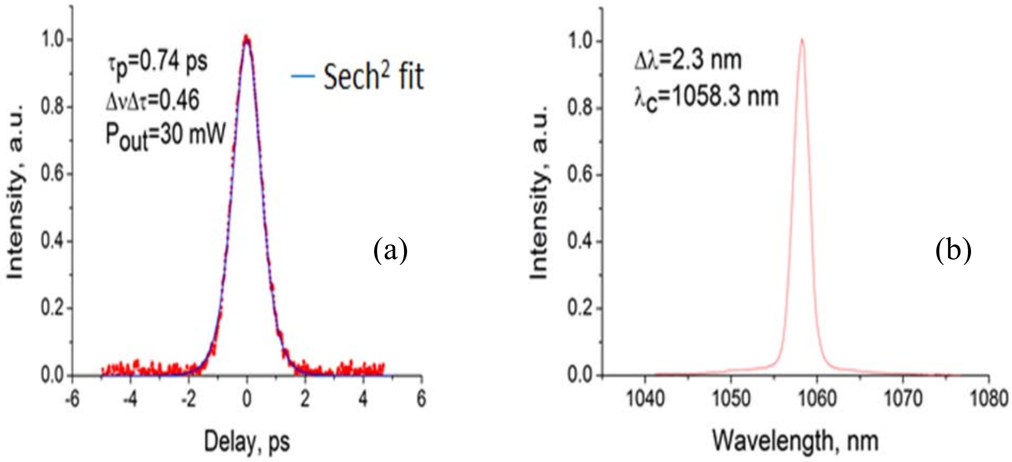

Figure 4-8. (a)Autocorrelation trace, and (b) optical spectrum measured at an output power of 30 mW for the mode-locked waveguide laser.

Next, the 2% OC was replaced by a 4% OC to extract more output power. The input-output characteristics for the laser are shown in Figure 4-9. CW operation was observed up to an input pump power of 156 mW with a corresponding output power of 12 mW. When the pump power was increased beyond 156 mW, Q-switched mode-locking was observed until an input power of 236 mW and an output power of 35 mW. This corresponds to an internal pulse energy of 0.18 nJ, which is consistent with the value of 0.2 nJ observed with the 2% OC. This is as expected, because the critical pulse energy to overcome Q-switched mode-locking is independent of the output coupler. Stable, self-starting mode-locking was achieved beyond this pump power. A maximum power of 81 mW was achieved and the slope efficiency for mode-locked operation was measured to be 27%. On increasing the pump power, the RF spectrum became unstable possibly due to the onset of multi-pulsing.

It should be noted that the slope efficiencies obtained using SESAMs is lower than those obtained during the CW characterisation (Figure 4-2). This can be explained by the increased losses due to 1) the non-saturable losses of the SESAM and 2) the gap between the mirror and the end-face.

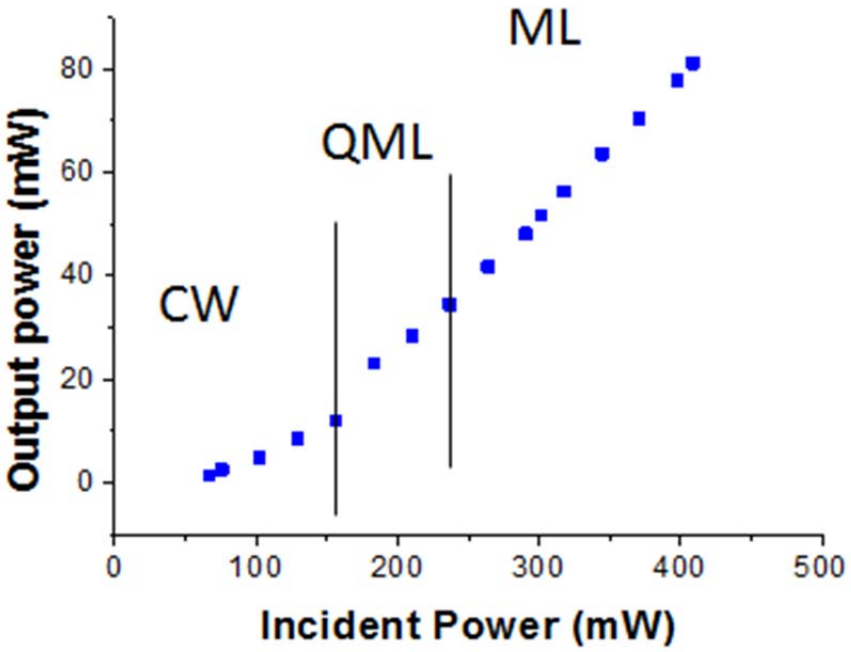

Figure 4-9.Input-output characteristics for the mode-locked waveguide laser with a 4% OC.

The autocorrelation trace and the output spectrum were measured at an output power of 81 mW and are shown in Figure 4-10 (a) and (b) respectively. A good fit to a sech^2 profile was found with pulse duration of 800 fs. The optical spectrum was centred at a wavelength of 1052 nm and had a FWHM bandwidth of 2.1 nm, giving a time-bandwidth product of 0.46.

Therefore it can be concluded that using a higher output coupler can be beneficial for extracting more output power without significantly compromising on the pulse widths and without increasing the time-bandwidth product.

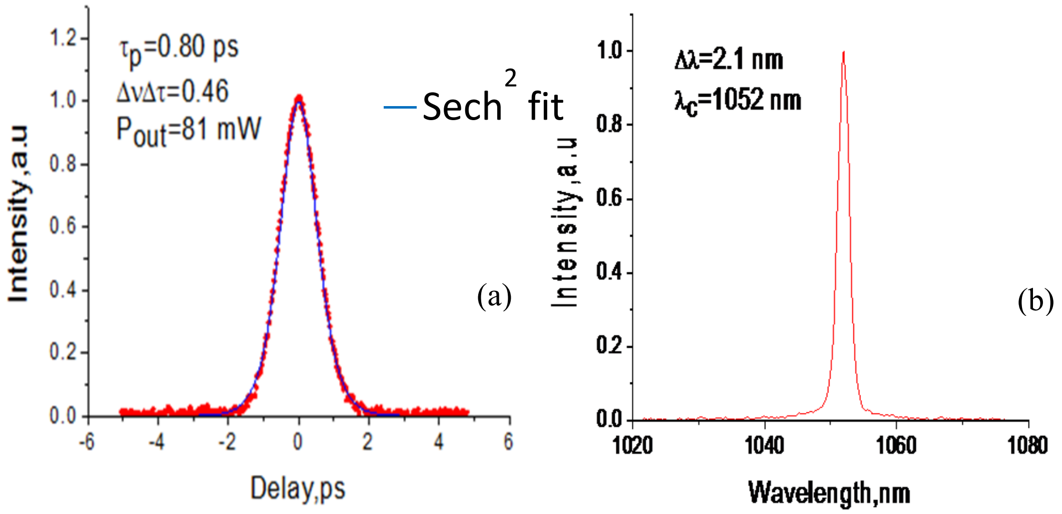

Figure 4-10. (a)Autocorrelation trace and (b) optical spectrum measured at an output power of 81 mW for the mode-locked waveguide laser.

4.2.3.2 9.4-mm-long waveguide

After the initial success with the 20-mm-long waveguide, and the discovery of the importance of the gap on the performance of the mode-locked laser, the setup was modified in order to precisely control the gap between the SESAM and the waveguide facet and hence accurately control the GVD. For the 20-mm-long waveguide laser experiments, the SESAM was end-butted directly onto the waveguide. However, for the shorter samples it was placed on a copper mount, which was on a flexure stage that allowed fine control over the separation between the SESAM and the waveguide. The separation was monitored by a combination of a ×100 objective and a CCD camera (as was shown in Figure 4-1).

A 980.6-nm laser diode delivering 750 mW of output power was used for the previous experiments and was also initially used for pumping the 9.4-mm-long waveguide sample. The absorption within the waveguide was measured by launching the pump into the waveguide and measuring the transmitted power with no mirrors attached. The absorption was found to be relatively low for this shorter waveguide with a measured pump transmission of ~8% (assuming a 100% launch efficiency) at lasing threshold as seen from Figure 4-11.

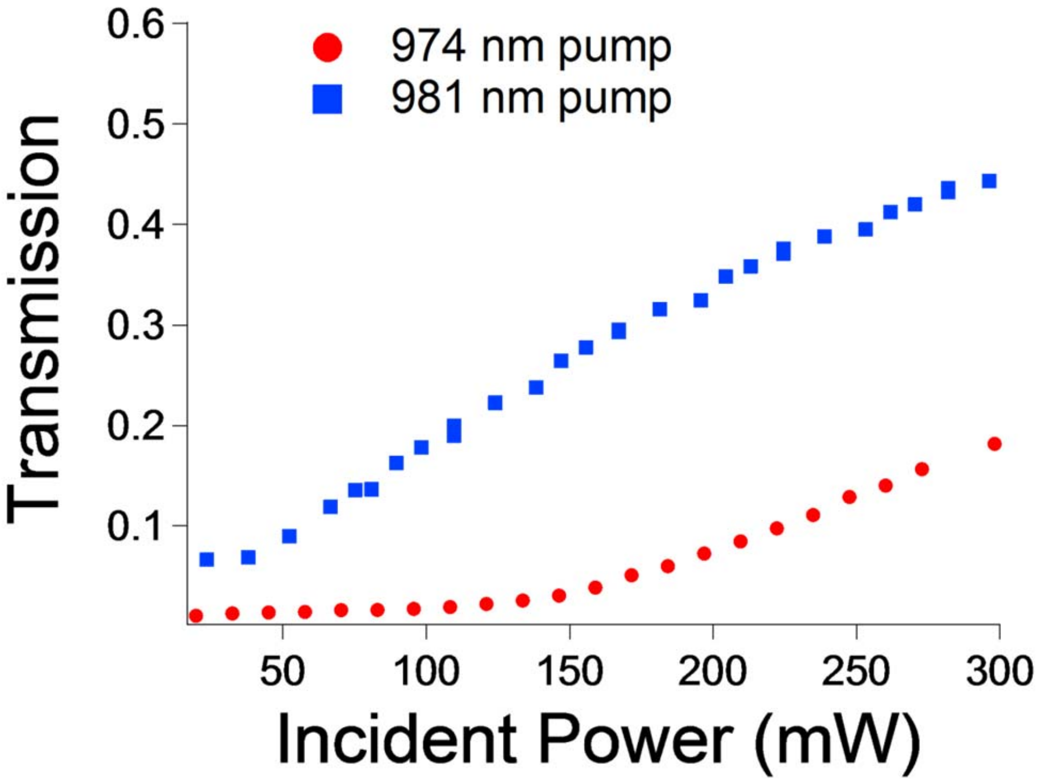

Figure 4-11. Transmission vs. Incident power for the 974 nm and 981 nm pumping.

The pump was then replaced by a 973.4 nm laser diode, which was closer to the peak of the absorption band and delivered similar incident power to the waveguide. Using the 973.4 nm pump, a transmission of ~2% was measured at threshold power, as seen from Figure 4-11. Therefore, 973.4 nm pumping was used for the 9.4-mm-long, 8-mm-long and 6.5-mm-long waveguides.

Stable mode-locking was achieved at an output power of 60 mW and for a gap of ~41 μm between the SESAM and the waveguide using a 2% OC. A clean and sharp peak was observed in the RF spectrum at a central frequency of 10.4 GHz, as seen in Figure 4-12. Mode-locked operation was not as stable (with the RF spectrum fluctuating between a single line and multiple lines) as that achieved for the 20-mm-long sample, possibly due to competition between 1030 nm and 1045 nm wavelengths observed during the laser operation.

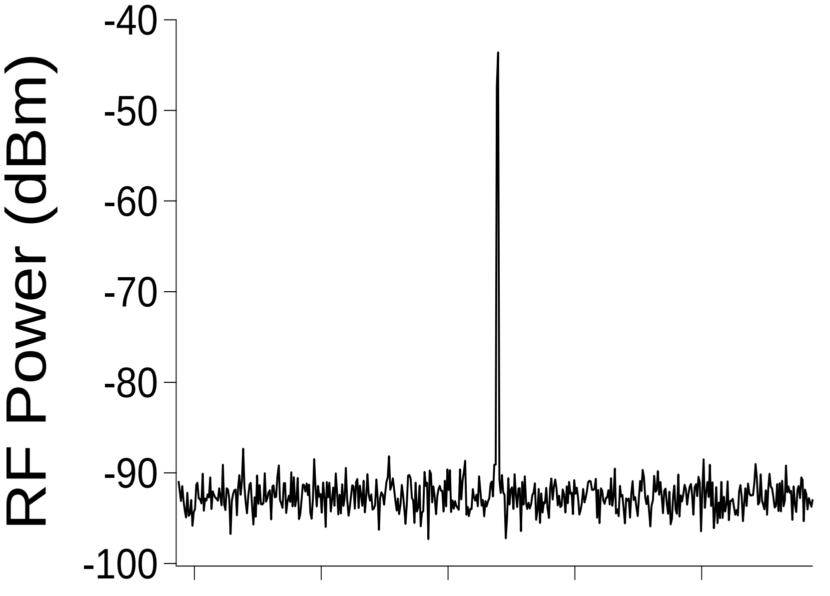

Figure 4-12. RF spectrum measured at an RBW of 10 kHz and a span of 10 MHz for the 9.4-mm-long mode-locked waveguide laser.

The autocorrelation trace is shown in Figure 4-13 (a) and was found to be a good fit to a sech^2 pulse with a FWHM width of 757 fs. The optical spectrum was centred at 1041.4

nm and had a FWHM bandwidth of 2.7 nm and is shown in Figure 4-13 (b). The time-bandwidth product was calculated to be 0.56.

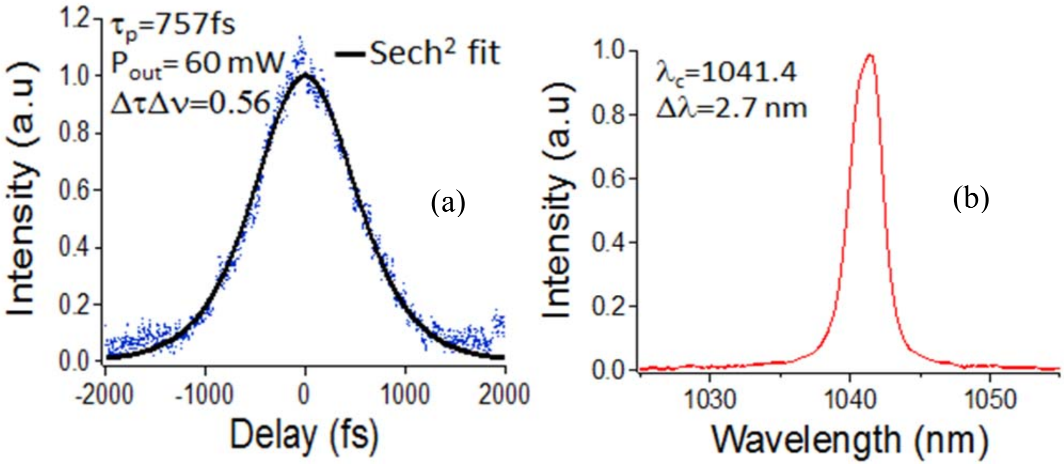

Figure 4-13. (a)Autocorrelation trace, and (b) optical spectrum measured at an output power of 60 mW for the mode-locked waveguide laser.

4.2.3.3 8-mm-long waveguide

Stable mode-locking was achieved with a gap of ~26 μm between the SESAM and the waveguide facet for the 8-mm-long waveguide laser at an output power of 45 mW using a 2% OC. The RF spectrum is shown in Figure 4-14 and a sharp peak is observed at a repetition-rate of 12 GHz.

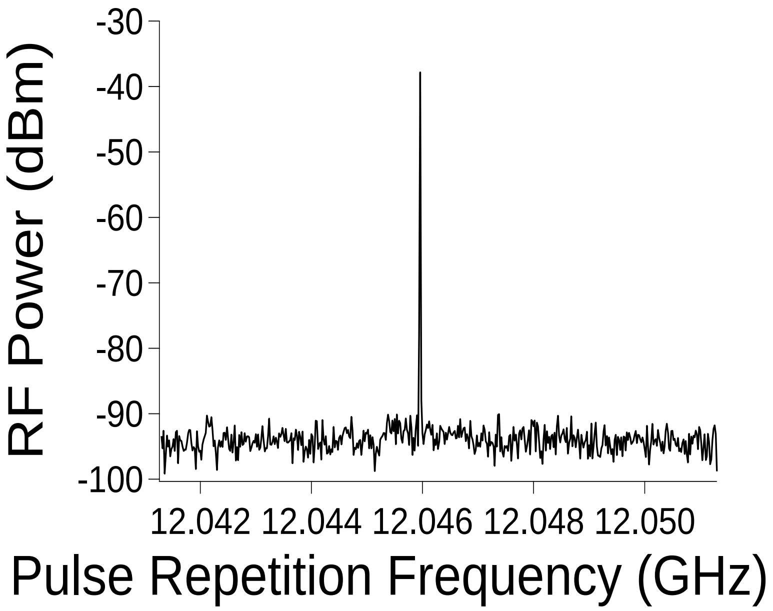

Figure 4-14. RF spectrum measured at an RBW of 10 kHz and a span of 10 MHz for the 8-mm-long mode-locked waveguide laser.

A pulse width of 824 fs was measured from the autocorrelation trace (Figure 4-15 (a)) and the central wavelength was measured to be 1045.7 nm (Figure 4-15 (b)) with a spectral bandwidth of 1.9 nm giving a time-bandwidth product of 0.43.

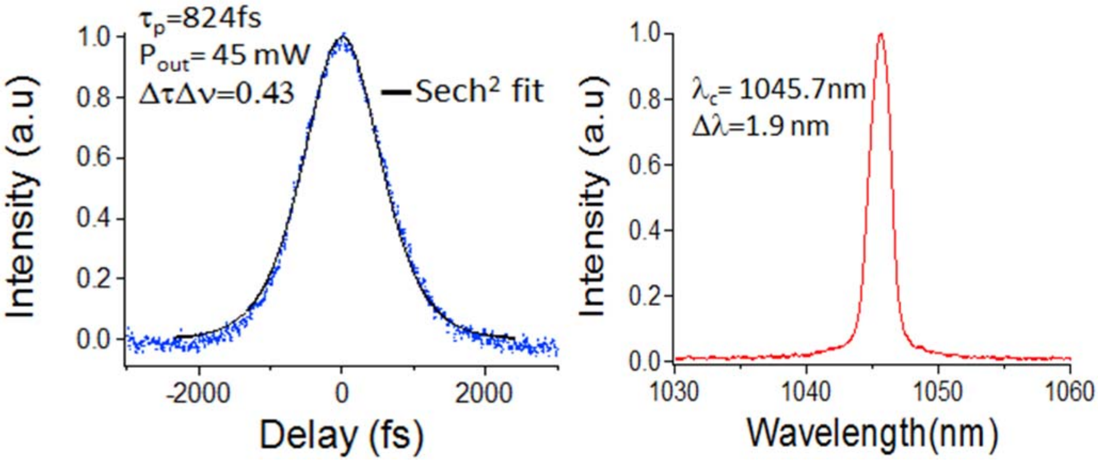

Figure 4-15. (a)Autocorrelation trace, and (b) optical spectrum measured at an output power of 45 mW for the mode-locked waveguide laser.

4.2.3.4 6.5-mm-long waveguide

Stable mode-locking was achieved with a gap of ~26 µm between the SESAM and the waveguide facet for the 6.5-mm-long waveguide laser at an output power of 27 mW using a 2% OC. The RF spectrum is shown in Figure 4-16 and it can be seen that a sharp peak was observed at a repetition-rate of 15.2 GHz.

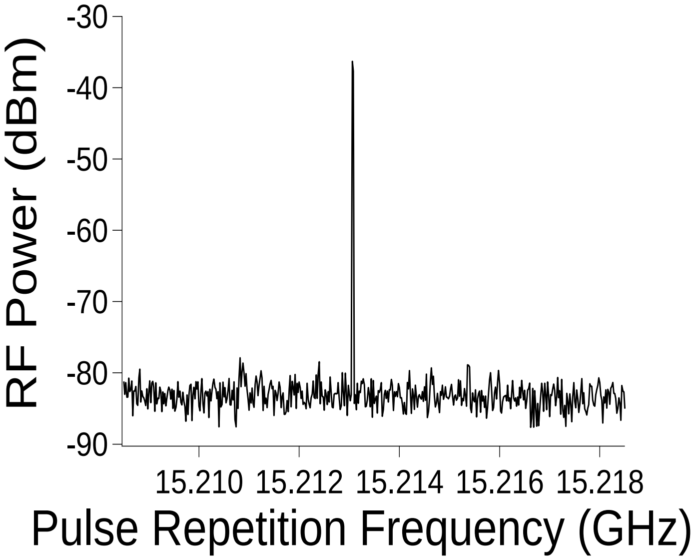

Figure 4-16. RF spectrum measured at an RBW of 10 kHz and a span of 10 MHz for the 6.5-mm-long mode-locked waveguide laser.

The autocorrelation trace and the optical spectrum are shown in Figure 4-17. The pulse width was found to be 811 fs and the optical spectrum had a bandwidth of 2.1 nm and was centred at 1047.4 nm. The time-bandwidth product was calculated to be 0.49.

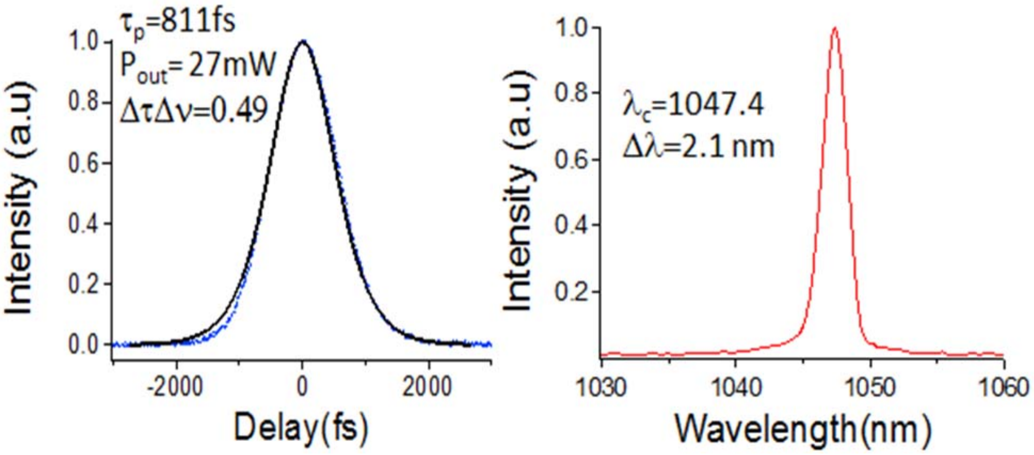

Figure 4-17. (a)Autocorrelation trace, and (b) optical spectrum measured at an output power of 27 mW for the mode-locked waveguide laser.

A photograph of the SESAM and the waveguide taken from the combination of the ×100 objective and the CCD camera is shown in Figure 4-18. The gap between the two end-facets can be clearly discerned.

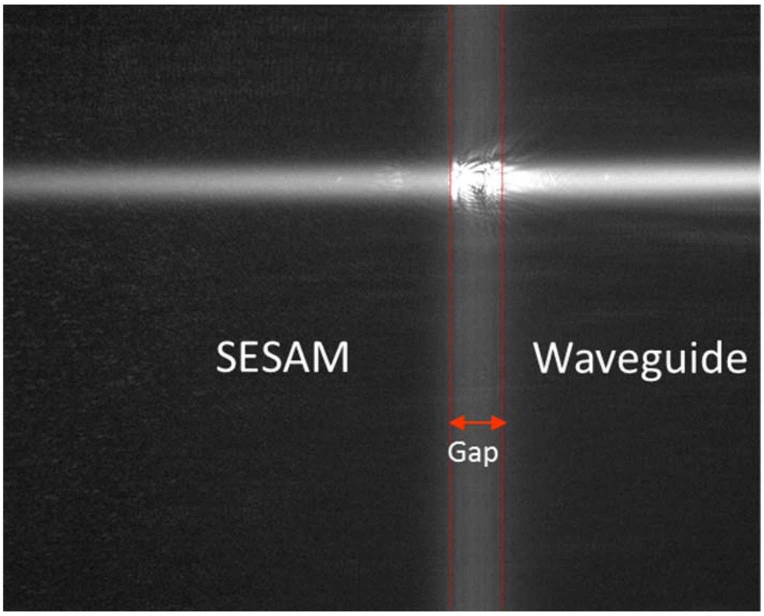

Figure 4-18. A photograph showing the gap of ~20 μm between the SESAM and the waveguide end-facet.

A summary of the results obtained for different waveguide samples using a 2% OC is shown in Table 4-1.

Table 4-1.Summary of the mode-locked results

Sample length (mm)	Repetition-rate (GHz)	Pulse Duration (fs)	Center wavelength (nm)	Time-bandwidth product	Output power (mW)
20	4.9	738	1058.3	0.46	32
9.4	10.4	757	1041.4	0.56	60
8	12	824	1045.7	0.43	45
6.5	15.2	811	1047.4	0.49	27

4.2.4 GTI effect

The low-threshold mode-locking and sub-picosecond pulse generation from our waveguide lasers can be attributed to a soliton formation mechanism, i.e. when the pulse phase shift due to self-phase modulation (SPM) in the gain medium is compensated by negative GVD. Indeed, stable mode-locking was observed at intra-cavity pulse energies in the range of 0.1-0.3 nJ, which are considerably lower than the calculated critical pulse energy of ~3.6 nJ (from equation 2.59) required to overcome Q-switching instabilities in the case of a non-soliton mode-locking regime [8].

The required negative GVD in our experiments originates from the micrometre-scale gaps between the SESAM and uncoated surfaces of the waveguide structure. Similar effects are also observed when the gap between the waveguide and the output coupler is controlled. This leads to the formation of equivalent GTI structures [9] that provide a sufficient amount of negative GVD suitable to support a soliton mode-locking regime, as was previously shown in the case of a bulk laser system [10]. The group delay dispersion (GDD) is the GVD multiplied by the length and is a function of t_0 which is the round-trip time for light in the gap (which depends on the size of the gap (*d*) and the refractive index (n)), the optical frequency ω, and the reflectivity of the waveguide R. The GDD is given by the following expression [11]:

$$GDD = -\frac{2\sqrt{R}(1-R)\sin(\omega t_0)}{\left[1+R-2\sqrt{R}\cos(\omega t_0)\right]^2} t_0^2,\ t_0 = \frac{2nd}{c} \quad (4.1)$$

The GDD vs. the gap has been plotted for a wavelength of 1058 nm in Figure 4-19. for different n (1 for an air–filled gap and 1.3 for fluorinert-filled gap) and a zoomed-in plot for gaps between 20 μm and 30 μm has been shown in Figure 4-20. As seen from Figure 4-19 and Figure 4-20, it is possible to introduce dispersion in excess of -7000fs^2 by increasing the gap to about ~30 μm. It should be noted, however, that the value of the GDD depends very sensitively on the GTI gap (~80 fs^2/nm) and, although, a precise control of the gaps was provided, it was not possible to fully balance the second order dispersion and the self-phase modulation, which explains the generation of slightly chirped pulses. It should also be noted that, as the gap is increased, the loss due to diffraction in free space also grows quickly.

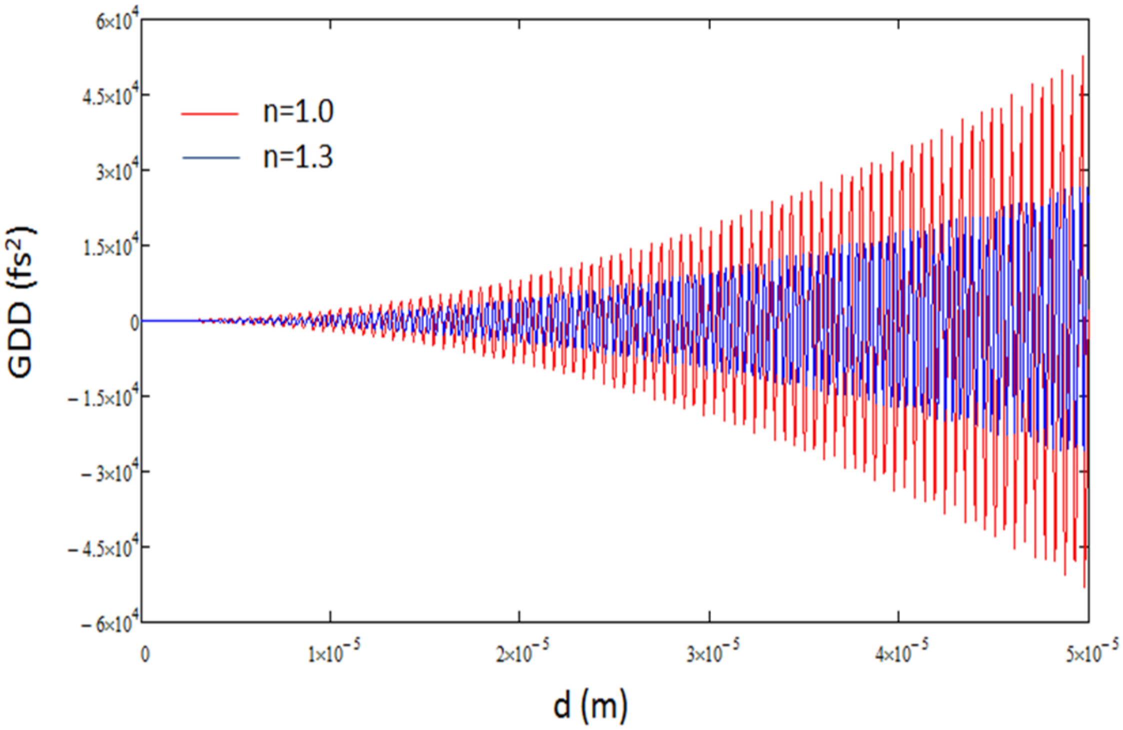

Figure 4-19. GDD vs. d for n=1 and n=1.3.

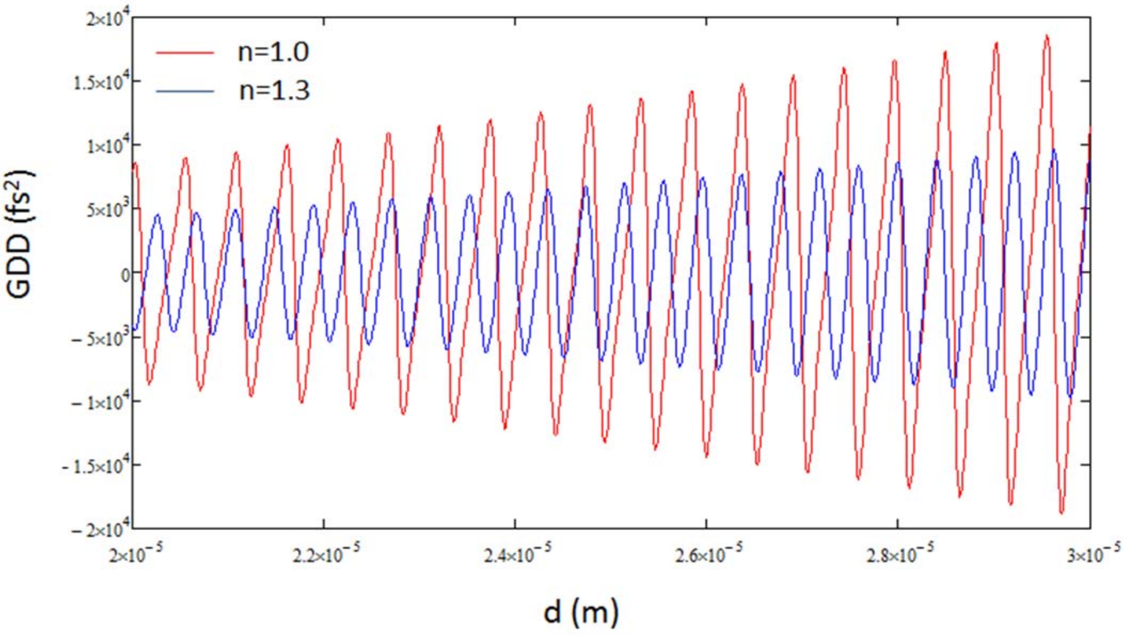

Figure 4-20. GDD vs. d for n=1 and n=1.3 for a gap between 20 μm and 30 μm.

During soliton mode-locking, the phase shift due to self-phase modulation is balanced by the phase shift due to dispersion and is given by [12]:

$$\frac{\delta E_P}{4\tau} = \frac{|D|}{\tau^2} \qquad (4.2)$$

where δ is the nonlinear coefficient, E_P is the pulse energy, D is the GDD and τ is 0.56 times the pulse duration measured at full width at half maximum (FWHM). From (4.2), the net GDD was estimated to be around -6200 fs^2 for the 20-mm-long-waveguide cavity with $= 178\,\mu rad/W$, $E_P = 0.33\,nJ$ and $\tau = 420\,fs$. The material dispersion in the cavity was calculated to be 920 fs^2 and so the estimated contribution from the GTI effect is -7120 fs^2. Using the modified equation (equation (2.60)) for the critical pulse energy in the soliton mode-locking case, the measured pulse energies are in good agreement with the calculated value of 0.095 nJ.

GDD vs. the wavelength has been plotted in Figure 4-21 for a gap of 26 μm. This shows that it might be possible for the wavelength to tune itself in order to get the correct dispersion in order to facilitate soliton mode-locking.

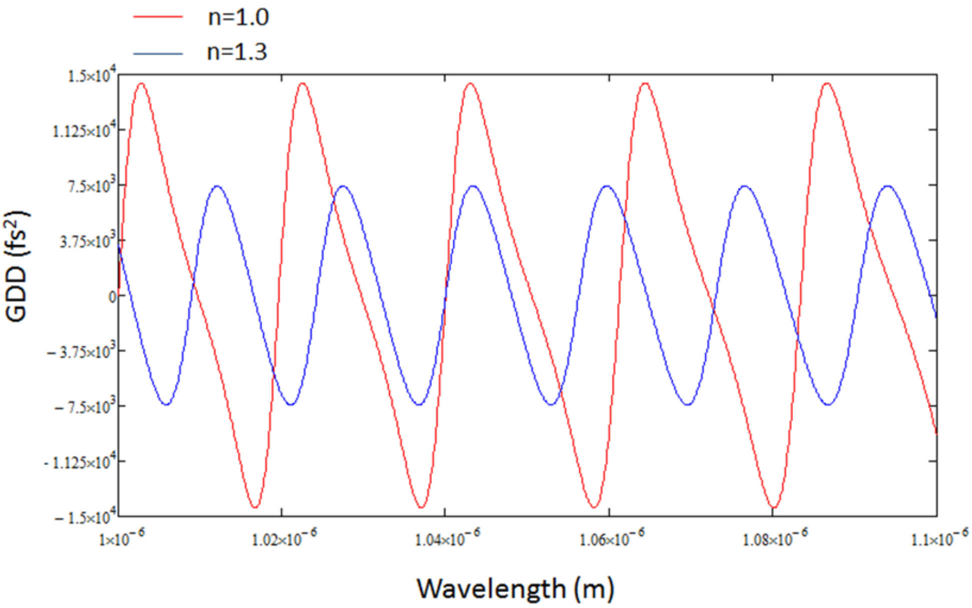

Figure 4-21. GDD vs. wavelength for different n for a gap of 26 μm.

4.3 Yb^{3+}:$RbTiOPO_4$

In the previous sub-section, mode-locking results achieved with ytterbium-doped phosphate glasses were discussed. In this section, $RbTiOPO_4$ (RTP) is investigated as a promising material for both non-linear applications and, when doped with Yb^{3+} for ultrafast waveguide laser operation. In this sub-section, the fabrication details of the RTP substrates and the epitaxial layers of (Yb,Nb):RTP are discussed. Preliminary laser results obtained with an (Yb,Nb):RTP planar waveguide are also presented. Finally, channel waveguides in (Yb,Nb):RTP fabricated by reactive ion-etching and ion-beam milling are discussed.

4.3.1 RTP crystal growth and LPE of (Yb,Nb):RTP

The RTP crystals used as substrates were grown at URV, Tarragona inside a tubular furnace [13] using the top-seeded solution growth method (TSSG). The super-saturation of the solution was obtained by slow cooling. An RTP seed parallel to the ***c***-crystallographic direction was used as this is the optimum orientation for the growth of high-quality RTP crystals. From these crystals it is possible to obtain substrates in the ***ab*** plane, which is of interest for the non-critical phase matching (type-II) second harmonic generation (SHG) [14] of fundamental radiation near 1 μm, corresponding to the emission wavelength of Yb^{3+}. All the substrates were cut perpendicular to the c-crystallographic axis and the surfaces were polished in preparation for epitaxial growth.

LPE growth of an (Yb,Nb):RTP thin film was carried out at URV, Tarragona in a furnace with a solution having composition of Rb_2O – P_2O_5 – (TiO_2 + Nb_2O_5 + Yb_2O_3) – WO_3 with concentration of 43.90-23.6-22.50-10.00 (mol%) respectively. The TiO_2 in the solution was partially substituted by 2 mol% Nb_2O_5 and 6 mol% Yb_2O_3. Nb_2O_5 is added to facilitate a higher concentration of Yb^{3+} via charge-compensation [15]. After the homogenisation of the solution, the saturation temperature was measured to be 1135 K. Next, the RTP substrates were slowly lowered into the furnace in order to minimise cracks due to thermal stress. The substrates were immersed into the solution and kept at a temperature of 1 K above the saturation temperature for 5 minutes to dissolve the outer region of the crystal. The temperature of the solution was then decreased to 9 K below the saturation temperature to super-saturate the solution and to allow stress-free epitaxial growth. The substrates were stirred at 60 rpm using a motor, and growth was allowed to occur for 6 hours.

The obtained epitaxial layers were studied at URV, Tarragona using a Sensofar PLμ 2300 interferometric microscope to measure the film thickness, which was initially 70 μm and then polished to a uniform thickness of either 10 μm for the planar waveguide or 5-6 μm for the channel waveguides. The composition of the epitaxial layer was determined by electron probe micro-analysis with a wavelength dispersive spectrometer (EPMA-WDS), using a Cameca SX-50 microprobe analyzer and the concentration of Yb^{3+} in the epitaxial layer was found to be 0.33 at.%, which corresponds to an Yb^{3+} concentration of 2×10^{20} cm^{-3}. The refractive index contrast in TM polarisation (E//***c***-axis) was measured at URV, Tarragona and was found to be 6×10^{-3} at a wavelength of 972 nm (from a Ti:sapphire laser) by the prism-coupling technique and the indices for the different crystallographic axes are shown in Table 4-2. The epitaxial layer was confirmed to be single-crystalline from X-ray diffraction measurements.

Table 4-2. Refractive indices of the substrate and the film.

	n_x (E//***a***)	n_y(E//***b***)	n_z (E//***c***)
substrate (n_{sub})	1.7675	1.7774	1.8573
film (n_{film})	1.7649	1.7778	1.8631
Δn (n_{film}-n_{sub})	-0.0026	0.0004	0.0058

4.3.2 Planar waveguide laser

For the planar waveguide experiments, a 10-μm-thick layer of (Yb,Nb):RTP was grown on the RTP substrate and the device was polished to a length of 6 mm as shown schematically in Figure 4-22. At 1 μm, this waveguide supports 3 modes for the E//***c*** polarisation.

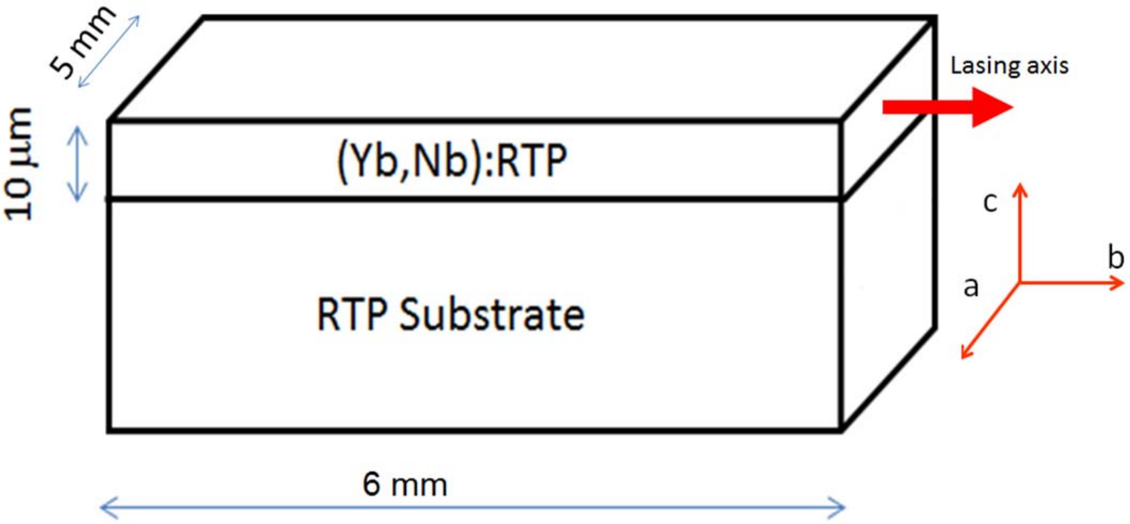

Figure 4-22. The dimensions of the (Yb,Nb):RTP waveguide.

The waveguide was pumped with a Ti:sapphire laser tuned to 900 nm with E//c (TM), as the absorption was highest for this configuration. The pump was focused with a ×10 objective to a spot size with a radius of 3 μm. The values of absorption (A), single-pass loss (L_s) and launch efficiency (η_L) were measured to be 0.66, 0.11 (or 0.8 dB/cm) and 0.9 respectively using the method described in section 3.3.2.3 (b). Thin dielectric mirrors were then butted directly onto the waveguide end-faces to form the laser cavity. Using an optical chopper the characteristic rise and decay of the fluorescence intensity (with lifetime ~2 ms) was monitored on a photodiode. On increasing the pump power, a fast and very strong increase in intensity indicated the point at which laser threshold had been achieved. Lasing was achieved on the TM mode for an HR/HR cavity with an absorbed power of 276 mW. This is just at the limit of capability of the Ti:sapphire laser system and therefore slope efficiency laser measurements were not possible. Pumping with single-emitter laser diodes with power up to 10 W will be of interest in the future. The calculated gain for total inversion is 0.69 cm^{-1} (total doping concentration times the emission cross-section at the lasing wavelength) whereas the measured loss is 0.19 cm^{-1}, hence the condition of gain > loss is only just satisfied. The gain is low in this material because of the low-doping concentration of Yb^{3+} during the epitaxial growth [13]. Therefore, it is important to produce (Yb,Nb):RTP films with even lower losses for efficient laser applications.

4.3.3 Channel waveguides by ion-beam milling

After these preliminary results with a planar waveguide, channel waveguides were fabricated in 5-μm-thick (Yb,Nb):RTP layer using ion-beam milling [16] in an attempt to reduce the threshold power.

4.3.3.1 Fabrication details

The sample was included in glue on a glass slide in order to remove any edge effects for the following photolithographic process. A 4-μm-thick layer of S1828 resist was spin-coated onto the sample before masking and subsequent development. A dark-field mask was used with waveguide widths from 3 μm to 10 μm, with a separation of 100 μm between them. The dark-field mask channels were carefully aligned along the ***a*** crystallographic direction in order to produce ribs on the substrate parallel to this direction. As can be seen in Table 4-2, the refractive index contrast between the doped layer and the un-doped substrate is positive for the ***b*** and ***c***-polarisations and negative for the ***a***-polarisation. Thus, guiding is possible in TM and TE regimes along ***a***, but only in TM along ***b***. The etching process was carried out in an Oxford Plasma Technology Ionfab 300 Plus system. The masked sample was held at 45º and rotated at 5 rpm during the process. An Ar^{+} ion-beam was accelerated at 500 V with a beam current of 100 mA. This beam etched the sample for 2 hours and 20 minutes to etch 3-μm-high ribs in the film. The resist was then removed by acetone and isopropanol followed by plasma-ashing.

A Sensofar PLμ 2300 optical imaging profiler was used to check the quality of the ribs. With this microscope the top widths of the ribs were measured to be in the range from 3 μm to 10 μm in agreement with the values of the mask used. The profile of the ribs was studied using a non-contact profiler (Zescope by Zemetrics). Figure 4-23 shows a 3-d image of a rib waveguide giving a qualitative idea of the smoothness of the etched side-walls.

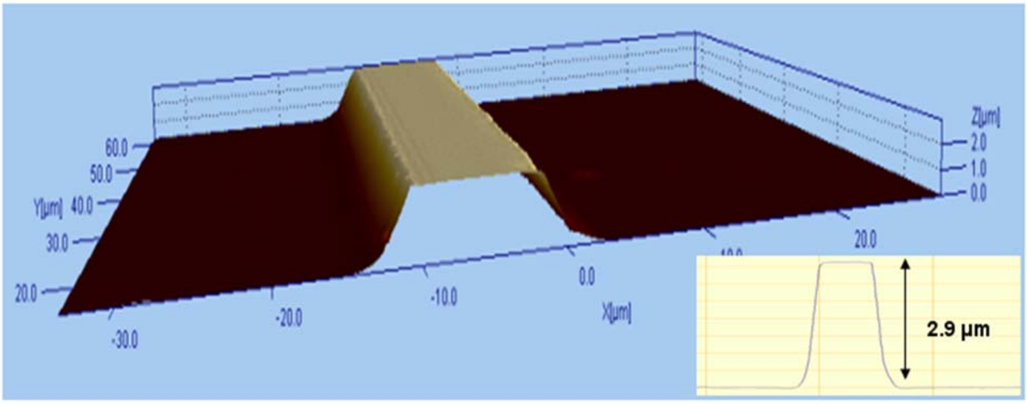

Figure 4-23. A 3-d profile of the etched waveguide measured by a non-contact profiler. Inset: 2-d profile of the waveguide.

The etch depth was 2.9 µm (resulting in an etch rate of 16.4 nm/min) as can be seen from the inset of Figure 4-23. It is important to note that the shape of the rib is not rectangular, but is trapezoidal. The end-faces of the waveguides were then polished with the sample sandwiched between two glass blocks to protect the edges. After polishing the end faces, the width of the rib base was found to be 4 µm larger than the width at the top, indicating that the slope of the rib walls was 56°. Figure 4-24 is a general view of the ribs in a top view regime using a scanning electron microscope (SEM) at URV Tarragona.

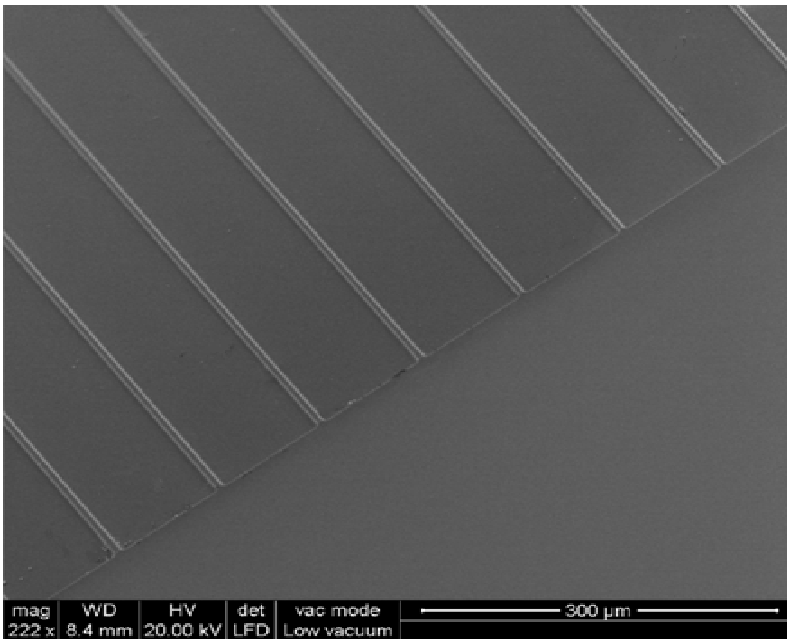

Figure 4-24. General top view of the rib waveguides by Scanning Electron Microscope (SEM).

In a more detailed view, Figure 4-25 shows ribs of 9 µm in width and the good quality of the rib walls is qualitatively confirmed.

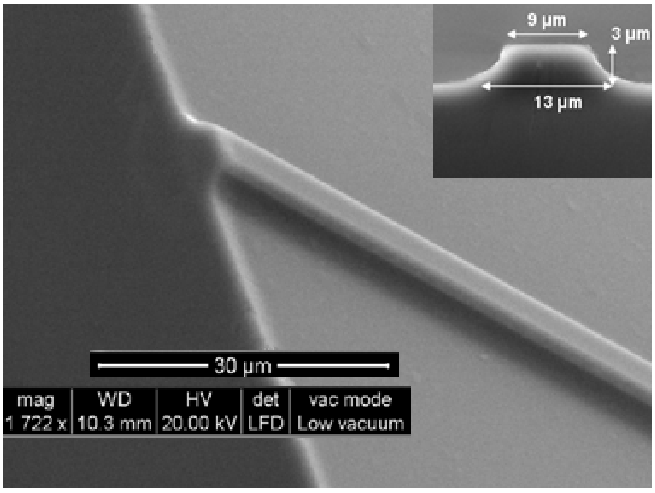

Figure 4-25. Detailed view of the 9-µm nominal-width rib waveguide by SEM, with the cross-section view in inset.

4.3.3.2 *Optical characterisation*

A ×10 objective microscope was used to couple the Ti:sapphire laser, operating at a wavelength of 900 nm, into the rib waveguide making a spot-size of 3 µm. The near-field pattern was measured in order to understand the energy distribution of the propagation modes for the pump wavelength. An output objective was used after the waveguide to image the waveguide mode on to a CCD camera. Figure 4-26 shows the near-field pattern of the rib with a 10 µm top-width.

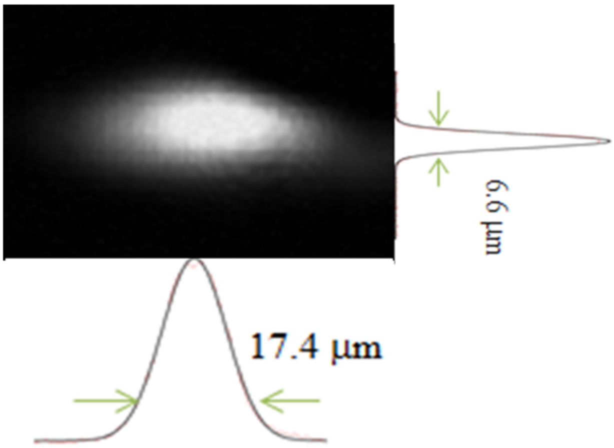

Figure 4-26. Near Field Pattern (NFP) of the fundamental mode at 900 nm for the 10 µm top-width rib

As expected, the mode is asymmetric, with Gaussian profiles with $1/e^2$ beam radii of 8.7 µm and 3.3 µm in the x and y-directions, respectively. Numerical modelling carried out using OlympIOs for the trapezoidal features resulted in $1/e^2$ beam radii of 7.4 µm and 2.2 µm in the x and y-direction respectively for the TM_{00} mode. The transmission losses were estimated to be ~3 dB/cm using the transmission method described in 3.3.2.3 (b). The second harmonic generation (SHG) inside the rib waveguide was checked at URV, Tarragona using a pulsed laser at 1140 nm from an optical parametric oscillator (OPO) (Vibrant HE 355 II + UV model from Opotech) coupled to the rib waveguides by a microscope objective. The OPO was tuned to obtain maximum efficiency of SHG for propagation along the ***a*** crystallographic direction. An achromatic half-wave plate was placed between the laser source and the sample at an angle of 22.5º to ensure that the TM and TE modes were excited simultaneously, which is required for type II SHG. The guided green light at 570 nm, obtained exclusively inside the channels, was imaged onto a CCD camera and is showed in Figure 4-27.

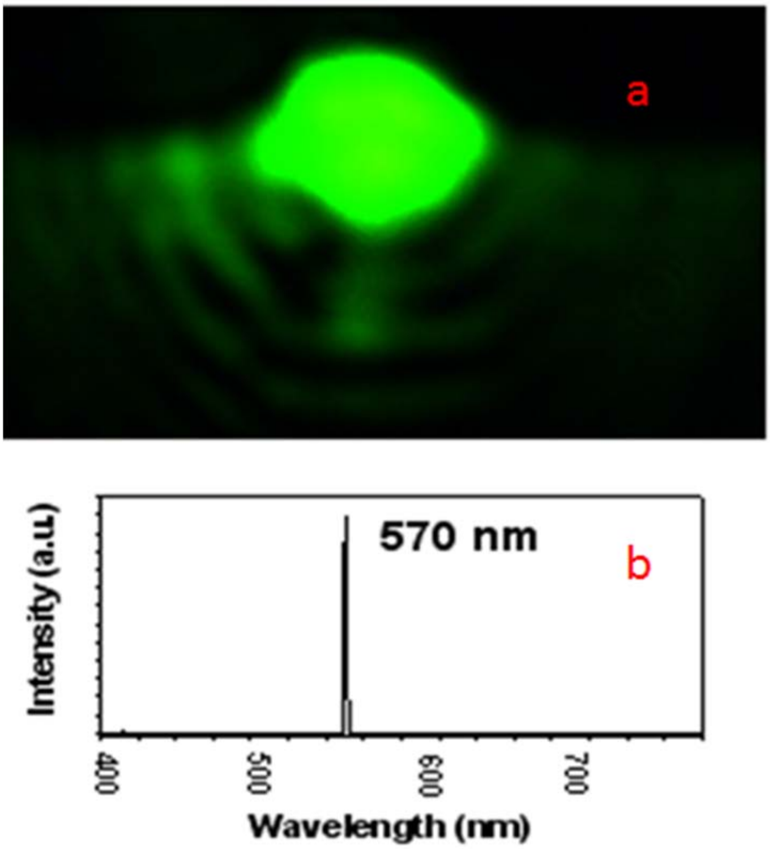

Figure 4-27. (a). CCD image of 570 nm green light from type II SHG of 1140 nm IR light and (b). Spectrum of the SHG light.

Unfortunately, experiments aimed at achieving laser performance in these waveguides were unsuccessful, which is consistent with the estimated high values of propagation loss.

4.3.4 Channel waveguides by reactive ion etching

Since laser action could not be achieved with channel waveguides fabricated by ion-beam milling, an alternative technique to pattern the waveguides i.e. reactive ion etching (RIE) was employed to try and reduce the propagation losses. This section describes the optimisation technique and the optical characterisation results of the waveguide. The effect of the RIE parameters on the etch rate and the surface roughness were systematically studied in order to optimise the etching process in RTP substrates and to thus fabricate low-loss channel waveguides in (Yb,Nb):RTP [17]. RTP substrates and one Yb,Nb:RTP/RTP planar waveguide were obtained from URV, Tarragona. All the optimisation and characterisation were carried out by the author.

4.3.4.1 Fabrication details

A 300-nm-thick uniform layer of chromium (Cr) was deposited on the RTP substrates using e-beam evaporation, following which a 1.3 μm layer of S1813 photoresist was patterned using photolithography to make a mask consisting of waveguide features of widths ranging from 1 μm to 10 μm in steps of 0.2 μm. The Cr layer was then etched using a chemical etchant and the resist was washed away using solvents. The hard-masked RTP substrates were then etched in an OPT Plasmalab 80 plus RIE system (Oxford Instruments) with an RF frequency of 13.56 MHz. Finally, the metal mask was chemically etched and the substrate was cleaned with solvents.

The RF power, the gas pressure and the ratio of the gases used (Ar and SF_6) were the three parameters that were varied during RIE. The starting parameters were chosen as: RF power of 250 W, a pressure of 50 mTorr, a total gas flow rate of 20 sccm and a gas ratio of 90:10::SF_6:Ar. The temperature was kept fixed at 20°C for all the experiments.

There is a lack of literature on the dry etching of RTP, but halides are known to form volatile compounds with KTP [18]. Since RTP and KTP are from the same family of crystals, with the K^+ ions replaced by the Rb^+ ions in RTP, fluoride gases were used as etching species in the experiments described here. The fluoride gas chosen was SF_6 as it provides more free fluorine radicals [19] in comparison to the other available fluoride gas, CHF_3. Ar is an inert gas and is used to bombard the surface thus making the etching process more physical. As a starting parameter, 90% SF_6 in the gas mixture was chosen to have a predominantly chemical etching process. The percentage of SF_6 in the gas mixture was varied from 90% to 10% to study the interplay between the physical and the chemical etching processes. The RF power, gas pressure and the gas ratios were then systematically varied to study their influence on surface roughness and the etch rate. The measured RMS surface roughness of the substrates before etching varied from 2 nm up to 5 nm from sample to sample; hence the change in the RMS surface roughness (after etching-before etching), as opposed to the absolute values, is presented in the next sub-section.

4.3.4.2 Optimisation procedure

With the gas pressure kept constant at 50 mTorr, the SF_6:Ar concentration ratio set at 90:10 and an etch time of 40 minutes, the etch rate for RTP, etch rate for the Cr mask and the surface roughness as a function of RF power is presented in Figure 4-28. It can be seen that the etch rate increases almost linearly with power, with an etch rate of up to 13 nm/min being obtained at an RF power of 350 W. The RMS surface roughness also increases as a function of RF power and a value of 3.4 nm is measured at 350 W. A good balance between the surface roughness and the etch rate was achieved for a power of 250 W and hence this power was fixed for the following experiments.

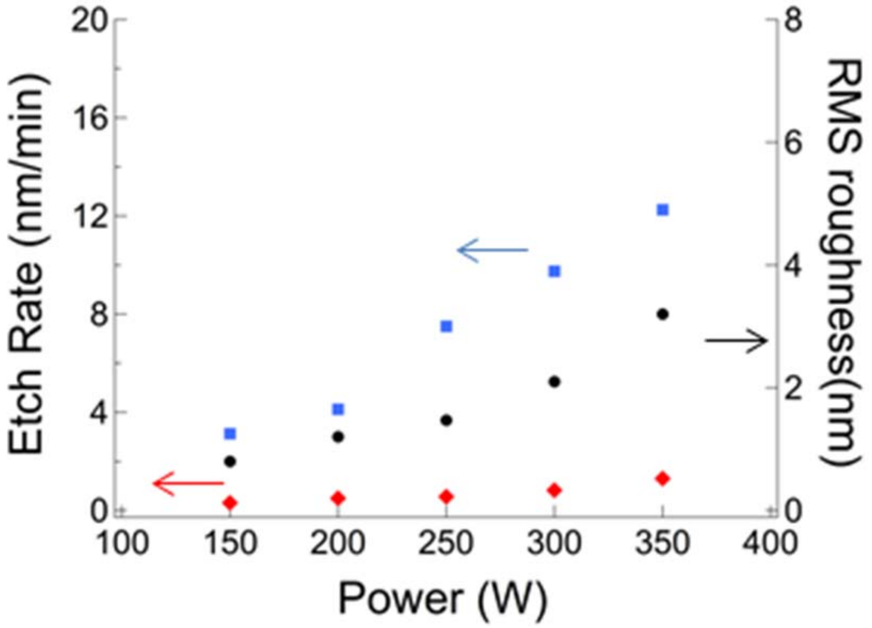

Figure 4-28. Etch rate of RTP (blue), etch rate of Cr (red) and the surface roughness (black) as a function of RF power.

At a fixed RF power of 250 W (from the previous optimisation) and a 90% SF_6 gas mixture, the etch rates and surface roughness were then measured as a function of the gas pressure, with the results plotted in Figure 4-29. It can be seen that the RTP etch rate decreases with the increasing pressure. This can be understood by the increased scattering of the etching species with pressure and a subsequent decrease in the mean free path for the radicals [20] resulting in a loss of kinetic energy. At a pressure of 50 mTorr, an etch rate of 8 nm/min and a surface roughness of 1.6 nm were observed. A pressure of 50 mTorr was then set as a balance between the etch rate and surface roughness.

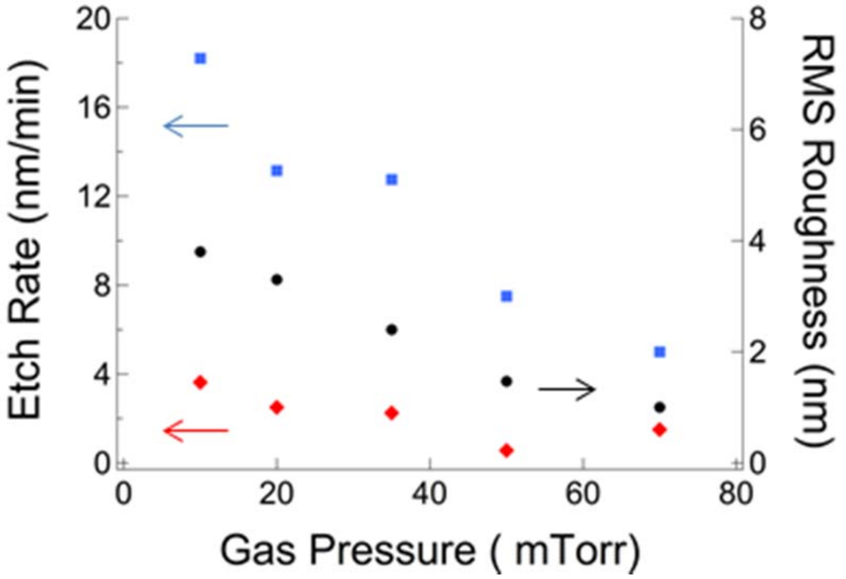

Figure 4-29. Etch rate of RTP (blue), etch rate of Cr (red) and the surface roughness (black) as a function of gas pressure.

At a power of 250 W and a gas pressure of 50 mTorr, the percentage of SF_6 in the gas chamber was varied. The results obtained for the etch rates and surface roughness are presented in Figure 4-30.

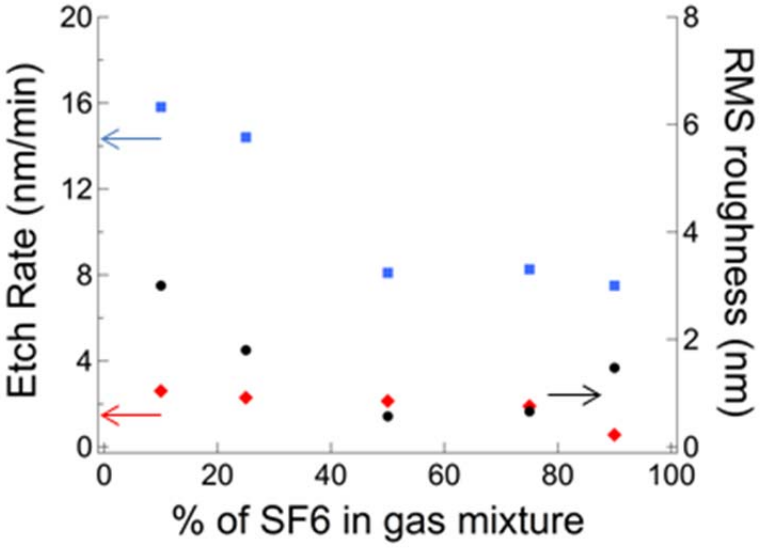

Figure 4-30. Etch rate of RTP (blue), etch rate of Cr (red) and the surface roughness (black) as a function of percentage of SF_6 in the gas mixture.

At low SF_6 concentrations and high Ar concentration, the etch rate of RTP is as high as 16 nm/min for 10% SF_6. However, the surface roughness is quite high (3.4 nm). This is primarily a physical etching process and a lot of the material is etched and sputtered by the Ar^+ ions, thus increasing the surface roughness. At high SF_6 concentrations, the etch rate is found to decrease whereas the surface roughness is found to increase slightly. An optimum for the surface roughness is reached with 50% SF_6 in the gas mixture. At 50% SF_6, the etch rate is about 8 nm/min and the surface roughness is <1 nm.

The selectivity (ratio of etch rates of RTP to chromium) was found to be greater than 5 for almost all the conditions. This facilitated the use of thin Cr layers (~300 nm) as masks for etching the waveguides.

The DC bias of the RIE chamber is a process-dependent parameter. For each measurement described above, the DC bias was measured and the etch rate of RTP and Cr versus the DC bias are plotted in Figure 4-31. It is important to note that all the data points do not have the same conditions, however the linear behaviour of the etch rate shows consistency in the plasma condition against the gas ratio, pressure and RF power. As seen from Figure 4-28, Figure 4-29 and Figure 4-30, an etch rate of 8-10 nm/min gives a good balance between etch rate and surface roughness, this corresponds to a DC bias of around -300V as seen from Figure 4-31.

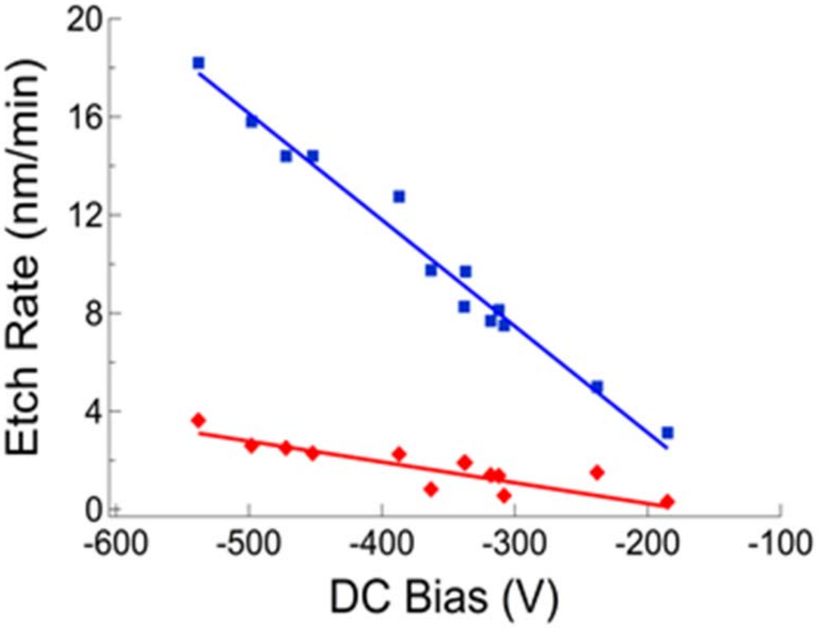

Figure 4-31. The etch rate of RTP (blue) and Cr (red) as a function of the measured DC bias.

4.3.4.3 *Fabrication of waveguides*

The optimised conditions discussed in the previous sub-section were used to fabricate waveguides along the ***b***-direction in an (Yb,Nb):RTP epitaxial layer with a thickness of 6 μm. The parameters used were: RF power of 250 W, gas pressure of 40 mTorr and gas flow rates of 10 sccm for both SF_6 and Ar (i.e an SF_6 concentration of 50%). The pressure was slightly reduced from 50 mTorr to 40 mTorr, to increase the etch rate without compromising on the surface roughness. The sample was etched for 135 minutes in order to fabricate single-mode waveguides in (Yb,Nb):RTP for propagation of light at wavelengths of 1 μm. Next, this waveguide sample was polished to a length of 7.5 mm. Following the polishing step, the sample was kept in acetone for 15 minutes in an ultrasonic bath followed by isopropanol and finally de-ionized (DI) water, also for 15 minutes each. To remove any residual water and moisture, the sample was blow-dried with N_2 and finally dehydrated in an oven at 90ºC for 10 minutes. The mask was removed by chemical etching, after which the sample was plasma-ashed in the RIE chamber for 20 minutes with an RIE power of 200 W, a pressure of 50 mTorr and O_2 flow rate of 10 sccm, which removed any organic impurities present on the waveguides. The SEM image of the end-facet of the waveguide is shown in Figure 4-32.

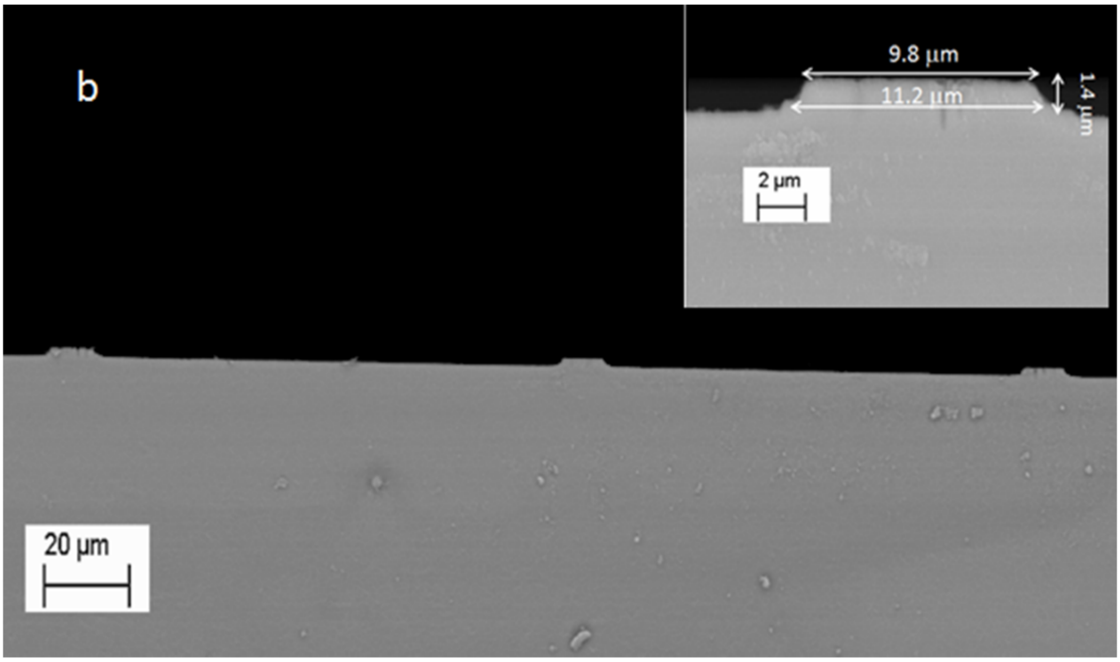

Figure 4-32. SEM image of the end-facet of the waveguide. Inset: a zoomed-in image of a waveguide.

The etch depth was measured, by a stylus profiler and from SEM measurements to be 1.4±0.1 µm, thus giving an etch rate of 10 nm/min. The surface roughness of the film before etching was measured to be 3±0.5 nm and increased to 8±0.5 nm after etching. This is slightly higher than what was expected from the values obtained during the optimisation, which could be understood by the fact that the film has a slightly different composition when compared to the substrate and the fact that a longer etch time was used. From Figure 4-32, it can be seen that for a waveguide with a top width of 9.8 µm, a side-wall angle of 63º is measured. Figure 4-33 shows the top-view and the side-view of the waveguides, qualitatively suggesting a reasonable etch quality and smooth side-walls, respectively.

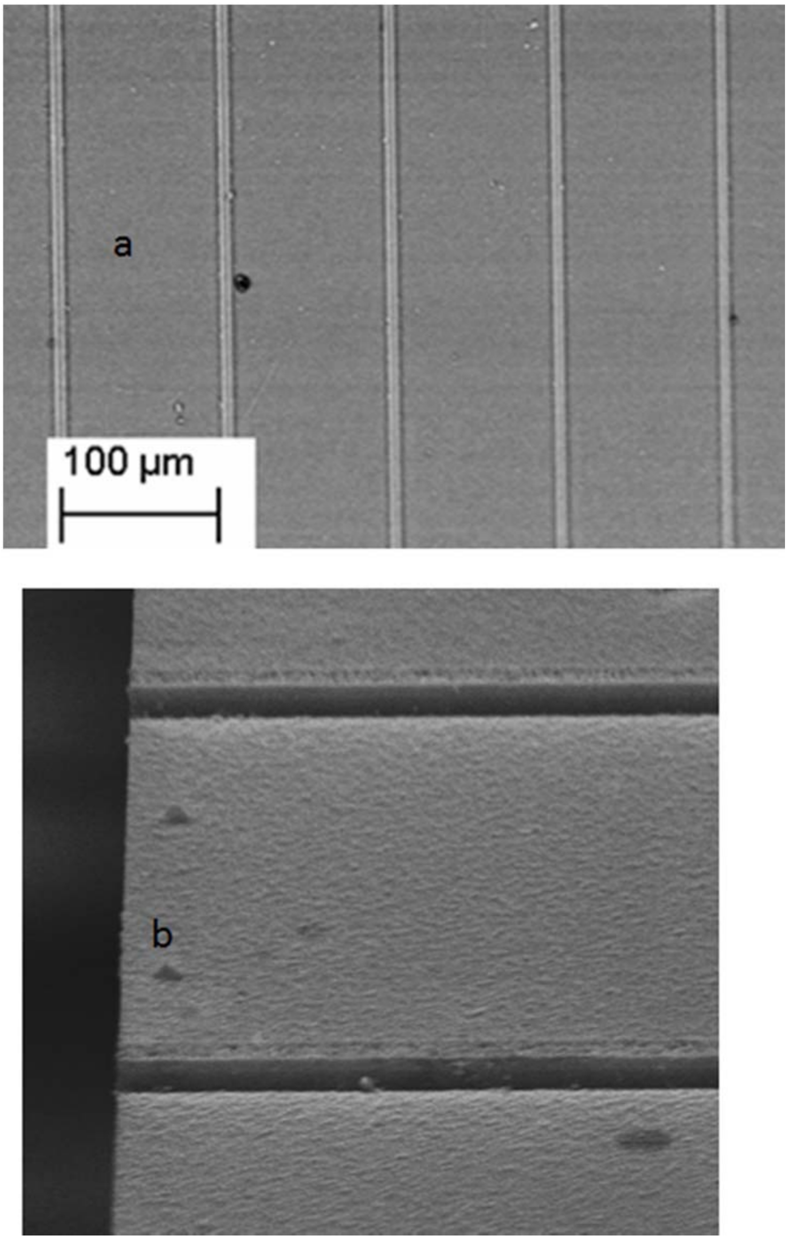

Figure 4-33 (a) Top-view of the etched waveguide sample and (b) SEM image taken by tilting the sample by 70° to show the side-wall quality.

The surface profile of the planar region and the ribs measured by a white-light interferometer profiler (Zescope by Zemetrics) is shown in Figure 4-34. It again appears that the surface quality is good, barring a few spikes.

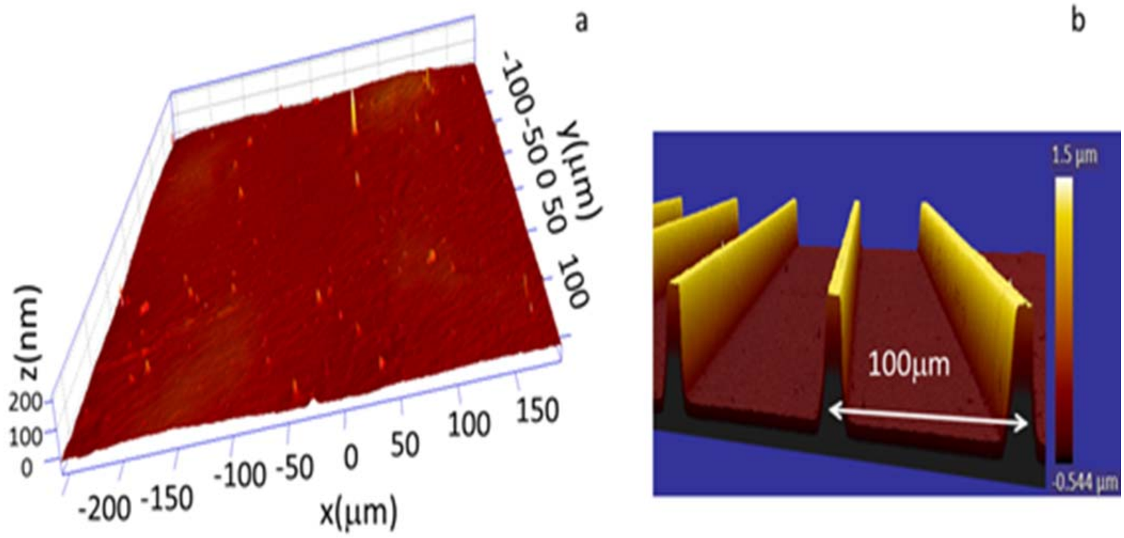

Figure 4-34. Surface profile of (a) an etched planar region and (b) a region with etched ribs.

4.3.4.4 Optical characterisation

The (Yb:Nb):RTP waveguide fabricated by RIE was optically characterised by end-coupling a fibre-coupled single-mode laser diode (3S photonics). The laser diode had a maximum output power of 750 mW and a wavelength of 980.6 nm, with a 3 dB spectral bandwidth of 1 nm. The pump beam was collimated using a lens with a focal length of 8 mm and was passed through a half-wave (λ/2) plate to control the polarisation. The pump was then coupled into the waveguide using a ×16 objective resulting in a beam with a waist radius of 3.2 μm. The output from the waveguide was collected using a ×6 objective and imaged on to a camera to measure the mode profile. The losses were estimated by measuring the transmitted pump power using a thermal power meter and comparing it to the incident light as described in section 3.3.2.3.

The waveguide structure is designed to be single mode at 981 nm and the simulated and measured TM profile is shown in Figure 4-35. The $1/e^2$ mode radii were measured to be 7.9 μm and 4.3 μm in the x and y-directions respectively. This is in good correlation with the simulated values of 7.6 μm and 3.4 μm (simulated by a commercially available software OlympIOs).

The transmission was measured at various levels of pump powers and the losses were estimated to be <3.5 dB/cm for the E//c crystallographic axis (TM).

On rotating the polarisation, the losses increased to >10 dB/cm for TE polarisation. This is consistent with the fact that the index contrast is negative for this polarisation as seen from Table 4-2 (E//a). It should be noted that in this configuration, the spectroscopy of (Yb,Nb):RTP means that TM is the preferred polarisation for lasing [21]. The loss for the TE polarisation would have to be further reduced before these waveguides can be used for self-frequency doubling applications.

Once again, experiments aimed at demonstrating laser action were performed but without success. Thus, despite successfully making channel waveguides, the propagation losses were again too high to allow laser operation in this low-gain material.

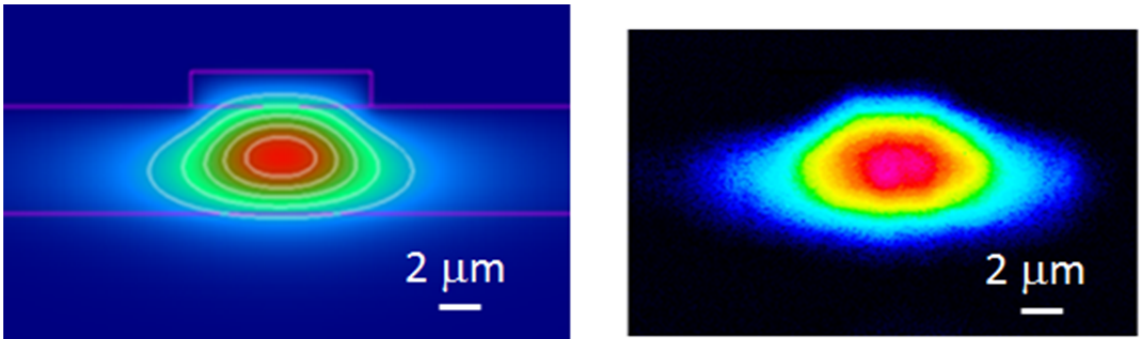

Figure 4-35.a: Simulation of the mode profile in an 8 µm wide (Yb,Nb):RTP rib waveguide at a wavelength of 0.98 µm. b: Measured near-field mode profile for the RIE etched waveguide.

4.3.5 Summary

In this section various (Yb,Nb):RTP waveguides, fabricated using different techniques were discussed. However, the propagation losses could not be reduced enough to support laser action. Therefore, this material was not pursued any further for mode-locking experiments.

4.4 Yb^{3+}:KY(WO$_4$)$_2$

As discussed in chapter 2, potassium double tungstates KY(WO$_4$)$_2$ or KYW, when doped with Yb^{3+} have a very broad emission bandwidth and are very promising for ultrafast applications around 1030 nm. There have also been recent reports of a Yb:KYW planar waveguide laser co-doped with Gd^{3+} and Lu^{3+}, operating as a pure 3-level system at the zero–phonon line at 981 nm [22] with a threshold power of 75 mW and a channel waveguide laser operating around 981 nm with an output power of 11 mW [23].

In this section, mirrorless lasing at 981 in an Yb,Gd,Lu:KYW laser with a very low threshold power of 23 mW is discussed [24]. The waveguides were fabricated in an "inverted-rib waveguide" geometry, with the substrate being etched and then overgrown with the active layer. The initial aim of these experiments was to realise a low-loss waveguide laser operating around 1030 nm, however due to the high propagation losses, the high-gain 981 nm laser operation was preferred.

4.4.1 Fabrication details

Substrates for the liquid-phase-epitaxy (LPE) growth were obtained (from URV Tarragona) from KYW bulk crystals grown by the top-seeded-solution-growth slow-cooling (TSSG-sc) technique in a vertical tubular furnace. The solute/solvent ratio was 12 mol% $KY(WO_4)_2$ / 88 mol% $K_2W_2O_7$. The analytical grade purity (99.99%) powder precursors were melted inside a cylindrical platinum crucible (~125 cm^3). The 300-g solution was homogenized by keeping the temperature 10 K above the expected saturation temperature T_s, for 6 hours. T_s was accurately determined by using a **b**-oriented KYW crystal seed placed in contact with the surface of the solution, rotating at 42 rpm, and by controlling its dissolution or growth with a precision of 10 µm. Thus T_s was established as the temperature at which neither dissolution nor growth of the crystal seed could be observed. The KYW bulk crystal started to grow from the seed in contact with the surface of the solution by slow cooling (0.15 K/hour) from T_s down to ~ 30 K below T_s. Once the cooling ramp was over, the grown crystal was slowly extracted from the supersaturated solution (at 0.1 mm/min) and held slightly above the surface of the solution to avoid cracking due to thermal shocks. Finally, the furnace was cooled at a rate of 20 K/hour down to room temperature. The as-grown KYW crystal was then cut in slices perpendicular to the **b**-crystallographic direction, with typical dimensions (10mm × 2.5mm × 25 mm) and polished to high quality.

The patterning of the substrate was carried out by the author at the Integrated Photonics Cleanroom (IPC) at the University of Southampton. A photoresist (S1828) layer was spun on the substrate, which was then photolithographically patterned by UV exposure and consequent development of the mask. The mask transferred onto the substrate was a dark-field mask with openings of widths 3 µm-10 µm in steps of 0.2 µm. This was then etched by ion-beam milling in an Ionfab 300 Plus Ion-beam system using inert Ar^+ ions. The sample was etched for 4 hours and 30 minutes with a current of 100 mA and a voltage of 500 V. The resist was then removed by solvents and plasma-ashing in an OPT Plasmalab 80 Plus Reactive Ion Etcher. The processing steps are shown in Figure 4-36.

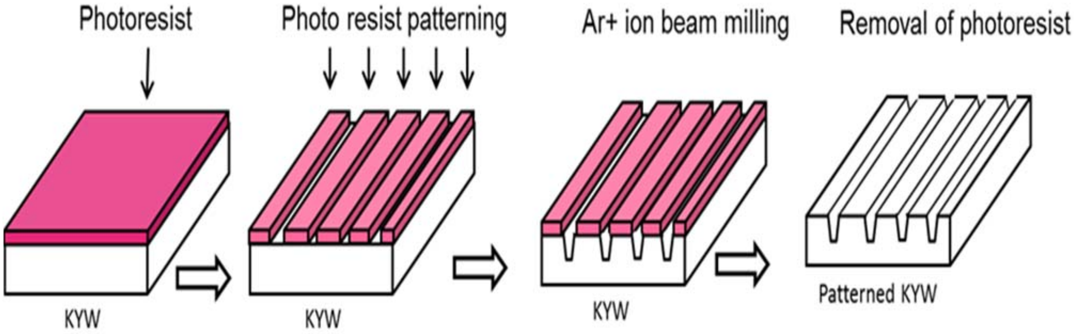

Figure 4-36. The etching steps of the KYW substrate.

The etch depth was measured by KLA Tencor P-16 Stylus Profiler and was found to be to be 5 µm as shown in Figure 4-37. The resulting grooves, fabricated parallel to the N_g optical direction, were used as the basis for growth of inverted rib waveguide structures, as described below.

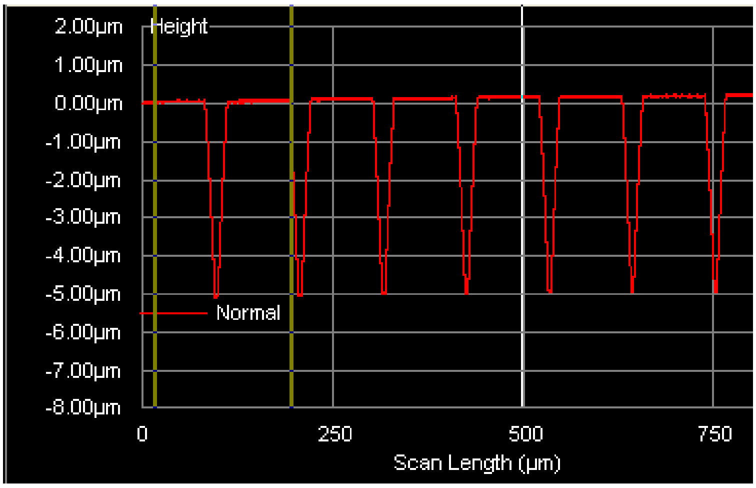

Figure 4-37. 2-d Profile of the etched KYW substrate

A KYW layer substituted with 18 mol% Gd, 25 mol% Lu and activated with 3 mol% Yb was grown over the microstructured KYW substrate by LPE [25], at URV Tarragona. Gd was introduced into the KYW matrix in order to increase the refractive index with respect to the substrate and Lu was added in compensation, to match the lattice parameter of the layer structure to that of the substrate [26]. In this case, 80 g of solution in the solute/solvent ratio 7 mol% $KY(WO_4)_2$/93 mol% $K_2W_2O_7$ were mixed inside a cylindrical platinum crucible (~50 cm^3). After homogenisation, the saturation temperature T_s was determined in the same way as for the KYW bulk crystals. The substrate was vertically dipped into the solution at 1 K above T_s over a period of 5 minutes with the aim of inducing dissolution of its surface and hence avoiding the introduction of defects in the subsequent layer growth. The epitaxial growth of the layer started on decreasing the temperature of the solution 3 K below T_s and finished 3 hours later by holding the substrate with the grown layer at 1 mm above the surface of the solution. The furnace was cooled down to room temperature at 15 K/hour. The layer had a thickness of 50 μm, measured with respect to the surface not exposed to the Ar^+-milling. The epitaxial layer grown over the etched face of the substrate was polished down to a thickness of <1μm. A KYW cladding layer was then grown over the channels by LPE, following the same procedure as for the doped layer. The growth of the active layer and cladding layer is summarised in Figure 4-38.

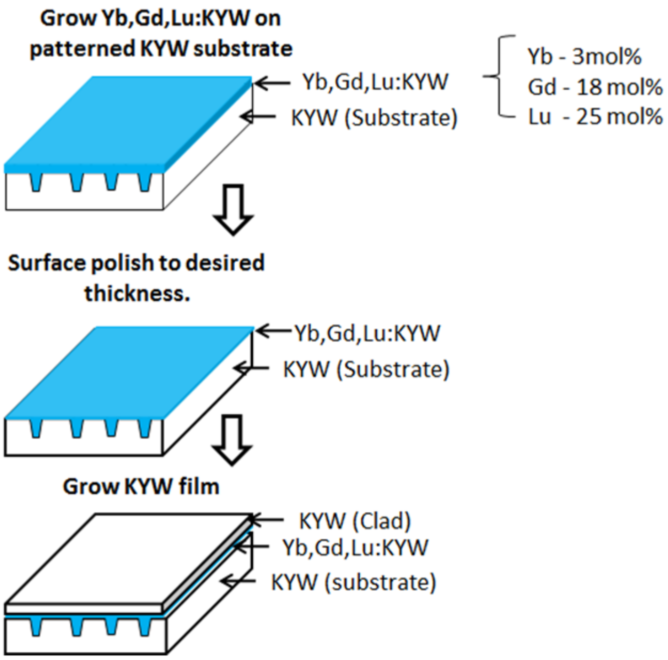

Figure 4-38. Growth of the active layer and the cladding layer.

The sample was then cut perpendicular to the N_g optical direction in such a way that light could be coupled into the inverted ribs either polarized horizontally ($\mathbf{E}//N_m$) or vertically ($\mathbf{E}//N_p$) whilst propagating parallel to N_g. The sample was then polished to a length of 3 mm. Figure 4-39 shows the SEM image of the end face of the waveguide. It can be seen that the polishing of the active layer to the desired thickness was not perfect, leading to a non-uniform thickness, which could be one of the major factors contributing to the high propagation loss as discussed later.

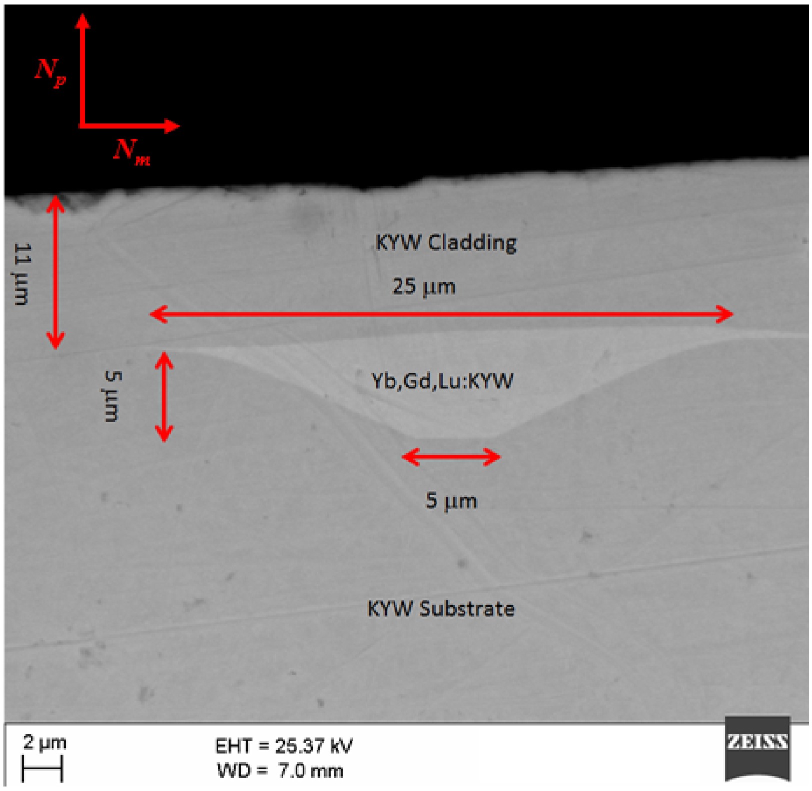

Figure 4-39. SEM cross- section view of the “inverted” waveguide

4.4.2 Laser experiments

The experimental setup for the laser experiments performed using the inverted rib waveguide was similar to that described in chapter 2. The waveguides were pumped by a Ti:sapphire laser tuned to 932 nm and was horizontally (TE) polarised. Lasing results at 981 nm and 1000 nm have been discussed in the following sub-sections.

4.4.2.1 Lasing at 981 nm

For this set of experiments, the first cavity formed was without the use of any external mirrors, the feedback being provided by the Fresnel reflections (11%) from each of the end-facets. The input and output powers were measured and the slope efficiency (for the combined output from both ends) was found to be 58% with respect to absorbed power (which was calculated by measuring transmission of the pump through the waveguide, on and off absorption near the threshold power as described in 3.3.2.3), with a threshold power of 23 mW. The maximum power extracted in this configuration was 17 mW. Similar experiments were repeated with different cavities ie: HR/Fresnel cavity, HR/24%T cavity and HR/6%T cavity. The results are presented in Figure 4-40 and summarized in table 1. The lowest threshold power obtained was 13 mW for the HR/6%T cavity.

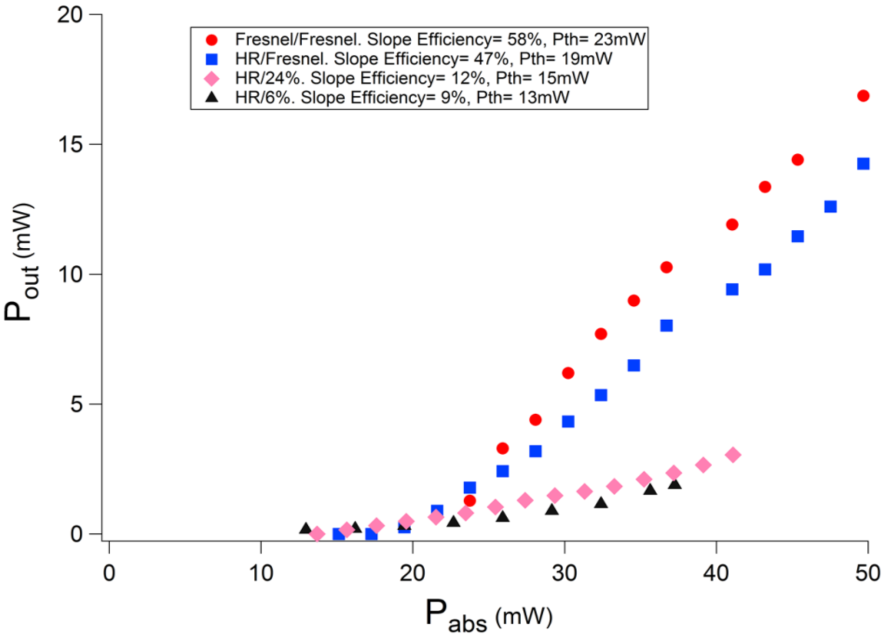

Figure 4-40. Output power (P_{out}) vs. Absorbed power (P_{abs}) for different cavity configurations.

Table 4-3. Summary of threshold powers and slope efficiencies for different cavities.

Cavity	Absorbed threshold power (mW)	Slope efficiency (%)
Mirrorless (Fresnel/Fresnel)	23	58
1 Mirror (HR/Fresnel)	19	47
HR/24%	15	12
HR/6%	13	09

The losses were estimated by a Caird analysis (section 3.3.2.1) and confirmed by transmission measurements (section 3.3.2.3) to be ~2.7 dB/cm, which is 1.7 dB/cm higher than that measured for a planar waveguide fabricated by LPE. This is also higher than previously reported values in this material [27], which may be attributed to the imperfect polishing of the active layer as seen from Figure 4-39. The output spectrum was measured by an optical spectrum analyser (OSA) and was centred at 980.8 nm as shown in Figure 4-41 and the laser output was horizontally polarized (E//$\boldsymbol{N_m}$).

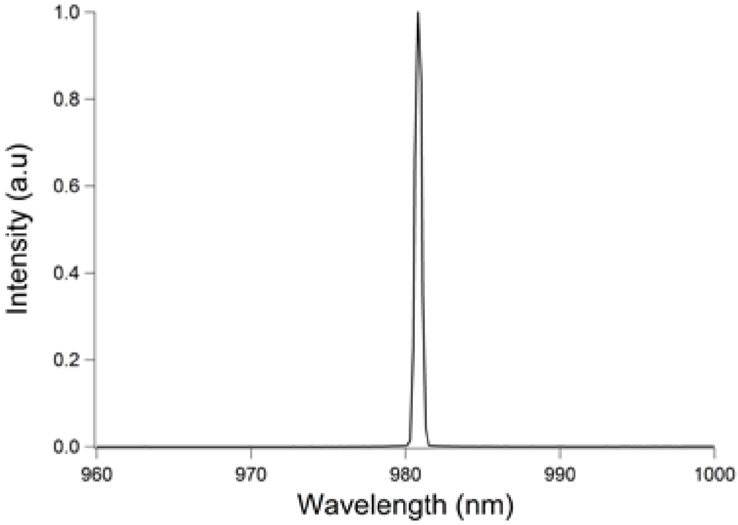

Figure 4-41. The measured spectrum centred at 980.8 nm.

The output beam was imaged onto a CMOS camera and is shown in Figure 4-42. The output is single-mode with beam radii of 4.8 μm and 3 μm in the x and y-direction respectively. The simulated (using OlympIOs commercial software) beam profiles is slightly different to with the predicted mode radii being 4.1 μm and 2.2 μm in the x and y-directions respectively. This may be due to the simulated structure being different to the somewhat irregular experimental structure seen in Figure 4-39.

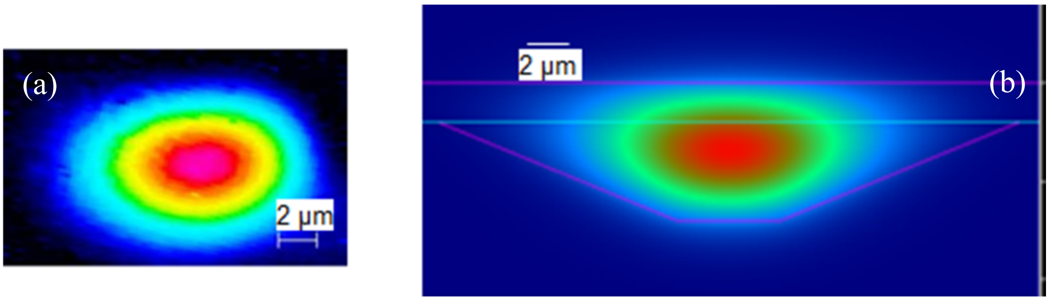

Figure 4-42. a. Measured laser mode. b. Simulated laser mode.

4.4.2.2 *Lasing at 999.8 nm*

The mirrors were changed for these set of experiments, with the input mirror having >99.8% transmission at 932 nm and <1% transmission at 999.8 nm and the output mirror having a transmission of 5% at 999.8 nm. The threshold was observed to be 8 mW and the slope efficiency was found to be 4.8%. The input-output characteristics are shown in Figure 4-43. The lasing wavelength was found to be 999.8 nm.

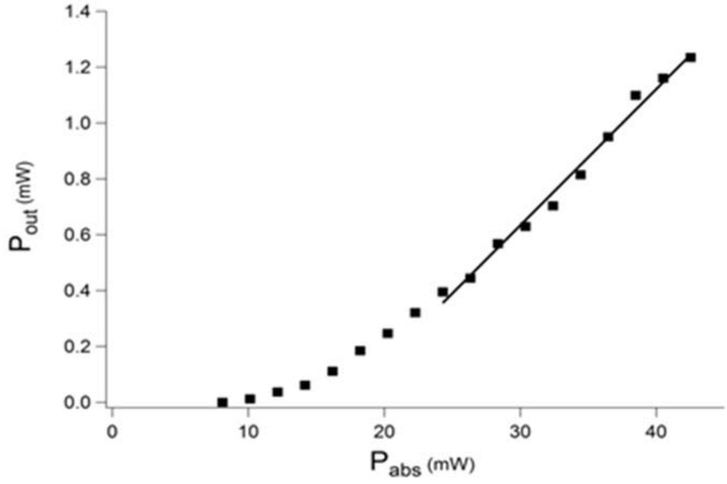

Figure 4-43. Output power (Pout) vs. Absorbed power (Pabs) for the HR/5% cavity.

On moving the launching objective horizontally, it was possible to achieve operation at 981 and 999 nm simultaneously as well as only at 981 nm as seen from Figure 4-44.

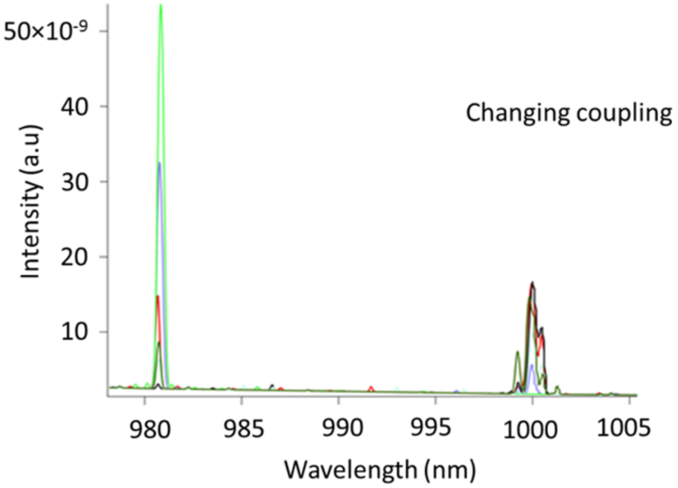

Figure 4-44. Effect of coupling on laser wavelength.

4.4.2.3 Discussions

As described in the previous sub-sections, 981 nm was the preferred lasing wavelength when compared to the more commonly operated 1024 nm transition. The evolution of the fluorescence spectra with increasing launch power was studied in the mirrorless cavity configuration. A fibre-coupled OSA was used to take these spectra with the fibre at the end of the waveguide and from the top of the waveguide. Figure 4-45 shows the measured spectra.

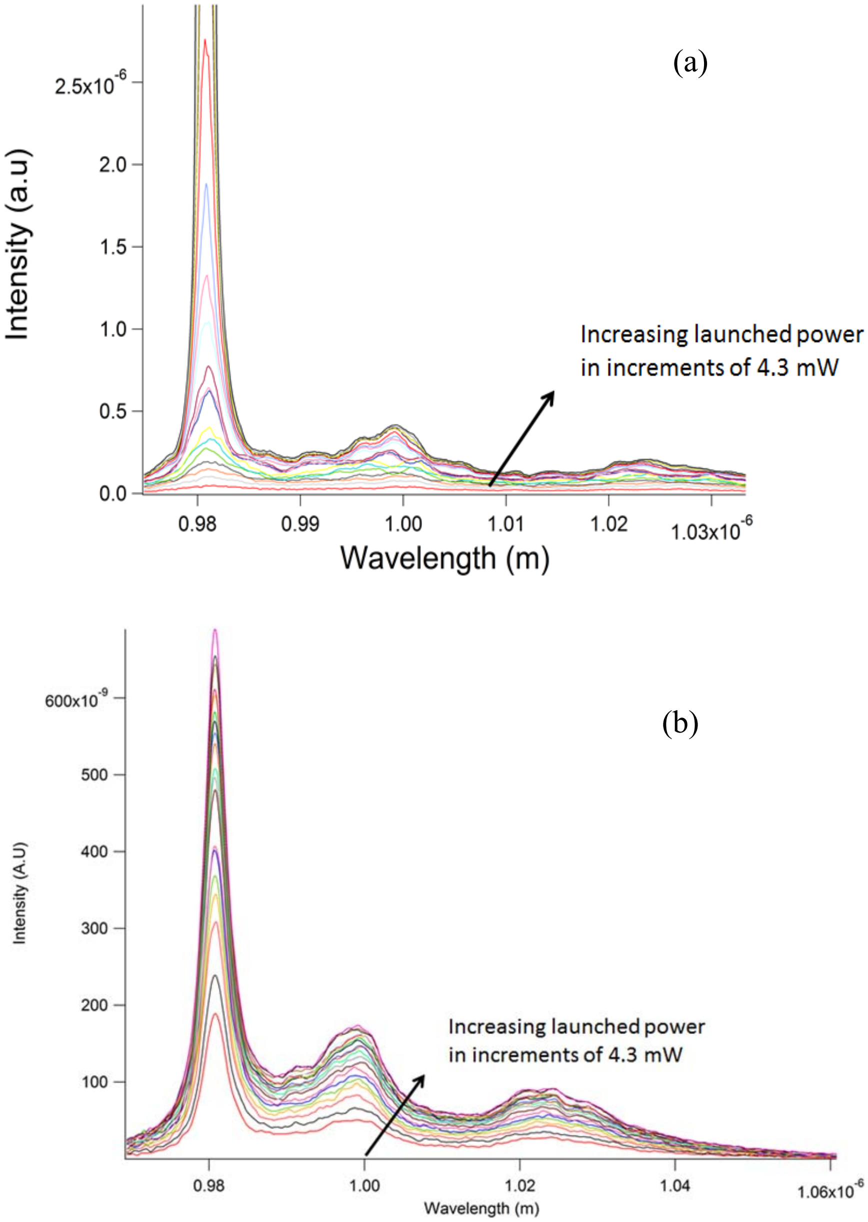

Figure 4-45. (a) Evolution of spectra with launched pump power measured end-on and (b) a. evolution of spectra with launched pump power measured from the top.

Figure 4-46 shows the extracted peak intensity for each power (measured from the end). It is clearly seen that most of the gain is taken by the 981 nm wavelength and hence is the preferred wavelength when compared to 999.8 nm and 1024 nm laser wavelength. This observation is consistent with calculations carried out assuming a propagation loss of 2.7 dB/cm. The calculated threshold powers for 1024 nm, 999.8 nm and 981 nm for a mirrorless cavity are 32 mW, 20 mW and 17 mW, hence the 981 nm wavelength reaches threshold first.

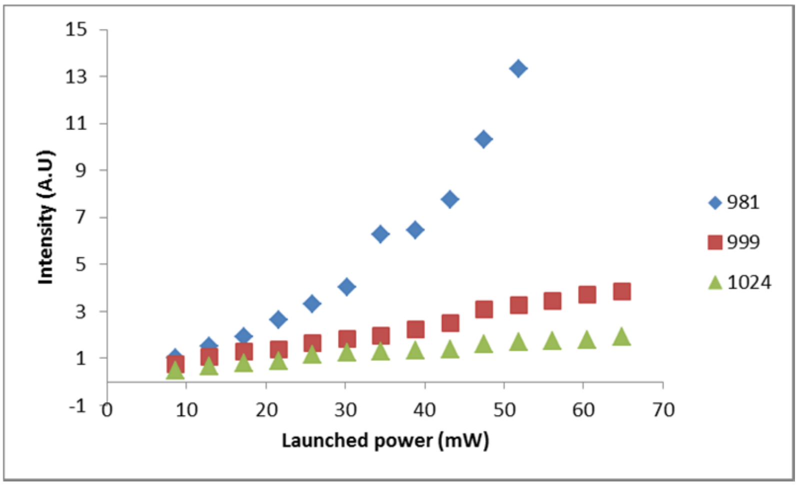

Figure 4-46. Extracted peak intensities for 981nm, 999.8 nm and 1024 nm as a function of power.

For the HR/5%T cavity the laser threshold is calculated to be 3.5 mW for the 1024 nm wavelength compared to 16.5 mW for the 981 nm and 3 mW for the 999.8 nm. Hence the 999.8 nm radiation reaches threshold first. In each case, the balance between gain, re-absorption loss, propagation loss and cavity loss allows selection between these wavelengths.

4.5 Conclusions

In this chapter, the first mode-locking results with an Yb^{3+}-doped waveguide laser have been presented. A fundamentally mode-locked repetition-rate of 4.9 GHz was achieved at a maximum output power of 81 mW and pulse durations as short as 740 fs, with an output wavelength of 1052 nm. A novel dispersion technique for waveguide lasers was employed using the Gires Tournois interferometer (GTI) effect by controlling the gap between the waveguide and the SESAM or the output coupler. Using shorter devices, this repetition-rate was increased to 15.2 GHz, which to date is the highest fundamental repetition-rate achieved from any solid-state waveguide laser. These devices are very promising for laser frequency metrology and medical applications.

Next, results with ytterbium-doped $RbTiOPO_4$ were presented as a potential ultrafast laser host compatible with fabrication of waveguide geometries. Laser action was demonstrated for the first time in an (Yb,Nb):RTP planar waveguide laser. The active layer was epitaxially grown to a thickness of 10 μm and a laser threshold power of 276 mW was observed. Unfortunately, due to the limitation of the pump power, the input-output characterisation could not be carried out, which will be done in the future with high power laser diodes. In order to reduce the threshold power of the (Yb,Nb):RTP waveguide laser, channels were fabricated in epitaxially grown films by ion-beam milling and reactive ion etching (RIE). Second harmonic generation was also observed at a wavelength of 570 nm for a fundamental wavelength of 1140 nm in waveguides fabricated by ion-beam milling. The propagation losses were measured to be 3 dB/cm. Unfortunately, these losses were too large for laser operation to be achieved. RIE was then investigated as an alternative fabrication technique using SF_6 and Ar gases. A systematic study of the RIE parameters (RF power, gas pressure and gas ratio) was carried out to optimize the etching. The first ever (Yb,Nb):$RbTiOPO_4$ channel waveguide fabricated by reactive ion etching was demonstrated with a propagation loss of 3.5 dB/cm. Once again propagation losses were found to be high and therefore laser action could not be demonstrated in these channel waveguides.

Yb:KYW was also investigated as a potential material system for ultrafast waveguide laser operation. However, once again the final propagation losses were found to be high and laser action was preferred at the high-gain 981 nm wavelength. Mirrorless lasing was demonstrated in an “inverted” Yb,Gd,Lu:KYW waveguide laser fabricated by ion-beam milling. Pure 3-level operation at 981 nm was observed with a slope efficiency of 58%. Using smaller output couplers, a threshold power as low as 13 mW was observed. Laser action was also observed at 999.8 nm using a different mirror set. Future work will involve etching Yb,Gd,Lu:KYW using smaller etch depths and less vigorous etching parameters to get losses as loss as 0.3 dB/cm as demonstrated by Geskus et al [27].

Although other authors have demonstrated low-loss Yb:KYW waveguide lasers [27], and very short pulses have been demonstrated in bulk Yb:KYW lasers [28], our preferred host for further experiments in ultrafast waveguide lasers is glass due to ease of fabrication of low-loss guides by ion-exchange, relative cheapness of the material and ease of incorporating other dopants, and the future possibility of incorporating such lasers in highly integrated optical circuits.

4.6 References

1. Veasey, D. L., Funk, D. S., Peters, P. M., Sanford, N. A., Obarski, G. E., Fontaine, N., Young, M., Peskin, A. P., Liu, W. C., Houde-Walter, S. N. and Hayden, J. S., *Yb/Er-codoped and Yb-doped waveguide lasers in phosphate glass.* Journal of Non-Crystalline Solids, 2000. **263-264**: p. 369-381.
2. Ulrich, R. and Torge, R., *Measurement of Thin Film Parameters with a Prism Coupler.* Appl. Opt., 1973. **12** (12): p. 2901-2908.
3. Kin S. C., *Construction of refractive-index profiles of planar dielectric waveguides from the distribution of effective indexes.* Lightwave Technology, Journal of, 1985. **3** (2): p. 385-391.
4. Choudhary, A., Lagatsky, A. A., Kannan, P., Sibbett, W., Brown, C. T. A. and Shepherd, D. P., *Diode-pumped femtosecond solid-state waveguide laser with a 4.9 GHz pulse repetition rate.* Opt. Lett., 2012. **37** (21): p. 4416-4418.
5. Lagatsky, A. A., Choudhary, A., Kannan, P., Shepherd, D. P., Sibbett, W. and Brown, C. T. A., *Fundamentally mode-locked, femtosecond waveguide oscillators with multi-gigahertz repetition frequencies up to 15 GHz.* Opt. Express, 2013. **21** (17): p. 19608-19614.
6. ISO standard, *11146 Lasers and laser-related equipment – Test methods for laser beam widths, divergence angles and beam propagation ratios*, 2005.
7. Kartner, F.X., Jung, I.D. and Keller, U., *Soliton mode-locking with saturable absorbers.* Selected Topics in Quantum Electronics, IEEE Journal of, 1996. **2** (3): p. 540-556.
8. Hönninger, C., Paschotta, R., Morier-Genoud, F., Moser, M. and Keller, U., *Q-switching stability limits of continuous-wave passive mode locking.* J. Opt. Soc. Am. B, 1999. **16** (1): p. 46-56.
9. Kuhl, J. and Heppner, J., *Compression of femtosecond optical pulses with dielectric multilayer interferometers.* Quantum Electronics, IEEE Journal of, 1986. **22** (1): p. 182-185.
10. Krainer, L., Paschotta, R., Moser, M. and Keller, U., *77 GHz soliton modelocked Nd:YVO*$_4$ *laser.* Electronics Letters, 2000. **36** (22): p. 1846-1848.
11. Diels, J.-C. and Rudolph, W., *Femtosecond Optics*, in *Ultrashort Laser Pulse Phenomena* 2006, Academic Press: Burlington. p. 61-142.
12. Kärtner, F.X. and Keller, U., *Stabilization of solitonlike pulses with a slow saturable absorber.* Optics Letters, 1995. **20** (1): p. 16-18.
13. Cugat, J., Sole, R. M., Carvajal, J. J., Pujol, M.C., Mateos, X., Diaz, F. and Aguilo, M., *Crystal growth and characterization of* $RbTi_{1-x-y}Yb_xNb_yOPO_4/RbTiOPO_4$ *(001) non-linear optical epitaxial layers.* CrystEngComm, 2011. **13** (6): p. 2015-2022.
14. Carvajal, J. J., Solé, R., Gavaldà, Jna, Massons, J., Segonds, P., Boulanger, B., Brenier, A., Boulon, G., Zaccaro, J., Aguiló, M. and Díaz, F., *Spectroscopic and second harmonic generation properties of a new crystal:Yb-doped* $RbTiOPO_4$*.* Optical Materials, 2004. **26** (3): p. 313-317.
15. Carvajal, J. J., Nikolov, V., Solé, R., Gavaldà, Jna, Massons, J., Aguiló, M. and Díaz, F., *Crystallization Region, Crystal Growth, and Characterization of Rubidium Titanyl Phosphate Codoped with Niobium and Lanthanide Ions.* Chemistry of Materials, 2002. **14** (7): p. 3136-3142.

16. Cugat, J., Choudhary, A., Sole R., Carvajal, J.J., Massons, J., Shepherd, D.P., Diaz, F. and Aguilo, M., *Ar^+ ion milling rib waveguides on nonlinear optical (Yb,Nb):RTP/RTP epitaxial layers*. Optical Materials Express, 2013. **3** (11): p.1912-1917.
17. Choudhary, A., Cugat, J., Pradeesh, K., Solé, R., Díaz, F., Aguiló, M., Chong, H. M. H. and Shepherd, D. P., *Single-mode rib waveguides in (Yb,Nb):$RbTiOP_4$ by reactive ion etching.* Journal of Physics D: Applied Physics, 2013. **46** (14): p. 145108.
18. Kohler, M., *Etching in Microsystem Technology*, 1999, Weinheim: Wiley-VCH Verlag GmbH.
19. Legtenberg, R., Jansen, H., de Boer, M. and Elwenspoek, M., *Anisotropic Reactive Ion Etching of Silicon Using $SF_6/O_2/CHF_3$ Gas Mixtures.* Journal of The Electrochemical Society, 1995. **142** (6): p. 2020-2028.
20. Choi, H.J. and Lee, B.T., *Inductively Coupled Plasma Reactive Ion Etching of SiC Single Crystals Using NF_3-Based Gas Mixtures.* Journal of Electronic Materials, 2003. **32** (1): p. 1-4.
21. Mateos, X., Petrov, V., Peña, A., Carvajal, J. J., Aguiló, M., Díaz, F., Segonds, P. and Boulanger, B., *Laser operation of Yb^{3+} in the acentric $RbTiOPO_4$ codoped with Nb^{5+}*. Opt. Lett., 2007. **32** (13): p. 1929-1931.
22. Geskus, D., Aravazhi, S., Wörhoff, K. and Pollnau, M., *High-Gain $KY(WO_4)_2$:Yb^{3+} Planar Waveguide Laser at the Zero-Phonon Line*. 2010 in *Conference on Lasers and Electro-Optics*.
23. Geskus, D., Aravazhi, S., Wörhoff, K. and Pollnau, M., *High-power, broadly tunable, and low-quantum-defect $KGd_{1-x}Lu_x(WO_4)_2$:Yb^{3+} channel waveguide lasers.* Opt. Express, 2010. **18** (25): p. 26107-26112.
24. Choudhary, A., Bolaños, W., Kannan, P., Carvajal, J.J., Aguilò, M., Diaz, F. and Shepherd, D.P., *Low-threshold, mirrorless emission at 981 nm in an Yb,Gd,Lu:KYW inverted rib waveguide laser*. 2013. Proc. SPIE 8599, Solid State Lasers XXII: Technology and Devices, 859905
25. Bolaños, W., Carvajal, J. J., Mateos, X., Murugan, G. S., Subramanian, A., Wilkinson, J. S., Cantelar, E., Lifante, G., Aguiló, M. and Díaz, F., *$KY_{0.58}Gd_{0.22}Lu_{0.17}Tm_{0.03}(WO_4)_2$ buried rib waveguide lasers.* Optical Materials, 34, (2), 475-480.
26. Bolaños, W., Carvajal, J.J., Pujol, M. C., Mateos, X.,Lifante, G., Aguiló, M. and Díaz, F., *Epitaxial Growth of Lattice Matched $KY_{1-x-y}Gd_xLu_y(WO_4)_2$ Thin Films on $KY(WO_4)_2$ Substrates for Waveguiding Applications.* Crystal Growth & Design, 2009. **9** (8): p. 3525-3531.
27. Geskus, D., Aravazhi, S., Grivas, C., Wörhoff, K. and Pollnau, M., *Microstructured $KY(WO_4)_2$:Gd^{3+}, Lu^{3+}, Yb^{3+} channel waveguide laser.* Opt. Express. **18** (9): p. 8853-8858.
28. Kuleshov, N. V., Lagatsky, A. A., Podlipensky, A. V., Mikhailov, V. P. and Huber, G., *Pulsed laser operation of Yb-doped $KY(WO_4)_2$ and $KGd(WO4)_2$* Optics Letters, 1997. **22** (17): p. 1317-1319.

Chapter 5 Er, Yb-doped glass waveguides

5.1 Introduction

In the previous chapters, continuous wave (CW) and mode-locking results obtained with Yb^{3+}-doped waveguides operating near 1 μm were presented. Er^{3+}-doped gain media are widely used to develop lasers operating around 1.5 μm, primarily for applications in telecommunications. This motivation has meant that most of the limited work in mode-locked waveguide lasers to date has been based on Er-doped materials. However, these tended to use extended cavities and hence the repetition-rates have been lower than 1 GHz [1-6]. More recently a fully integrated waveguide laser has been demonstrated with a repetition-rate of 400 MHz and power levels of about 1 mW [7]. In this device, the saturable absorber element was end-butted on the waveguide and dispersion compensation was achieved on the chip itself by using an un-doped waveguide section with negative dispersion [7].

In this chapter, mode-locking results obtained in waveguides fabricated by ion-exchanging a commercially available Er, Yb-doped phosphate glass (IOG-1, Schott glass technologies, Inc) are presented. Yb^{3+}-sensitizer ions are co-doped with Er^{3+} within the glass matrix to increase the absorption of the pump owing to the small absorption cross sections of the Er^{3+} ions. A monolithic cavity was formed by end-butting a semiconductor saturable absorber mirror (SESAM) and output coupling (OC) mirrors directly to the waveguide and dispersion compensation was achieved through the Gires-Tournois interferometer (GTI) effect [8] by controlling the gap between the SESAM and the waveguide.

Quantum dot (QD) SESAMs [9] have been recently developed as an improvement over conventional quantum well SESAMs giving low non-saturable losses, low saturation fluence and fast recovery times. The concentration of the QDs can also be controlled during fabrication to achieve the desired modulation depth for stable mode-locking for very high repetition-rates (> 1 GHz). Until recently, GaAs-based QD SESAMs have been used to demonstrate mode-locking around the 1.3-μm spectral regime [9]. However, due to challenges in material engineering it is very difficult to fabricate QD SESAMs for 1.5 μm.

InP-based platforms are used for fabricating optical devices near 1.5 μm, however InP-based QDs have not been perfected yet.

The first ever demonstration of mode-locked operation around 1.5 μm using an InGaAs/InGaAs QD-SESAM was demonstrated recently using a bulk Er,Yb glass laser with a repetition-rate of 10 GHz and an output power of 8 mW [10]. For the experiments described in this chapter, a similar QD-SESAM fabricated by researchers at the University of Sheffield was employed, resulting in a repetition-rate of up to 6.8 GHz. A dot in well (DWELL) structure was used for these experiments, which is described in section 5.3. To the best of my knowledge, this is the first ever demonstration of mode-locked operation of a waveguide laser using a quantum dot SESAM at any wavelength. 6.8 GHz is also the highest reported repetition-rate from a fundamentally mode-locked waveguide laser at 1.5 μm. The fabrication of the waveguides and the modelling of the mode profile was carried out by Dr. Pradeesh Kannan.

5.2 Fabrication of waveguides

Commercially available phosphate glasses from Schott Glass Technologies Inc. (IOG-1), doped with 1.16 wt. % erbium (Er) and 4.77 wt. % ytterbium (Yb) were used as the host material. Ion-exchange was carried out using the processing steps outlined in chapter 3. The dimensions of the glass substrates used for fabrication were 2.5cm × 2.5cm × 0.2cm. After metal masking with mask opening widths of 1 μm to 10 μm in steps of 0.2 μm, these glass substrates were kept immersed for 30 minutes in a molten mixture of 45% KNO_3 – 50% $NaNO_3$ – 5% $AgNO_3$ (mol%) in a furnace at 325°C. After the ion-exchange and mask removal, the glass samples were polished to lengths of 20 mm and 14.5 mm, respectively.

The refractive index profile of the ion-exchanged glass was measured in a planar waveguide fabricated using the same processing steps as the channel waveguide, except for the metal masking. M-line measurements were performed by prism coupling and the diffusion depth was found to be 14.6 μm and the index contrast between the surface and the substrate was found to be 5.1×10^{-3} at 1553 nm. The fundamental mode at 1553 nm was simulated by a commercially available waveguide modelling package (RSoft CAD) for a waveguide fabricated using a mask opening of 6 μm, corresponding to the waveguides used to obtain the laser results discussed in the following sections. The $1/e^2$ beam radii were found to be 9 μm and 5.7 μm along the horizontal and vertical directions, respectively, as shown in Figure 5-1.

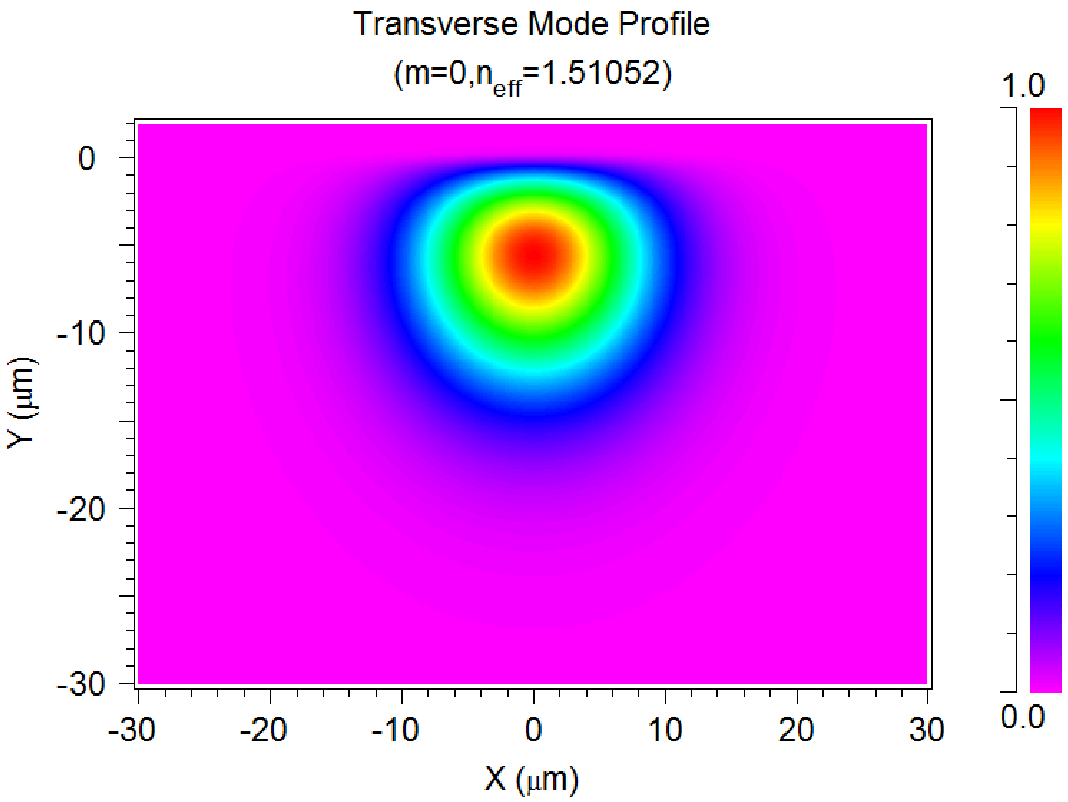

Figure 5-1. The simulated mode profile at 1553 nm for the waveguide fabricated using a 6 μm mask opening.

5.3 Quantum dot SESAM structure

The 1550 nm QD-SESAM structure was grown in a solid-source III-V molecular beam epitaxy machine (VG 90 by Oxford Plasma systems). A distributed Bragg reflector (DBR) structure consisting of 31 pairs of GaAs (115 nm) and $Al_{0.98}Ga_{0.02}As$ (134 nm) was grown on a semi-insulating GaAs 100 substrate. On top of the DBR mirror [10], one DWELL structure was grown. The DWELL structure consisted of a 1 nm layer of $In_{0.18}Ga_{0.82}As$, the InGaAs/GaAs quantum dot layer and 6 nm $In_{0.31}Ga_{0.69}As$ layer. Finally, a GaAs capping layer was grown on top of the DWELL structure. The In-layers were grown at 530°C and the GaAs layers were grown at a temperature of 565°C.

A schematic of the QD-SESAM structure is shown in Figure 5-2 and the reflectivity curve of the SESAM was measured by Dr. Alexander Lagatsky at the University of St. Andrews and is shown in Figure 5-3. A similar QD SESAM has a saturation fluence (F_{sat}) of 9 μJ/cm^2 and a modulation depth (ΔR) of 0.4% and non-saturable losses (ΔR_{ns}) <0.1% as discussed in [10].

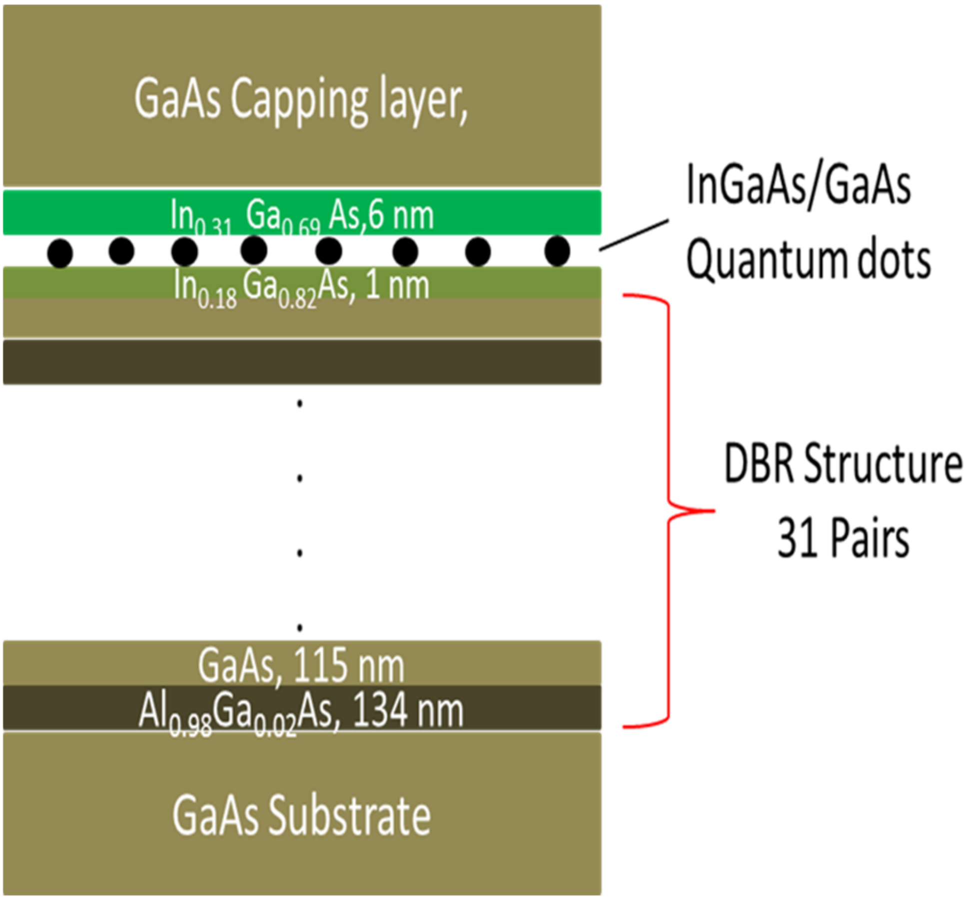

Figure 5-2. The QD SESAM Structure

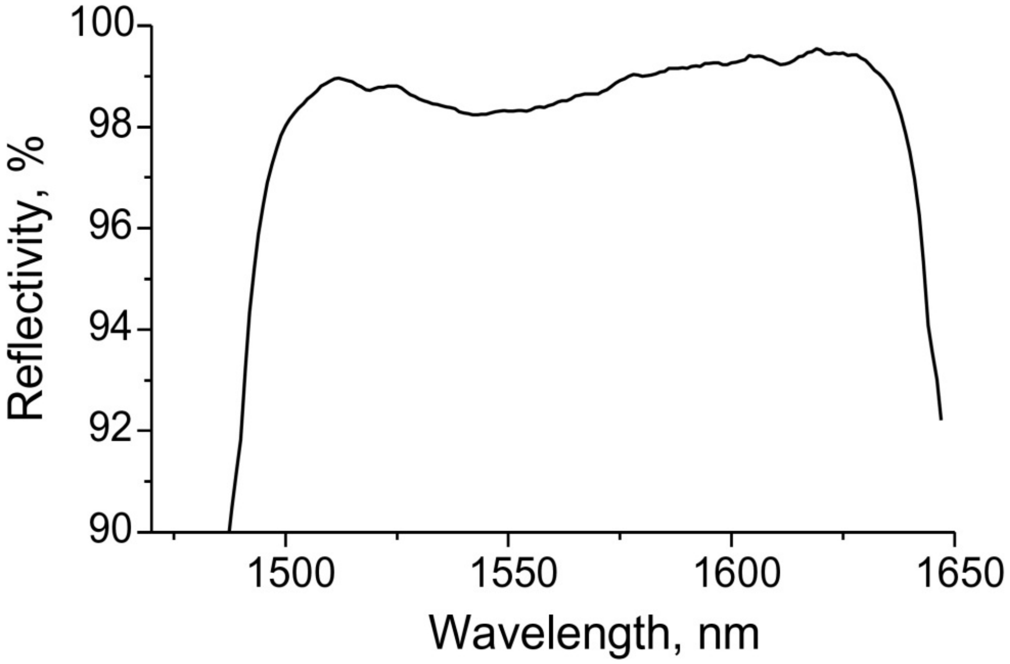

Figure 5-3. The reflectivity curve for the Quantum Dot SESAM.

5.4 CW characterisation

For CW lasing experiments, a 2% OC (R=98% at 1550 nm and R<1% at 974 nm) and a high reflectivity mirror (R>99.8% at 1550 nm) were end-butted on the 14.5-mm-long and 20-mm-long waveguides using fluorinert (FC-70, Sigma Aldrich). The waveguide was held on a thermo-electrically cooled copper mount kept at a constant temperature of 18°C as the performance was found to deteriorate at room temperature (i.e. CW output power was found to be 10% lower). The pump laser was a fibre-coupled, single-mode laser diode from 3S photonics with a central wavelength of 973.4 nm and a maximum average power of 850 mW. The experimental setup is similar to Figure 3-6, except with a high reflector (HR) mirror in place of a SESAM. The pump was collimated by a ×20 objective having a focal length of 8 mm and was then launched into the waveguide using a ×10 objective with a focal length of 15.4 mm resulting in a launched spot radius of 6.4 µm. The output power (P_{out}) versus input power (P_{in}) characteristics obtained with the 14.5-mm-long sample is shown in Figure 5-4.

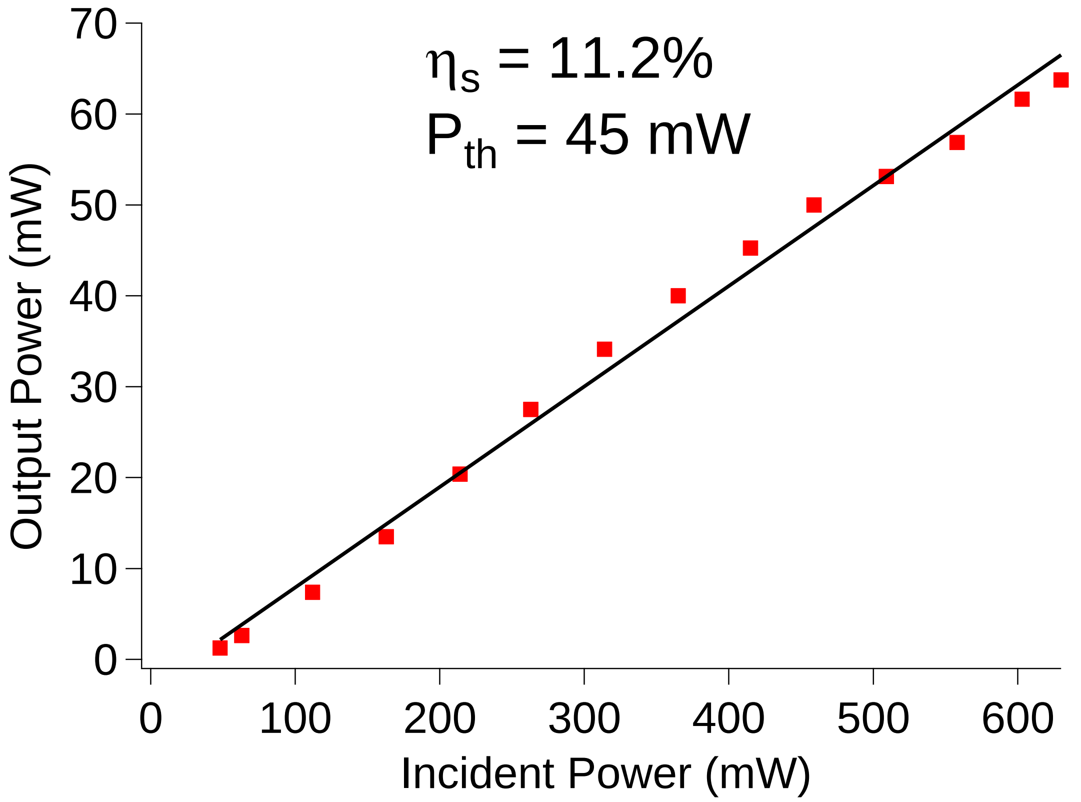

Figure 5-4. Output power against input power characteristics for the 14.5-mm-long waveguide sample.

The slope efficiency was measured to be 11.2% and the threshold power was 45 mW for a waveguide fabricated by a mask opening of 6 μm. The laser spectrum was measured by an optical spectrum analyser (OSA) and was centred at 1558 nm. The upper limit on the propagation loss was estimated to be 0.15 dB/cm by using the measured value of the slope efficiency and equation 2.55, with an assumption of a perfect overlap between the pump mode and the laser mode and a perfect launch of the pump into the waveguide. The transmission of the pump at different powers was measured through the waveguide after removing the mirrors and the results are presented in Figure 5-5. It can be seen that the transmission at threshold power is less than 1% (assuming a 100% launch efficiency), implying that around threshold the absorption should be >99% and hence this length of the waveguide is sufficient for efficient absorption.

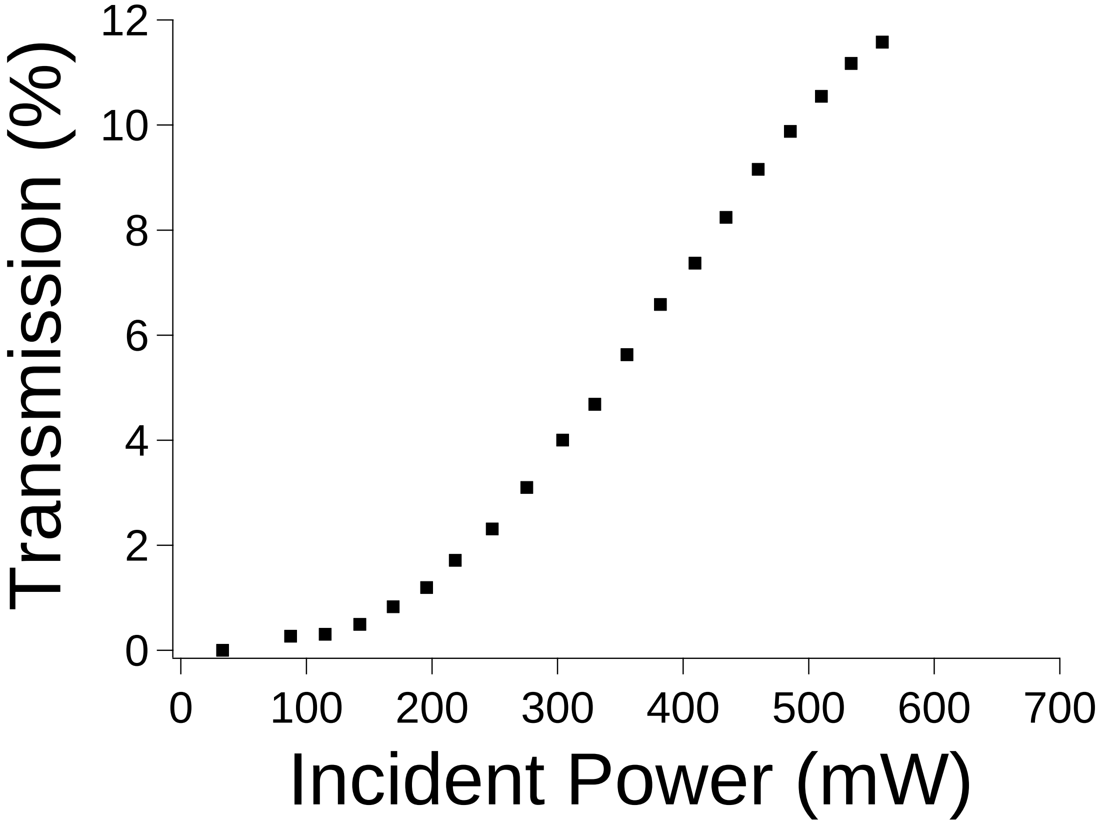

Figure 5-5. Transmission measurement for 14.5 mm long sample.

The output power versus input power curve obtained with the 20-mm-long waveguide is shown in Figure 5-6. The slope efficiency was measured to be 5.5% and the threshold power for lasing was found to be 76 mW. The spectrum was centred at 1564 nm, which is slightly longer than was observed with the 14.5-mm-long waveguide. This is as expected as the use of a longer guide favours operation on the more 4-level transition with reduced re-absorption losses. Using a similar method as for the 14.5-mm-long waveguide, the propagation losses were estimated to be less than 0.25 dB/cm. The slightly higher loss is attributed to the sample to sample variation in fabrication. As seen from Figure 5-5, most of the pump is absorbed within the 14.5-mm-length, and hence the longer length only introduces more re-absorption loss and propagation loss to the cavity. This is the reason for the higher threshold power and the lower maximum output power obtained from this waveguide. The pump mode radii were measured by imaging the output from the waveguide onto a CMOS camera using a lens of focal length 16.9 mm and then using Gaussian beam propagation to calculate the actual spot sizes at the waveguide facet. The beam radii were measured to be 8.1 µm and 5.3 µm along the horizontal and vertical directions, respectively in good correlation with the values of 7.5 µm and 4.9 µm simulated using RSoft CAD.

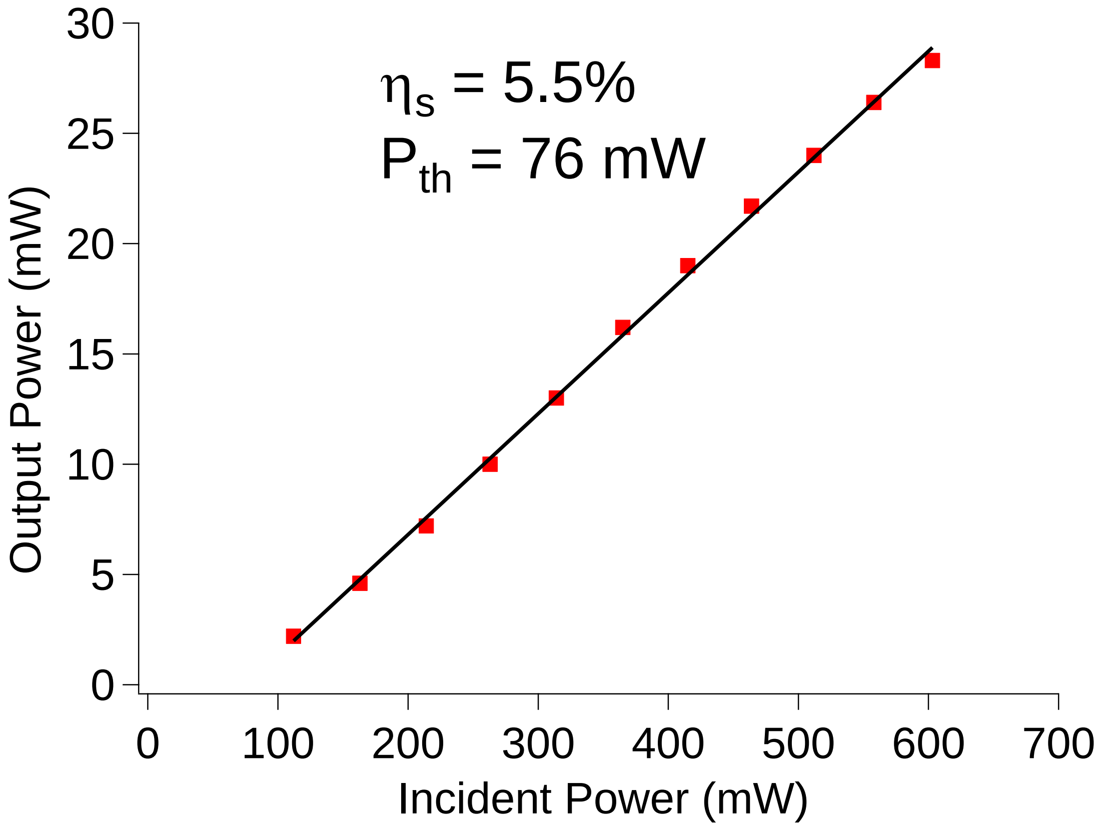

Figure 5-6. Output power against input power characteristics for the 20-mm-long waveguide sample.

5.5 Mode-locking experiments

5.5.1 20-mm-long sample

The HR mirror was replaced by the QD-SESAM for the mode-locking experiments. The QD-SESAM was kept on a 3-axis stage with two additional degrees of freedom to control the tip and tilt of the SESAM to enable alignment with the waveguide. The distance between the SESAM and the waveguide was carefully monitored by using a combination of a ×100 objective lens and a CCD camera kept above the waveguide setup. The control of the gap introduces dispersion in the cavity due to the GTI effect, as discussed in the previous chapter. This in turn reduces the mode-locking threshold due to soliton mode-locking. For the 20-mm-long sample, the laser was found to operate in the Q-switched mode-locking regime at an incident pump power of 415 mW and an output power of 5.6 mW. The Q-switched pulses were recorded using a fast photo-detector (> 25 GHz Bandwidth) and a slow oscilloscope (500 MHz Bandwidth). The system response time was not fast enough to resolve the individual pulses, but the Q-switched pulse envelope was measured and found to have a pulse width of 106 ns and is shown in Figure 5-7. The pulse Q-switched pulse train is shown in Figure 5-8 and the repetition-rate was measured to be 370 kHz.

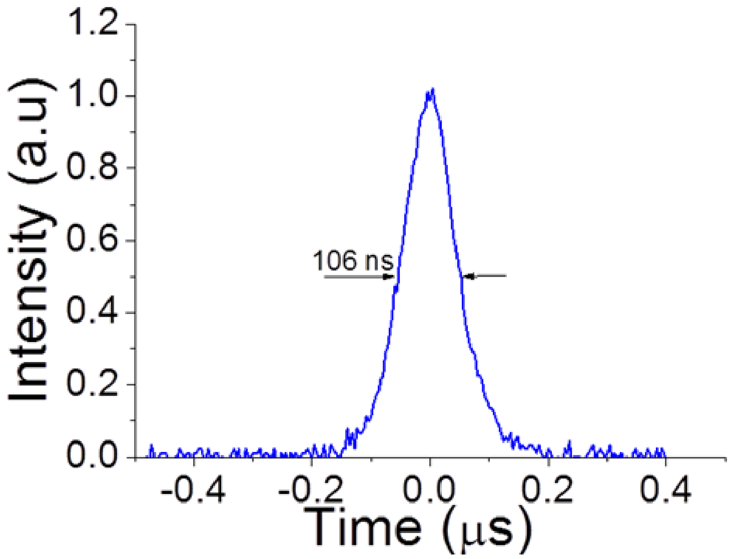

Figure 5-7. Q-switch pulse envelope obtained during Q-switched mode-locking.

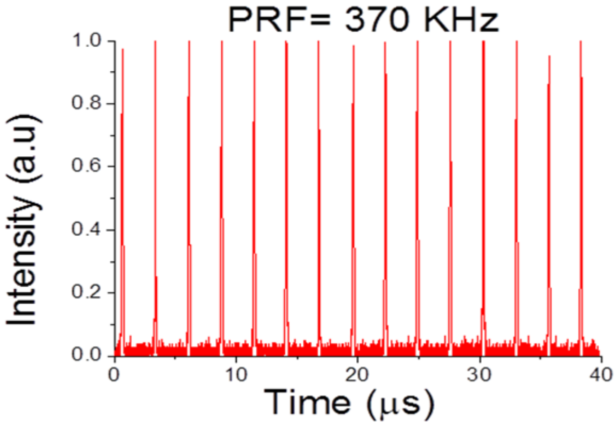

Figure 5-8. The pulse train for the Q-switched pulses.

Q-switched mode-locking was confirmed by radio frequency (RF) spectrum analyser measurements, from the occurrence of multiple peaks. At a pump power of 513 mW, self-starting CW mode-locking was observed with a corresponding output power of 6.7 mW. The air gap between the SESAM and the waveguide was ~ 13 μm and the net round-trip group velocity dispersion (GVD) was estimated to be – 2000 fs^2 using equation (4.2) (the contribution due to the waveguide was -840 fs^2 and the contribution from the GTI was -1160 fs^2). The output power versus input power characteristics of the mode-locked waveguide laser clearly showing the different regimes of operation are shown in Figure 5-9. It can be seen that a maximum power of 9 mW was obtained during stable mode-locked operation.

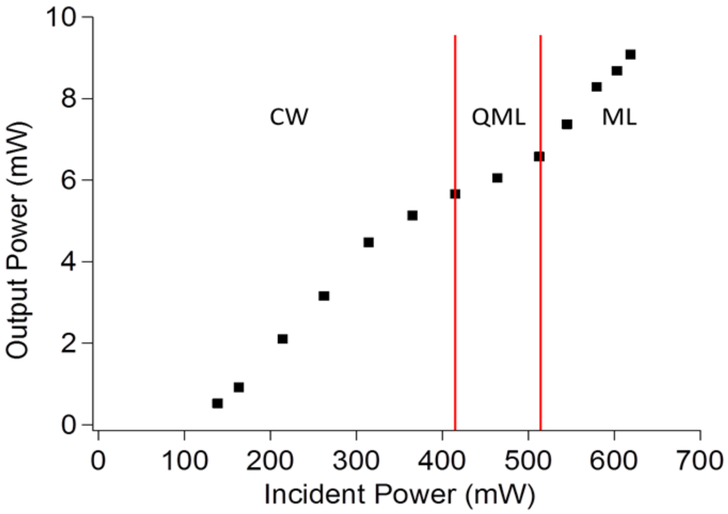

Figure 5-9. Output power versus input power characteristics for the 20-mm-long mode-locked waveguide laser.

The RF spectrum for the mode-locked pulses was recorded using a resolution bandwidth of 10 kHz and a span of 10 MHz and is shown in Figure 5-10. A clean, sharp peak is observed at 4.85 GHz.

The autocorrelation trace was measured at an output power of 9 mW and is shown in Figure 5-11. The blue curve is a sech^2 fit to the experimental data (red dots) and gives a pulse duration of 2.5 ps. The corresponding optical spectrum is shown in Figure 5-12 and it can be seen that the spectrum has a bandwidth of 1.15 nm and is centred at 1556 nm. The pulses have a time-bandwidth product of 0.36, indicating nearly transform-limited sech^2 pulses.

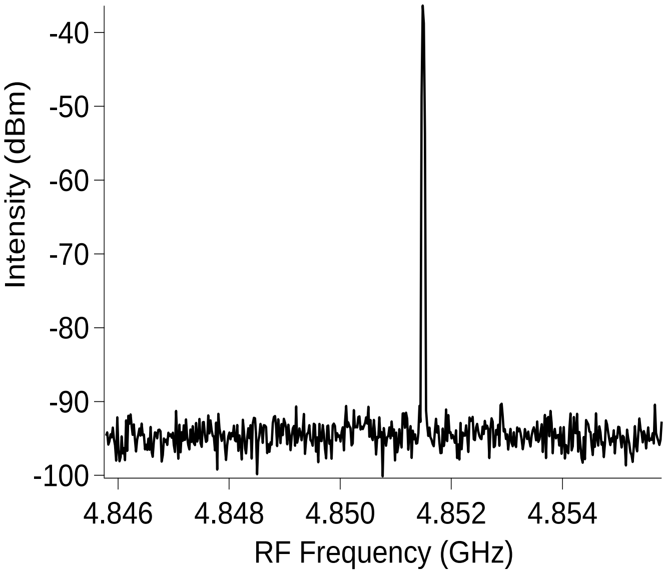

Figure 5-10. RF spectrum for the 20-mm-long waveguide sample.

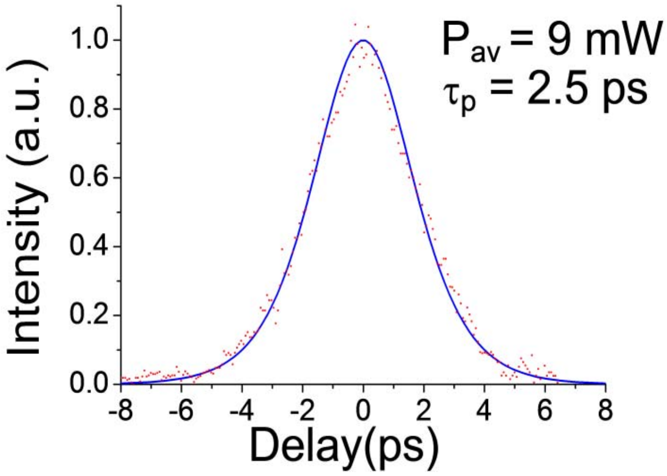

Figure 5-11. Autocorrelation trace for the 4.8 GHz waveguide laser. Red- experimental data, blue line- sech^2 fit.

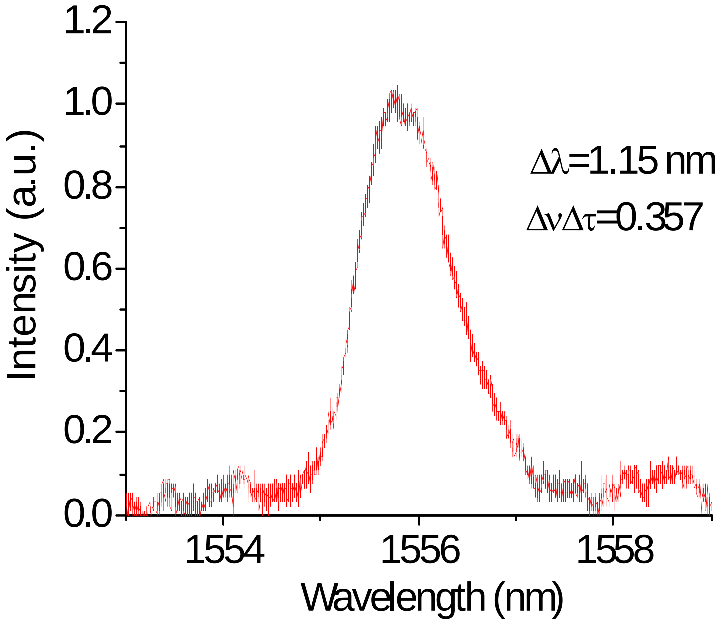

Figure 5-12. Optical spectrum for the 4.8 GHz waveguide laser at a mode-locked power of 9 mW.

5.5.2 14.5-mm-long sample

The output power versus input power characteristics obtained using the 14.5-mm-long waveguide are shown in Figure 5-13. Q-switched mode-locking was observed at a pump power of 464 mW and a corresponding output power of 14 mW. When the pump power was increased to 558 mW, self-starting mode-locking was observed with an output power of 25 mW. As seen from Figure 5-13 a maximum power of 30 mW was obtained for the maximum pump power. The gap between the QD-SESAM and the waveguide was ~13 µm, as in the previous case. The RF spectrum was measured at a span of 10 MHz and a bandwidth of 10 kHz and is shown in Figure 5-14. It can again be seen that the peak is clean and sharp and is centred around 6.8 GHz.

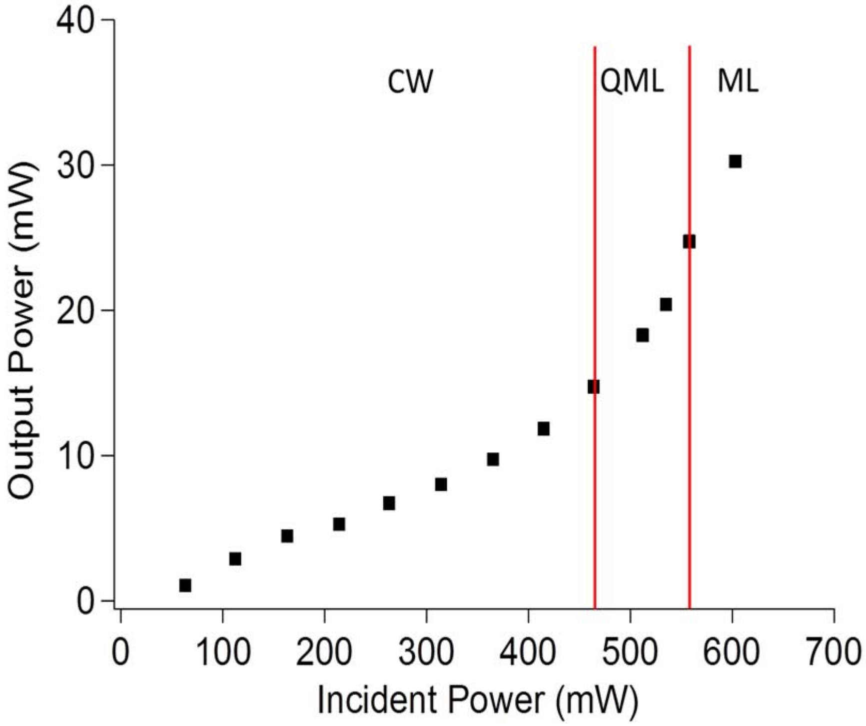

Figure 5-13. Pin-Pout characteristics for the 14.5 mm long sample.

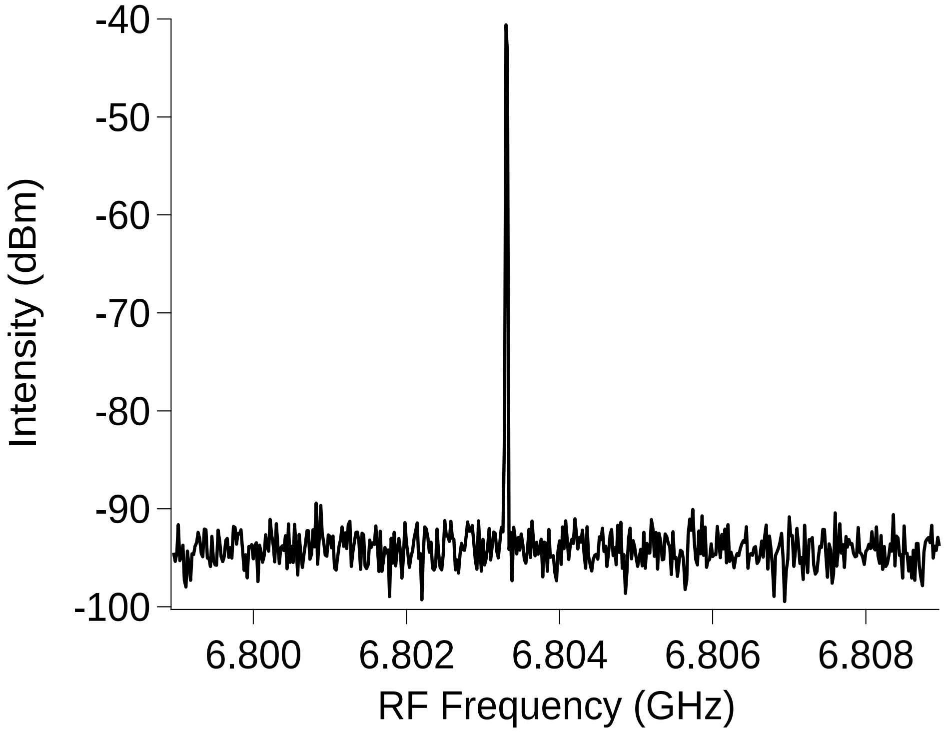

Figure 5-14. RF spectrum centred at 6.8 GHz for the 14.5-mm-long waveguide.

The autocorrelation trace measured at an output power of 30 mW is shown in Figure 5-15. The pulse duration was measured to be 5.4 ps and gives a reasonable fit to a sech^2 profile.

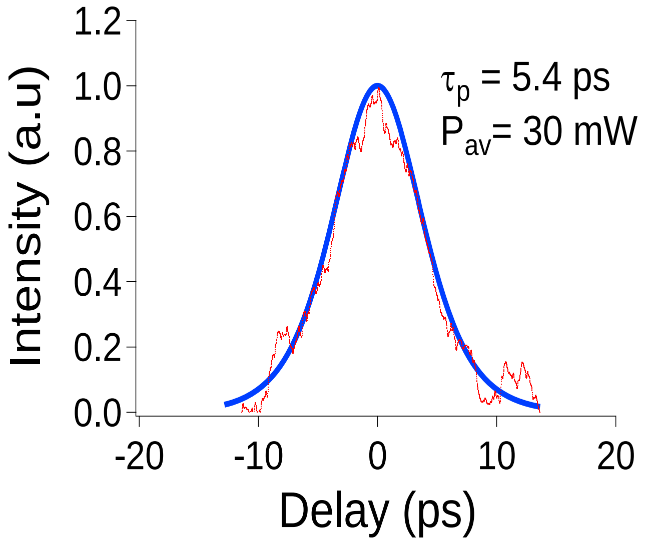

Figure 5-15. Autocorrelation trace for the 6.8 GHz waveguide laser. Red- experimental data, blue line- sech^2 fit

The optical spectrum is centred at 1544.5 nm and has a bandwidth of 0.76 nm and is shown in Figure 5-16. The resulting time-bandwidth product is 0.52, which implies slightly chirped pulses.

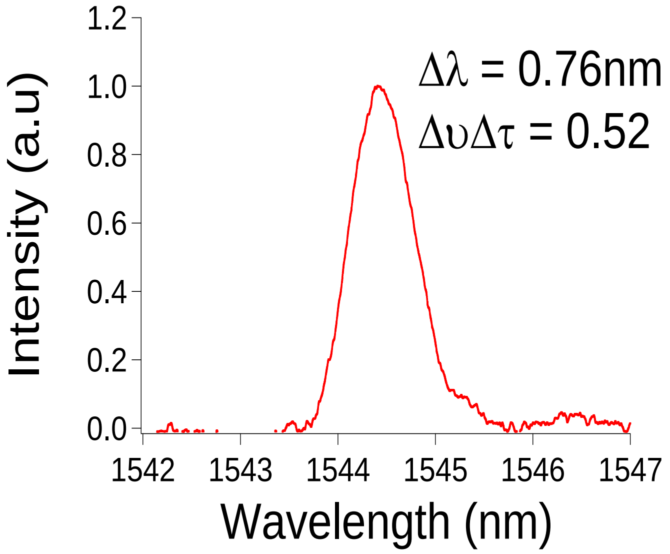

Figure 5-16. Optical spectrum for the 6.8 GHz waveguide laser at an output power of 30 mW.

5.5.3 Repetition-rate tuning

After mode-locking was achieved at a central frequency of 6.8033 GHz, the dependence of the repetition-rate on the pump power was studied. The pump power was increased from 586 mW to 684 mW (by going 10% beyond the normal operating current of the laser diode). The repetition-rate was observed to decrease on increasing the pump power, as is seen from Figure 5-17, with a maximum shift in frequency of 1090 kHz. A similar effect has been previously used to stabilize a waveguide laser operating at a repetition-rate of 750 MHz, in combination with a piezo-controlled SESAM [5], achieving a timing jitter of 14 fs. This shift in the repetition-rate was attributed to atomic dispersion [11]. Atomic dispersion should actually reduce the refractive index for the lasing wavelength when pumped with higher powers, which would increase the repetition-rate in contradiction to what is observed in Figure 5-17. The thermo-optic coefficient (dn/dT) for this glass is negative, which would also mean a decrease in the refractive index with increasing temperature. Since a decrease in the repetition-rate was observed with increase in the pump power, it is believed that the thermal expansion of the glass dominates the other two effects.

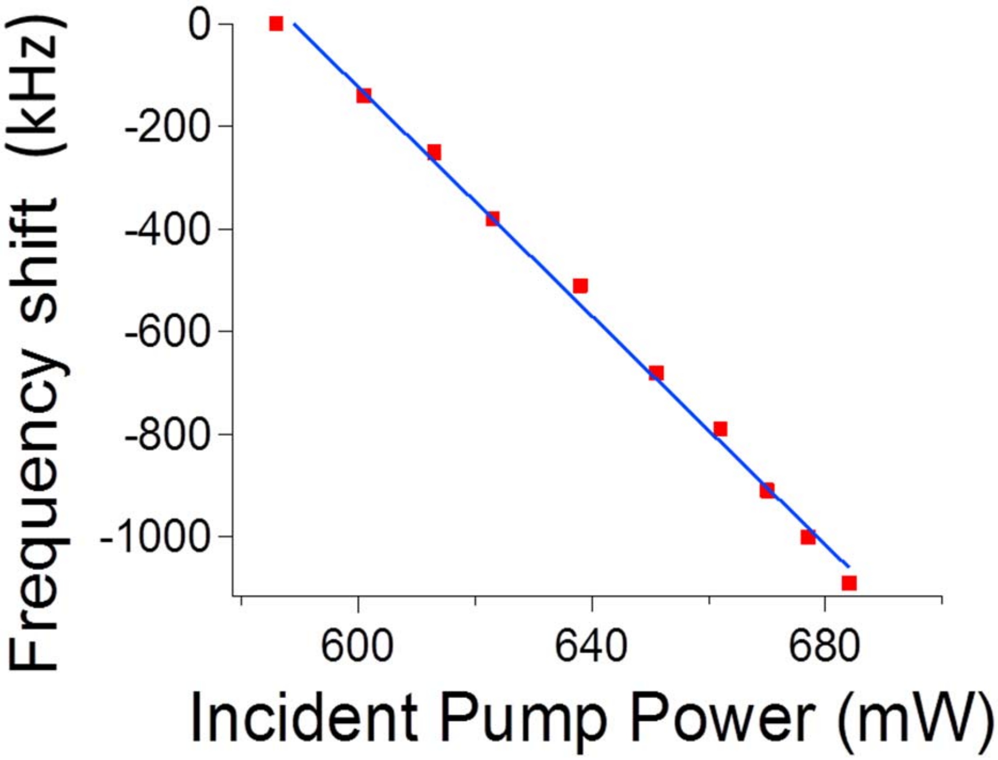

Figure 5-17. Change in frequency as a function of incident pump power.

5.6 Conclusions

In this chapter, the mode-locking results obtained around 1.5 μm have been discussed. A standard photolithographic ion-exchange technique was used to make low-loss (<0.3 dB/cm) waveguides in a commercially available phosphate glass (IOG-1 from Schott Glass Technologies Inc.) doped with erbium ions and ytterbium ions. The ion exchange was carried out at 325°C in a molten mixture of 45% KNO_3 – 50% $NaNO_3$ – 5% $AgNO_3$ (mol%). The waveguide samples used for the CW and mode-locking experiments were 20-mm and 14.5-mm in length giving maximum output powers of 28 mW and 64 mW, respectively, under CW operation.

A dot in well (DWELL) SESAM structure fabricated by researchers at the University of Sheffield was used to mode-lock the Er,Yb: IOG-1 glass waveguides. Diode-pumped, self-starting, fundamentally mode-locked operation was demonstrated using the novel DWELL SESAM. The 20-mm-long waveguide had a mode-locking output power threshold of 6.7 mW and a maximum output power of 9 mW was obtained during operation. Nearly transform-limited pulses as short as 2.5 ps were obtained at a wavelength of 1556 nm and a repetition-rate of 4.85 GHz.

For the 14.5-mm-long sample, self-starting mode-locking was demonstrated at a repetition-rate of 6.8 GHz. To the best of my knowledge, this is the highest repetition-rate to have been reported for a fundamentally mode-locked waveguide laser in the 1.5 μm spectral regime [12]. This is also the first mode-locked operation of a waveguide laser using a QD-SESAM. The mode-locking threshold was found to be at an output power of 25 mW and a maximum power of 30 mW was obtained during mode-locked operation. Slightly chirped pulses with a time-bandwidth product of 0.52 were obtained with a pulse width of 5.4 ps at a central wavelength of 1545 nm.

Fine control of the repetition-rate was demonstrated using the 14.5-mm-long waveguide. On increasing the pump power by 100 mW the repetition-rate was found to decrease by 1.09 MHz. This has been attributed to the thermal expansion of the waveguide with increasing pump power, which increases the length of the waveguide sample and in turn reduces the repetition-rate of the waveguide. This effect could potentially be used to help stabilize the waveguide cavity for frequency comb applications. The most common way of cavity stabilisation is using piezo-controlled cavity elements to finely control the cavity length. This however, includes moving parts and is often prone to noise and also needs external mechanical control. Using the pump power to control the frequency is simpler and could be a route towards on-chip integration of frequency combs. Future work could also include power-scaling via master-oscillator power-amplifier (MOPA) configurations.

5.7 References

1. Valle, G.D, Osellame, R., Galzerano, G., Chiodo, N., Cerullo, G., Laporta, P., Svelto, O., Morgner, U., Rozhin, A. G., Scardaci, V. and Ferrari, A. C., *Passive mode locking by carbon nanotubes in a femtosecond laser written waveguide laser.* Applied Physics Letters, 2006. **89** (23): p. 231115.
2. Beecher, S. J., Thomson, R. R., Psaila, N. D., Sun, Z., Hasan, T., Rozhin. A. G., Ferrari, A. C. and Kar, A. K., *320 fs pulse generation from an ultrafast laser inscribed waveguide laser mode-locked by a nanotube saturable absorber.* Applied Physics Letters, 2010. **97** (11): p. 111114.
3. Schlager, J. B., Callicoatt, B. E., Silverman, K. L., Mirin, R. P., Sanford, N. A. and Veasey, D. L., *Mode-locked erbium/ytterbium co-doped waveguide laser*. in *Lasers and Electro-Optics, 2001. CLEO '01.*
4. Schlager, J. B., Callicoatt, B. E., Mirin, R. P. and Sanford, N. A., *Passively mode-locked waveguide laser with low residual jitter.* IEEE Photonics Technology Letters, 2002. **14** (9): p. 1351-1353.
5. Schlager, J. B., Callicoatt, B. E., Mirin, R. P., Sanford, N. A., Jones, D. J. and Ye, J., *Passively mode-locked glass waveguide laser with 14-fs timing jitter.* Opt. Lett., 2003. **28** (23): p. 2411-2413.
6. Sun, Z., Hasan, T.,Torrisi, F., Popa, D., Privitera, G., Wang, F., Bonaccorso, F., Basko, D.M. and Ferrari, A.C., *Graphene Mode-Locked Ultrafast Laser.* ACS Nano, 2010. **4** (2): p. 803-810.
7. Hyunil, B., Hanjani, A., Frolov, S., Ippen, E. P., Pudo, D., Shmulovich, J. and Kartner, F. X., *Integrated Low-Jitter 400-MHz Femtosecond Waveguide Laser.* Photonics Technology Letters, IEEE, 2009. **21** (12): p. 763-765.
8. Krainer, L., Paschotta, R., Moser, M. and Keller, U., *77 GHz soliton modelocked Nd:YVO$_4$ laser.* Electronics Letters, 2000. **36** (22): p. 1846-1848.
9. Lagatsky, A. A., Leburn, C. G., Brown, C. T. A., Sibbett, W., Zolotovskaya, S. A. and Rafailov, E. U., *Ultrashort-pulse lasers passively mode locked by quantum-dot-based saturable absorbers.* Progress in Quantum Electronics. **34** (1): p. 1-45.
10. Zhang, Z. Y., Oehler, A. E. H., Resan, B., Kurmulis, S., Zhou, K. J., Wang, Q., Mangold, M., Suedmeyer, T., Keller, U., Weingarten, K. J. and Hogg, R. A., *1.55 µm InAs/GaAs Quantum Dots and High Repetition Rate Quantum Dot SESAM Mode-locked Laser.* Scientific Reports, 2012. **2**: p. 477.
11. Fleming, S.C. and Whitley, T.J., *Measurement and analysis of pump-dependent refractive index and dispersion effects in erbium-doped fiber amplifiers.* Quantum Electronics, IEEE Journal of, 1996. **32** (7): p. 1113-1121.
12. Choudhary, A., Lagatsky, A. A., Zhang, Z. Y., Zhou, K. J., Wang, Q., Hogg, R. A., Pradeesh, K., Rafailov, ,E. U., Sibbett, W., Brown, C. T. A. and Shepherd, D. P., *A diode-pumped 1.5 µm waveguide laser mode-locked at 6.8 GHz by a quantum dot SESAM.* Laser Physics Letters, 2013. **10** (10): p. 105803.

Chapter 6 Tm-doped glass waveguides

6.1 Introduction

In the previous chapters, CW and mode-locking results obtained around 1 μm and 1.5 μm have been discussed. The 2 μm "eye-safe" spectral regime is becoming increasingly important owing to a variety of applications in spectroscopy [1], LIDAR [2] and medicine [3].

As discussed in chapter 2, the $^3F_4 \rightarrow ^3H_6$ transition of the Thulium (Tm^{3+}) ion is commonly used for the development of lasers operating around 2 μm. Tm^{3+}-doped laser gain media have a broad absorption band near 800 nm, for which there are a large variety of pump laser diodes available in the market today. High-power, diode-pumped Tm^{3+}-doped solid-state lasers can therefore offer compact and efficient sources for 2-μm radiation. The broad emission bandwidth is also beneficial for the production of short optical pulses and ultrafast operation has been achieved in various gain media [4-6]. Another attractive feature is that cross-relaxation between the $^3H_4$ and $^3H_6$ levels allow an internal quantum efficiency of up to two.

Using Tm^{3+}-doped media in a low-loss waveguide geometry can deliver efficient lasers with a reduced threshold power and can also be a step towards the realisation of compact and integrated sources. The planar waveguide geometry allows good thermal management, which is beneficial for high-power operation [7]. Tm^{3+}-doped crystal waveguide lasers have been previously demonstrated in planar geometry in YAG [8], YLF [9], KYW [10] and $LiNbO_3$ [11] and in channel geometry in KYW [12] and $LiNbO_3$ [13]. A slope efficiency as high as 70% has been achieved for a Tm^{3+}:KYW channel waveguide laser fabricated by a combination of liquid-phase epitaxy and ion-beam milling [12]. Q-switched operation has also been demonstrated recently in a planar Tm:KYW waveguide laser fabricated by liquid-phase epitaxy [14].

Glass-based laser hosts are relatively cheap and simple to fabricate, they offer a broad emission bandwidth and compatibility with low-loss ion-exchange waveguide fabrication techniques. Tm^{3+}-doped glass waveguide lasers have been fabricated in a lead-germanate glass by ion-implantation [15], and in fluorogermanate glass [16] and ZBLAN glass [17] by femtosecond writing. As discussed in the previous chapters, ion-exchange is a cheap and simple technique for fabricating low-loss channel waveguides in glasses. However, to date there has been limited work on the ion-exchange of Tm^{3+}-doped glass waveguides [18, 19] with the focus being on the S-band amplification near 1.4 μm [19].

In this chapter, the first ion-exchanged thulium-doped waveguide laser operating near 1.9 μm is presented [20]. A novel combination of ion-exchange and ion-beam milling was used to fabricate waveguides, with propagation losses of ~0.3dB/cm. A threshold power of as low as 44 mW was achieved for a cavity formed by high reflectivity (HR) mirrors and a slope efficiency of up to 6.8% was observed for a HR/10% output coupler (OC) cavity. An extension of this work is the development of mode-locked waveguide laser sources near 2 μm, which could open up opportunities such as pumping of mid-infrared frequency combs [21]. All the experiments discussed in this chapter were carried out by the author with the exception of the fabrication of waveguides and the modelling of the modes, which was carried out by Dr. Pradeesh Kannan, and the fabrication of the glass, which was carried out by Dr. Xian Feng.

6.2 Fabrication details

The germanate glass was fabricated by a standard melting and quenching technique. The glass melt had a composition of 65.5 mol% GeO_2, 12 mol% Al_2O_3, 4.5 mol% BaO and 18 mol% Na_2O which was then doped with 1 mol% of Tm_2O_3 which corresponds to an ion concentration of $4\times10^{20}cm^{-3}$. The annealed glasses were then sliced to dimensions of 20 mm x 20 mm x 2 mm and were polished to optical quality for the fabrication of channel waveguides. Initially, a similar ion–exchange procedure as described in chapter 3 was carried out. However, it was found that the glass reacted with the chemical etchant (Al etchant from OM group, inc) used during the etching of the aluminium (Al) mask, resulting in very rough glass surfaces.

The fabrication process was therefore slightly modified to avoid the chemical removal of the metal mask and this is shown in Figure 6-1. First, a 35 ± 5-nm-thick layer of aluminium was deposited on the germanate glass using an electron-beam evaporation system. Next, the photoresist layer was spun on the glass sample and channel opening widths between 1 μm and 10 μm, in steps of 0.2 μm, were photolithographically transferred. After this step, the masked glass sample was put in an Ar^+ ion-beam milling system (Ionfab 300 Plus from Oxform plasma) and the resist mask pattern was transferred to the metal. The parameters used in the etching were current = 100 mA, voltage = 500 V and etching time = 150 seconds.

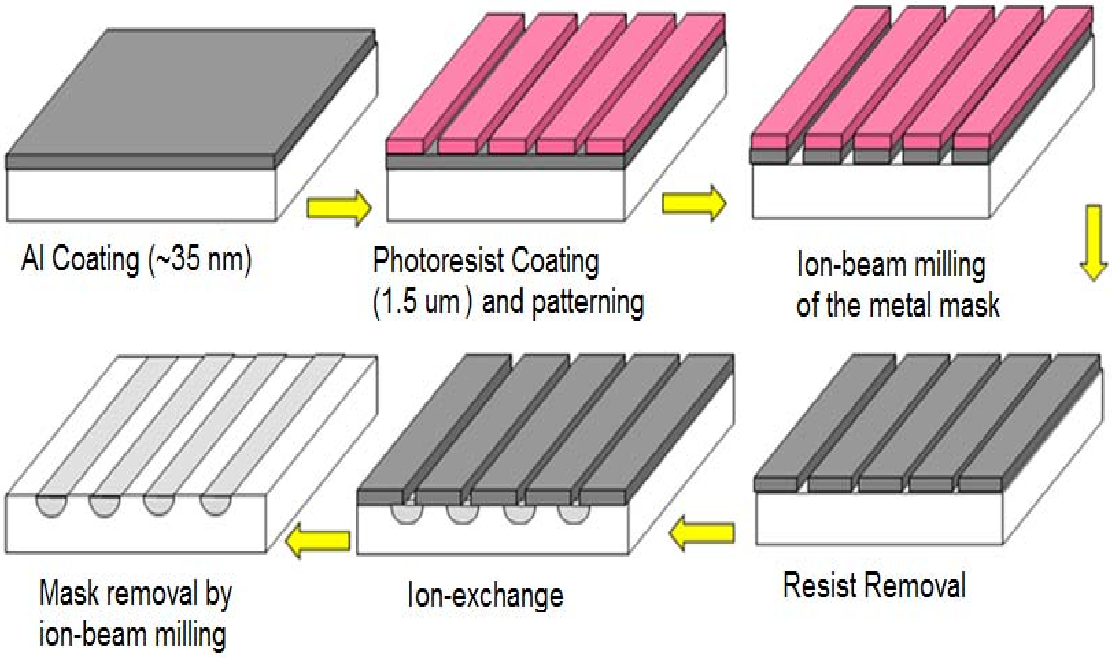

Figure 6-1. The modified fabrication process to fabricate channel waveguides in Tm: germanate glass

The photoresist was removed using acetone and the glass was kept in the ion-exchange furnace for 300°C for 20 minutes in a molten salt mixture of 43 mol% KNO_3 – 55 mol% $NaNO_3$ – 2 mol% $AgNO_3$. Following the ion-exchange step, the metal mask was removed using ion-beam milling. Since the unmasked glass is also etched during this step, due to ion-beam milling being a non-selective process, a 50-nm depression was formed in the waveguide region as shown in Figure 6-2 (for a waveguide fabricated by a channel opening width of 9 µm). To minimise the etching of the glass during the etching of the metal (to define the mask) and during the mask removal step, a very thin layer of metal layer (~35 nm) was used as a mask as compared to the 200-nm-thick layers as described in chapter 4 and in chapter 5. A thicker layer of metal mask would mean that a greater tolerance (to make sure that the metal layer is etched all the way through) would have to be kept during the masking stage, which will lead to a deeper etching of the glass. Also, during the mask removal step, since the glass and metal have similar etch rates, a thicker mask would have meant an etch depth of >100 nm in the glass. Finally, the glass samples were end-polished to a length of 11.5 mm.

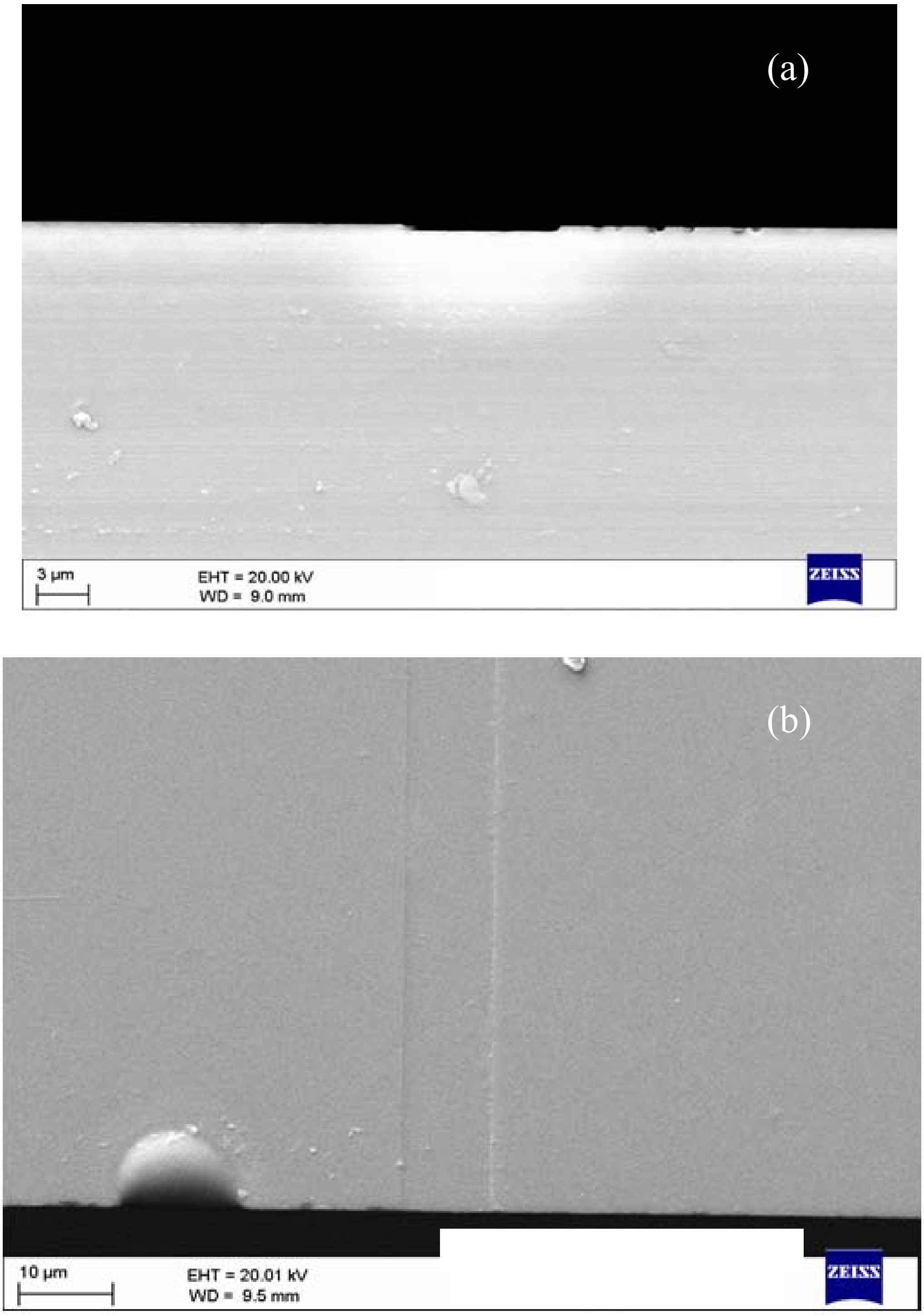

Figure 6-2. (a) End facet view of the waveguide, and (b) the top view of the waveguide after fabrication

6.3 Optical characterisation

The refractive index was measured using the prism coupling technique in a planar ion-exchanged waveguide fabricated with the same ion-exchange parameters as for the channel waveguides. The diffusion depth was found to be 4.6 µm and the index contrast (Δn) was 0.06 at 1553 nm. The waveguide supports 5 modes at 632.8 nm, 2 modes at 1553 nm and 1 mode at 1900 nm (the index at 1900 nm was found by fitting the measured refractive indices to the Sellmeier equations [22]). Hence, it can be concluded that this waveguide is single-mode at the laser wavelength.

The absorption spectrum of a polished piece of bulk glass measured using a Cary 500 spectrophotometer (Varian Ltd, Oxford, UK) is shown in Figure 6-3. It can be seen that the maximum absorption coefficient (α) is at 790 nm and has a value of 2.3 cm^{-1}. This wavelength is easily accessible by a Ti:sapphire laser, which was used as the pump source for the laser experiments.

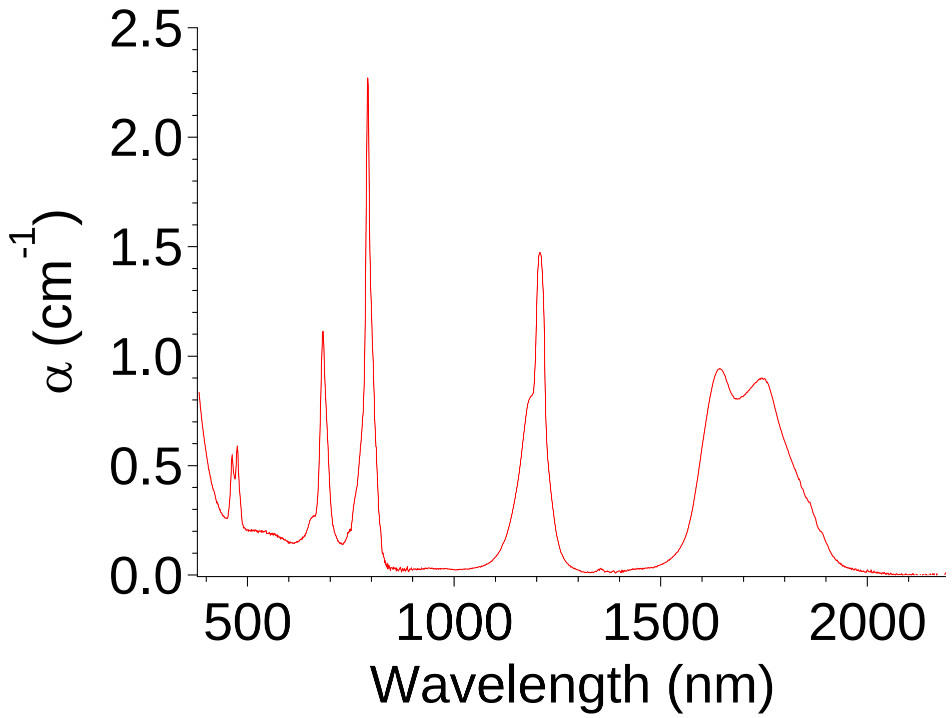

Figure 6-3. The absorption spectrum measured using a spectrophotometer.

A McCumber analysis carried out by Dr. Pradeesh Kannan [23, 24] was applied to the measured absorption spectrum to calculate the emission cross-sections shown in Figure 6-4. The emission is peaked at a wavelength of 1865 nm and has a value 2.3×10^{-21} cm^2.

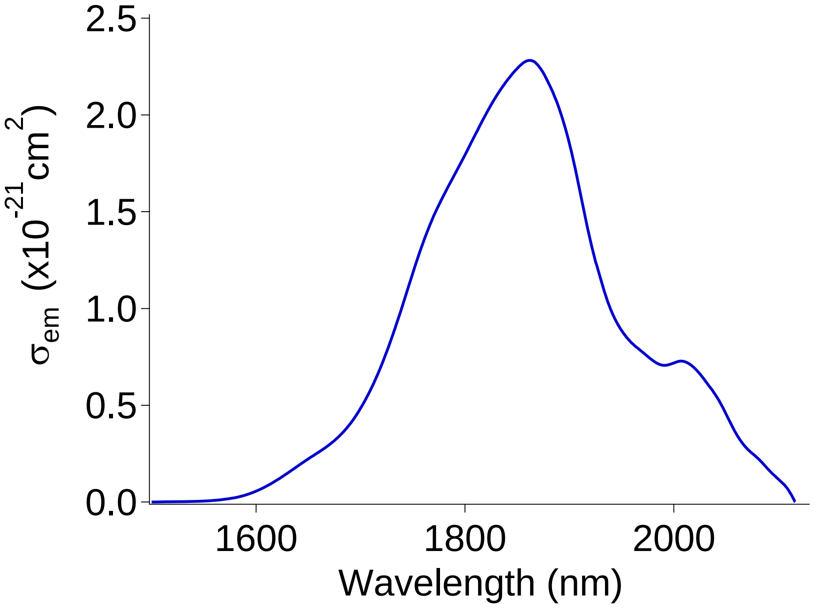

Figure 6-4. The calculated emission cross-section from McCumber analysis.

6.4 CW lasing experiments

6.4.1 Experimental setup

The ion-exchanged, 11.5-mm-long Tm^{3+}:germanate glass waveguide was mounted on a thermo-electrically-cooled copper mount using silver conductive paint and was kept at a temperature of 15°C. As seen from Figure 6-3, the absorption peaks at 790 nm, therefore a titanium sapphire laser tuned to a wavelength of 790 nm and delivering a maximum power of 500 mW was used to pump the waveguide. The pump power incident on the waveguide was controlled by a variable neutral density filter and a half-wave plate controlled the polarisation, which was kept horizontal. The pump light was coupled into the waveguide by an aspheric lens of focal length 11 mm. The transmission through the waveguide was measured at the absorption wavelength (790 nm) and away from absorption (840 nm) as described in section 3.3.2.3. From this method a launch efficiency of 80% and absorption of 85% were estimated. A mechanical chopper was installed in the pump beam, and the chopped output was focussed on an InGaAs detector for fluorescence lifetime measurements. The fluorescence lifetime was measured to be 0.8 ms from this measurement.

6.4.2 Laser results

A thin dielectric mirror (thickness = 175 µm) with a reflectivity of >99.8% at the lasing wavelength and reflectivity of ~ 32% at the pump wavelength was used as the high reflectivity (HR) mirror for the waveguide cavity. It was butted to the input facet of the waveguide and was held in position with fluorinated liquid (FC-70 from Sigma Aldrich). Another similar HR mirror was end-butted on the output facet of the waveguide and hence an HR/HR laser cavity was formed. All the waveguides were tested for their continuous wave (CW) performance and the lowest threshold power was observed for the waveguide fabricated with a mask opening width of 9 µm. On increasing the pump power (P), lasing was observed at an absorbed threshold power (P_{th}) of only 44 mW. The output from the waveguide was passed through a glass filter (RG-1000) and was measured to be less than 1 mW. The central lasing wavelength (λ_{lasing}) was measured with an optical spectrum analyser (OSA) from Yokogawa AQ6375 and was found to be 1885 nm. The output from the waveguide was filtered using a germanium window (to remove any 1.5 µm fluorescence and the pump) and was focussed on the InGaAs photodetector to measure the angular frequency (ω) of the relaxation oscillations and to estimate the loss as described in 3.3.2.2. The plot for ω^2 vs. r is shown in Figure 6-5 where r is defined as $P/P_{th} - 1$. The cavity loss was derived using the slope of the linear fit to the experimental data and the propagation loss was found to be 0.3 dB/cm (assuming no losses due to mirror butting).

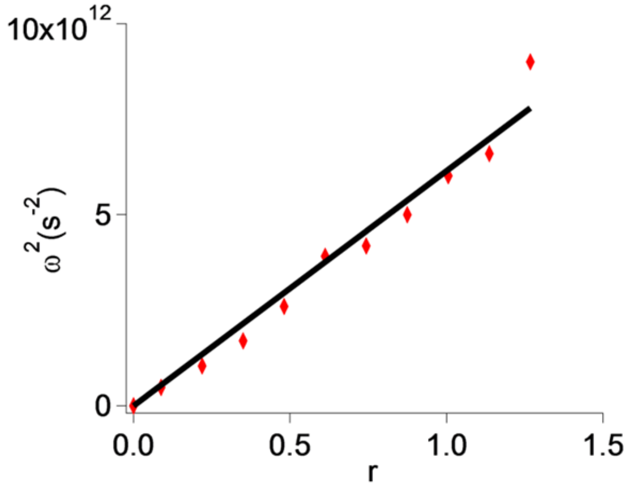

Figure 6-5. Plot of the square of the relaxation oscillation frequency against the number of times above threshold measured for an HR/HR cavity.

Next, bulk mirrors with a thickness of 6 mm and with transmissions of 6% and 10% at the laser wavelengths were used as OCs. The input-output characteristics are shown in Figure 6-6.

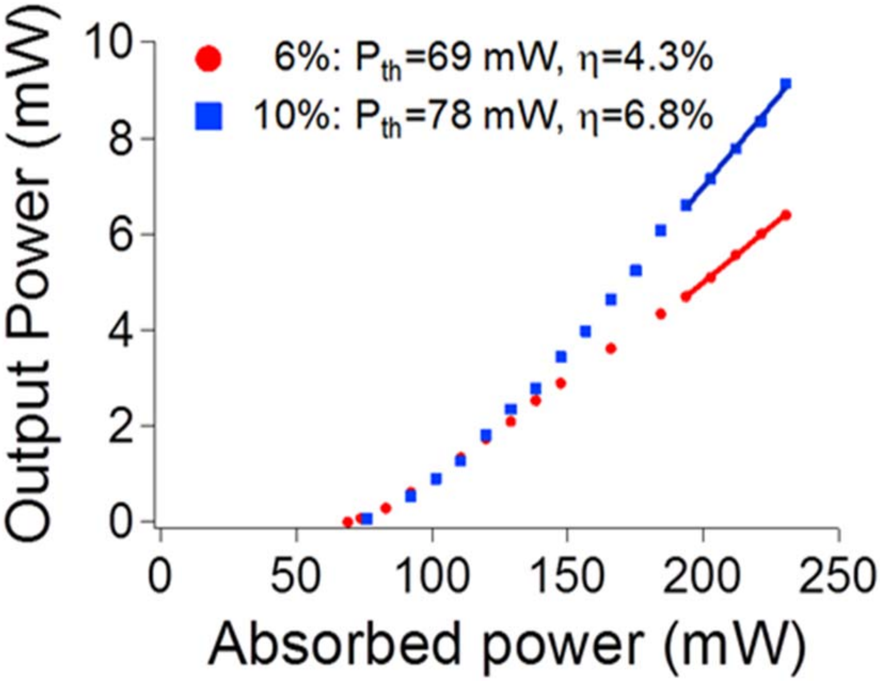

Figure 6-6. Input-output characteristics of the Tm: germanate waveguide laser for a 6% OC and a 10% OC.

The mirrors were placed on a 5-axis (x, y, z, tip and tilt) kinematics mount. The tip and tilt were adjusted to align the mirror with the end facet and it was moved as close as possible to the waveguide end-face to achieve efficient laser action. A laser threshold of 69 mW was observed for the 6% OC and a slope efficiency of 4.3% was measured. For the 10% OC, a threshold power of 78 mW was observed and a slope efficiency of 6.8% was measured. The laser spectra were measured by an OSA and were found to be centred at a wavelength of 1884 nm and 1881 nm for the 6% and 10% OC respectively. The laser spectrum measured with the 10% OC is shown Figure 6-7 and the envelope has a full-width-at-half-maximum (FWHM) bandwidth of 1.9 nm.

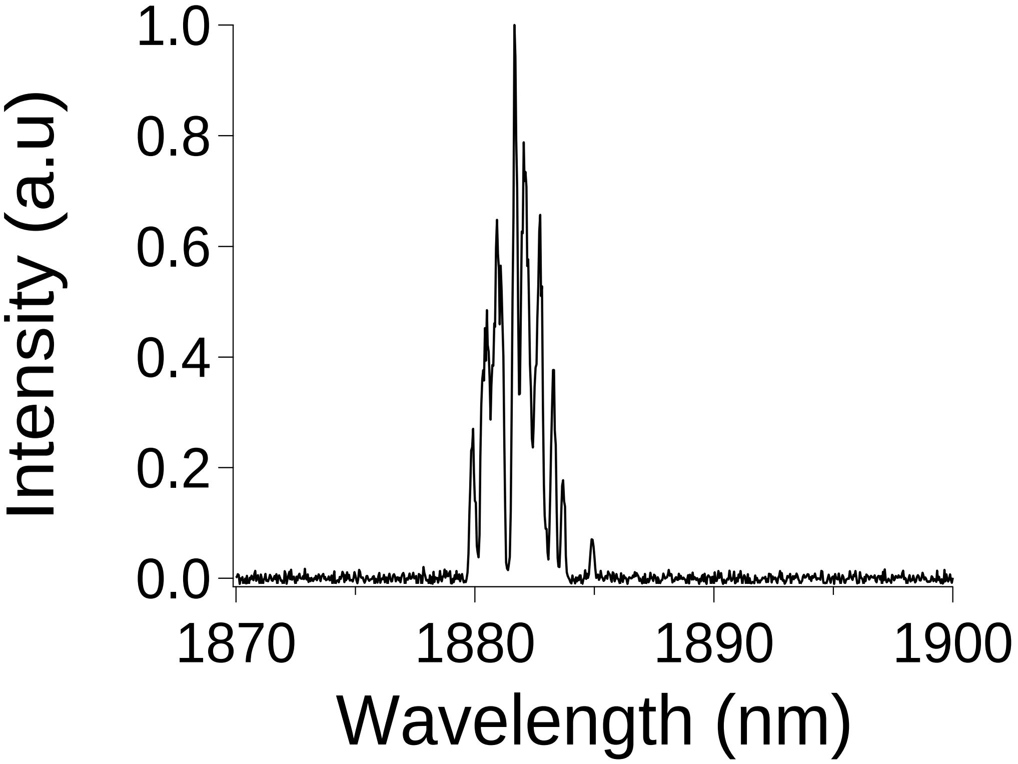

Figure 6-7. Laser spectrum for the HR/10% cavity.

The relaxation oscillations were also measured for both the OCs using a similar procedure as for the HR/HR cavity. The plots of ω^2 vs. r for the HR/6% cavity and the HR/10% cavity are shown in Figure 6-8 (a) and Figure 6-8 (b) respectively. It was found that the (total cavity loss - output coupler loss) was consistently 1.5 dB more than what was found in the case of the HR/HR cavity. This additional loss can be attributed to the misalignment between the waveguide facet and the mirror and imperfect end-butting. Due to the mirrors being aligned manually using a kinematic mount, a small angle could have remained between the waveguide and the mirror. This introduces significant loss to the laser mode when compared to the case of the thin HR mirror, which was directly end-butted on the waveguide facet. A possible route to reduce this loss is direct deposition of the dielectric coating on the waveguide facets or the use of thin OC mirrors.

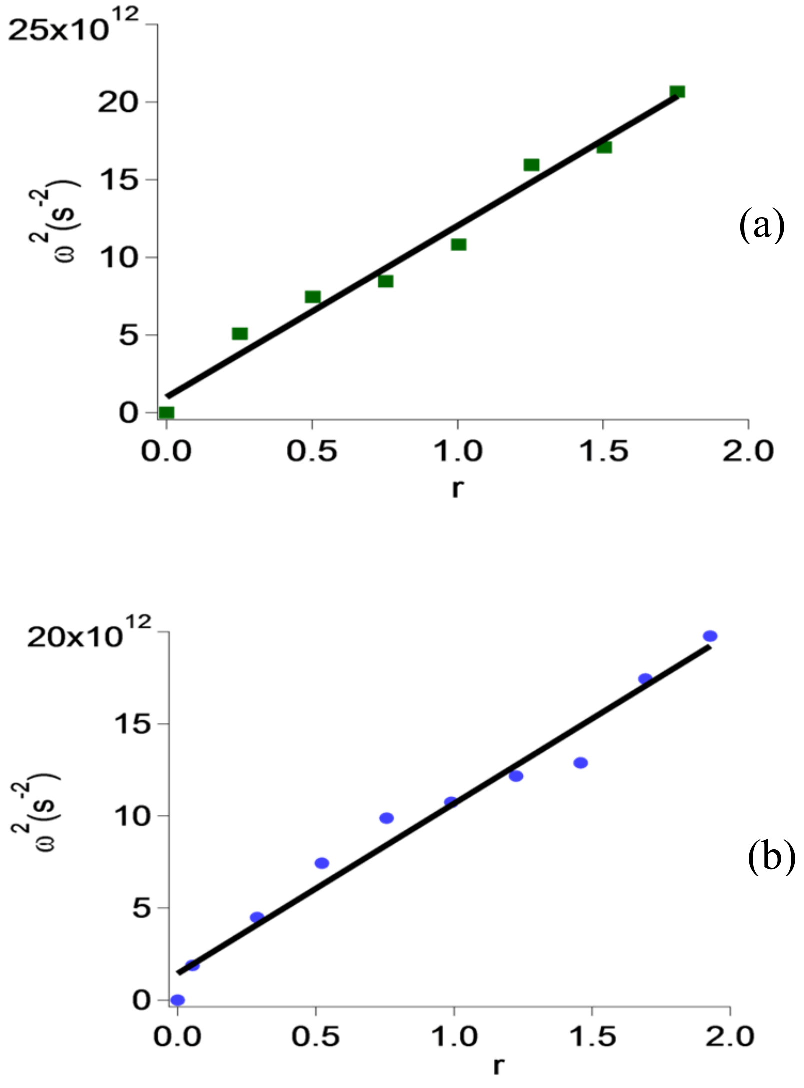

Figure 6-8. Plot of the square of the relaxation oscillation frequency against the number of times above threshold measured for an (a) HR/6% cavity, and (b) HR/10% cavity.

6.4.3 Beam characterisation

Beam characterisation was carried out by imaging the output from the waveguide on to a CMOS camera. The measured pump mode is shown Figure 6-9 (a), and the 1/e^2 beam radii were measured to be 6.2 µm and 3.2 µm in the horizontal and vertical directions, respectively. The simulated pump mode profile using a commercially available waveguide modelling software (RSoft) is shown in Figure 6-9 (b). The simulated mode sizes were calculated to be 5.1 µm and 2.1 µm in the horizontal and vertical directions respectively. This discrepancy between the measured and simulated values might be due to the 50 nm etch in the waveguide region as seen from Figure 6-2 which was not included in the modelling.

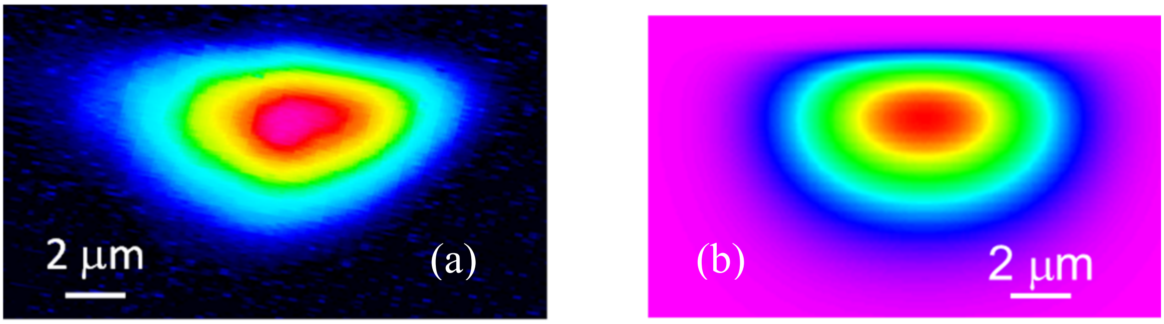

Figure 6-9. (a) Measured mode-profile, and (b) simulated mode-profile at 790 nm.

6.5 Discussions

The internal quantum efficiency (η_q), gives an indication of the degree of cross-relaxation in the Tm^{3+}-doped gain media. A quantum efficiency of two implies that all the ions are participating in the cross-relaxation mechanism. This is controlled by the doping concentration of Tm^{3+} ions. η_q was estimated by fitting the measured values of the slope efficiency (η) to the following equation [25]:

$$\eta = \frac{\nu_l}{\nu_p}\eta_q\eta_{ol}\frac{T}{T+L} \qquad (6.1)$$

where, ν_p is the pump frequency, ν_l is the laser frequency, T is the output coupler transmission, L is the estimated round-trip losses from relaxation oscillation measurements (excluding the output coupler transmission) and η_{ol} is the overlap factor estimated to be ~0.8 from the quasi-3-level-laser analysis of Risk [25]. Using the experimentally observed values, the internal quantum efficiency was found to be 1.15. This value of slightly >1 indicates that the laser is benefiting from some cross-relaxation, which helps to populate the upper laser level. However, the slope efficiency may be improved with even higher doping of Tm^{3+} ions in the glass matrix. From this estimated value of 1.15 for η_{ol}, the threshold powers were calculated for each of the laser cavity and are shown in Table 6-1.

Table 6-1. Summary of results for the Tm:germanate waveguide laser

OC	P_{th} Measured (mW)	P_{th} Theory (mW)	η_s Measured (%)	λ_{lasing} (nm)
HR	44	37	-	1885
6%	69	64	4.3	1884
10%	78	67	6.8	1881

From Table 6-1, it can be seen that there is a good agreement between the measured and calculated values of the threshold powers, further validating the estimation of the internal quantum efficiency. The current value of n_q would allow slope efficiencies of up to nearly 50%. This has not been achieved due to the fact that the propagation losses are high in relation to the output coupling. This could be increased by reducing the alignment losses by direct coating of dielectric mirrors on the waveguides.

6.6 Conclusions

In this chapter, CW lasing results of Tm:germanate glass waveguides around 2 μm has been presented. A novel combination of ion-exchange and ion-beam milling was used to fabricate low-loss waveguides in the Tm^{3+}-doped germanate glass. To the best of my knowledge, this work represents the first ion-exchanged Tm:glass waveguide laser. Laser threshold was reached at an absorbed pump power of 44 mW in a laser cavity formed by end-butting two thin high reflectivity mirrors on the end facet of the waveguide (HR/HR cavity). The laser wavelength was centred at 1885 nm and the propagation losses were estimated to be 0.3 dB/cm, using the relaxation oscillations method.

When one of the HR mirrors was replaced by a bulk mirror with a transmission of 6%, a slope efficiency of 4.3% was found and the threshold power increased to 69 mW. The laser wavelength was 1884 nm. With a 10% output coupler, a threshold power of 78 mW, a slope efficiency of 6.8% and a central wavelength of 1881 nm were observed. As a comparison, the slope efficiency for a Tm^{3+}-doped fluorogermanate glass channel waveguide laser fabricated by femtosecond writing [16] was 6% and the incident threshold power was 80 mW. However, the total cavity loss was found to have increased by 1.5 dB when using thick output coupling mirrors, which require manual alignment, compared to the case of the directly butted thin-mirror HR/HR cavity. This additional loss is due to the misalignment between the waveguide facet and the mirror. The value of the internal quantum efficiency was estimated to be 1.15 which indicates some degree of cross-relaxation.

The performance of the laser can be improved by:

1. Increasing the doping concentration of the Thulium ions in the glass matrix. This will increase the internal quantum efficiency.
2. Use of thin dielectric mirrors or direct coating of mirrors to reduce misalignment losses.
3. Using a higher output coupling mirror to increase the slope efficiency, at the cost of increased threshold pump power requirement.

Future work would involve replacement of the HR mirror with saturable absorber elements to realise high repetition-rate mode-locked sources around 2 μm and the implementation of diode-pumping using commercially available laser diodes. Such diode-pumped, efficient, laser sources could have a variety of applications, including acting as pumps for mid-IR frequency combs [21].

6.7 References

1. Walsh, B.M., *Review of Tm and Ho materials; spectroscopy and lasers.* Laser Physics, 2009. **19** (4): p. 855-866.
2. Henderson, S. W., Suni, P. J. M., Hale, C. P., Hannon, S. M., Magee, J. R., Bruns, D. L. and Yuen, E. H., *Coherent laser radar at 2 μm using solid-state lasers.* Geoscience and Remote Sensing, IEEE Transactions on, 1993. **31** (1): p. 4-15.
3. Theisen, D., Ott, V., Bernd, H.-W., Danicke, V., Keller, R. and Brinkmann, R., *Cw high-power IR laser at 2 μm for minimally invasive surgery.* Proc. SPIE 5142, Therapeutic Laser Applications and Laser-Tissue Interactions, 2003: p. 96-100.
4. Lagatsky, A. A., Calvez, S., Gupta, J. A., Kisel, V. E., Kuleshov, N. V., Brown, C. T. A., Dawson, M. D. and Sibbett, W., *Broadly tunable femtosecond mode-locking in a Tm:KYW laser near 2 μm.* Opt. Express, 2011. **19** (10): p. 9995-10000.
5. Lagatsky, A.A., Antipov, O.L., and Sibbett, W., *Broadly tunable femtosecond Tm:Lu_2O_3 ceramic laser operating around 2070 nm.* Opt. Express, 2012. **20** (17): p. 19349-19354.
6. Lagatsky, A. A., Koopmann, P., Fuhrberg, P., Huber, G., Brown, C. T. A. and Sibbett, W., *Passively mode locked femtosecond Tm:Sc2O3 laser at 2.1 μm.* Opt. Lett., 2012. **37** (3): p. 437-439.
7. Mackenzie, J. I., Mitchell, S. C., Beach, R. J., Meissner, H. E. and Shepherd, D. P., *15 W diode-side-pumped Tm:YAG waveguide laser at 2 μm.* Electronics Letters, 2001. **37** (14): p. 898-899.
8. Rameix, A., Borel, C., Chambaz, B., Ferrand, B., Shepherd, D. P., Warburton, T. J., Hanna, D. C. and Tropper, A. C., *An efficient, diode-pumped, 2 μm Tm:YAG waveguide laser.* Optics Communications, 1997. **142** (4–6): p. 239-243.
9. Bolanos, W., Starecki, F., Benayad, A., Brasse, G., Ménard, V., Doualan, J.-L., Braud, A.,Moncorgé, R. and Camy, P., *Tm:$LiYF_4$ planar waveguide laser at 1.9 μm.* Opt. Lett., 2012. **37** (19): p. 4032-4034.
10. Rivier, S., Mateos, X., Petrov, V., Griebner, U., Romanyuk, Y. E., Borca, C. N., Gardillou, F. and Pollnau, M., *Tm:$KY(WO_4)_2$ waveguide laser.* Opt. Express, 2007. **15** (9): p. 5885-5892.
11. de Sandro, J. P., Jones, J. K., Shepherd, D. P., Hempstead, M., Wang, J. and Tropper, A. C., *Non-photorefractive CW Tm-indiffused Ti:$LiNbO_3$ waveguide laser operating at room temperature.* Photonics Technology Letters, IEEE, 1996. **8** (2): p. 209-211.
12. van Dalfsen, K., Aravazhi, S., Grivas, C., García-Blanco, S. M. and Pollnau, M., *Thulium channel waveguide laser in a monoclinic double tungstate with 70% slope efficiency.* Opt. Lett., 2012. **37** (5): p. 887-889.
13. Cantelar, E., García, J. A. Sanz-, Lifante, G., Cussó, F., and Pernas, P. L., *Single polarized Tm^{3+} laser in Zn-diffused $LiNbO_3$ channel waveguides.* Applied Physics Letters, 2005. **86** (16): p. 161119-3.
14. Bolaños, W., Carvajal, J. J., Mateos, X., Cantelar, E., Lifante, G., Griebner, U., Petrov, V., Panyutin, V. L., Murugan, G. S.,Wilkinson, J. S., Aguiló, M. and Díaz, Francesc, *Continuous-wave and Q-switched Tm-doped $KY(WO_4)_2$ planar waveguide laser at 1.84 μm.* Opt. Express, 2011. **19** (2): p. 1449-1454.
15. Shepherd, D. P., Brinck, D. J. B., Wang, J., Tropper, A. C., Hanna, D. C., Kakarantzas, G. and Townsend, P. D., *1.9-μm operation of a Tm:lead germanate glass waveguide laser.* Opt. Lett., 1994. **19** (13): p. 954-956.

16. Fusari, F., Thomson, R. R., Jose, G., Bain, F. M., Lagatsky, A. A., Psaila, N. D., Kar, A. K., Jha, A., Sibbett, W. and Brown, C. T. A., *Lasing action at around 1.9 μm from an ultrafast laser inscribed Tm-doped glass waveguide.* Opt. Lett., 2011. **36** (9): p. 1566-1568.
17. Lancaster, D. G., Gross, S., Ebendorff-Heidepriem, H., Kuan, K., Monro, T. M., Ams, M., Fuerbach, A. and Withford, M. J., *Fifty percent internal slope efficiency femtosecond direct-written* Tm^{3+}*:ZBLAN waveguide laser.* Opt. Lett., 2011. **36** (9): p. 1587-1589.
18. Luo, T., Jiang, S., Hu, Y., Conti, G.N., Honkanen, S., Mendes, S.B. and Peyghambarian, N., *Germanate glass channel waveguides for infrared waveguide lasers*. in *Quantum Electronics and Laser Science Conference, 1999. QELS '99*. 1999. Baltimore, Maryland.
19. Yang, D.L., Pun, E.Y.B., and Lin, H., Tm^{3+} *doped ion-exchanged aluminum germanate glass waveguide for S-band amplification.* Applied Physics Letters, 2009. **95** (15): p. 151106-3.
20. Choudhary, A., Kannan, P., Mackenzie, J. I., Feng, X. and Shepherd, D. P., *Ion-exchanged* Tm^{3+}*:glass channel waveguide laser.* Opt. Lett., 2013. **38** (7): p. 1146-1148.
21. Leindecker, N., Marandi, A., Byer, R. L., Vodopyanov, K. L., Jiang, J., Hartl, I.,Fermann, M. and Schunemann, P.G., *Octave-spanning ultrafast OPO with 2.6-6.1 μm instantaneous bandwidth pumped by femtosecond Tm-fiber laser.* Opt. Express, 2012. **20** (7): p. 7046-7053.
22. Sellmeier, W., *Zur Erklärung der abnormen Farbenfolge im Spectrum einiger Substanzen.* Annalen der Physik, 1871. **219** (6): p. 272-282.
23. McCumber, D.E., *Einstein relations connecting broadband emission and absorption spectra.* Physical Review, 1964. **135**: p. A954-A957
24. Zhang, L., Zhang, J., Yu, C. and Hu, L., *A method for emission cross section determination of* Tm^{3+} *at 2.0 μm emission.* Journal of Applied Physics, 2010. **108** (10): p. 103117.
25. Risk, W.P., *Modeling of longitudinally pumped solid-state lasers exhibiting reabsorption losses.* J. Opt. Soc. Am. B, 1988. **5** (7): p. 1412-1423.

Chapter 7 Conclusions and future work

7.1 Thesis summary

This thesis has dealt with the development of compact mode-locked waveguide laser sources that have repetition-rates in excess of 1 GHz with target applications in optical frequency metrology and non-linear microscopy. A basic material requirement for such laser sources is that the gain media should have a broad emission bandwidth and be compatible with fabrication of low-loss waveguides. To this end, various gain media operating at different wavelengths were investigated to evaluate their performance. Ion-exchanged waveguides in rare-earth-doped phosphate glass showed the most promising results and were used for the mode-locking experiments. Mode-locked waveguide lasers operating near 1 μm and 1.5 μm were demonstrated with multi-GHz repetition rates and picosecond or sub-picosecond pulse durations. The highlight results with specific laser hosts are described below.

7.1.1 (Yb,Nb):RbTiOPO4

(Yb,Nb):RbTiOPO$_4$ (RTP) has a broad emission bandwidth around 1060 nm and is a very promising non-linear crystal, making it a good candidate for the development of mode-locked lasers and self-frequency-doubled lasers. Using liquid-phase epitaxy, low-loss (~1 dB/cm) (Yb,Nb):RTP waveguides were fabricated on RTP substrates. CW lasing was demonstrated for the first time in a planar (Yb,Nb):RTP waveguide laser at a threshold power of ~280 mW. The slope efficiency could not be calculated because of the limitation of the pump power. Future work involves the high power diode-pumping of this waveguide to fully characterise its laser performance.

Channel waveguides were then fabricated in (Yb,Nb):RTP by ion-beam milling to try and reduce the threshold power for lasing. Smooth side-walls were obtained and single-mode waveguides were demonstrated with propagation losses of ~3 dB/cm. Second harmonic light at 570 nm was also generated when it was pumped by an optical parametric oscillator (OPO) at 1140 nm [1].

Next, channel waveguides were fabricated in (Yb,Nb):RTP by reactive ion etching (RIE) using SF$_6$ and Ar gases. A systematic approach to optimise the RIE of RTP was taken, where the gas pressure, RF power and gas concentration were varied to minimise the surface roughness without having an overly long etch time. The optimised parameters were RF power of 250 W, gas pressure of 40 mTorr and gas flow rates of 10 sccm for Ar and 10 sccm for SF_6. Using these parameters single-mode rib waveguides in the (Yb,Nb):RTP film were fabricated that demonstrated waveguiding at 980 nm with a propagation loss of ~3.5 dB/cm [2].

Lasing was not achieved in the (Yb,Nb):RTP channel waveguides fabricated by reactive ion etching or ion-beam milling because of high propagation losses. Thus this material was not pursued in the project for mode-locking experiments.

7.1.2 Yb:KY$(WO_4)_2$

Yb:KY$(WO_4)_2$ (Yb:KYW) also possesses a broad emission bandwidth around 1030 nm and is very commonly used to generate ultra-short pulses in bulk laser systems.

In order to fabricate channel waveguides in this material, grooves with dimensions in the order of a few micrometres were etched into a KYW substrate by ion-beam milling, following which a layer of Yb:KYW was grown on the substrate by liquid-phase epitaxy [3]. A cladding layer of KYW was overgrown on the active layer to effectively produce "inverted-rib" waveguides in Yb:KYW. The propagation loss was measured to be ~2.6 dB/cm, which prevented the low-gain wavelength 1030 nm from lasing. Pure 3-level operation was observed from this waveguide with a lasing wavelength of 981 nm. A slope efficiency as high as 58% was achieved without any mirrors and a threshold power as low as 13 mW was obtained when mirrors were used to provide laser feedback. With a different mirror set, laser action was achieved at a wavelength of 999.8 nm with a slope efficiency of 5%. Yb:KYW remains a material of great interest for the realisation of mode-locked waveguide lasers, however the production of high quality Yb:KYW planar waveguides was problematic. In future, when good quality films are obtained, it is expected sub-500 fs pulses could be obtained at high output powers. The use of channel waveguide structures that require shallower etching should also help to reduce the additional losses that these etching processes can bring [4].

7.1.3 Mode-locked Yb:phosphate glass

Yb-doped glass is an attractive medium for integrated optics because of the low-cost and ease in fabrication of devices via ion-exchange, and it also has a broad emission bandwidth suitable for the production of ultrashort pulses.

Low-loss, ion-exchanged waveguides were fabricated in a commercially available Yb-doped phosphate glass (IOG-1 from Schott glass technologies, Inc). The waveguides were polished to lengths of 20 mm, 9.4 mm, 8 mm and 6.5 mm to give different repetition-rates. A mode-locked laser cavity was formed by end-butting a SESAM and an output coupler on the facets of the waveguides. Mode-locked Yb-doped glass waveguide laser operation was demonstrated, for the first time, at a repetition-rate of 4.9 GHz, a maximum power of 80 mW, a pulse duration of 740 fs and a central wavelength of 1058 nm [5].

A simple technique of dispersion control was utilised to operate the laser in the soliton mode-locking regime. A gap was introduced between the waveguide and the output coupler, which was controlled to change the total intra-cavity dispersion via the Gires-Tournois Interferometer (GTI) effect. It was found that the mode-locking performance was highly dependent on this gap, with no mode-locking achieved when the gap was reduced to zero.

With shorter waveguide samples, even higher repetition-rates were achieved. For a 9.4-mm-long sample, a repetition-rate of 10.4 GHz was achieved with a pulse width of 757 fs and an output power of 60 mW. A repetition-rate of 12 GHz was achieved for the 8-mm-long waveguide sample at a pulse duration of 824 fs and an output power of 45 mW. For the shortest 6.5-mm-long waveguide sample, the highest ever reported repetition-rate of 15.2 GHz from a waveguide laser was achieved at an output power of 27 mW and a pulse duration of 811 fs [6].

These results have opened up the field for the realisation of mode-locked waveguide lasers by simply end-butting the SESAMs on waveguide lasers and by exploiting the GTI effect. Future work may rely on integrated dispersion control within the SESAM itself for a more stable configuration.

7.1.4 Mode-locked Er,Yb:phosphate glass

1.5 µm is an important wavelength regime in the near infra-red for telecom applications. After mode-locking was achieved in Yb:phosphate glass, channel waveguides were fabricated in an Er,Yb:phosphate glass (IOG-1 from Schott) using a similar ion-exchange technique as that used for the Yb:phosphate glass waveguides. The waveguides were polished to a length of 20 mm and 15 mm in order to achieve mode-locking at different repetition-rates.

The mode-locked laser cavity was formed by a novel SESAM consisting of a dot in well (DWELL) structure and negative dispersion was introduced by controlling the gap between the SESAM and the waveguide via the GTI effect.

With the 20-mm-long waveguide sample, self-starting mode-locking was achieved at a repetition-rate of 4.8 GHz and pulse duration of 2.5 ps and a maximum output power of 9 mW. A repetition-rate of as high as 6.8 GHz was achieved with the 15-mm-long sample at a pulse duration of 5.4 ps and a maximum output power of 30 mW. The wavelength of operation for both the mode-locked lasers was around 1550 nm. The repetition-rate was finely tuned by more than 1 MHz by varying the pump power, which may be useful for future stabilisation without having any moving parts in the cavity.

This is the highest repetition-rate to have ever been reported from a fundamentally mode-locked waveguide laser around the 1.5 μm spectral regime. Also this is the first waveguide laser to be mode-locked by a quantum dot SESAM [7].

7.1.5 Tm:germanate glass

2 μm is an important “eye-safe” wavelength regime for various applications, such as spectroscopy, medical surgery and LIDAR. The next step in the project was to develop mode-locked sources in this spectral regime to target these important applications. To achieve this, an ion-exchangable Tm:germanate glass was fabricated with a high Tm^{3+} concentration in order to increase the quantum efficiency via the well-known cross-relaxation process in thulium ions.

Ion-exchange was carried out in this glass and it was polished to a length of 11.5 mm, corresponding to a repetition-rate of 8 GHz, if mode-locked. The propagation losses were measured by a relaxation oscillations technique and were found to be 0.3dB/cm at the laser wavelength. A threshold power as low as 44 mW was achieved with a cavity formed by two highly reflecting mirrors at a wavelength of 1885 nm. The highest slope efficiency of 6.8% was achieved with a 10% output coupler with a maximum output power of 10 mW. Based on these results a quantum efficiency of 1.15 was estimated [8].

This is an encouraging result for the possibility of future mode-locked operation, as low propagation loss waveguides and low thresholds for laser operation near 1.9 μm have been demonstrated. However, this performance could be improved by doping the glass with a higher concentration of Tm^{3+} ions in an attempt to increase the quantum efficiency and by reducing the mirror alignment losses.

7.2 Future work

7.2.1 Power-scaling

In the previous section, the results obtained during the course of the project were summarised. Mode-locked operation was achieved at wavelengths of 1 μm and 1.5 μm with a repetition-rate of up to 15 GHz. It will be of interest to power-scale these devices to increase their range of potential applications. Three different strategies can be employed to achieve this:

1. *High power pumping of planar ion-exchanged waveguides*. In this scheme, a planar ion-exchanged waveguide can be fabricated and then pumped with commercially available 10 W single-emitter diodes with a good beam quality in the guided direction ($M^2 \approx 1$), and a moderate beam quality ($M^2 \approx 40$) in the non-guided direction. This can potentially lead to a single stage source with an output power of ~1 W. However, high-power pumping of glass may not be ideal due to thermal issues. Also, there is a high probability of SESAM damage at such high average powers. Nevertheless, if this could be achieved, scaling the mode size in the non-guided plane by a factor of ~10 would lead to typical modelocked output power regimes of the order of ~1W rather than the ~100 mW typically achieved so far as this would produce the same fluence on the SESAM.

2. *Master Oscillator Power Amplifier (MOPA) using fibre amplifiers*. The mode-locked waveguide laser can be used as a seed source for various cascaded fibre amplifiers which can potentially amplify the seed to about 40 W. A block diagram for such a system is shown in Figure 7-1. The output from the amplifier stages can be compressed to give near transform-limited pulses. These high-power, multi-GHz pulses can be fed for example into a photonic crystal fibre for super-continuum generation as has previously been demonstrated using an ultrafast VECSEL seed source [9].

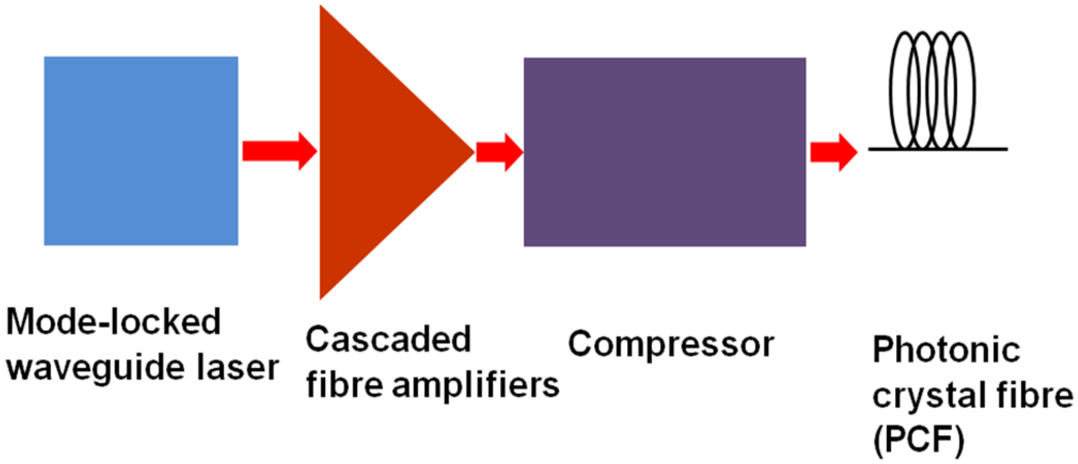

Figure 7-1. Block diagram for the amplification scheme of the mode-locked waveguide laser.

3. *Master Oscillator Power Amplifier (MOPA) using a single-stage waveguide amplifier.* The output from the mode-locked waveguide laser source can be amplified by another ion-exchanged waveguide. This can be an attractive option for the realisation of integrated high power mode-locked multi-GHz systems. A more attractive alternative to this configuration is the realisation of the seed and the amplifier stage on one integrated chip as seen from Figure 7-2. Such a concept may be achieved via flame hydrolysis deposition [10] which could allow the necessary localised deposition.

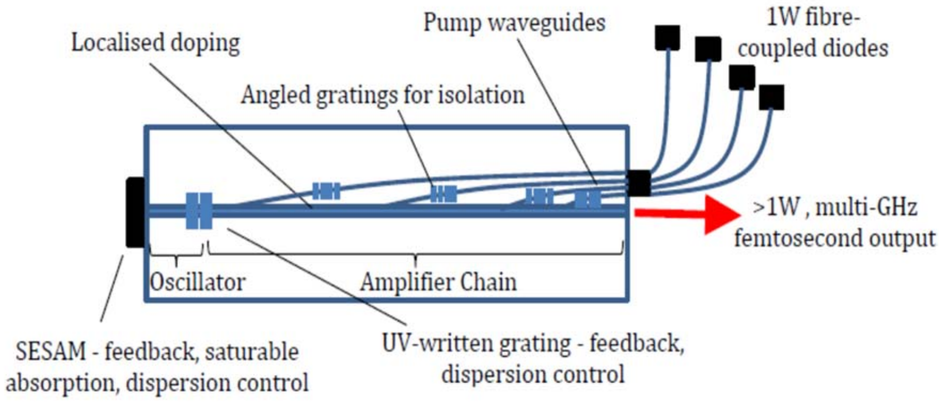

Figure 7-2. A concept for an integrated seed and amplifier solution delivering 1 W at multi-GHz repetition rates.

7.2.2 Mode-locking of Tm:germanate glass

During the course of this project, only CW operation was demonstrated in an ion-exchanged Tm:germanate waveguide laser. To try and increase the slope efficiency of the laser, new glass has been fabricated with a higher doping concentration. Experiments with this waveguide will be carried in the future to confirm the improvement in performance. Following which, mode-locking experiments will be carried out to try and develop a multi-GHz source in the mid-infrared, which could have applications in mid-IR frequency combs.

7.2.3 Mode-locking of Yb:KYW

Yb:KYW is a very promising candidate for mode-locking applications because of a broad emission bandwidth, better power handling properties compared to glass and a higher gain. Low-loss channels have previously been demonstrated in this material by Geskus et al. [4] and if such waveguides could be sourced they are obvious candidates for mode-locking experiments.

7.2.4 Applications of mode-locked, multi-GHz waveguide lasers

The next step after the realisation of the mode-locked sources is their trial in various applications. For many applications, such as those exploiting the frequency comb provided by such sources, the source will need to be stabilised, either by having piezo-electric components on the mirror and/or by controlling the pump power. Reduction of the pulse duration to sub-200 fs would also be of benefit for continuum generation and/or further investigating the balance between self-phase modulation and the GVD within our soliton mode-locked systems would be useful in this respect. Many other applications, such as nonlinear microscopy or even femtosecond micro-machining would benefit from the power scaling schemes noted above.

7.3 References

1. Cugat, J., Choudhary, A., Sole R., Carvajal, J.J., Massons, J., Shepherd, D.P., Diaz, F. and Aguilo, M., *Ar^+ ion milling rib waveguides on nonlinear optical (Yb,Nb):RTP/RTP epitaxial layers*. Optical Materials Express, 2013. **3** (11): p.1912-1917.
2. Choudhary, A., Cugat, J., Pradeesh, K., Solé, R., Díaz, F., Aguiló, M., Chong, H. M. H. and Shepherd, D. P., *Single-mode rib waveguides in (Yb,Nb):$RbTiOP_4$ by reactive ion etching.* Journal of Physics D: Applied Physics, 2013. **46** (14): p. 145108.
3. Choudhary, A., Bolaños, W., Kannan, P., Carvajal, J.J., Aguilò, M., Diaz, F. and Shepherd, D.P., *Low-threshold, mirrorless emission at 981 nm in an Yb,Gd,Lu:KYW inverted rib waveguide laser*. 2013. Proc. SPIE 8599, Solid State Lasers XXII: Technology and Devices, 859905
4. Geskus, D., Aravazhi, S., Grivas, C., Wörhoff, K. and Pollnau, M., *Microstructured $KY(WO_4)_2$:Gd^{3+}, Lu^{3+}, Yb^{3+} channel waveguide laser.* Opt. Express. **18** (9): p. 8853-8858.
5. Choudhary, A., Lagatsky, A. A., Kannan, P., Sibbett, W., Brown, C. T. A. and Shepherd, D. P., *Diode-pumped femtosecond solid-state waveguide laser with a 4.9 GHz pulse repetition rate.* Opt. Lett., 2012. **37** (21): p. 4416-4418.
6. Lagatsky, A. A., Choudhary, A., Kannan, P., Shepherd, D. P., Sibbett, W. and Brown, C. T. A., *Fundamentally mode-locked, femtosecond waveguide oscillators with multi-gigahertz repetition frequencies up to 15 GHz.* Opt. Express, 2013. **21** (17): p. 19608-19614.
7. Choudhary, A., Lagatsky, A. A., Zhang, Z. Y., Zhou, K. J., Wang, Q., Hogg, R. A., Pradeesh, K., Rafailov, ,E. U., Sibbett, W., Brown, C. T. A. and Shepherd, D. P., *A diode-pumped 1.5 μm waveguide laser mode-locked at 6.8 GHz by a quantum dot SESAM.* Laser Physics Letters, 2013. **10** (10): p. 105803.
8. Choudhary, A., Kannan, P., Mackenzie, J. I., Feng, X. and Shepherd, D.P., *Ion-exchanged Tm^{3+}:glass channel waveguide laser.* Opt. Lett., 2013. **38** (7): p. 1146-1148.
9. Head, C. R., Chan, H.-Y., Feehan, J. S., Shepherd, D. P., Alam, S., Tropper, A. C., Price, J. H. V. and Wilcox, K. G., *Supercontinuum Generation with GHz Repetition Rate Femtosecond-Pulse Fiber-Amplified VECSELs.* Photonics Technology Letters, IEEE, 2013. **25** (5): p. 464-467.
10. Guilhot, D. A., Emmerson, G. D., Gawith, C. B. E., Watts, S. P., Shepherd, D. P., Williams, R. B. and Smith, P. G. R., *Single-mode direct-ultraviolet-written channel waveguide laser in neodymium-doped silica on silicon.* Optics Letters, 2004. **29**(9): p. 947-949.